



Derivative synthesis of the transcriptional inhibitor α -amanitin and the translational inhibitor cycloheximide

Citation

Hoang, Eileen Mai-Huong. 2021. Derivative synthesis of the transcriptional inhibitor α -amanitin and the translational inhibitor cycloheximide. Doctoral dissertation, Harvard University Graduate School of Arts and Sciences.

Permanent link

<https://nrs.harvard.edu/URN-3:HUL.INSTREPOS:37370085>

Terms of Use

This article was downloaded from Harvard University's DASH repository, and is made available under the terms and conditions applicable to Other Posted Material, as set forth at <http://nrs.harvard.edu/urn-3:HUL.InstRepos:dash.current.terms-of-use#LAA>

Share Your Story

The Harvard community has made this article openly available.
Please share how this access benefits you. [Submit a story](#).

[Accessibility](#)

HARVARD UNIVERSITY
Graduate School of Arts and Sciences



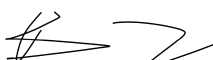
DISSERTATION ACCEPTANCE CERTIFICATE


The undersigned, appointed by the
Department of Chemistry & Chemical Biology
have examined a dissertation entitled:

Derivative synthesis of the transcriptional inhibitor α -amanitin
and the translational inhibitor cycloheximide

presented by: Eileen Mai-Huong Hoang

candidate for the degree of Doctor of Philosophy and hereby
certify that it is worthy of acceptance.

Signature 
Typed name: Professor Brian B. Liao

Signature 
Typed name: Professor Emily Balskus

Signature 
Typed name: Professor Christina Woo

Date: 25 June 2021

**Derivative synthesis of the transcriptional inhibitor α -amanitin
and the translational inhibitor cycloheximide**

A dissertation presented

by

Eileen Mai-Huong Hoang

to

The Department of Chemistry and Chemical Biology

in partial fulfillment of the requirements

for the degree of

Doctor of Philosophy

in the subject of

Chemistry

Harvard University

Cambridge, Massachusetts

June 2021

© 2021 – Eileen Mai-Huong Hoang

All rights reserved

**Derivative synthesis of the transcriptional inhibitor α -amanitin
and the translational inhibitor cycloheximide**

Abstract

The following work focuses on my efforts towards the synthesis of the transcriptional inhibitor α -amanitin and the translational inhibitor cycloheximide as a means to exploit the potential of these natural products as probes for developing new biochemical methods. The first half of this thesis details my work to access derivatives of α -amanitin, a naturally occurring cytotoxin that is found in several species of poisonous mushrooms and demonstrates incredible selectivity and binding affinity to eukaryotic RNA Polymerase II (Pol II). We devised a modular synthesis of a click-compatible α -amanitin that would be amenable to late-stage derivatization. Our strategy was reliant on the linear assembly of amino acid building blocks - many of which were non-canonical - followed by the key Savigne-Fontana macrocyclization to access the unique cysteine-tryptophan tryptathionine side chain linkage. This portion of my thesis details the synthesis of a solid-phase peptide synthesis-compatible bromopyrroloindoline, the enantioselective synthesis of (2*S*,3*R*,4*R*)-4,5-dihydroxy-isoleucine (DHlle), and finally the assembly of the bicyclic peptide framework to furnish the desired amanitin derivatives.

The second half of this thesis outlines the work towards the synthesis and characterization of potent cycloheximide (CHX) analogues. Due to its ability to effectively freeze ribosomes along mRNA, CHX has long been employed as a biochemical tool to study protein synthesis, and more recently has gained the role as the *de facto* inhibitor used for ribosome profiling. The remaining chapters of this dissertation will outline our lab's previous total synthesis of CHX and related analogues as well as our development of a semi-synthetic route to C13-amido CHX derivatives that is reliant on a diastereoselective C-H amination. This chapter is concluded with our mechanistic exploration of our most potent CHX analogue, using sequencing-based analysis and cryogenic electron microscopy to investigate the rationale of the increased activity of these synthetic derivatives.

Table of Contents

Abstract	iii
Table of Contents	iv
List of Abbreviations	vi
Chapter 1: An introduction to α-amanitin	1
1.1. α -amanitin: overview, biosynthesis, related compounds	1
1.2. Mechanism of action	3
1.3. Biochemical applications of α -amanitin	8
1.4. How do we access α -amanitin and derivatives?	11
1.5. Early SAR	12
1.6. The first reported total synthesis of amanitin analogues	13
1.7. The tryptathionine bridge and the Savige-Fontana reaction	14
1.8. The longstanding synthetic challenge of DHIIe	18
1.9. Early syntheses of DHIIe	19
1.10. The synthesis of a propargylated amanitin analogue by Zhao <i>et al.</i>	21
1.11. The first total synthesis of α -amanitin by Matinkhoo <i>et al.</i>	23
1.12. Recently published total syntheses of α -amanitin	26
Chapter 2: Efforts towards the synthesis of amanitin analogues	33
2.1. α -amanitin: our goals and strategy	33
2.2. Synthesis of an oxidized tryptophan-glycine dimer	35
2.3. An aside: notes on the synthesis of 6-Trp(OH)	37
2.4. Failed efforts towards the synthesis of (2 <i>S</i> ,3 <i>R</i> ,4 <i>R</i>)-dihydroxyisoleucine	39
2.5. A second attempt at synthesizing DHIIe	41
2.6. A successful strategy for accessing DHIIe	43
2.7. An aside: utilizing an abandoned route for synthesizing desmethyl DHIIe	45
2.8. Assembly of α -amanitin derivatives	47
2.9. Our strategy	47
2.10. Assembly of the monocyclic heptapeptide	47

2.11. Bicyclization	50
2.12. Some other derivatives of interest	52
2.13. Summary and conclusion	55
2.14. Experimental section	55
Chapter 3: An introduction to cycloheximide	78
3.1. Cycloheximide: overview	78
3.2. Mechanism of action	79
3.3. Related eukaryotic translation inhibitors	80
3.4. Biochemical applications of cycloheximide	82
3.5. Previous total syntheses of cycloheximide	83
3.6. Cycloheximide: our goals and interests	85
3.7. Laying the groundwork: the total synthesis of cycloheximide and analogues	85
3.8. The synthetic route to cycloheximide	86
3.9. Analogue generation and assessment	88
3.10. Curious behavior at carbon 13	92
Chapter 4: Semi-synthetic route to CHX C13-amido analogues	93
4.1. Introduction: how to access C13-functionalized CHX analogues	93
4.2. A semi-synthesis of C13-amido CHX derivatives	93
4.3. DMS-MaPSeq of CHX and 2.46	95
4.4. Abandoned efforts towards photo-labeling the ribosome	96
4.5. Summary and conclusion	98
4.6 Experimental section	99
References	110
Appendix A: Catalog of spectra	116

List of Abbreviations

Å	angstrom
Ac	acetyl
acac	acetylacetonate
ADC	antibody-drug conjugate
Bn	benzyl
Boc	<i>tert</i> -butyloxycarbonyl
BOM	benzyloxymethyl
Bu	butyl
°C	degrees Celsius
CAN	cerium(IV) ammonium nitrate
cat.	catalytic
Cbz	carbobenzyloxy
cDNA	complementary DNA
CHX	cycloheximide
<i>cis</i>	<i>L.</i> , on the same side
COD	cyclooctadiene
COMU	(1-Cyano-2-ethoxy-2-oxoethylideneaminoxy)dimethylamino-morpholino-carbenium hexafluorophosphate
Cryo-EM	cryogenic electron microscopy
CuAAC	Copper catalyzed azide-alkyne cycloaddition

DABSO	1,4-diazabicyclo[2.2.2]octane bis(sulfur dioxide) adduct
Davis reagent	2-(phenylsulfonyl)-3-phenyloxaziridine
DBCO	dibenzocyclooctyne
DBU	1,8-diazabicyclo[5.4.0]undec-7-ene
DCC	<i>N,N'</i> -dicyclohexylcarbodiimide
DCE	1,2-dichloroethane
dd	Doublet of doublets
ddd	Doublet of doublet of doublets
DHlle	(2 <i>S</i> ,3 <i>R</i> ,4 <i>R</i>)-4,5-Dihydroxyisoleucine
DIPAMP	1,2-Bis(2-methoxyphenyl)(phenylphosphino)ethane
DIPEA	diisopropylethyl amine
DIPT	diisopropyl tartrate
DMAP	dimethylaminopyridine
DMDO	dimethyldioxirane
DMF	<i>N,N</i> -dimethylformamide
DMS	dimethyl sulfate
DMS-MaPseq	dimethyl sulfate mutational profiling with sequencing
DMSO	dimethyl sulfoxide
DNA	deoxyribonucleic acid
dNTP	deoxyribonucleotide triphosphate
DPPA	diphenylphosphoryl azide

DSC	<i>N,N'</i> -disuccinimidyl carbonate
<i>E</i>	<i>Ger.</i> , entgegen
EDC	1-ethyl-3-(3-dimethylaminopropyl)carbodiimide
ee	enantiomeric excess
equiv	equivalent
ESI	electrospray ionization
esp	$\alpha,\alpha,\alpha',\alpha'$ -tetramethyl-1,3-benzenedipropionic acid
Et	ethyl
Fmoc	9-Fluorenylmethoxycarbonyl
Fpi	3a-Fluoropyrrolo[2,3- <i>b</i>]indoline, 3a-fluoropyrrolo[2,3- <i>b</i>]indoline-2-carboxyl
FP-T300	<i>N</i> -Fluoro-2,4,6-trimethylpyridinium triflate, <i>N</i> -fluoro-2,4,6-collidinium triflate
g	gram
GmPOPB	Proline oligopeptidase B from <i>Galerina marginata</i>
h	hour(s)
HATU	1-[Bis(dimethylamino)methylene]-1 <i>H</i> -1,2,3-triazolo[4,5- <i>b</i>]pyridinium 3-oxid hexafluorophosphate
HBSS	Hank's balanced salt solution
HOBt	1-Hydroxybenzotriazole
Hpi	3a-hydroxypyrrolo[2,3- <i>b</i>]indoline
HPLC	high-performance liquid chromatography
HRMS	high-resolution mass spectrometry

Hyp	<i>trans</i> -Hydroxyproline
Hz	hertz
IC ₅₀	Half maximal inhibitory concentration
icCL-seq	in-cell click selective crosslinking with RNA sequence profiling
Ipc	Isopinocampheyl
<i>J</i>	coupling constant (in Hz)
KHMDS	potassium bis(trimethylsilyl)amide
K _i	inhibition constant
LDA	lithium diisopropylamide
LiHMDS	lithium hexamethyldisilazide
LTM	lactimidomycin
M	molar (mols/liter)
m	multiplet
μ	micron
<i>m</i> CPBA	<i>meta</i> -chloroperoxybenzoic acid
Me	methyl
MSA	methanesulfonic acid
Mg	milligram
MHz	megahertz
MIDA	<i>N</i> -methyliminodiacetic acid
min	minute(s)

mL	milliliter
mmol	millimole
mol	mole
MS	mass spectrometry
MsCl	methanesulfonyl chloride
<i>m/z</i>	mass-to-charge ratio
NBS	<i>N</i> -bromosuccinimide
NET-seq	Native elongating transcript sequencing
NMM	<i>N</i> -methylmorpholine
NMO	<i>N</i> -methylmorpholine- <i>N</i> -oxide
NMR	nuclear magnetic resonance
NTP	ribonucleotide triphosphate
MTM	methylthiomethyl
OPP	<i>O</i> -propargyl puromycin
OSu	<i>N</i> -hydroxysuccinimide
OTf	trifluoromethanesulfonate
PBS	phosphate-buffered saline
PCR	polymerase chain reaction
PEG	polyethylene glycol
PG	protecting group
pH	hydrogen ion concentration

Ph	phenyl
PIDA	phenyliodine(III) diacetate
Pin	pinacol, pinacolate
Pol II	RNA polymerase II
POP	prolyl oligopeptidase
ppm	parts per million
PPTS	pyridinium <i>p</i> -toluenesulfonic acid
PTSA	<i>p</i> -toluenesulfonic acid
PyBOP	(Benzotriazol-1-yloxy)tripyrrolidinophosphonium hexafluorophosphate
q	quartet
R	general substituent
<i>R</i>	rectus (Cahn-Ingold-Prelog system)
<i>R_f</i>	retention factor
RNA	ribonucleic acid
RPF	ribosome-protected fragment
RT	room temperature
S	sinister (Cahn-Ingold-Prelog system)
s	second(s); singlet
SAR	structure-activity relationship
Selectfluor	1-chloromethyl-4-fluoro-1,4-diazoniabicyclo[2.2.2]octane bis(tetrafluoroborate)
SPPS	solid-phase peptide synthesis

<i>syn</i>	<i>L.</i> , with
t	triplet
T3P	propylphosphonic anhydride
TBAF	tetrabutylammonium fluoride
TBAI	tetrabutylammonium iodide
TBS	<i>tert</i> -butyldimethylsilyl
TBDPS	<i>tert</i> -butyldiphenylsilyl
Teoc	2-(trimethylsilyl)ethoxycarbonyl
TFA	trifluoroacetic acid
TFE	2,2,2-trifluoroethanol
THF	tetrahydrofuran
TIPS	triisopropylsilyl
TLC	thin-layer chromatography
TMS	trimethylsilyl
<i>trans</i>	<i>L.</i> , across
Trt	trityl, triphenylmethyl
TSTU	<i>N,N,N',N'</i> -tetramethyl- <i>O</i> -(<i>N</i> -succinimidyl)uranium tetrafluoroborate
UV	ultraviolet
X	general substituent
Z	<i>Ger.</i> , zusammen
δ	chemical shift

Chapter 1: An introduction to α -amanitin

1.1. α -amanitin: overview, biosynthesis, related compounds

α -amanitin (**Figure 1.1, I.1**) is a naturally occurring cytotoxin that is found in several poisonous mushrooms, including the “death cap” *Amanita Phalloides*. Since its initial isolation in 1940^{1,2}, the natural product has gained considerable infamy due to not only its toxicity – boasting a remarkably low LD₅₀ of 50-100 ug/kg – but also its unique structure. α -amanitin is the most well-known of the amatoxins, a family of bicyclic octapeptides originating from the *Amanita* genus of mushrooms (though amatoxins have later been isolated from certain species of the genera *Galerina*, *Lepiota*, and *Conocybe*). This family of cytotoxins is responsible for the majority of fatal mushroom poisonings, no doubt in part to their ability to resist degradation via high temperatures, enzymes, and acid³. Amatoxins are transcriptional inhibitors that bind to eukaryotic RNA Polymerase II (Pol II) but demonstrate varying binding affinity to the enzyme; these discrepancies in toxicity profiles have served as valuable tools in probing the structure-activity relationships (SAR) of α -amanitin and related derivatives (**Table 1.1**)⁴.

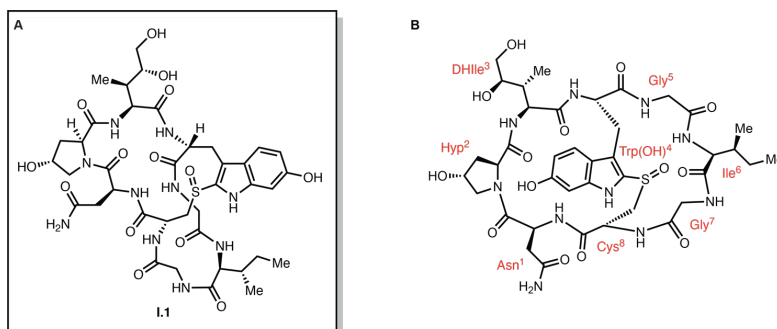
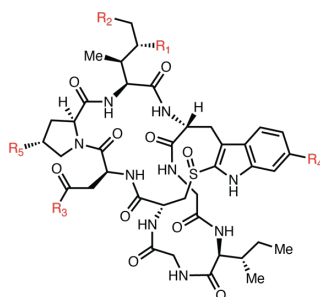


Figure 1.1. A) The structure of α -amanitin. **B)** Numbering for the eight residues present in the natural product.

Though initially assumed to be produced via nonribosomal peptide synthetases, amatoxins are ribosomally encoded^{5,6}. The biosynthesis of α -amanitin commences with the ribosomal production of a 35-amino acid propeptide encoded by the *AMA1* gene in *Amanita bisporigera*. The peptide sequence of α -amanitin is flanked by two conserved Pro residues within the propeptide, which is liberated via a prolyl

oligopeptidase (POP). Previous investigations have shown that a dedicated POP, GmPOPB, is not only responsible for the initial cleavage of the propeptide,⁷ but also performs a second cleavage event that results in the head-to-tail cyclization between Pro² and Ile³ in the mature polypeptide. There is still much to be elucidated about GmPOPB regarding its role in the production of α -amanitin, especially given that its particular enzymatic specificity has not yet been sufficiently explained; there is not a sequence or structural motif that seems to account for the enzyme's specificity for the 35-amino acid propeptide of α -amanitin.

Table 1.1. Members of the amatoxin family of natural products. Listed K_i values were obtained using Pol II isolated from calf thymus; LD₅₀ values were obtained using white mice⁴.



	Compound	R ₁	R ₂	R ₃	R ₄	R ₅	K _i (nM)	LD ₅₀ (mg/kg)
I.1	α -amanitin	CH ₂ OH	OH	OH	NH ₂	OH	2.3	0.3
I.2	β -amanitin	CH ₂ OH	OH	OH	OH	OH	2.5	0.5
I.3	γ -amanitin	CH ₃	OH	OH	NH ₂	OH	5	0.2
I.4	ϵ -amanitin	CH ₂ OH	OH	OH	OH	H	-	0.3-0.6
I.5	amanin	CH ₂ OH	OH	OH	OH	H	5	0.3
I.6	amaninamide	CH ₂ OH	OH	OH	NH ₂	H	5	20
I.7	amanullin	CH ₃	H	OH	NH ₂	OH	10	>20
I.8	amanullinic acid	CH ₃	H	OH	OH	OH	-	>20
I.9	proamanullin	CH ₃	H	H	OH	OH	-	>20

While there is a substantial amount of information we lack regarding the initial truncation and macrocyclization of the α -amanitin peptide sequence, there is even less known with regards to the post-translational oxidation events that lend the natural product its uniquely modified structure. These events include the hydroxylation of Pro, Trp, and Ile residues, as well as the internal Cys-Trp crosslink that lends α -amanitin its rigid, bicyclic structure. The formation of the thioether bridge is followed by its diastereoselective oxidation to the (*R*)-sulfoxide. However, neither the order nor the exact effectors of these events are currently known.

The same biosynthetic mysteries persist for other amatoxin-related poisons, most notably the phallotoxins, whose most prominent member is the well-studied phalloidin. The phallotoxins bear a striking resemblance to the amatoxins – namely the rigid, bicyclic structure and heavily modified peptide sidechains. However, the phalloxin base structure contains seven amino acids in comparison to the amatoxin's eight, stemming from a ribosomally-produced peptide precursor of 34 amino acids encoded by the *PHA1* gene in *Amanita* mushrooms. Going beyond structural differences, the activities of these two classes of toxins are also dissimilar. While the amatoxins are remarkably specific and potent inhibitors of Pol II, the phallotoxins are selective inhibitors of filamentous actin (F-actin) and do not demonstrate any affinity to Pol II. This difference in protein target between the two toxin subclasses provides further intrigue with regards to the structural origin of α -amanitin's mechanism of action with regards to transcriptional inhibition.

1.2. Mechanism of action

Poisoning induced by ingestion of amatoxins results in acute liver failure and necrosis. α -amanitin is capable of surviving absorption in the digestive tract and consequently travels to the liver, where hepatic uptake is mediated by a nonspecific physiological transport system normally reserved for bile salts. There, α -amanitin binds to eukaryotic Pol II, inhibiting transcription and therefore the production of mRNA. The severe deficiency of protein synthesis results in widespread cell death over the course of several days and is generally fatal if left untreated.

α -amanitin's notoriety stems from both its incredible selectivity and binding affinity to Pol II. The cytotoxin boasts a nanomolar K_d for its protein target and is selective for Pol II vs. Pol I and Pol III. Although the specific inhibition of Pol II by α -amanitin was initially reported in the 1970s, the structural basis of the

small molecule-protein interaction was not known until a co-crystal structure (2.8 Å) of α -amanitin bound to yeast Pol II was published in 2002 (**Figure 1.2**)⁸. The structures obtained by Kornberg et al. indicate that α -amanitin does not interact with the Pol II nucleotide binding site; indeed, this observation is corroborated by biochemical studies showing that drug binding has no influence on the affinity of Pol II for nucleoside triphosphates. Instead, α -amanitin acts as an allosteric inhibitor and binds to a structure within Pol II called the “bridge helix”, which extends between the interface of the two largest protein subunits, Rpb1 and Rpb2. The small molecule limits the mobility of the bridge helix as well as the Pol II trigger loop, an enzymatic structure that undergoes conformational “folding” to catalyze nucleotide addition of RNA. The bridge helix and trigger loop work in tandem to mediate the translocation of the polymerase along the DNA template; their restriction due to α -amanitin reduces nucleotide incorporation to only a few per minute as opposed to thousands and effectively halts active transcription.

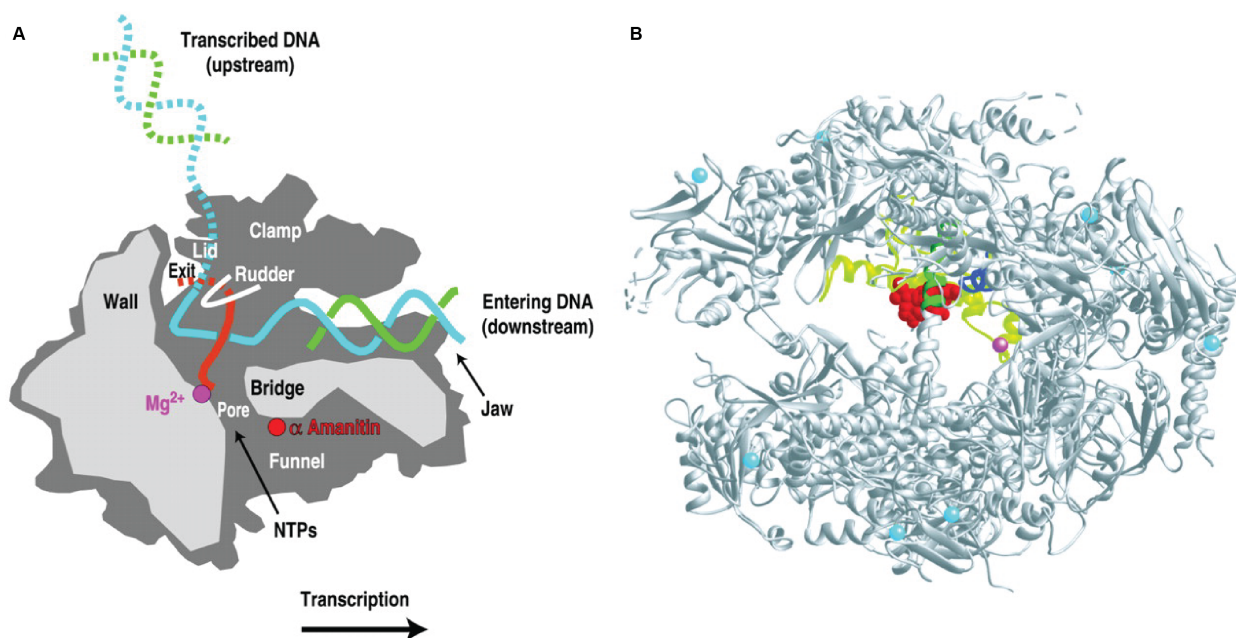
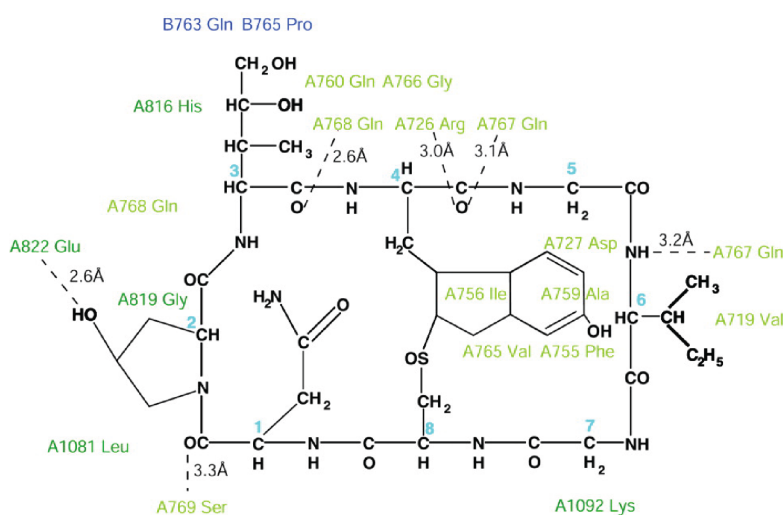


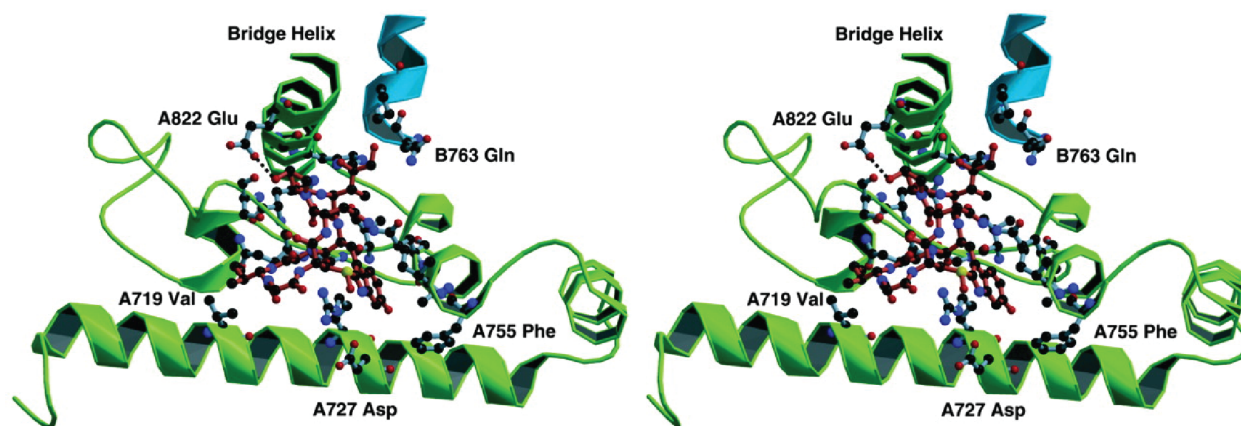
Figure 1.2. A) A cutaway view of the Pol II transcribing complex that shows the binding position of α -amanitin (red dot), located beneath the bridge helix, near the interface of subunits Rpb1 and Rpb2. Note that the binding location of the small inhibitor is relatively removed from the enzyme active site. **B)** Ribbons representation of the Pol II structure. α -amanitin is red, zinc atoms are shown in light blue, the active site

magnesium is magenta, the region of Rpb1 around α -amanitin is light green (funnel) and dark green (bridge helix), the region of Rpb2 near α -amanitin is dark blue. Figures reproduced with permission from Klug⁹ and Bushnell *et al*⁸.

Key interactions between α -amanitin and Pol II have been uncovered due to the initial crystal structures obtained by Kornberg (**Table 1.2**). In addition, derivatives of α -amanitin, both natural and synthetic, have provided the means to fully probe the structure-activity relationship of the infamous toxin. A particular interest has been dedicated to the binding contributions of α -amanitin's noncanonical amino acids; this concern is of special interest to those synthetically minded, as the numerous modified residues result in a considerable increase with regards to the synthetic complexity of the molecule. The yeast Pol II structures suggest a strong interaction with the α -amanitin hydroxyproline (Hyp) and a glutamic acid within the bridge helix (Glu822 in yeast Pol II). Subsequent cryo-EM structures of the inhibited Pol II elongation complex also indicate that Hyp interacts directly with the trigger loop (His 1108 in mammalian Pol II; His1085 in yeast Pol II), further underscoring that Hyp is critical for inhibition.

Table 1.2. Hydrogen bonds between α -amanitin and *S. cerevisiae* Pol II. α -amanitin residues are numbered corresponding to the scheme in **Figure 1.1 B**. Reproduced with permission from Bushnell *et al*. Copyright (2002) National Academy of Sciences, U.S.A.⁸





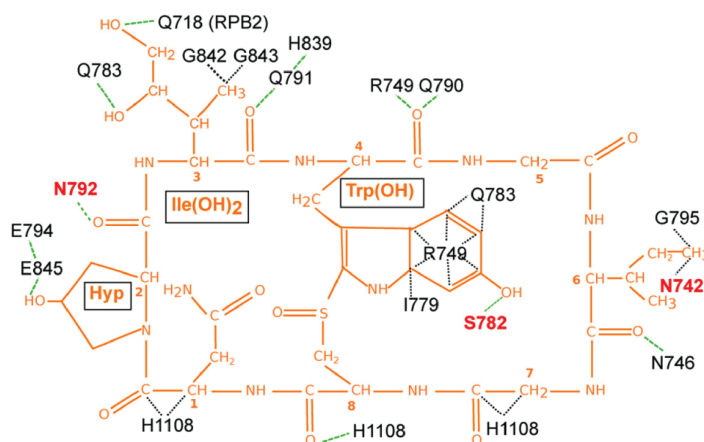
α -amanitin residue	α -amanitin atom	yeast Pol II residue (Rpb1)	Pol II atom	distance (Å)
Hyp ²	O	Ser769	N	3.3
Hyp ²	OD2	Glu822	OE1	2.6
DHlle ³	O	Gln768	OE1	2.6
Trp(OH) ⁴	O	Arg726	NH1	3.0
Trp(OH) ⁴	O	Gln767	N	3.1
Gly ⁵	N	Gln767	O	3.2

The role of the heavily oxidized (2*S*,3*R*,4*R*)-4,5-dihydroxy-isoleucine (DHlle) in enzyme inhibition was not so clear cut. The yeast Pol II crystal structure suggests an indirect interaction between the backbone carbonyl of DHlle and a residue within the bridge helix, but no obvious evidence that the side chain hydroxyls participate in any critical interactions within the binding pocket. Proamanullin, an amatoxin that lacks both the hydroxyl of Hyp and those of DHlle, displays inhibitory activity that is roughly 20,000-fold less than that of α -amanitin. This decrease in activity was initially attributed entirely to the ablation of the Hyp hydroxyl, in part due to conflicting data regarding the necessity of the DHlle hydroxyl groups. The derivative amanullin retains the oxidized side chain of Hyp but not that of DHlle and displays inhibitory activity at a 4-fold decrease compared to α -amanitin (**Table 1.1**, entry I.7). However, a later reported synthesis and

in-cell assay of amanullin reports that the derivative is inactive against CHO cells, suggesting that the role of DHlle in Pol II inhibition could not be fully explained using the current available structural data.

Kornberg's co-crystal structures were a prominent step forward in elucidating both the structural basis for Pol II inhibition by α -amanitin as well as uncovering more details about the mechanism of transcription itself. However, we have only recently seen the publication of a structure of α -amanitin bound to mammalian Pol II (in contrast to yeast Pol II). Cryo-EM structures published by Cramer *et al.* in 2018¹⁰ presents the Pol II EC inhibited by α -amanitin, highlighting several additional interactions with metazoan-specific residues that explain the cytotoxin's higher binding affinity for metazoan vs. yeast Pol II (nanomolar vs. micromolar, respectively) (**Table 1.3**). Many of the reported interactions between α -amanitin and the yeast Pol II EC were also observed in the mammalian cryo-EM structures, an unsurprising consequence of the high conservation of residues within the drug binding pocket. However, two additional hydrogen bonds of note were reported: one between the indole ring of α -amanitin's 6-hydroxy-tryptophan (6-Trp(OH)) and Pol II RPB1 Ser782; and another between the backbone carbonyl of DHlle and RPB1 Asn792.

Table 1.3. Hydrogen bonds between α -amanitin and *S. scrofa* Pol II. α -amanitin residues are numbered corresponding to the scheme in **Figure 1.1 B**. Reproduced with permission from Liu *et al*¹⁰.



α -amanitin residue	α -amanitin atom	mammalian Pol II residue (Rpb1)	Pol II atom	distance (Å)	present in yeast Pol II EC α -amanitin complex
Hyp ²	OD(D)	Glu845	OE1(A)	3.1	yes
Hyp ²	O(A)	Asn792	N(D)	3.6	yes
Hyp ²	O(A)	Asn792	ND2(D)	2.8	no
DHlle ³	OD(A)	Gln718 (RPB2)	NE2(D)	2.8	yes
DHlle ³	OG(A)	Gln783	NE2(D)	3.5	yes
DHlle ³	O(A)	Gln791	NE2(D)	3.6	yes
Trp(OH) ⁴	O(A)	Arg749	NE	3.6	yes
Trp(OH) ⁴	O(A)	Gln790	N(D)	2.5	yes
Trp(OH) ⁴	OH2	Ser782	OG	2.5	no
Ile ⁶	O(A)	Asn746	ND2(D)	3.7	yes
Cys ⁸	O(A)	His1108	NE2	3.6	yes

1.3. Biochemical applications of α -amanitin

α -amanitin's remarkable specificity and binding affinity for eukaryotic Pol II makes the small molecule an attractive tool for cancer therapeutics and biochemical applications. Of particular note is the development of antibody-drug conjugates (ADCs) that use α -amanitin as a toxic payload. Multiple aspects of α -amanitin make the small molecule a prime candidate for antibody conjugation. It's extremely potent, which lessens the concentration needed to induce cell death. α -amanitin is target selective, moreover its protein target is one of the most essential enzymes for cell survival. The toxin is stable under physiological conditions, water soluble, and offers several points of conjugation that allows the drug to retain its activity. Critically, α -amanitin is effective against rapidly dividing cells as well as quiescent cells; its inhibition of Pol II triggers degradation of the polymerase and results in apoptosis. The use of ADCs also circumvents the issue of α -amanitin's cell impermeability; the hydrophilic nature of the small molecule generally precludes its passive uptake into most human cell types barring hepatocytes¹¹.

Numerous amanitin-based ADCs have been synthesized, some of which have cleared pre-clinical trials. A nowhere near inclusive list of examples include the conjugation of α -amanitin to an anti-Thy IgG to target T lymphoma cells¹², anti-BCMA antibody (B-cell maturation antigen) to target multiple myeloma¹³,

and an anti-EpCAM (epithelial cell adhesion molecule) antibody against pancreatic carcinoma¹⁴. These studies represent advances not only with an eye towards targeted cancer treatments, but also lends invaluable insight into what synthetic modifications α -amanitin can tolerate. Generally, amanitin-based ADCs utilize one of three points of conjugation: the 6-hydroxyl group located on the Trp indole ring; the 5-hydroxyl of the DHlle; or the side chain amide of Asn side. This demonstrates that the small molecule's inhibitory activity can indeed withstand the appending of large functional groups such as an antibody; however, it is noted that certain combinations of conjugation point and linker can adversely affect the cytotoxicity of the corresponding ADC¹¹. The use of the 6-Trp(OH) for example is generally accompanied by a lysosomally-cleaved linker for payload release to circumvent issues with diminished toxicity due to conjugation.

α -amanitin's highly selective affinity for Pol II is also a powerful tool for probing the fundamental process of transcription and subsequently, gene expression¹⁵. Initially, the major regulatory steps of RNA synthesis as mediated by Pol II were believed to be the recruitment of the polymerase to the gene promoter and transcription initiation. However, the process of Pol II elongation, which refers to the attachment of nucleotides to a growing chain of RNA, has garnered increasing amounts of interest. This is in no small part due to the revelation that numerous checkpoints that control transcriptional elongation are frequently mutated in disease. Consequently, numerous techniques have cropped up with the goal of elucidating the mechanisms of elongation *in vivo*, most of which rely on mapping genome-wide Pol II density.

Chromatin immunoprecipitation and sequencing (ChIP-seq) is a well-established technique that allows *in vivo* mapping of protein-chromatin interactions and can be used to measure Pol II occupancy on a particular DNA template. However, the data produced from ChIP-seq is of limited spatial and temporal resolution and provides no clue if the identified Pol II molecules are engaged in active transcription. More recently, high throughput sequencing methods tailored specifically for Pol II have allowed for nucleotide-resolution of polymerase positioning as well as unveiled several aspects of transcriptional regulation that could not be probed with conventional density mapping techniques¹⁶⁻¹⁸. Of note is the development of native elongating transcript sequencing (NET-seq), which uses α -amanitin to freeze Pol II molecules and identify the nascent transcripts produced by actively transcribing molecules (**Figure 1.3**).

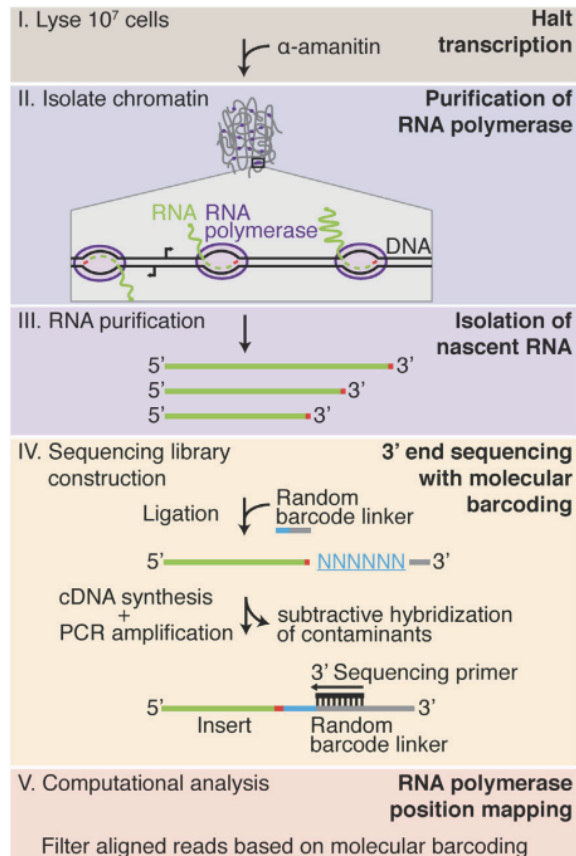


Figure 1.3. Overview of the key steps of NET-seq. The transcription inhibitor, α -amanitin, is introduced at cell lysis and is maintained through all purification steps. Engaged RNA polymerase is purified through the isolation of chromatin. The 3' end of the co-purified nascent RNA (red) is ligated to a linker containing a mixed random hexameric sequence (blue) that serves as a molecular barcode. After cDNA synthesis, contaminant species are removed by hybridization. PCR amplification results in a DNA-sequencing library with the sequencing primer binding site proximal to the random hexamer barcode. Finally, the 3' ends of the sequenced nascent RNA are aligned to the human genome, yielding RNA polymerase density at nucleotide resolution. Analysis of the molecular barcode allows reads arising from DNA library construction artifacts to be filtered out. Reproduced with permission from Mayer *et al*¹⁸.

NET-seq provides multiple advantages over previous Pol II mapping strategies – nucleotide-resolution, strand specificity, polymerase directionality, and sites of Pol II pausing. Furthermore, capturing nascent transcripts can allow for the identification of unstable, pre-processed RNA species that are not

captured with other sequencing techniques. While NET-seq is already an impressive method of studying transcriptional elongation, the use of a small molecule inhibitor offers vast potential for improvement via probe derivatization. For example, appending a pull-down handle to α -amanitin would allow for the direct isolation of nascent transcripts and circumvent the current ultracentrifugation purification that is both tedious and low-yielding.

1.4. How do we access α -amanitin and derivatives?

Despite the potential of the cytotoxin as a powerful tool for therapeutic and biochemical applications, access to α -amanitin and related derivatives is still challenging. Several avenues of accessing amatoxins include isolation from mushrooms, enzyme-based semi-synthetic methods, and of course, chemical synthesis. Several genera of mushrooms house members of the amatoxins: extraction of *Amanita*, *Galerina*, and *Lepiota* results in varying amounts of predominantly α -, β -, and γ -amanitin¹¹. Unsurprisingly, this process is time-consuming and relatively low yielding, in part due to the tedious process of separating the different amatoxins after their initial extraction. Fermentation-based isolation is the most commonly used method but still suffers from low yields, long processing times, and high costs. Enzyme-based semi-synthetic methods for accessing bicyclic toxins are of particular interest, but unfortunately not an immediately realistic goal. Given what we currently know about the biosynthesis of α -amanitin, a feasible route to the cytotoxin would be the chemical synthesis of the known 35-amino acid propeptide, followed by the enzymatic cleavage and macrocyclization using a dedicated prolyl oligopeptidase (POP). However, the current dearth of knowledge concerning the post-translational processing of α -amanitin means that there is no easy enzymatic solution with regards to the internal bicyclization, sulfoxidation, and side chain hydroxylations.

With the above in mind, chemical synthesis remains the most feasible method of procuring α -amanitin and related derivatives. Furthermore, improvement upon current natural product isolation strategies does not address the desire for more varied α -amanitin analogues. Though nearly all amanitin-based ADCs and probes use the natural product as a synthetic starting block, this precludes the systemic derivatization of the molecule that is necessary for detailed SAR analysis. The majority of α -amanitin SAR data has been gleaned in the period between the late 1970s and early 1990s and have generally only produced analogues that stem from direct modification of the cytotoxin after natural product isolation. The

few totally synthetic derivatives lack key oxidative features that result in a decrease in cytotoxic activity. Key derivatives and SAR data will be expanded upon in the following sections.

1.5. Early SAR

The history of the study and synthetic efforts towards α -amanitin and related analogues is marked with several temporal gaps. Much of the SAR and initial synthetic attempts at accessing α -amanitin were produced in the 80s and 90s, with little progress seen in the interim between this initial wave of interest and the very recent publications of the molecule's total synthesis starting in 2018. This difficulty in accessing synthetic analogues of α -amanitin has resulted in a general lack of structure-activity relationship for the cytotoxin. Initial SAR after α -amanitin was first isolated came primarily through comparison to known amatoxins and direct modification of the natural product. Common modifications of the natural product are mediated through the non-canonical 6-Trp(OH) and DH1le, in no small part due to the interest of finding suitable sites of conjugation for the synthesis of biochemical probes and ADCs. For example, regioselective methylation^{19,20} as well as arylazo-coupling²¹ of the 6-hydroxyl of 6-Trp(OH) both produce derivatives that retain the inhibitory activity of the parent compound, highlighting the indole as a natural choice for bioconjugation strategies. Interestingly, dialkylation products in which α -amanitin is modified at the indole nitrogen of 6-Trp(OH) in addition to the phenol have shown to have relatively little effect on the toxicity profile of the resulting compound. However, given that O-alkylation is always observed first, the indole nitrogen is not generally considered a candidate for functionalization.

While direct modification of the 6-Trp(OH) phenol has historically yielded highly potent compounds, similar modifications of the DH1le sidechain diol are overall less successful. Reported chemical modifications of the DH1le diol include etherification, periodate cleavage, and manipulation of its oxidation state, but only yielded analogues that were significantly less toxic in comparison to α -amanitin²⁰. Furthermore, attempts to target the other aliphatic side chains of α -amanitin are often foiled due to the higher accessibility and reactivity of the DH1le diol. Nevertheless, these synthetic as well as naturally occurring amanitin derivatives have proven valuable in SAR studies, especially given the longstanding lack of an enantioselective synthesis of DH1le. In addition to the studies focused on α -amanitin's complex building blocks, early SAR studies in the 1980s were impressively able to investigate the inhibitory

importance of the (*R*)-sulfoxide contained within the natural product's tryptathionine bridge¹⁹, the configuration of which is shared by both α -amanitin and β -amanitin. Production of the (*S*)-sulfoxide of 6-Trp(OMe) α -amanitin (a derivative known to retain the natural toxin's inhibitory activity) resulted in a 20-fold decrease in toxicity. Surprisingly, the corresponding thioether and sulfone demonstrated inhibition on par with the unmodified natural product. As such, many synthetic efforts towards α -amanitin derivatives forgo the diastereoselective sulfoxidation of the tryptathionine bridge in favor of the thioether.

1.6. The first reported total synthesis of amanitin analogues

A viable route to α -amanitin is no trivial task; the first total synthesis of the natural product has only recently been published in 2018 (*vide infra*)²². Several aspects make α -amanitin a formidable synthetic challenge. Unsurprisingly, some of the major obstacles are the synthesis of the non-canonical (2*S*,3*R*,4*R*)-4,5-dihydroxy-isoleucine (DHlle), the 6-hydroxy-tryptophan (6-Trp(OH)), and the intra-annular tryptathionine bridge and its enantioselective oxidation to the (*R*)-sulfoxide. Although these barriers have impeded a synthetic route to α -amanitin in its entirety, synthesis of less complex derivatives of the natural product has proven useful in determining the most critical features responsible for the toxin's activity. However, very few of these synthetic derivatives have been shown to retain the full potency of α -amanitin.

Zanotti, Birr, and Wieland are credited with the first reported synthesis of amaninamide, which omits the 6-hydroxytryptophan and DHlle in favor of their canonical counterparts²³. Already known for their extensive work in uncovering the SAR of α -amanitin via related amatoxins and analogues derived from the direct chemical modification of the natural product, Zanotti and coworkers report the synthesis of a linear octapeptide containing an N-terminal Hpi moiety and an internal trityl side chain protected cysteine (**Figure 1.4**). Thioether formation was performed via an intramolecular Savige-Fontana reaction, followed by macrolactamization to furnish the bicyclic product. Oxidation of the thioether bridge produced the final sulfoxidated bicycle, in a separable 2:1 diastereomeric mix in favor of the (*S*)-sulfoxide.

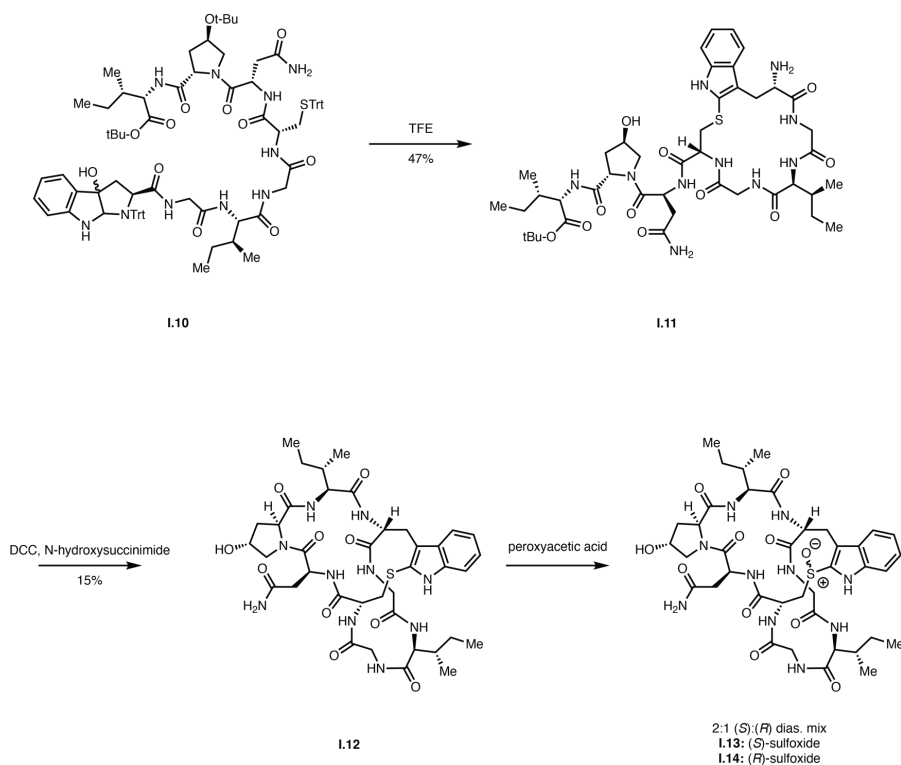


Figure 1.4. The first reported synthesis of amaninamide, credited to Zanotti and coworkers²³.

The installation of the tryptathionine bridge via the acid-mediated Savige-Fontana cyclization with an N-terminal Hpi remains by far the most widely utilized strategy for accessing amanitin derivatives, even upon the shift from solution-phase to predominantly solid-phase peptide synthesis for assembling the linear precursor peptide. The vast majority of synthetic amanitin derivatives produced during the ensuing years take advantage of the strategy published by Zanotti *et al.*, including the exclusion of (2*S*,3*R*,4*R*)-DHlle and 6-Trp(OH) from the final product.

1.7. The tryptathionine bridge and the Savige-Fontana reaction

Zanotti's use of the Savige-Fontana reaction to install the amanitin tryptathionine bridge has remained the most prominent method of obtaining the natural product's indole-thiol crosslink. The Cys-Trp side chain-side chain linkage is one of the defining characteristics of the amatoxins, wherein the 2-position of the tryptophan indole is substituted with the sulfur of the cysteine side chain²⁴. Indeed, the tryptathionine bridge

is largely responsible for lending α -amanitin and related molecules their rigid, bicyclic framework, an appealing structural quality that often translates to increased stability and higher on-target binding due to lowered conformation plasticity^{25,26}.

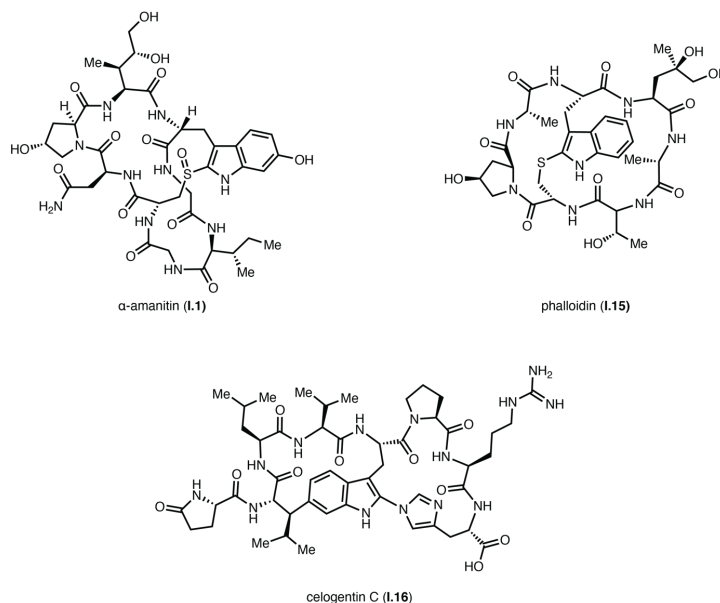


Figure 1.5. Examples of bicyclic peptide natural products. The intra-annular tryptathionine bridge is only found in the amatoxin and phallotoxin family of compounds, though the sulfur at the bridge position exists in different oxidation states. Celogentin C boasts two unusual tryptophan cross links: one that connects the leucine β -carbon to the C6 indole and another that connects the imidazole N1 of histidine to the C2 indole. The same architecture is common to the entire celogentin family.

Crosslinked structures are a prevalent motif among both natural and synthetic peptide molecules, but the tryptathionine bridge is exclusive to the amatoxin and phallotoxin families, if present in different oxidation states – amanitins contain a sulfoxide at the bridge position, while phallotoxins contain the thioether (**Figure 1.5**). Derivatives of either family that lack the tryptathionine linkage have shown to be virtually inactive against their protein targets².

The tryptathionine bridge has received considerable synthetic interest in the pursuit of amatoxin and phallotoxin derivatives, no doubt due to its critical role in binding affinity for each molecule's respective

binding partner. The earliest documented synthesis of an indole-thioether linkage is attributed to Wieland and coworkers in 1969, wherein the cysteine thiol is converted to the sulfenyl chloride and undergoes nucleophilic attack by the tryptophan indole in glacial acetic acid²⁷. This strategy has proved its utility in the solution-phase synthesis of several phallotoxins but has demonstrated limited use for solid-phase-based methods^{28,29}. The tedious protection group strategies, by-product formation, and inability to exploit linear peptide synthesis in the construction of these analogues have all contributed to the decreased use of sulfenyl halide-based tryptathionylation, especially in the wake of the Savige-Fontana reaction.

The acid-mediated reaction between a free cysteine thiol and a tryptophan indole was first reported in 1976³⁰. The Savige-Fontana reaction has since become by far the most common and well-documented method of obtaining the tryptathionine bridge found in α -amanitin and related molecules. At the crux of the original prep was 3 α -hydroxypyrrolo[2,3-*b*]indoline, 3 α -hydroxypyrrolo[2,3-*b*]indoline-2-carboxyl (Hpi), obtained through the reaction of tryptophan with peroxyacetic acid at depressed temperatures to produce a mixture of diastereomers (**Figure 1.6**). Upon addition of cysteine in 25% trifluoroacetic acid, Hpi acts as a suitable electrophile for the free cysteine thiol and forms tryptathionine good yield. Furthermore, this reaction was found to be chemoselective for the cysteine thiol as no products due to reaction with other amino acid side chains were observed.

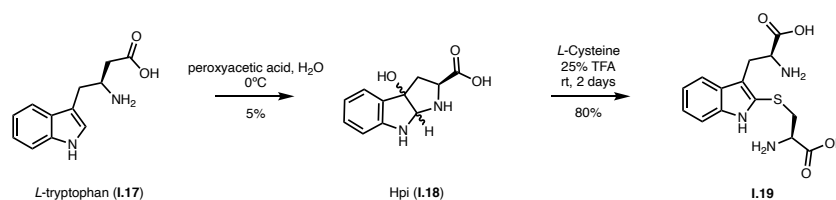
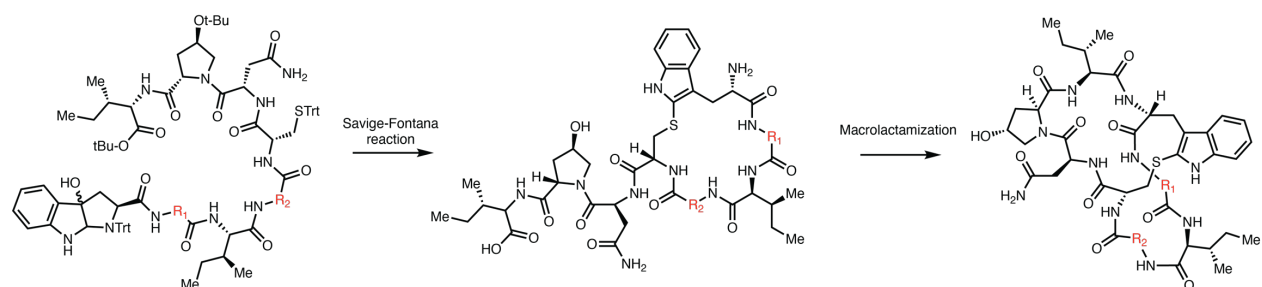


Figure 1.6. The first reported synthesis of Hpi (**1.19**) and its acid mediated reaction with *L*-cysteine as reported by Savige and Fontana³⁰.

Perhaps most critically, protection of the Hpi C-terminus with the acid labile Boc group allows Hpi to serve as a compatible monomer for standard Fmoc-based SPPS³¹. Following their report of the first totally synthetic amanitin derivatives in 1981, Zanotti and coworkers made full use of the Savige-Fontana

reaction in later published syntheses of several other amanitin derivatives that replace DHlle with other hydrophobic sidechains³² and explore modification of the two glycine residues (**Table 1.4**)³³.

Table 1.4. The synthetic amanitin analogues reported by Zanotti *et al.*³³. Employment of the acid-mediated Savige-Fontana reaction allows for the initial side chain-side chain macrocyclization, followed by the head-to-tail macrolactamization to afford the bicyclic products.



	R ₁	R ₂
1.20	<i>L</i> -Ala	Gly
1.22	<i>D</i> -Ala	Gly
1.23	Gly	<i>D</i> -Ala
1.24	<i>D</i> -Ala	<i>D</i> -Ala

This strategy of accessing tryptathionine-bridged cyclic peptides persists as the most prevalent method of synthesizing amatoxin and phallotoxin derivatives. Briefly, a linear precursor peptide is synthesized on acid-labile resin, containing an internal Cys(Trt) residue and N^α-Boc-Hpi installed at the N-terminus. Treatment with TFA is concomitant with resin cleavage, global deprotection, and tryptathionylation. The Savige-Fontana reaction is believed to occur via the deprotection of the Hpi N-terminus and the subsequent protonation of the amino nitrogen, leading to bond cleavage between N^α and the adjoining carbon (**Figure 1.7**). Nucleophilic attack at the C2 position by the free cysteine thiol results in the rearomatization of the

indole side chain as well as the ejection of the leaving group at C γ , producing the thioether linkage and the macrocyclic peptide. Bicyclization is then performed via standard solution-phase peptide bond formation.

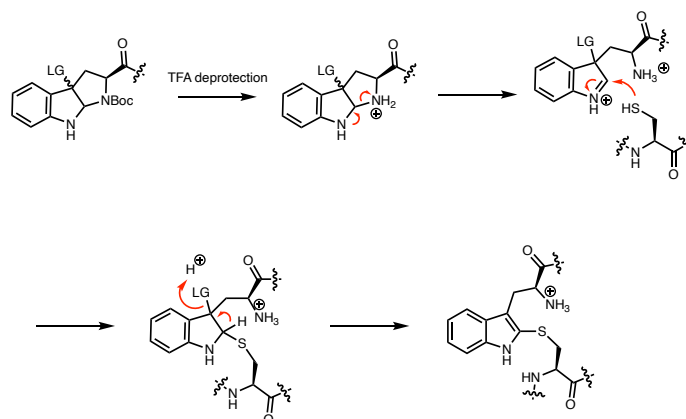
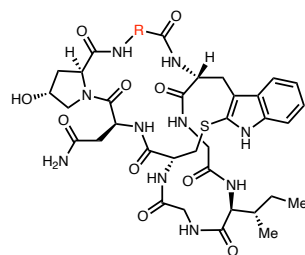


Figure 1.7 Proposed mechanism for the Savige-Fontana reaction.

1.8. The longstanding synthetic challenge of DHlle

One of the most notable obstacles towards a total synthesis of α -amanitin is obtaining the non-canonical DHlle amino acid. Despite its deceptively simple structure, DHlle contains 3 contiguous stereocenters: an α -stereocenter, secondary methyl, and secondary hydroxyl in an all-anti configuration. However, the considerable difficulty of accessing the desired isomer has resulted in a notable paucity in efficient synthetic routes, and consequently nearly every synthetic derivative of α -amanitin substitutes DHlle with some other hydrophobic or noncanonical amino acid^{32,33}. Synthetic derivatives containing Ile in place of DHlle exhibit roughly 32-fold less inhibitory activity than the natural product, a relatively low decrease in comparison to replacement with Val, Leu, or Ala. Furthermore, ablation of the 5-hydroxyl of DHlle has a remarkably lower effect on Pol II inhibition vs. that of the 4-hydroxyl (**Table 1.5**).



	R	K _i (relative to α-amanitin)
I.1	DHlle	1
I.25	Ile	32
I.26	Val	128
I.27	Leu	1400
I.28	Ala	2700

Table 1.5. S-deoxy-amaninamide analogues that are derivatized at DHlle. Listed inhibition constants relative to α-amanitin were obtained using calf thymus Pol II³².

1.9. Early syntheses of DHlle

Given the longstanding interest in α-amanitin and by extension, DHlle, it is unsurprising that numerous attempts to synthetically access the dihydroxylated building block have been reported. Though few can boast that they are selective for the desired (2*S*,3*R*,4*R*) isomer, there have nonetheless been several published strategies to synthesize the heavily modified isoleucine derivative. The following section will discuss several early synthetic investigations of DHlle; more recent routes towards the building block will be discussed in later sections in the context of their respective total syntheses of α-amanitin.

The first non-enantioselective synthesis of the DHlle lactone is attributed to Wieland and coworkers in 1967, which commences with diethyl ethylidenemalonate (**Figure 1.8**)³⁴. A racemic mixture of all eight stereoisomers of lactone **I.32** was produced. Though the desired diastereomer only existed as a minor component, Wieland's work marked the first published synthesis of DHlle.

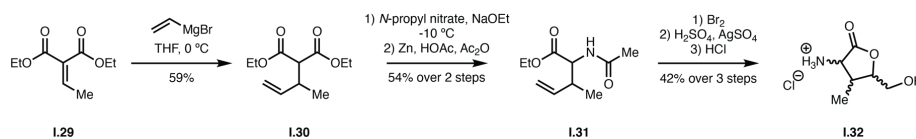


Figure 1.8. The first published synthesis of DHlle by Wieland and coworkers details the non-enantioselective synthesis of the DHlle lactone **I.32**³⁴.

Several years later, Bartlett *et al.* reported the diastereoselective synthesis of the DHlle lactone by utilizing an ester-enolate Claisen rearrangement as their key step (**Figure 1.9**)³⁵. The Bartlett group's interest in DHlle stemmed from their studies on exploiting the ester-enolate Claisen rearrangement as a method to produce γ,δ -unsaturated amino acids.

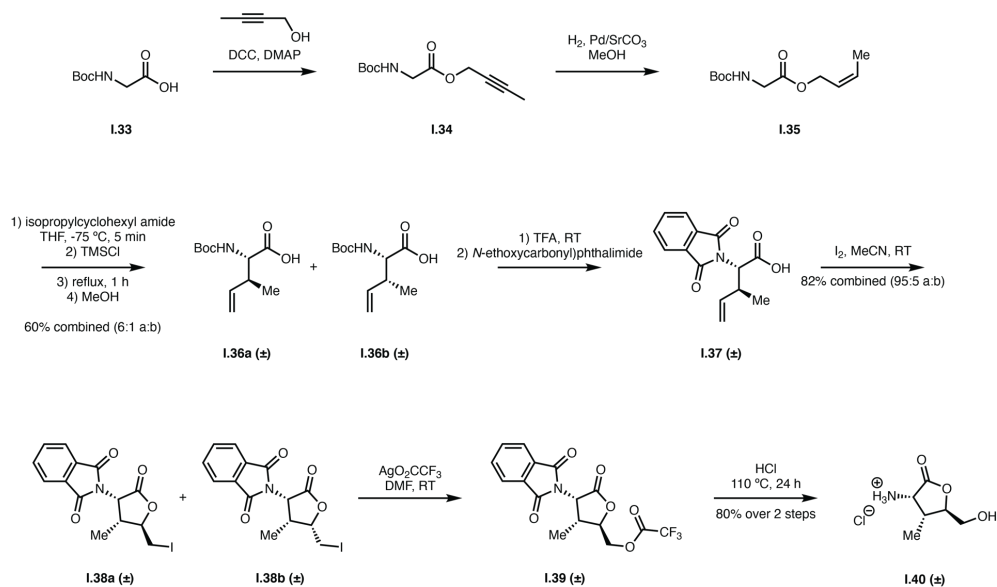


Figure 1.9. Bartlett and coworkers' route for the diastereoselective synthesis of the DHlle lactone³⁵. The inability to separate the desired natural product diastereomer from a racemic mixture diminishes the route's overall synthetic utility.

The *cis*-crotyl ester of *N*-Boc-glycine was prepared as the substrate for the Claisen rearrangement based on previous reactions using the *trans*-crotyl ester equivalent. Rearrangement of the *trans*-crotyl *N*-Boc-glycine resulted in an enantiomeric mixture of the undesired dehydro-*allo*-isoleucine as the major product, surmised to stem from the configuration of the favored enolate structure in the transition state. Assuming a chair-like transition state, the intermediate is proposed to have the enolate oxygen and the deprotonated carbamate positioned *cis* relative to each other. As predicted, rearrangement of the *cis*-crotyl ester produced the desired dehydro-isoleucine isomer, present as a *D/L* enantiomeric mix. With these results in hand, Bartlett and coworkers turned to a stereoselective iodolactonization for the alkene functionalization,

which demonstrated the best diastereoselectivity upon replacement of the amine Boc with a phthaloyl group and using iodine in acetonitrile. Hydrolysis of the iodolactone followed by saponification led to a racemic mixture of dehydro-*L*-isoleucine lactone, though Bartlett and coworkers note ~10% epimerization at C α upon conversion of the iodinated lactone to the DHlle lactone. While a remarkable improvement over Wieland's completely non-stereoselective synthesis, Bartlett's route to the DHlle lactone demonstrates several issues that decrease its overall synthetic utility, most conspicuously that the final natural product diastereomer is inseparable from the racemic product mixture. Regardless of these shortcomings, there has been a dearth of published reports that improve upon Bartlett's 1982 synthesis until recently. An uptick of interest in devising a total synthesis of α -amanitin has in turn produced a several syntheses for DHlle (*vide infra*).

1.10. The synthesis of a propargylated amanitin analogue by Zhao *et al.*

Taking advantage of the foundational work done by Zanotti, Wieland, and others, the Perrin lab has made remarkable strides forward in the synthesis and cytotoxic assessment of amanitin analogues. The use of solid phase peptide synthesis had since been proven to be a viable strategy for accessing synthetic analogues of the amatoxins and phallotoxins²⁸, and is demonstrated by Zhao and coworkers in their 2015 synthesis of S-deoxy click-compatible amanitin analogues³⁶.

A linear heptapeptide was assembled on the acid labile 2-chlorotrityl chloride resin with an Hpi group appended to the N-terminus, substituting *N*-propargyl asparagine in place of the canonical amino acid found in the natural product (**Figure 1.10**). The linear peptide was subjected to TFA, cleaving the resin concomitantly with the removal of the side chain protecting groups and allowing nucleophilic addition of the free cysteine thiol to the unprotected Hpi moiety. With the macrocyclized heptapeptide in hand, Zhao and coworkers obtained the final bicyclic structure via successive peptide couplings with DHlle. The activated NHS-ester of the fully-protected DHlle monomer was coupled to the free Gly N-terminal, after which Fmoc deprotection and desilylation of DHlle allowed for the final peptide formation between the DHlle amine and the Hyp C-terminus. The final macrolactamization was performed with a diastereomeric mixture of DHlle, resulting in four bicyclic compounds. The diastereomer containing the correct configuration of DHlle was

determined after separation and assessment of each individual isomer indicated that only one analogue demonstrated cytotoxicity comparable to the parent compound.

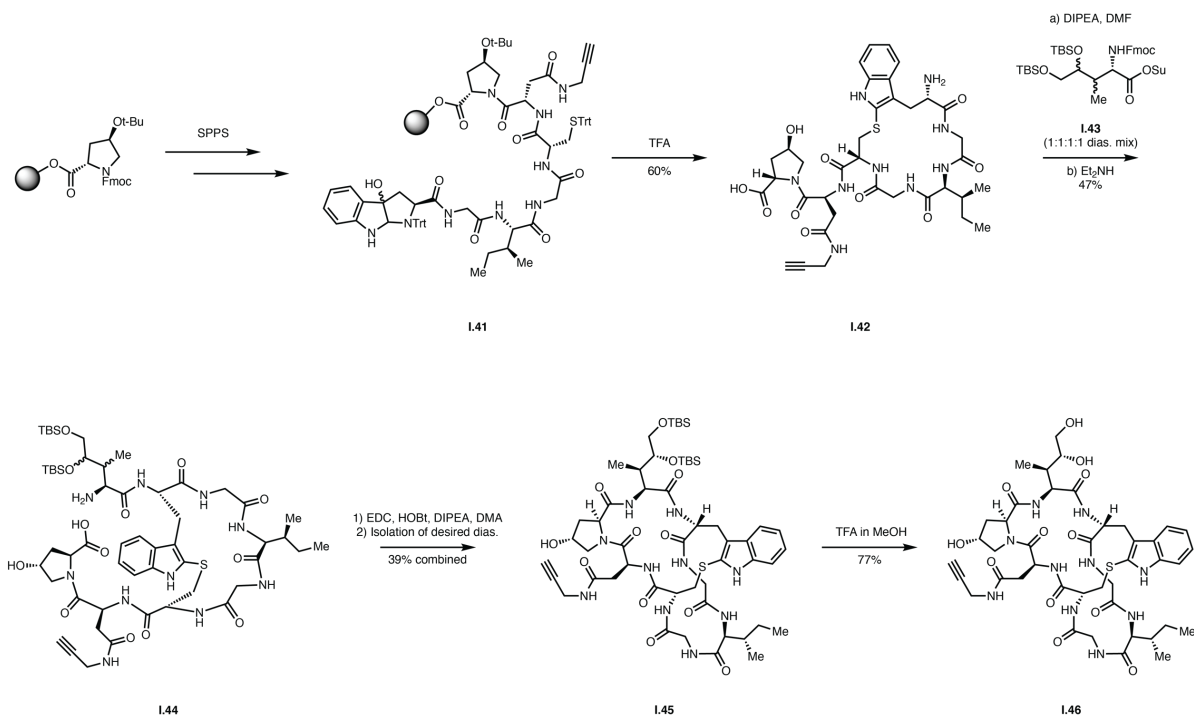


Figure 1.10. Synthesis of a propargylated amanitin analogue as reported by Zhao and coworkers³⁶.

It is noteworthy that the route utilized by the Perrin lab to obtain DHIIc was greatly inspired by Barlett's synthesis of dehydroisoleucine **I.49** (Figure 1.11). **I.49** was obtained as a racemate with 9:1 diastereoselectivity in favor of the desired diastereomer and was subsequently subjected to Upjohn dihydroxylation. Interestingly, Zhao and coworkers report that Sharpless' asymmetric dihydroxylation (AD) showed no stereoselectivity with AD-mix- α nor AD-mix- β , and instead persisted with standard dihydroxylation to obtain all four DHIIc diastereomers. Following TBS protecting of the resulting hydroxyl groups as well as replacement of the amine Cbz with Fmoc furnished a diastereomeric mixture of DHIIc that was adequately protected for solid-phase peptide synthesis. However, resolving the DHIIc monomers was not successful, and the diastereomeric mixture was directly incorporated into the amanitin heptapeptide monocyte to yield four diastereomers of the bicyclic octamer (**I.50a** (\pm) and **I.50b** (\pm)). HPLC resolution of

the diastereomeric mix isolated one toxic analogue, presumably that which contained the (2S,3R,4R) configuration of DHIIe. The lack of selectivity of the dihydroxylation as well as difficulty associated with purifying the resulting diastereomers decreases the overall appeal of this synthesis; however, the cytotoxic assessment of the corresponding bicycles resulted in evidence that the configuration of DHIIe is indeed critical for activity.

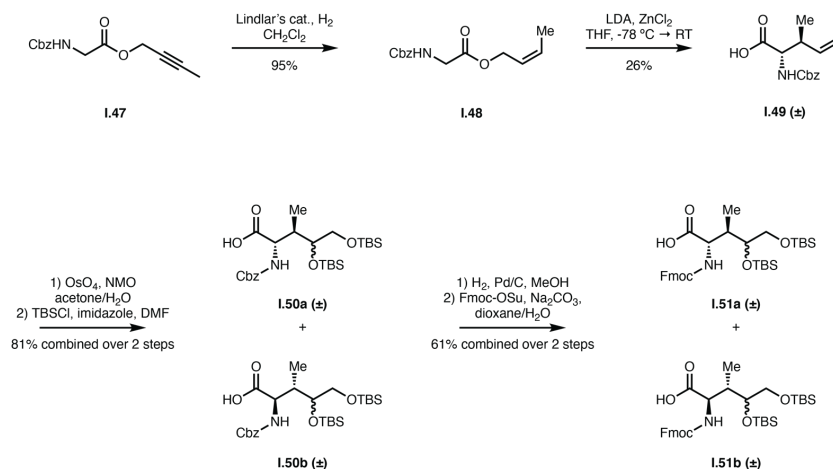


Figure 1.11. Zhao *et al.* report the synthesis of 4 diastereomers of DHIIe en route to obtaining biofunctionalized amanitin derivatives³⁶. HPLC resolution of the DHIIe diastereomers was only possible after peptide coupling to the macrocyclic scaffold.

1.11. The first total synthesis of α -amanitin by Matinkhoo *et al.*

The Perrin lab retains a similar strategy for their 2018 total synthesis of α -amanitin²², synthesizing a linear heptapeptide on resin in the following sequence: Hyp(OtBu), Asn(Trt), Cys(Trt), Gly, Ile, Gly, 6-BMIDA-Fpi (**Figure 1.12**). Global deprotection and tryptathionylation was carried out using a 1:1 mixture of TFA/DCM and furnishing monocyclic heptapeptide **1.53**. The MIDA-boronate was converted to the boronic acid, then oxidatively deborylated to produce the corresponding phenol.

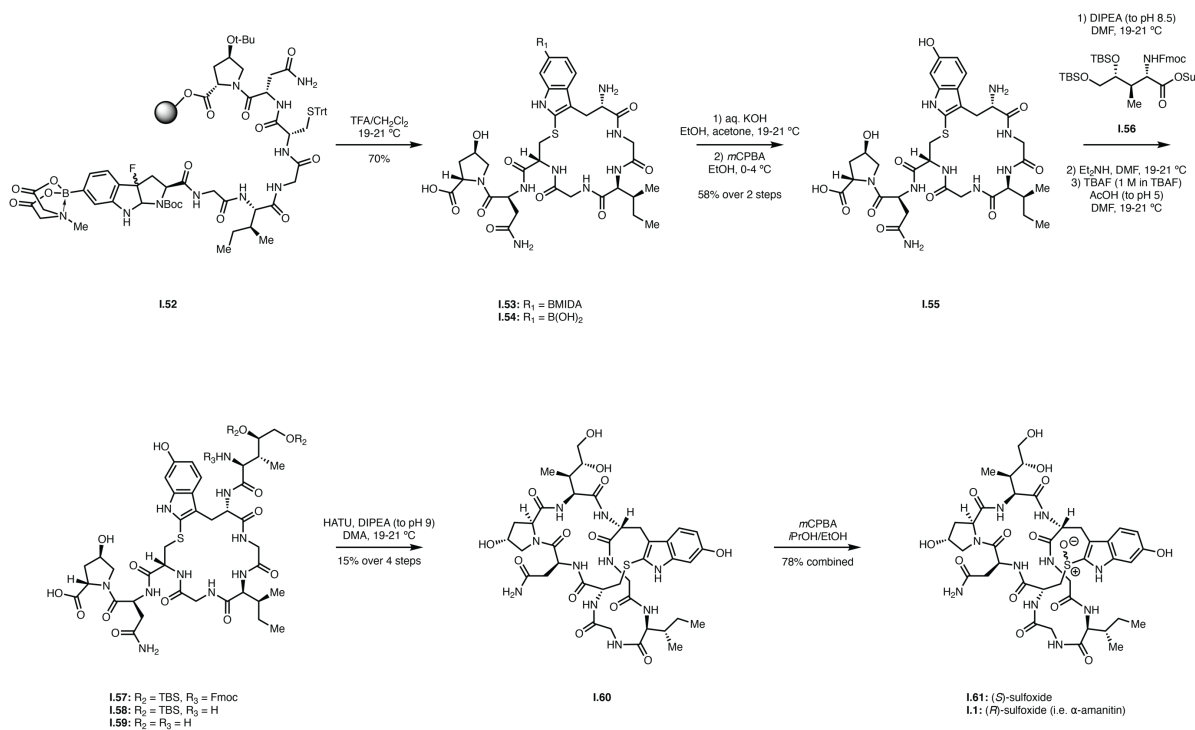


Figure 1.12. The total synthesis of α -amanitin reported by Matinkhoo et al²².

As in their previous synthesis, macrolactamization was performed with a series of peptide couplings with the final residue, DHlle. However, the presence of 6-Trp(OH) necessitated a series of pH adjustments, lest the oxidatively sensitive group lead to undesired byproducts upon the final series of reactions. Finally, diastereoselective sulfoxidation of the thioether to the corresponding (*R*)-sulfoxide using *m*CPBA concluded the total synthesis of the natural product.

Given our own failures regarding the synthesis of 6-OH-Trp (outlined in Chapter 2), we were highly interested in the method in which the Perrin lab obtained the elusive tryptophan derivative in their total synthesis of α -amanitin²². Intriguingly, the authors detail a similar thought process regarding the use of Baran's regioselective borylation to install a latent hydroxyl group onto the tryptophan indole but faced similar difficulties with attempts to synthesize the corresponding Hpi derivative using DMDO. Instead, a solution was found in the use of an electrophilic fluorinating reagent as the oxidant of choice (**Figure 1.13**).

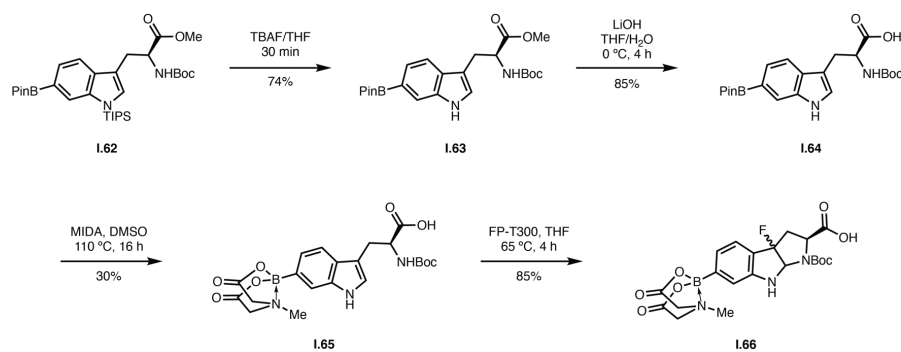


Figure 1.13. The synthesis of 6-BMIDA-Fpi **I.66** as reported by Matinkhoo *et al*²².

Protecting the boronate using *N*-methyliminodiacetic acid (MIDA) smoothly produced 6-MIDA-Trp from NBoc-Trp(TIPS)-OMe, which was subjected to fluorocyclization by 1-fluoro-2,4,6-trimethylpyridinium triflate to give a mixture of *syn-cis* and *anti-cis* 3a-fluoro-6-MIDA-boronyl-1,2,3,3a,8,8a-hexa-hydroppyrrolo-[2,3-*b*]indolyl-*N*^ε-Boc-2-carboxylate (6-BMIDA-Fpi). Incorporation of 6-BMIDA-Fpi into a linear peptide and exposure to Savigne-Fontana reaction conditions resulted in the successful tryptathionylation and formation of the desired macrocycle, with a mixture of the MIDA-boronate and OH observed at the tryptophan C6 position. At its time of publication, the synthesis of 6-BMIDA-Fpi by Matinkhoo and coworkers was the only practical report of a building block that yields the oxidatively sensitive 6-hydroxy tryptathionine crosslink of α -amanitin upon acid-mediated macrocyclization. However, the subsequent years following the Perrin lab's initial report yielded several total syntheses of α -amanitin, and with them variations on the synthesis of a peptide coupling-compatible tryptophan monomer.

Matinkhoo and coworkers also report an independent route to DHlle. Unlike the majority of previous syntheses that begin with glycine and install the side chain, the route starts with a protected acetaldehyde as the latent dihydroxylated side chain of the amino acid (**Figure 1.14**). Brown crotylation of 2-(benzyloxy)acetaldehyde installed the β -methyl and γ -hydroxyl with high enantioselectivity in a single step. After dihydroxylation and oxidative cleavage of the olefinic intermediate the authors turned to an asymmetric Strecker reaction to impart the desired configuration at C α .

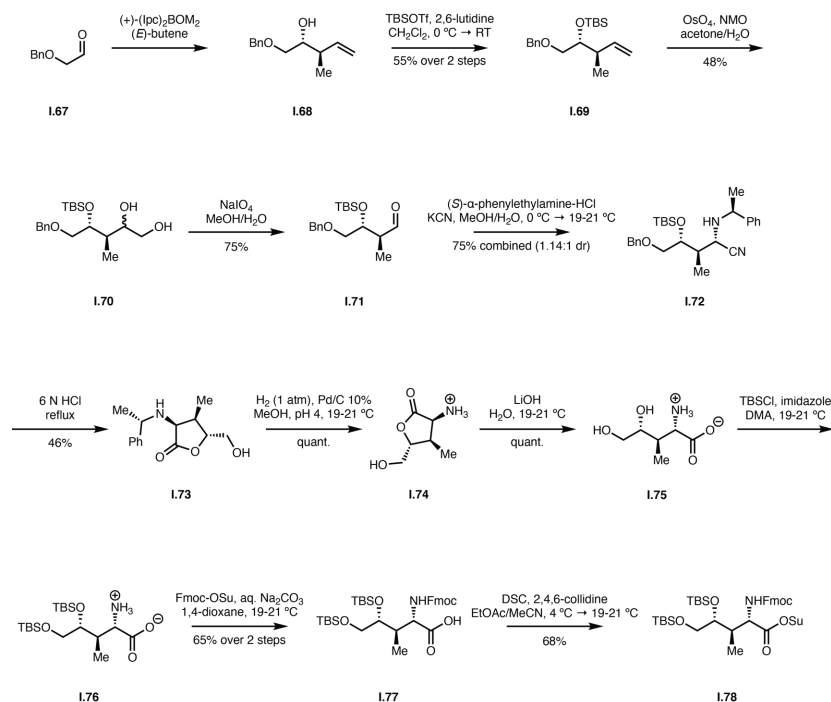


Figure 1.14. The synthesis of SPPS-compatible DHIIe as reported by Matinkhoo *et al.* in their total synthesis of α -amanitin²².

The mismatched Strecker reaction resulted in modest selectivity (1.14:1) in favor of the desired diastereomer, though the two isomers were readily separable by standard silica gel chromatography. Nitrile hydrolysis under acidic conditions also removed the TBS and Bn protecting groups, resulting in γ -lactone formation. Removal of the chiral auxiliary and recrystallization of the resulting HCl salt allowed the absolute configuration of the α -, β -, and γ -carbons to be determined by X-ray diffraction confirming that all three stereogenic centers matched those of the natural product diastereomer of DHIIe. Lactone saponification followed by silylation of the diol and Fmoc protection of the amine yielded the solid-phase compatible DHIIe in preparation for its incorporation into α -amanitin.

1.12. Recently published total syntheses of α -amanitin

Several reports of the total synthesis of α -amanitin have followed in the wake of the Perrin lab's 2018 seminal work. The total synthesis from Lutz and coworkers³⁷ takes advantage of the well-documented

synthesis of Hpi to install the tryptathionine linkage in their total synthesis of α - and β -amanitin. The authors begin their synthesis of the tryptophan building block with 6-benzyloxyindene-3-carbaldehyde (**Figure 1.15**), opting to install the amino acid scaffold from the pre-oxidized indole as opposed to starting from *L*-tryptophan. Protection of the nitrogen indole with Cbz followed by Horner-Wadsworth-Emmons and enantioselective hydrogenation furnished fully protected tryptophan derivative **1.82**. Replacement of the 6-OH Cbz with an acetal group provided a suitable substrate for oxidative cyclization, which was performed using the photosensitizer rose bengal in contrast to the traditionally utilized DMDO, resulting in the SPPS-compatible 6-acetoxy-3 α -hydroxyhexahydropyrroloindole-2-carboxylic acid **1.85**.

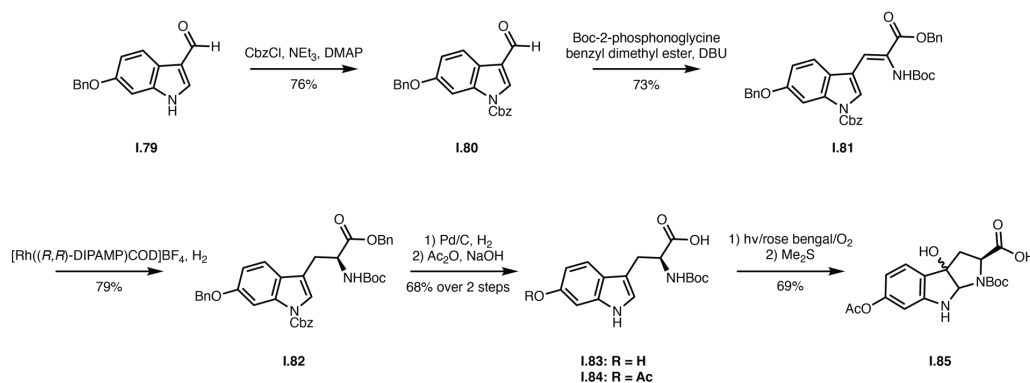


Figure 1.15. Synthesis of protected Hpi by Lutz and coworkers³⁷. Oxidative cyclization is performed using the photosensitizer rose bengal in place of the more frequently employed DMDO.

Lutz and coworkers also report an independent route for the DHlle building block. The synthesis relies on the use of an olefinic intermediate for asymmetric dihydroxylation, starting from commercially available 4-methyl aspartate ester (**Figure 1.16**). The secondary methyl group was installed using LiHMDS and methyl iodide after the reductive amination with benzaldehyde and phenyl fluorenyl protection of the free amine, producing a 5:1 ratio in favor of the desired diastereomer. Regioselective reduction of the methyl ester with LiAlH₄ furnished alcohol **1.89**. Interestingly, the authors found that the undesired 1,2-*syn* diastereomer underwent lactonization, the 1,2-*anti* diastereomer does not, facilitating their isomeric separation. The olefin was installed by oxidation and homologation, followed by swift

dihydroxylation using AD-mix β . Acetylation of the resulting diol and removal of the N-terminal protecting groups yielded DHlle monomer **1.95**.

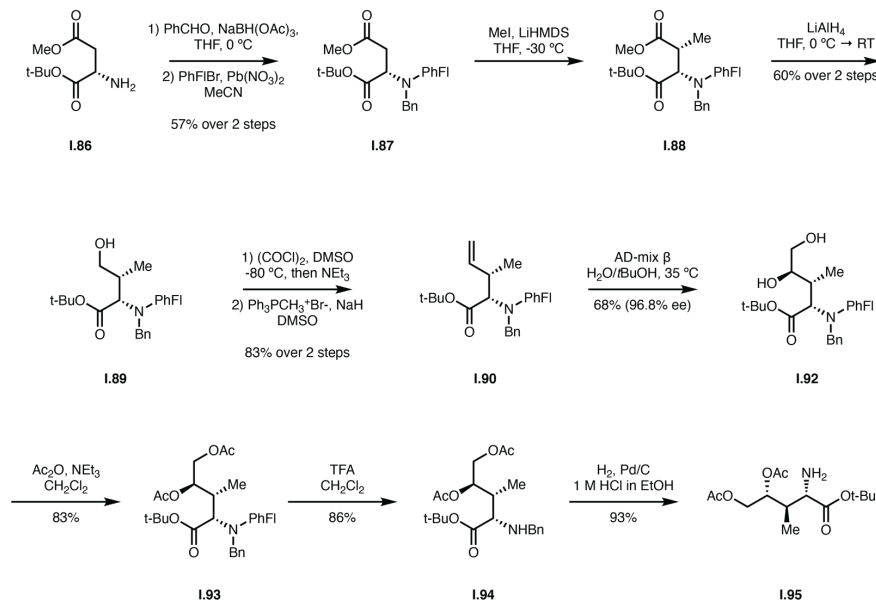


Figure 1.16. Synthesis of DHlle starting from 4-methyl aspartate ester as reported by Lutz *et al*⁶⁷.

While Lutz and coworkers utilize a similar solid phase strategy as that exploited by the Perrin lab, the entirety of the octapeptide is assembled on resin, made possible by use of Fmoc-Hyp-OAll for the initial immobilization on THP resin (**Figure 1.17**). Allyl deprotection followed by attachment of DHlle to the C-terminus preceded the sequential attachment of the remaining residues, ending with the attachment of 6'-acetoxy-*N*-Boc-Hpi to the N-terminus. Savige-Fontana cyclization of the octapeptide was performed upon exposure of the resin to TFA, followed by head-to-tail cyclization. As with the previously described syntheses by Matinkhoo and Siegert, sulfoxidation was achieved via treatment with *m*CPBA to produce the sulfoxide final product in a 2:1 diastereomeric ratio in favor of the (*R*)-sulfoxide diastereomer.

Siegert *et al.* have also obtained an independent route for the total synthesis of α -amanitin. In contrast to the both Matinkhoo and Lutz, Siegert achieves the amanitin bicyclic scaffold by solution-phase peptide assembly³⁸. Most intriguingly is the choice to synthesize 6-Trp(OH) and obtain the Cys-Trp side chain bridge in advance of constructing the linear peptide sequence and monocycle (**Figure 1.18**).

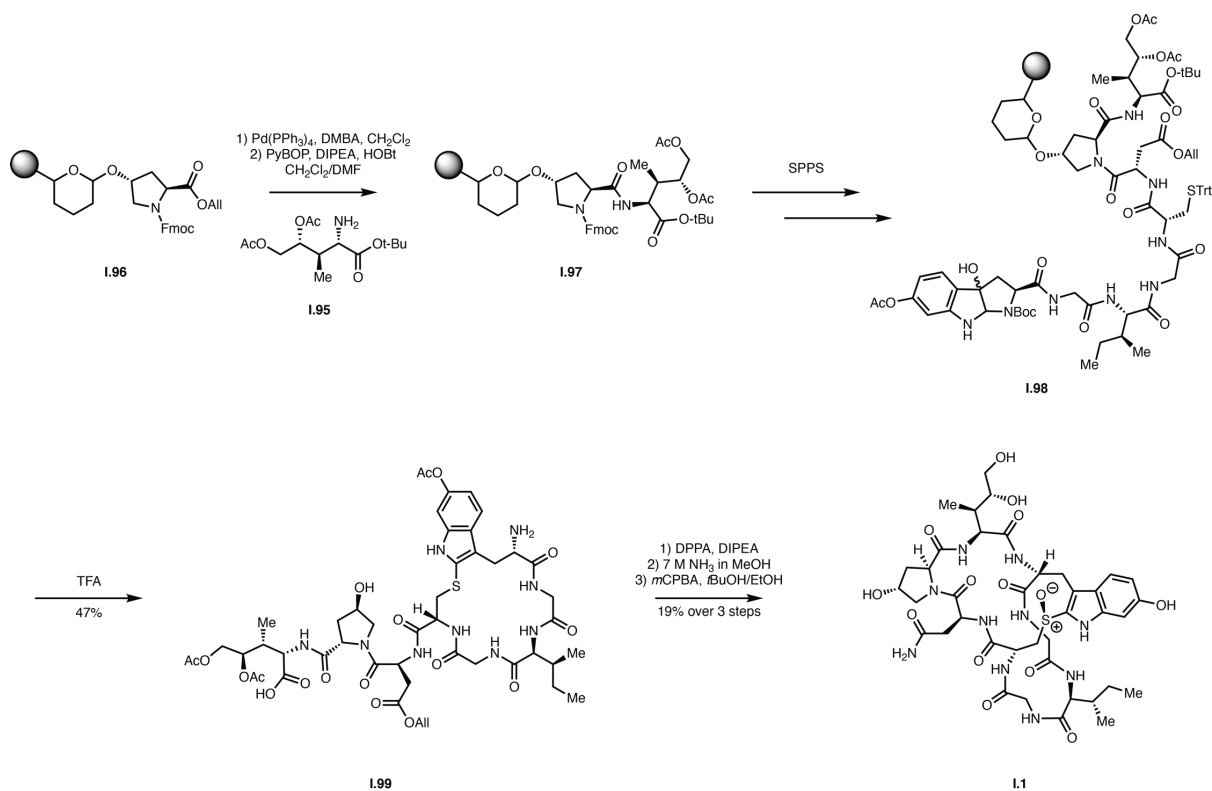


Figure 1.17. The total synthesis of α -amanitin reported by Lutz *et al*³⁷.

While the previously described Trp building blocks exploit the Hpi structure in anticipation of a Savigne-Fontana reaction, Siegert and coworkers describe a clever method of accessing 6-hydroxytryptophan starting from 6-benzyloxyindol due to their alternative method of accessing the intra-annular Cys-Trp linkage. Siegert *et al.* chose to construct the peptide backbone starting from the oxidized side chain (**Figure 1.18**). Alkylation of the protected heterocycle using *L*-serine produced racemic tryptophan **1.101** which was subjected to dynamic kinetic resolution to produce 6-benzyloxy-*L*-tryptophan. The free amine was protected with TeocOSu, resulting in *N*-Teoc-6-benzyloxy-*L*-tryptophan **1.105**.

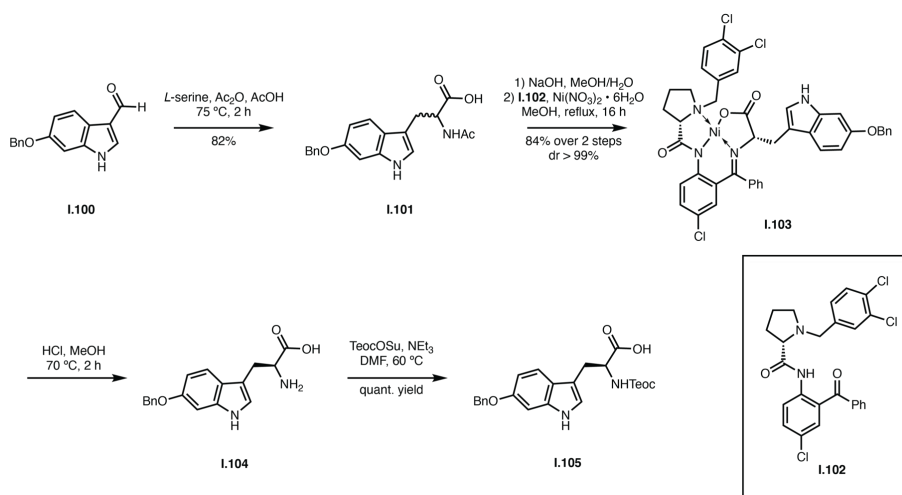


Figure 1.18. Synthesis of *N*-Teoc-6-benzyloxy-*L*-tryptophan **I.105** by Siegert and coworkers³⁸. The lack of reliance of the Savige-Fontana reaction for the eventual installation of the tryptathionine bridge allows the use of a protected 6-Trp(OH) instead of an Hpi derivative.

The synthesis of DHlle is performed in seven steps starting from glycine *tert*-butyl ester (**Figure 1.19**). Trifluoroacetylation of the free amine followed by ruthenium-catalyzed asymmetric alkylation using a chiral allylic carbonate yielded olefinic intermediate **I.111** in good yield (88%), diastereomeric ratio (86:14), and enantiomeric excess (98%) in favor of the desired 1,2-*anti* product. The amine protecting group was replaced with an Fmoc in preparation for installation of the diol via Upjohn dihydroxylation, wherein stereoselectivity was found to be controllable with the use of a biphasic solvent mixture of H₂O/CHCl₃. Silylation of the diol with TBSCl and removal of the *t*-Bu group furnished the suitably protected DHlle monomer. While this synthetic route echoes many of the previous attempts to access DHlle, the improved selectivity of the asymmetric allylic alkylation and dihydroxylation serves as a vast improvement over prior reports.

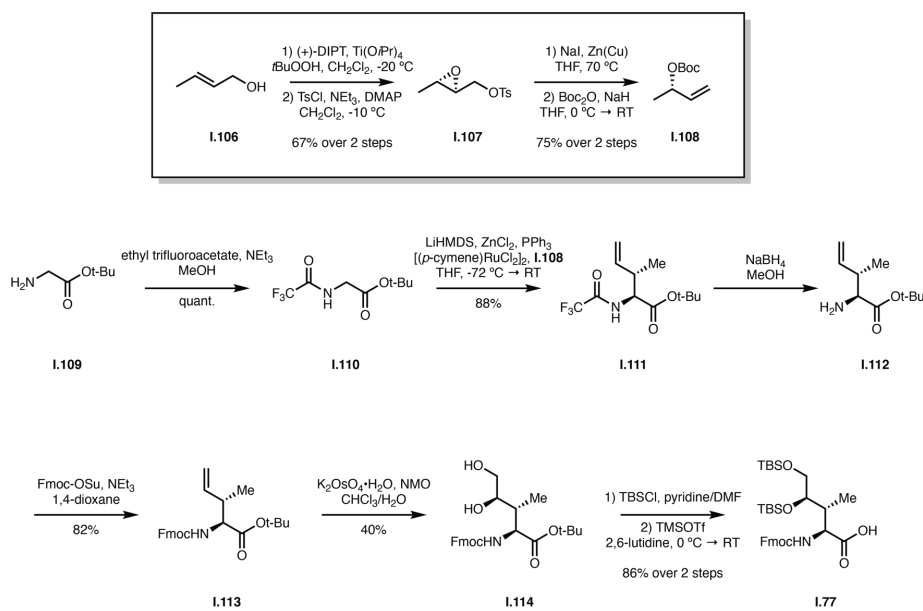


Figure 1.19. Synthesis of protected DHlle by Siegert and coworkers³⁸.

Unlike the vast majority of previously described syntheses, Siegert and coworkers preinstall the tryptathionine bridge by formation of the sulfonyl chloride of *N*-Boc-*L*-Cysteine-*O*tBu and subsequent S_EAr with the protected 6-hydroxytryptophan monomer, resulting in dimeric cysteine-tryptophan building block **I.115** in advance of macrocyclization. Obtaining the side chain-side chain linkage and initial macrocyclization in separate steps eliminates the need to rely on an Hpi-based derivative to furnish the desired tryptathionine bridge, opening up more synthetically diverse pathways to amanitin analogues. Piecing together the Cys-Trp dipeptide with H-Gly-Ile-Gly-OH tripeptide produced linear intermediate **I.117**. Macrolactamization furnished monocycle **I.118** in advance of the separate couplings of DHlle and Asn-Hyp dipeptide to the pentapeptide. Closing the bicycle through one final peptide bond coupling followed by *m*CPBA sulfoxidation of the tryptathionine afforded the target molecule. Due to the convergent assembly of the macrocyclic structure and the preinstallation of the tryptathionine linkage, Siegert and coworkers have achieved one of the few syntheses that diverge from the general synthetic route initially laid out by Zanotti, Barr, and Wieland in 1981.

Chapter 2: Efforts towards the synthesis of amanitin analogues

2.1. α -amanitin: our goals and strategy

Our goals regarding this project have been reshaped many times. The following section will outline the strategies and steps taken to complete these goals up until the project's termination. The essence of this endeavor was to produce biofunctionalized derivatives of α -amanitin for their use in various biochemical protocols. As mentioned in the preceding sections, α -amanitin is an extremely attractive natural product due to its remarkable selectivity and inhibitory activity against Pol II and appending the cytotoxin with one or more bioorthogonal handles opens up great potential for improving upon currently existing biological assays as well as the invention of new biotechnologies that are reliant on Pol II binding. We took particular interest in previous reports of amanitin analogues accessed via copper catalyzed alkyne-azide cycloaddition (CuAAC) chemistry, in which the precursor contains a terminal alkyne incorporated within the α -amanitin Asn side chain³⁶. We envisioned that a click-compatible handle would be invaluable for numerous biological applications, and furthermore thought of incorporating multiple bioorthogonal functionalities into the molecule in addition to the alkyne enrichment handle. Among these possibilities was incorporating a group with covalent functionality into the amanitin scaffold as a way to access irreversible Pol II inhibitors; an invaluable asset for streamlining techniques such as NET-seq that would greatly benefit from an improved Pol II purification workflow.

With this goal in mind, we turned our attention to the overall strategy for assembling our desired derivatives. This strategy was broken down into several main goals: synthesis of the modified tryptophan and isoleucine amino acids, installation of the Cys-Trp side chain crosslink, and bicyclization via head-to-tail peptide bond formation. Of these concerns, special attention was given to the intra-annular Cys-Trp linkage. The tryptathionine bridge is a hallmark structural feature of the amatoxins and phallotoxins and is unsurprisingly a major source of intrigue surrounding the structural design of the two cytotoxin families^{24,29}. As described in Chapter 1, the most common method of obtaining this Cys-Trp crosslink is through the acid-mediated Savigne-Fontana reaction, in which a hydroxypyrrroloindoline undergoes nucleophilic attack by the Cys thiol to produce a thioether side chain-side chain bridge that can be subsequently oxidized to the corresponding sulfoxide³⁰.

We decided to employ a similar blueprint as previous syntheses of α -amanitin and related molecules, including the key cyclization that produces the tryptathionine bridge (**Figure 2.1**). This necessitates the use of the modified tryptophan building block, Hpi, which is incorporated into a linear heptameric peptide assembled via solid-phase peptide synthesis (SPPS). Critically, both the resin and side chain protecting groups utilized in the assembly of the linear heptamer are acid labile such that subjecting **I.42** to Savigny-Fontana reaction conditions results in resin cleavage and global deprotection simultaneously with macrocyclization. The bicyclic octamer is obtained by coupling the final residue, DHlle, to the tryptophan N-terminus and the hydroxyproline C-terminus of the monocyclic heptapeptide.

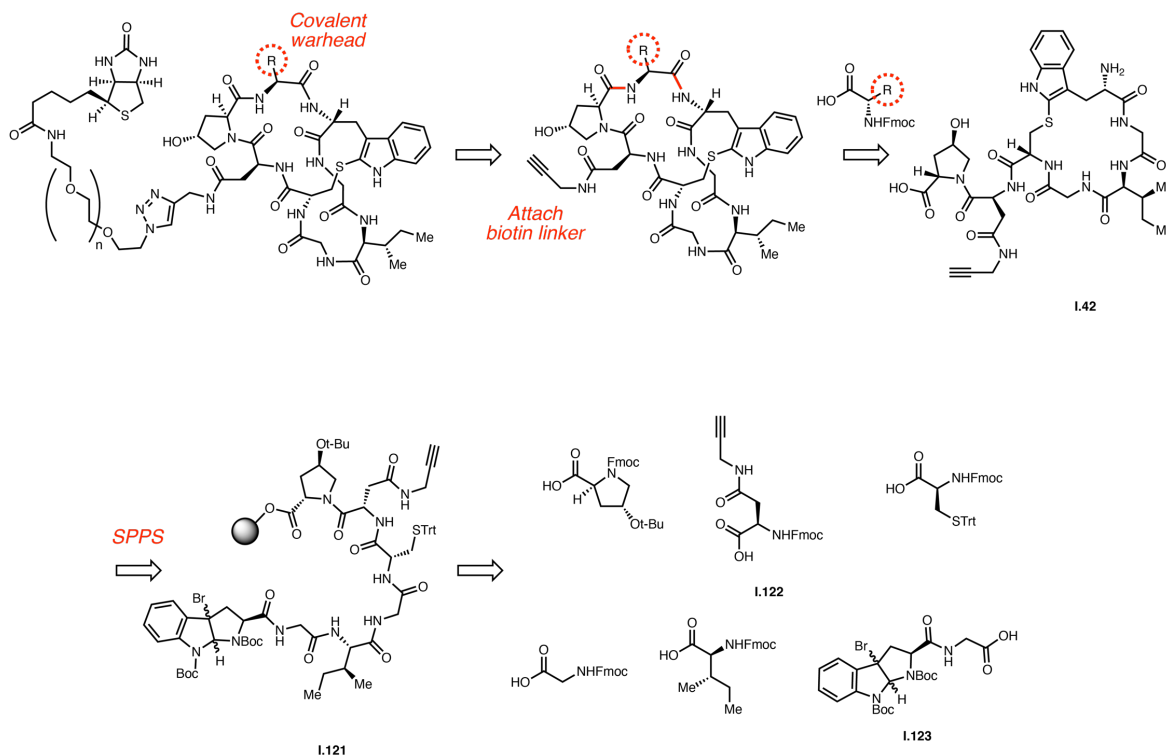


Figure 2.1. Retrosynthesis for accessing biofunctionalized α -amanitin derivatives.

Our overall synthetic plan was influenced by several factors, one of which was our decision to utilize the position of DHlle as the installation point for other potential functionalities. While we were interested in synthesizing an alkyne-functionalized amanitin containing DHlle, we also believed that we could leverage

the DHlle position as an installation point for an amino acid derivative with an electrophilic group that could potentially react with a protein residue within the Pol II binding pocket. We approached this fully aware of the role that DHlle plays in the binding affinity of α -amanitin for Pol II, surmising that formation of an irreversible covalent bond within the protein binding pocket would compensate for the loss in non-covalent interactions attributed to the DHlle diol. Importantly, the overall synthetic route involves the late-stage incorporation of DHlle, resulting in a more efficient route for analogues that utilize the DHlle position as the variable amino acid.

2.2. Synthesis of an oxidized tryptophan-glycine dimer

We began our synthetic exploration of amanitin derivatives with the tryptophan building block for several reasons. As previously mentioned, our synthetic strategy relies on the use of the Savige-Fontana reaction to install the trademark tryptathionine bridge that lends α -amanitin its rigid, bicyclic structure. This reaction necessitates the use of an oxidized tryptophan derivative that is susceptible to nucleophilic attack by a free thiol upon exposure to acidic conditions. In this chapter, we will discuss the published strategies employed to synthetically access tryptathionine, our own modified synthesis of an oxidized tryptophan dimer, and our brief, but eventually abandoned foray into producing an SPPS-compatible tryptophan building block containing the elusive 6-hydroxy indole.

Historically, Hpi is the building block of choice for the Savige-Fontana reaction. However, other variations of oxidized tryptophan are viable partners for tryptathionylation, assuming they stay true to the oxidation state of Hpi. This proved valuable when devising our own synthesis of an oxidized tryptophan building block for the synthesis of amanitin derivatives, though our initial foray into this leg of the synthesis had originally planned to stick to the published literature.

We approached the synthesis of the oxidized tryptophan building block with several points in mind. Firstly, adherence to previously published syntheses of amanitin derivatives requires an oxidized tryptophan residue at the N-terminus of the linear peptide precursor. Secondly, given what is known about the role of 6-Trp(OH), we believed that absence of the 6-hydroxyl of the Trp residue would bear no crippling consequence to the overall utility of our desired analogues. In essence, we decided to forego innovation in this portion of the overall synthetic strategy in favor of speed and consequently planned to replicate the

published synthesis of Trt-Hpi-Gly-OMe³⁹ (**Figure 2.2**); however, our final oxidized tryptophan derivative ended up containing several modifications.

There are several methods to generate Hpi and derivatives from tryptophan: reports include photosensitized oxidation⁴⁰, oxidative deselenation⁴¹, and most commonly, use of a mild oxidation agent such as 3,3-dimethyldioxirane (DMDO). While peroxyacetic was the original reagent used by Savige and Fontana to obtain Hpi, improved yields have been demonstrated upon the switch to DMDO⁴². With this in hand, May and coworkers produced a series of tryptophan-ylated amino acids that could be oxidized to the corresponding Hpi amino acids with high yield and relative ease²⁹. Given their lab's interest in producing bicyclic peptides, these derivatives were synthesized with the ultimate goal of effecting a Savige-Fontana macrocyclization of a linear peptide following SPPS. Of note is the route to Tr-Hpi-Gly-OMe, as glycine occupies the position adjacent to tryptophan in the amanitins. Satisfyingly, exposure of Tr-Trp-Gly-OMe to DMDO at low temperature produced the corresponding Hpi tricycle in good yield (70% yield of a 1:1 diastereomeric mixture).

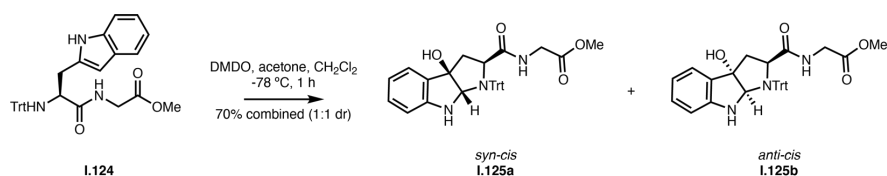


Figure 2.2. The oxidation of Tr-Trp-Gly-OMe to the corresponding Tr-Hpi-Gly-OMe as a *syn-cis* and *anti-cis* diastereomeric mixture as reported by May *et al*³⁹.

In our hands, we found that Boc protection of the tryptophan N^α to be more stable than tritylation. Furthermore, installation of Boc at the indole nitrogen to be similarly helpful and necessary given our choice to employ N-bromosuccinimide (NBS) as our oxidative cyclization agent in place of DMDO. Bromocyclization of a fully protected tryptophan using NBS and pyridinium *p*-toluenesulfonate to produce 3a-bromo-1,2,3,3a,8,8a-hexahydropyrrolo[2,3-b]indole-2-carboxylate (3a-Br-Hpi) was found to be more scalable and convenient in comparison to generating DMDO for Hpi formation⁴³. As with DMDO treatment, we observed a mixture of *syn-cis* and *anti-cis* diastereomers after bromocyclization. However, with the

knowledge that the divergent stereochemistry would be ablated upon tryptathionylation and that both isomers readily undergo the desired reaction, we found separation to be unnecessary. As reported by May *et al.*, saponification of the C-terminal methyl ester with aqueous LiOH was rapid and occurred with minimal byproduct formation to yield the desired 3a-Br-Hpi-Gly in anticipation of its incorporation of the amanitin precursor peptide (**Figure 2.3**).

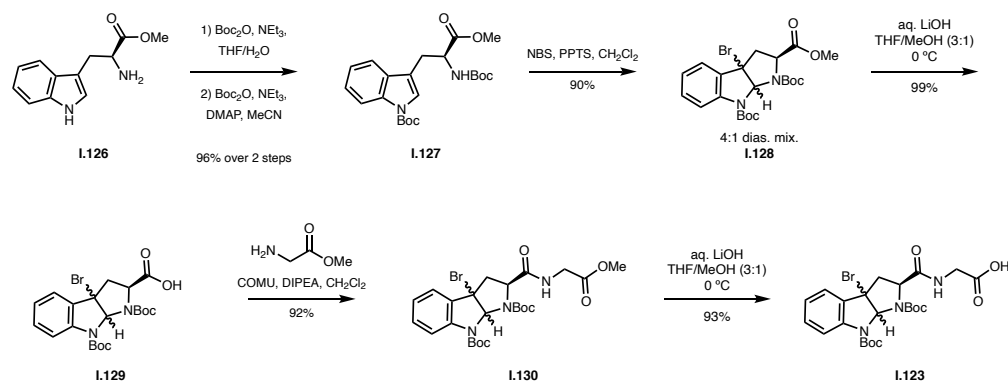


Figure 2.3. Complete synthetic route to NBoc-3a-Br-Hpi(Boc)-Gly-OH from *L*-Trp-OMe.

2.3. An aside: notes on the synthesis of 6-Trp(OH)

As we mentioned in our goals for this project, our initial objectives for this project consisted of synthesizing potent amanitin probes for their use in biochemical applications. Furthermore, the relative inessentiality of the 6-hydroxyl of α -amanitin for activity meant that we deprioritized the inclusion of the extra functional group upon preparation of our building blocks for SPPS. Compounding these concerns was the lack of reported protocols on the synthesis of 6-hydroxy-tryptophan, most likely stemming from the oxidative instability of the indole side chain with the extra OH at C6. However, we were intrigued by work from the Baran lab that reports the successful and selective C6 borylation of tryptophan as an intermediate in the total synthesis of Verruculogen and Fumitremorgin A⁴⁴. Feng and coworkers utilize an iridium-catalyzed C-H borylation to carry out the difficult functionalization of the NBoc-Trp(TIPS)-OMe indole C6 position. Screening reaction conditions revealed that optimal regioselectivity and yield of 6-BPin-Trp were obtained with the use of 1,10-phenanthroline as the ligand (**Figure 2.4**). Critical to this strategy was the installation

of a sterically bulky triisopropylsilane group on the indole nitrogen as a means to block the preferential reaction at the C2 and C7 position, though 5-BPin-Trp is observed as a minor regioisomer.

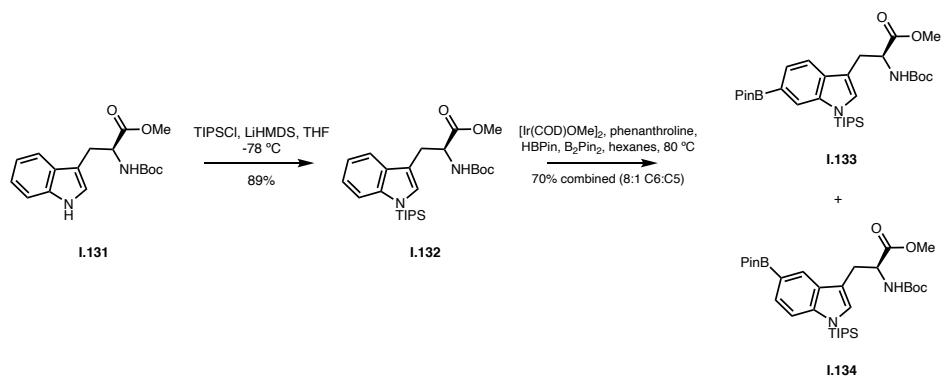


Figure 2.4. Ligand-controlled C-H borylation of protected tryptophan **1.132** reported by Feng *et al*⁴⁴. enabled access to C6- borylated product **1.133** with C5-borylated **1.134** observed as a minor isomer.

Spurred by these results, we contemplated exploiting the regioselective borylation to install the C6 hydroxyl of α -amanitin. Replication of the C-H borylation reported by the Baran group was successful; furthermore, testing the oxidative deborylation of 6-BPin yielded the desired 6-OH directly from the 6-BPin-Trp (**Figure 2.6 A and B**). Our issues, however, stemmed from the incompatibility of bromocyclization with the substitution at the indole C6. Protection of the C6-hydroxyl with a benzyl group and performing NBS-mediated cyclization after removal of the N-indole TIPS yielded no detectable product; similarly frustrating was the lack of product formation from our attempts to perform the directed borylation on the tricyclic product. We suspected that the additional substitution at the indole C6 (whether present as a boronate or the protected hydroxyl) imparts increased susceptibility to oxidation at the C2 position, resulting in generation of the oxindole as the major byproduct. Given the overall goals of our project, we ultimately decided to abandon this route and simply stick with the 3a-Br-Hpi-Gly dimer for our linear peptide precursor.

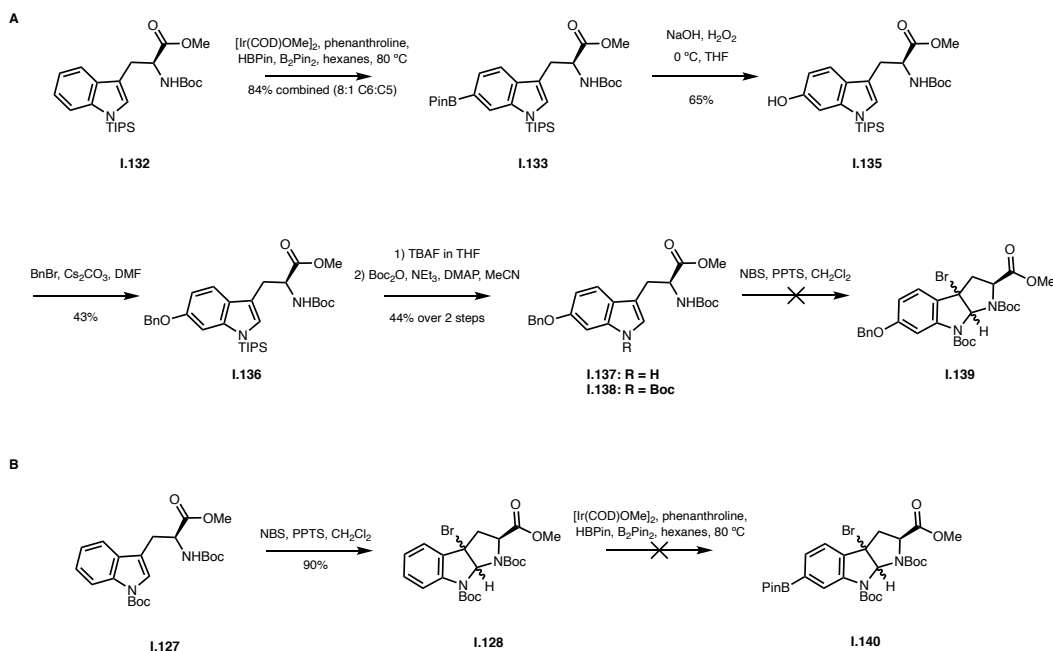


Figure 2.5. Replication of the directed C-H borylation reported by the Baran lab was met with success. However, our attempts to maintain or install the latent C6 hydroxyl both before **A)** and after **B)** bromocyclization were not.

2.4. Failed efforts towards the synthesis of (2S,3R,4R)-dihydroxyisoleucine

My foray into the synthesis of DHle came at the beginnings of my doctorate studies in 2016. At this point in time, the Perrin lab had not yet published their total synthesis of α -amanitin and there was no enantioselective synthesis of DHle. We took great interest in their 2015 publication by Zhao *et al.* regarding the synthesis of S-deoxy amanitin analogues, in part due to our own goals of developing biochemically useful amanitin probes. We sought to improve upon the currently published syntheses of DHle and though we eventually came across an enantioselective route to the desired building block, there were several failed pathways leading to our success. The following section will detail the reasoning and result of these attempts, including a previously failed pathway that was repurposed to generate the C3-desmethyl derivative of DHle.

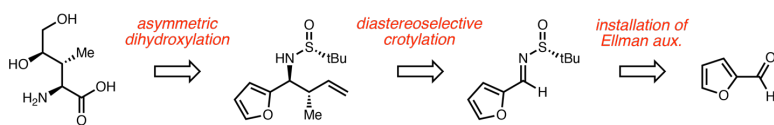


Figure 2.6. Initial retrosynthesis of DHIIe wherein the stereocontrol of the key crotylation is imparted by Ellman's *tert*-butanesulfinamide.

Like Perrin and coworkers, we believed that diastereoselective crotylation was an attractive strategy. This would install the α - and β -carbon stereocenters in a single step as well as provide an olefinic intermediate for asymmetric dihydroxylation (**Figure 2.6**). We decided on the use of Ellman's *tert*-butanesulfinamide to control the facial selectivity of the crotylation at the α -center⁴⁵. Although the diastereoselective allylation of enantioenriched sulfinyl imines is well-established, there are far fewer reports detailing face or *anti:syn* selectivity of the analogous crotylation. Exploration of the literature turned up the work of Olga Soares do Rego Barros *et al.* reporting the indium-mediated diastereoselective crotylation of chiral *N-tert*-butanesulfinyl imines using crotyl bromide in which the (*R*)-isomer of Ellman's auxiliary with (*E*)-crotyl bromide produced predominantly the 1,2-*anti* diastereomer in addition to high face selectivity⁴⁶. The crotylation is proposed to proceed through a chair-like transition state that involves the chelation of both the imino nitrogen and the sulfinyl oxygen to control the resulting configuration at the α -amine, while the *anti:syn* selectivity stems from use of the *Z* vs. *E* isomer of the crotylating reagent (**Figure 2.7**).

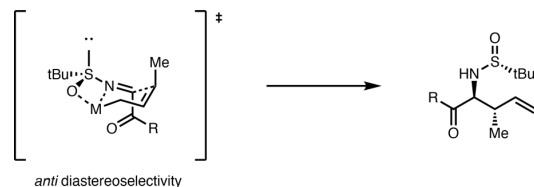


Figure 2.7. Proposed transition state of the indium-mediated crotylation of *N-tert*-butanesulfinyl imines. The use of (*E*)-crotyl bromide should result in formation of predominantly the *anti*-isomer.

Emboldened by our literature search, we decided on the use of a furan moiety to serve as a latent carboxylic acid and proceeded with the condensation of furfuraldehyde with (*R*)-*tert*-butanesulfinamide to furnish sulfinyl aldimine **I.142** in good yield (**Figure 2.8**). In our hands, we found that the facial selectivity at the amine center to be in good agreement with that of the literature, but no detectable selectivity for the desired *trans* vs. *syn* isomer. Furthermore, separation of the two isomers was intractable using standard purification techniques. We were tempted to cut our losses and abandon the synthesis at this stage. However, we recognized that the diastereomeric mixture of intermediate **I.143** could serve as a test substrate for Sharpless dihydroxylation. Employment of AD-mix β was expected to result in formation of the secondary hydroxyl *anti* relative to the amino center, regardless of the configuration of the methyl group at the β -carbon, resulting in 2 major diastereomers. However, our results were similar to those previously reported by Zhao *et al.* in their attempts to perform asymmetric dihydroxylation of a DHlle intermediate³⁶. NMR of the crude reaction revealed the formation of all four possible diastereomers, which we were unable to separate. While we were initially on the fence about trying to optimize the crotylation in an attempt to impart *anti:syn* selectivity, not being able to rely on the Sharpless asymmetric dihydroxylation was an additional drawback that led us to think of alternative paths. However, we did find this overall strategy well suited to generation of the desmethyl analogues of DHlle (*vide infra*).

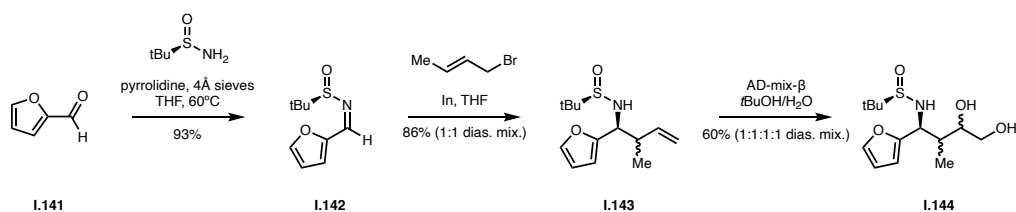


Figure 2.8. An abandoned route to DHlle using Ellman's auxiliary to direct an indium-mediated crotylation.

2.5. A second attempt at synthesizing DHlle

Though slightly discouraged from our initial endeavor, there were certain aspects of our abandoned route to DHlle that we believed were worthy of further exploration, most notably the use of furan as the latent carboxy-terminus and Ellman's auxiliary to install the α -amino center with near-perfect selectivity. In

contrast to our first synthetic pathway wherein the starting material provides the latent amino acid backbone and the side chain is installed in subsequent steps, we took this opportunity to try and set the configuration of the side chain stereocenters before that of the α -carbon (**Figure 2.9**). To this end, we chose (*D*)-malic acid as our building block of choice, eliminating the need to set the stereochemistry of the γ -carbon ourselves. We envisioned that methylation via LiHMDS and methyl iodide could furnish α -alkylated dimethyl malonate with high selectivity, as reported previously⁴⁷. As in our initial route to DHlle, we decided to take advantage of a chiral imine formed by condensation with *tert*-butanesulfinamide to install the amine; however, the addition to the chiral aldimine served to incorporate the latent carboxylic acid in lieu of an olefinic intermediate as in our prior attempt.

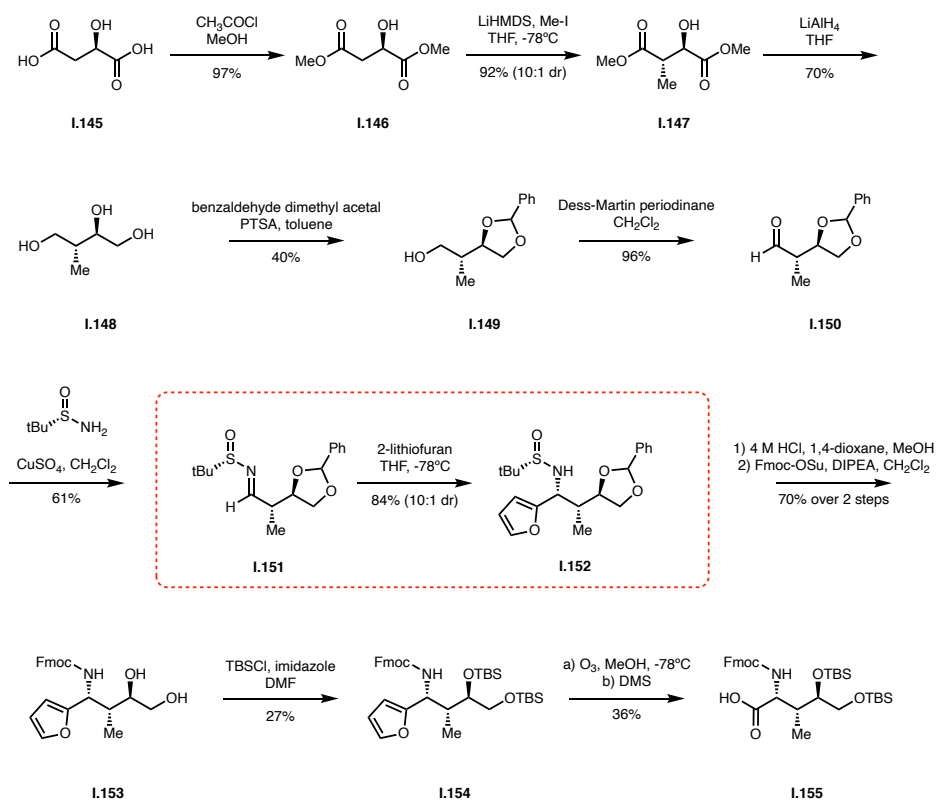


Figure 2.9. A second failed attempt at developing an enantioselective route to DHlle starting from (*D*)-malic acid.

We began with the esterification of (*D*)-malic acid, which was subjected to LiHMDS and methyl iodide to furnish **I.147** in good yield and 10:1 diastereomeric ratio in favor of the desired isomer. Reduction using LiAlH₄ produced triol **I.148**, which was swiftly followed by protection of the diol as a benzylidene acetal and then oxidation of the remaining hydroxyl to the corresponding aldehyde. Condensation with (*S*)-tert-butanesulfonamide and addition of 2-lithiofuran produced intermediate **I.152**. With all stereogenic centers set, the remaining steps served to exchange the protecting groups to those compatible with Fmoc-based SPPS chemistry as well as unveil the carboxylic acid. Acid-mediated cleavage of the chiral auxiliary and the acetal was followed by Fmoc protection of the amine as well as silylation of the diol with TBSCl, albeit with poor yield (presumably stemming from the steric congestion surrounding the γ -hydroxyl). Finally, ozonolysis produced the desired carboxylic acid upon reductive workup.

Having made it through the entire route, what remained was assignment of the relative stereochemistry of the α -, β -, and γ -centers. It is important to note that at this point in time, the Perrin lab had published their 2018 total synthesis of α -amanitin, providing us with an authentic to which we could compare our own isolated product. To our dismay, we found that the NMR of our isolated product did not match that provided by Matinkhoo *et al.*, suspecting that the benzylidene acetal was interfering with the facial selectivity of the furan addition to the sulfinyl aldimine. We found ourselves at a crossroads. The issues with installing the α -center may be circumvented by use of a different diol protecting group, but we were dubious about the poor yields obtained at the tail end of the synthesis. We considered optimizing the conditions of the diol silylation could increase the product yield to a respectable amount, we were more concerned about our ability to improve the final ozonolysis. While there were several aspects of this pathway that were attractive, our ultimate decision to abandon the use of furan as the carboxylic acid synthon was one of the main reasons we turned to our next and final strategy.

2.6. A successful strategy for accessing DHlle

Though we were further discouraged by our second abandoned synthetic pathway, there were several aspects that we thought were worth retaining. The overall strategy of installing the amino acid backbone versus the side chain was still appealing to us, and so we were not willing to completely relinquish the convenience of using a starting material with the diol already situated. We turned back to the literature for

fresh inspiration and were delighted to find work from the Hanessian lab that would be well-suited to our needs^{48,49}. Hanessian *et al.* report their findings of the stereocontrolled addition of lithium dimethylcuprate with γ -alkoxy, α,β -unsaturated esters in the presence of trimethylsilyl chloride. Results showed that employment of protected ester **I.159** resulted in 14:1 *anti:syn* selectivity upon conjugate addition, wherein a nonchelated approach appears to account for the observed selectivity. Furthermore, hydroxylation of the corresponding potassium enolate installs a heteroatom at the α -center syn to the β -carbon, which we envisioned could be easily inverted (**Figure 2.10**).

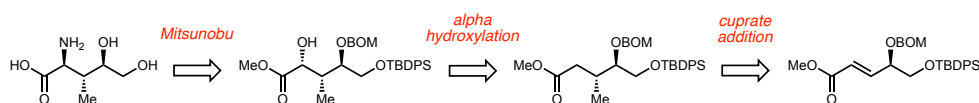


Figure 2.10. Final retrosynthetic strategy for DHlle.

Therefore, we envisioned a new pathway to DHlle generously inspired by the work of Hanessian and coworkers, beginning with (*S*)-2,2-dimethyl-1,3-dioxolane-4-carboxaldehyde (**Figure 2.11**). Chain extension via Horner-Wadsworth-Emmons was followed by acid-mediated acetal cleavage. Protection of the primary hydroxyl as a silyl ether and the secondary hydroxyl as a BOM ether afforded α,β -unsaturated ester **I.159** in preparation for cuprate addition. We were delighted to see that both conjugate addition and subsequent hydroxylation using Davis' oxaziridine produced a single diastereomer by NMR.

At this point in our pathway, we decided to take stock of the remaining transformations to be done, most of which were concerned with adjusting the present functional groups to be compatible with SPPS. Firstly: inversion of the α -stereocenter, which we planned to accomplish via azidation. The azide would face subsequent reduction to the amine, which would then be protected with an Fmoc group. Secondly: unveiling the carboxylic acid in anticipation of standard peptide coupling conditions. Thirdly: swapping out the BOM ether at the γ -position with a silyl ether. We were quite aware that deprotection of the γ -hydroxyl would result in lactone formation, which would necessitate saponification (and reveal the carboxylic acid as well). With this in mind, palladium-catalyzed hydrogenation was employed to remove the BOM ether, which predictably resulted in γ -lactonization.

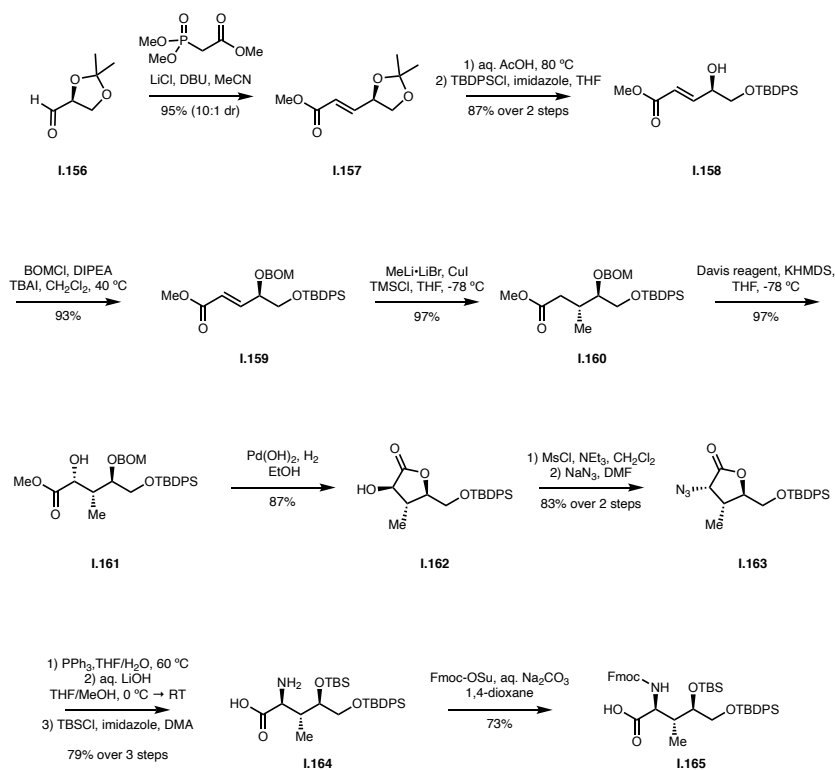


Figure 2.11. Complete synthetic route to DHlle starting from (S)-2,2-Dimethyl-1,3-dioxolane-4-carboxaldehyde.

We decided to address inversion of the α -stereocenter at this point, treating the lactone with mesyl chloride followed by sodium azide to furnish aza-lactone **I.163** before reduction to the corresponding amine. This reaction sequence was followed by saponification of the lactone, which was directly concentrated and redissolved in DMA. TBSCl and imidazole were added to cap the secondary hydroxyl as the silyl ether. Finally, Fmoc protection of the amine resulted in a fully protected DHlle peptide monomer. Comparison of our final product with the authentic provided by Matinkhoo *et al.* was done by replacing the TBDPS protecting group on the primary hydroxyl with TBS. Thankfully, we found our synthetic DHlle to be a match.

2.7. An aside: utilizing an abandoned route for synthesizing desmethyl DHlle

Before delving into our assembly strategy for α -amanitin derivatives, we thought that it would be worth mentioning the synthesis of 1,3-*syn* and 1,3-*anti* desmethyl DHIIe, which was accomplished using the overall strategy of one of our abandoned routes towards DHIIe. Although we and others have not experienced success with the selective dihydroxylation of an olefinic intermediate on our quest for DHIIe, we imagined that the lack of selectivity was not as pressing an issue for accessing the desmethyl compound for two reasons: firstly, assuming good face selectivity upon installing the α -amine, dihydroxylation would produce only two diastereomers, not four as in the case of dihydroxylation after crotylation; and secondly, we imagined that incorporation of the 1,3-*anti* desmethyl DHIIe into a bicyclic amanitin derivative may provide a useful point of comparison in future cytotoxicity assays and we therefore saw a way in which we could access both the 1,3-*syn* and 1,3-*anti* desmethyl compounds in a single pathway.

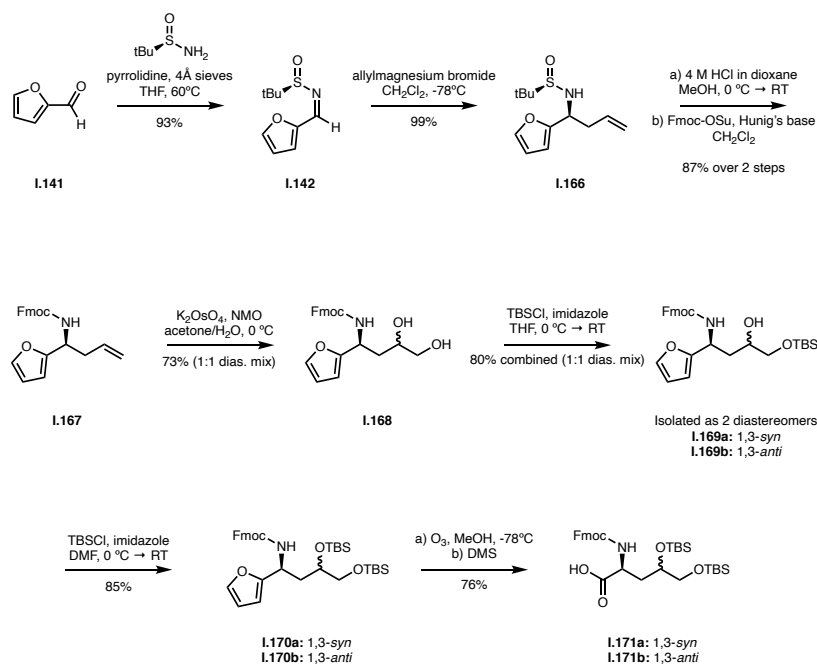


Figure 2.12. Full synthetic pathway to 1,3-*syn* and 1,3-*anti* desmethyl DHIIe.

As before in our initial journey towards DHIIe, condensation of furfuraldehyde with (*R*)-*tert*-butanesulfinamide followed by allylation furnished the protected α -amine as a single diastereomer, which was swiftly removed of the chiral auxiliary and Fmoc protected. Upjohn oxidation provided diol **I.168** as a

1:1 mixture of diastereomers which were easily separable by flash column chromatography after silylation of the primary hydroxyl with TBSCl. The 1,3-*syn* and 1,3-*anti* diastereomers were assigned using intermediates **I.169a** and **I.169b** after Fmoc deprotection of the amine and forming the cyclic carbamate with *N,N*-carbonyldiimidazole. We completed the rest of the route by silylation of the γ -hydroxyl and ozonolysis to unveil the carboxylic acid in good yield.

2.8. Assembly of α -amanitin derivatives

At the time that I undertook this project, there was no published total synthesis of α -amanitin. Despite its desirable inhibitory properties, the difficulty in accessing the non-canonical amino acids that are vital for cytotoxic activity have precluded the synthesis of the cytotoxin. Nevertheless, the years preceding the first total synthesis of α -amanitin have been littered with numerous reports on accessing related derivatives. Though simplification of the more synthetically challenging aspects of the small molecule results in analogues less potent than the parent compound, these historical publications laid the groundwork for the ensuing total syntheses of α -amanitin that have appeared within the past several years. The following chapter will detail our own attempts to emulate the results of our predecessors and the progress made up until the termination of this project.

2.9. Our strategy

In the wake of the total synthesis of α -amanitin by Matinkhoo and coworkers in addition to the well-established strategy for accessing analogous bicyclic peptides as outlined above, we ultimately committed to synthesizing our own derivatives using a similar solid phase-based pathway. There were several analogues that were realized from our efforts, all accessed through the general route that has historically garnered useful analogues of the amatoxins. We paid particular attention to the route used by Zhao and coworkers in their synthesis of propargylated amanitin derivatives³⁶. As we were interested in accessing click-compatible analogues, we decided to retain the Perrin's lab incorporation of *N*-propargyl-asparagine for bioconjugation post-peptide synthesis (see **Figure 2.1**).

2.10. Assembly of the monocyclic heptapeptide

As outlined in previous work by the Perrin lab, we planned to utilize the acid labile 2-chlorotrityl chloride resin for the immobilization of *trans*-hydroxyproline (Hyp(OtBu)), synthesizing a linear heptapeptide by sequential coupling of the following: Asn(propargyl), Cys(Trt), Gly, Ile, and finally, the previously-described 3a-Br-Hpi-Gly dimer (*vide supra*). The linear heptapeptide was then subjected to neat TFA at ambient temperature to effect resin cleavage, global deprotection of all side chain protecting groups, and nucleophilic addition of the free cysteine thiol to Hpi.

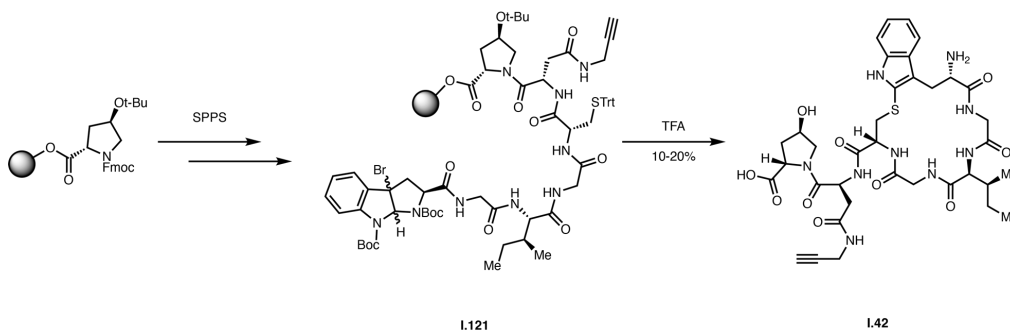


Figure 2.13. Our adherence to previously published conditions for the Savige-Fontana cyclization of **I.42**.

HPLC purification and mass spectrometry of the putative product peak revealed the presence of the desired monocyclic heptamer, indicating that the desired thioether formation was successful. In our hands, we found that the yield of the monocyclic heptamer to hover around 20%, in contrast to the 40-60% reported by Zhao *et al.* We were understandably discouraged by the subpar macrocyclization yields; coupled with the difficulties in performing the downstream bicyclization (*vide infra*), we decided that improving the yield of the Savige-Fontana reaction would be crucial if we were to have any hope in producing a wide suite of analogues. For screening purposes, we decided to assemble the linear heptapeptide precursor via solution phase peptide synthesis, eliminating any variables that may be attributed to the solid support (**Figure 2.14**).

Reaction yields were determined by HPLC using caffeine as an internal standard. While we found that decreasing the molarity of the reaction had a positive effect on product formation, the most noticeable uptick in reaction yield were due to the use of the dimethyl sulfide as a cation scavenger as well as decreasing the reaction temperature (**Table 2.1**).

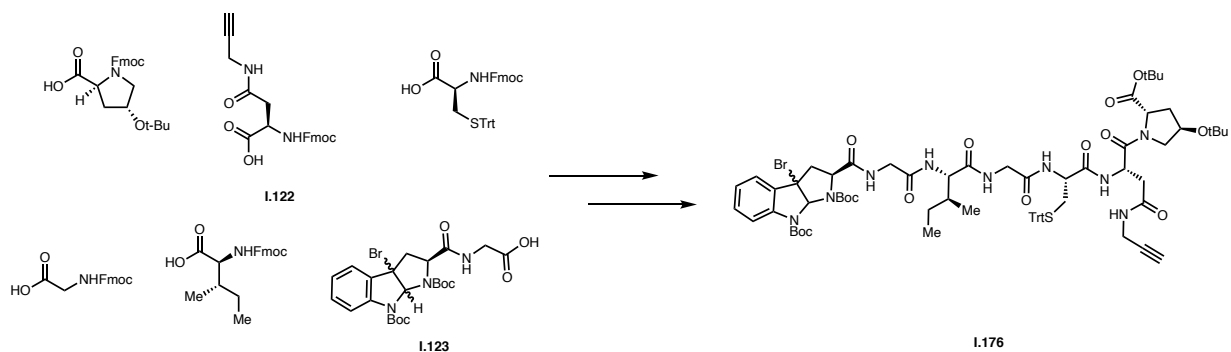
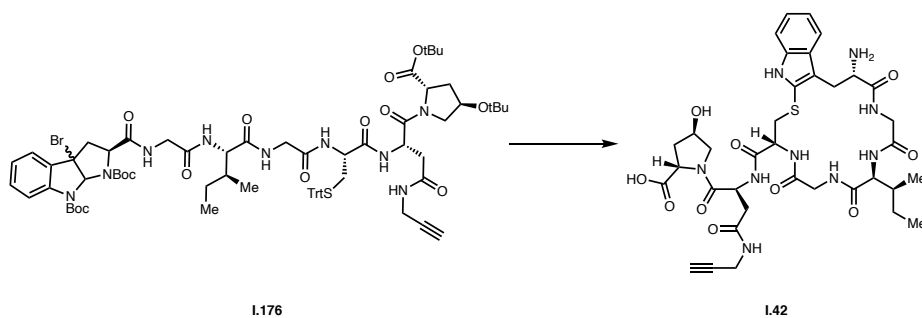


Figure 2.14. Solution-phase assembly of linear heptapeptide **I.176**.

Employing what we gleaned from our reaction condition screen, we found the most success in performing the Savige-Fontana reaction by the slow addition of the linear heptapeptide precursor in methylene chloride to a pre-cooled solution of TFA and 20 equivalents of dimethyl sulfide. The reaction was allowed to stir at 0 °C overnight, after which the mixture was directly concentrated and purified using reversed-phase HPLC. Satisfyingly, we were consistently able to produce isolated yields on par with those reported by the Perrin lab. It is necessary to note that we believe that the coelution of an uncharacterized byproduct with the desired macrocycle may have produced false inflation of calculated product yields, resulting in some entries in which the reaction yield is over 100%.

Table 2.1. A selection of conditions screened for the Savige-Fontana cyclization of heptapeptide **I.176** to macrocycle **I.42**. Yields were calculated based on the co-injection of an HPLC standard.



Molarity (M)	Additive (20 eq.)	Equiv dimethyl sulfide	Temperature (°C)	Reaction time (h)	Yield (%)
0.01	-	-	25	12	9
0.005	-	-	25	12	13
0.0005	-	-	25	12	24
0.005	Thioanisole	-	25	12	16
0.005	Thiophenol	-	25	12	0.4
0.005	Anisole	-	25	12	10
0.005	Dimethyl sulfide	20	25	12	50
0.005	p-cresol	-	25	12	12
0.005	m-cresol	-	25	12	8
0.005	-	10	25	12	47
0.005	-	40	25	12	43
0.005	-	20	-10	12	99
0.005	-	20	-20	12	105

2.11. Bicyclization

After our optimization of the Savigne-Fontana macrocyclization as well as the suitably protected DHlle in hand, it was a matter of course to follow through with completing the bicyclic scaffold of the final molecule. There remained four obstacles in way of our final product: peptide bond formation between DHlle and the monocyclic heptamer, removal of the DHlle N-terminus Fmoc group, desilylation of the DHlle diol, and closing the bicycle via one final coupling between DHlle and Hyp (**Figure 2.15 A**).

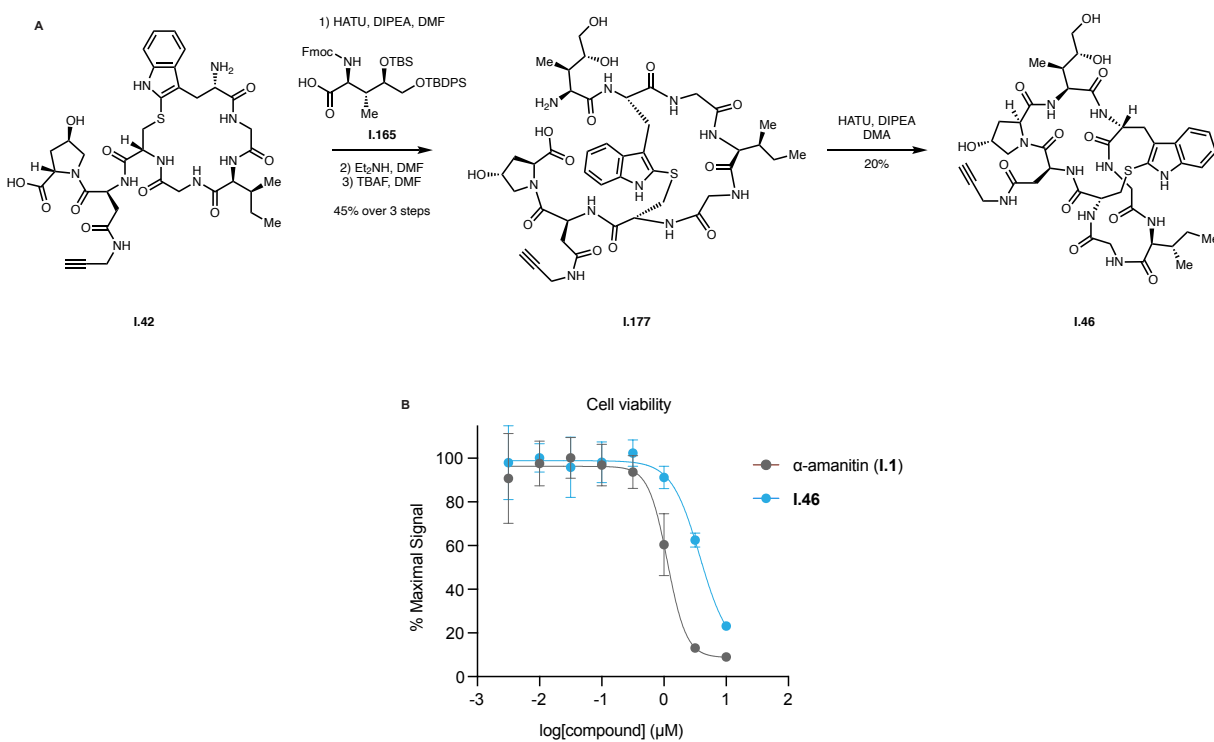


Figure 2.15. A) Bicyclization to furnish product **I.46** and **B)** cytotoxicity assessment of **I.46** over a two-day treatment of K562 cells.

The DHlle building block was dissolved in a minimal amount of DMF and preactivated for 30 minutes using HATU and DIPEA. After the addition of the monocyclic heptamer, the reaction was allowed to stir overnight. The Fmoc group was then removed by direct addition of 10 equivalents of diethylamine to the reaction mixture. We quickly found that attempts to purify the silylated intermediate via HPLC resulted in suboptimal purity due to the relatively nonpolar nature of the protected diol. Thus, we decided to perform the initial peptide coupling to form the monocyclic octamer as well as Fmoc removal and desilylation in a single pot, believing that the polarity of the completely deprotected octamer would be more amenable to reversed-phase purification. Intermediate **I.177** was isolated in roughly 45% yield over three steps before being subjected to the final peptide bond formation. The monocycle was dissolved in DMA before the addition of HATU and DIPEA to the reaction mixture. After 12 hours, the reaction was directly concentrated and HPLC purified to isolate the desired bicyclic octapeptide. Upon treatment of K562 cells, we were delighted to find that this compound displayed toxicity comparable to that of the natural product, with a

calculated IC_{50} of 4.5 μ M (**Figure 2.15 B**). **Figure 2.16** summarizes the bicyclic structures were successfully obtained as well as two that we were not – namely benzyl glycine **I.182** and an aryl sulfonyl fluoride **I.183** (*vide infra*).

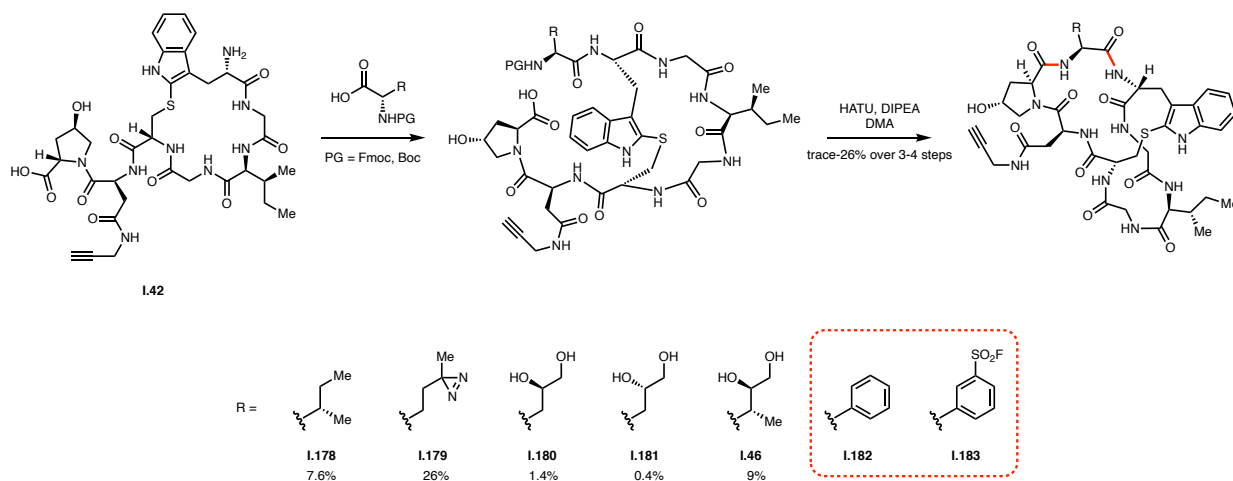


Figure 2.16. A selection of propargylated amanitin derivatives that were synthesized, with varying success.

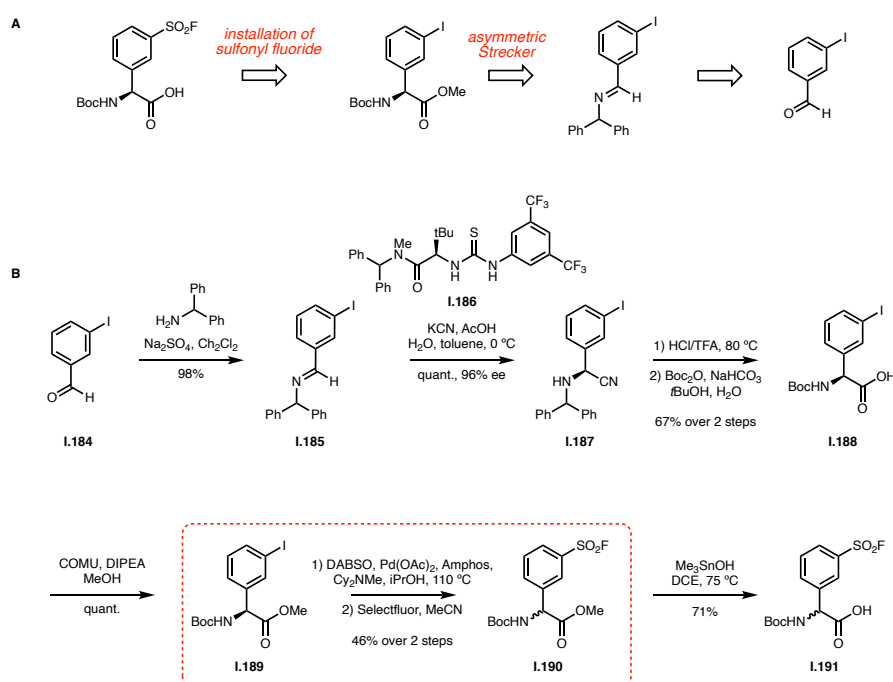
2.12. Some other derivatives of interest

At the commencement of this project, we were interested in the installation of additional functional groups onto α -amanitin in addition to the alkyne handle. We were particularly intrigued at the prospect of installing a covalent warhead to create an irreversible Pol II inhibitor, and so we embarked on several attempts to synthesize a covalent amanitin.

One of the most critical points of our aspirations was choosing the point of installation for our covalent warhead. Examination of the structure of α -amanitin within the mammalian Pol II binding pocket as well as our assembly strategy to access synthetic amanitins ultimately led us to derivatize the position of the DH11e residue. DH11e is the last residue coupled to form the bicyclic scaffold, and therefore derivatization at this position would allow for the most convergent pathway for generating amanitin analogues. Additionally, the orientation of α -amanitin within the Pol II binding pocket places the side chain of DH11e proximal to Tyr827, which we believe to have enhanced nucleophilicity due to its proximity to

His839. We therefore surmised that placement of an electrophilic sulfonyl fluoride in place of the DHlle diol to be an attractive strategy for installing a covalent bond between Pol II and our amanitin derivative.

Sifting through the literature, we concluded that the most facile method of synthesizing a sulfonyl fluoride-containing amino acid was to perform a late-stage installation of the sulfonyl fluoride through an aryl halide (**Figure 2.17**). The amino acid scaffold would be obtained through an asymmetric Strecker reaction wherein stereocontrol is exerted through a thiourea-based chiral catalyst.



Imine formation using 3-iodobenzaldehyde and benzhydrylamine was performed in preparation for conversion to the α -aminonitrile. The Strecker reaction proceeded smoothly to furnish α -aminonitrile **I.187** in near quantitative yield and 96% ee, which was then subjected to hydrolysis and Boc protection of the primary amine and methylation of the carboxylic acid.

At this point, we had a suitably protected amino acid; our remaining challenge was the installation of the sulfonyl fluoride itself. We utilized a palladium-catalyzed cross coupling to access the aryl sulfinate from the halide, followed by reaction with Selectfluor to obtain the desired sulfonyl fluoride. However, we

were perplexed to find that ^{19}F NMR revealed a mixture of two diastereomers. We surmised that the basic conditions used for installing the sulfonyl fluoride were responsible for α -epimerization. Unfortunately, the diastereomers were inseparable in our hands using both normal and reversed-phase chromatography. Nonetheless, we removed the methyl group residing on the C-terminus of the sulfonyl fluoride residue and attempted to couple the diastereomeric mixture to the macrocyclic heptamer. We separated the diastereomers by HPLC in the hopes that, despite our lack of confidence in assigning the diastereomers, we could at least determine whether bicyclization was feasible. Frustratingly, traces of our reversed-phase purification indicated that two separate product peaks contained what we believed to be the bicyclic product, leading us to believe that the peptide coupling conditions were basic enough to cause further α -epimerization of the aryl sulfonyl fluoride. While we proceeded to collect the bicyclic products formed, not much else of utility came from this exercise.

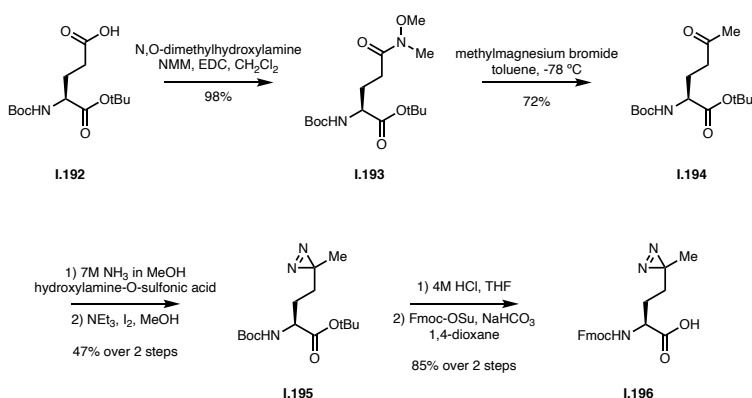


Figure 2.18. Synthesis of diazirine **I.196**.

Although our attempts to install a sulfonyl fluoride as a covalent handle were ultimately unfruitful, we did persist and succeed in appending a photoaffinity tag to the amanitin structure in the form of compound **I.179**. Our synthesis of photo-methionine was adapted from that of Vila-Perelló *et al.*⁵⁰ and accomplished starting from a doubly protected glutamic acid, which was converted to the Weinreb amide, followed by methylation. Installation of the diazirine was performed by subjecting the side-chain carbonyl to 7M ammonia in methanol and iodine-mediated oxidation of the diaziridine intermediate. Deprotection of

both the N- and C-termini was followed by capping the primary amine with an Fmoc group in anticipation of peptide coupling. Attachment to the monocyclic heptamer proceeded smoothly, yielding the desired bicycle in 26% yield over 3 steps and furnishing dual-functional amanitin **1.179** with both a click-compatible terminal alkyne and a covalent warhead in the form of a diazirine.

2.13. Summary and conclusion

This chapter describes our efforts towards the synthesis of several propargylated derivatives of α -amanitin. This was accomplished through the synthesis of two key amino acid building blocks: an oxidized tryptophan residue in the form of a bromopyrroloindoline as well as a fully protected DHlle. Our strategy capitalized on the use of the Savige-Fontana reaction as the key macrocyclization step en route to the bicyclic scaffold of our amanitin derivatives, followed by bicyclization using DHlle as the joining point for the monocyclic intermediate. While this overall assembly remains the most prominent for those generating amanitin analogues and was especially advantageous to us due to our chosen point of derivatization (i.e. the DHlle residue), there were several points in which we surmised whether an alternate construction of the bicyclic framework would be beneficial. This became a particularly salient point upon the discovery that the last few amide bond formations to obtain the bicycle were generally low yielding. We concluded that this could originate from the steric constraint associated with closing the bicycle using the position of the DHlle and could be circumvented by installation of all amide bonds to create the 8-membered macrocycle prior to the installation of the intra-annular tryptathionine bridge. This strategy sacrifices some of the convergent nature of our original route but may very well result in improved overall yield.

2.14. Experimental section

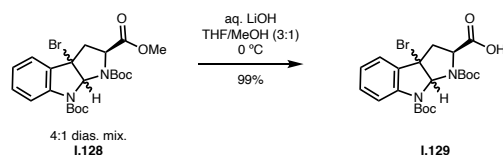
Materials and Methods

Organic Chemistry. All reactions were performed in oven-dried or flame-dried glassware under a positive pressure of nitrogen unless otherwise noted. Column chromatography was performed with a Biotage Isolera system employing silica gel 60 (230-400 mesh, Silicycle). Celite filtration was performed using Celite® 545 (EMD Millipore). Analytical thin-layer chromatography (TLC) was performed using 0.25 mm silica gel 60 F254 (EMD Millipore). TLC plates were visualized by fluorescence quenching under ultraviolet light (UV)

and exposure to a solution of ceric ammonium molybdate, *p*-anisaldehyde, or potassium permanganate stain followed by heating on a hot plate. Reversed-phase chromatography was performed on an Agilent 1200 series HPLC using water and acetonitrile as a mobile phase and Agilent Pursuit C18 as a stationary phase.

Commercial reagents and solvents were used as received with the following exceptions: tetrahydrofuran (THF), diethyl ether (Et₂O), dichloromethane (CH₂Cl₂), toluene (PhMe), acetonitrile (MeCN), and *N,N*-dimethylformamide (DMF) were degassed with argon and passed through a solvent purification system (designed by Pure Process Technology) utilizing alumina columns.

NMR spectra were recorded with a Varian INOVA-500 spectrometer, are reported in parts per million (δ), and are calibrated using residual undeuterated solvent as an internal reference (CDCl₃: δ 7.26 for ¹H NMR and δ 77.00 for ¹³C NMR; CD₃CN: δ 1.94 for ¹H NMR and δ 118.26; CD₃OD: δ 3.31 for ¹H NMR and δ 49.00 for ¹³C NMR). Data for ¹H NMR spectra are reported as follows: chemical shift (δ ppm) (multiplicity, coupling constant (Hz), integration). Multiplicities are reported as follows: s = singlet, d = doublet, t = triplet, q = quartet, m = multiplet, br = broad, or combinations thereof. High-resolution mass spectra (HRMS) were recorded using electrospray ionization (ESI) mass spectroscopy experiments on an Agilent 6210 TOF LC/MS.

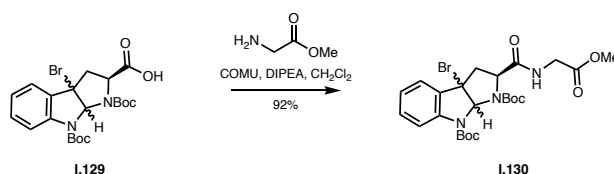


Carboxylic acid I.129

Lithium hydroxide (0.500 g in 18 mL water, 20.7 mmol, 2.0 equiv) was added dropwise to a stirring solution of I.128 (5.00 g, 10.0 mmol, 1.0 equiv) in 52 mL of 3:1 tetrahydrofuran/methanol at 0 °C. The reaction was warmed to RT and allowed to stir for 2 h. The reaction mixture was cooled to 0 °C, followed by dropwise

addition of 10% v/v hydrochloric acid solution until the mixture reached pH 3.0. The reaction mixture was extracted with three portions of ethyl acetate. The combined organic layers were washed with brine, dried over sodium sulfate, filtered, and concentrated. The crude residue was purified by flash column chromatography (1-20% methanol/dichloromethane gradient) to yield **I.129** (0.990 g, 20.5 mmol, 99%) as a white solid.

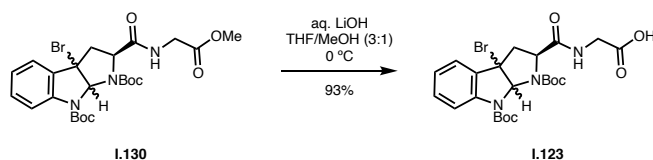
^1H NMR (500 MHz, CDCl_3) δ 7.56 (br s, 1H), 7.37 (d, $J = 7.7$ Hz, 1H), 7.33 (t, $J = 7.8$ Hz, 1H), 7.14 (t, $J = 7.5$ Hz, 1H), 6.40 (s, 1H), 3.90 (dd, $J = 10.3, 6.3$ Hz, 1H), 3.27 (dd, $J = 12.7, 6.4$ Hz, 1H), 2.89 (dd, $J = 12.7, 10.3$ Hz, 1H), 2.11 (s, 9H), 1.59 (s, 9H).



Methyl ester **I.130**

A suspension of **I.129** (0.545 g, 1.13 mmol, 1.0 equiv), glycine methyl ester hydrochloride (0.170 g, 1.36 mmol, 1.2 equiv), and COMU (0.581 g, 1.36 mmol, 1.2 eq) in 5.7 mL dichloromethane was cooled to 0 °C, followed by addition of DIPEA (0.708 mL, 4.07 mmol, 3.6 equiv). The reaction mixture was allowed to warm to RT. After 12 h, the reaction was quenched with saturated aq ammonium chloride and extracted with three portions of ethyl acetate. The combined organic extracts were washed with aq saturated brine, dried over sodium sulfate, filtered, and concentrated. The crude residue was purified by flash column chromatography (20-50% ethyl acetate/hexane gradient) to yield **I.130** (0.575 g, 1.04 mmol, 92%) as a white solid.

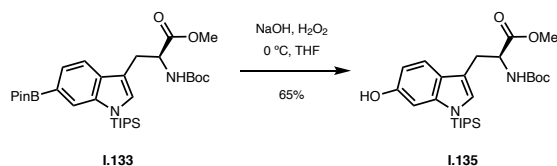
^1H NMR (500 MHz, CDCl_3) δ 7.51 (br s, 1H), 7.35 (dd, $J = 7.6, 1.4$ Hz, 1H), 7.33 – 7.26 (m, 1H), 7.11 (tt, $J = 7.6, 1.2$ Hz, 1H), 6.44 (s, 1H), 6.37 (s, 1H), 4.14 – 4.06 (m, 1H), 4.01 – 3.93 (m, 1H), 3.78 (dd, $J = 10.4, 6.2$ Hz, 1H), 3.73 (s, 3H), 3.20 (dd, $J = 12.8, 6.2$ Hz, 1H), 2.89 (dd, $J = 12.8, 10.4$ Hz, 1H), 1.36 (s, 8H).



Carboxylic acid I.123

Lithium hydroxide (0.086 g in 3.6 mL water, 3.6 mmol, 2.0 equiv) was added dropwise to a stirring solution of **I.130** (1.00 g, 1.81 mmol, 1.0 equiv) in 9.0 mL of 3:1 tetrahydrofuran/methanol at 0 °C. The reaction was warmed to RT and allowed to stir for 2 h. The reaction mixture was cooled to 0 °C, followed by dropwise addition of 10% v/v hydrochloric acid solution until the mixture reached pH 3.0. The reaction mixture was extracted with three portions of ethyl acetate. The combined organic extracts were washed with aq saturated brine, dried over sodium sulfate, filtered, and concentrated. The crude residue was purified by flash column chromatography (1-20% methanol/dichloromethane gradient) to yield **I.123** (0.927 g, 1.72 mmol, 93%) as a white solid.

¹H NMR (500 MHz, CDCl₃) δ 7.52 (br s, 1H), 7.38 (d, *J* = 7.6 Hz, 1H), 7.33 (t, *J* = 7.8 Hz, 1H), 7.15 (t, *J* = 7.6 Hz, 1H), 6.70 (s, 1H), 6.44 (s, 1H), 4.26 – 4.18 (m, 1H), 4.08 – 4.00 (m, 1H), 3.81 (dd, *J* = 10.6, 6.1 Hz, 1H), 3.26 (dd, *J* = 13.0, 6.1 Hz, 1H), 2.97 – 2.89 (m, 1H), 1.59 (s, 9H).

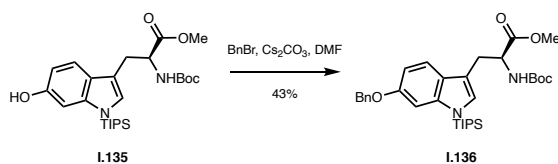


Phenol I.135

I.133 (1.07 g, 1.78 mmol, 1 equiv) was dissolved in dry THF (17.8 mL) and cooled to 0°C. 1% aq NaOH (17.8 mL) was added dropwise. Aq hydrogen peroxide (1.84 mL of 30% H₂O₂, 17.8 mmol, 10 equiv) was

added dropwise at 0°C and allowed to stir for 5 min. The reaction was quenched with 1:1 saturated ammonium chloride and sodium thiosulfate and then diluted with diethyl ether. The aq layer was then back extracted 3 times with diethyl ether. The combined organic layers were washed twice with 10% sodium thiosulfate and then once with saturated NaHCO₃ before washing with brine. The organic layer was then dried over sodium sulfate, filtered, and then concentrated *in vacuo*. The crude was purified via flash column chromatography (20% EtOAc in hexane). The fractions were cut, collected, and concentrated to yield **I.135** (0.568 g, 1.16 mmol, 65%) as a white foam.

¹H NMR (500 MHz, CDCl₃) δ 7.31 (d, *J* = 8.4 Hz, 1H), 6.95 (s, 1H), 6.88 (s, 1H), 6.65 (d, *J* = 8.7 Hz, 1H), 5.52 (d, *J* = 9.9 Hz, 1H), 5.09 (d, *J* = 8.2 Hz, 1H), 4.62 (q, *J* = 6.1 Hz, 1H), 3.62 (s, 3H), 3.21 (d, *J* = 5.7 Hz, 2H), 1.63 (h, *J* = 7.5 Hz, 3H), 1.43 (s, 9H), 1.12 (dd, *J* = 7.6, 2.1 Hz, 12H).

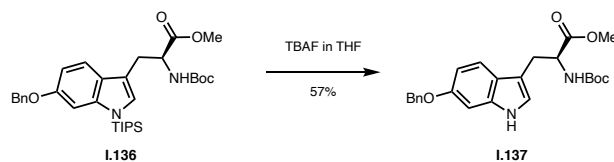


Benzyl ether **I.136**

I.135 (0.570 g, 1.16 mmol, 1 equiv) and CsCO₃ (0.454 g, 1.39 mmol, 1.2 equiv) were dissolved in DMF (7.0 mL). Benzyl bromide (0.165 mL, 1.39 mmol, 1.2 equiv) was added and the reaction mixture was allowed to stir at RT for 12 h. The reaction was quenched with saturated ammonium chloride and diluted with diethyl ether. The aq layer was back extracted 3 times with diethyl ether before washing the combined organic layers with brine. The organic layer was dried over sodium sulfate, filtered, and then concentrated *in vacuo*. The crude was purified by flash column chromatography (10-15% EtOAc in hexane) to furnish **I.136** (0.212 g, 0.499 mmol, 43%).

¹H NMR (500 MHz, CDCl₃) δ 7.34 (d, *J* = 8.6 Hz, 1H), 7.31 – 7.21 (m, 5H), 7.06 (d, *J* = 7.2 Hz, 2H), 6.81 (s, 1H), 6.71 (dd, *J* = 8.6, 2.1 Hz, 1H), 6.64 (d, *J* = 2.1 Hz, 1H), 5.17 (s, 2H), 5.07 (d, *J* = 8.2 Hz, 1H), 4.62

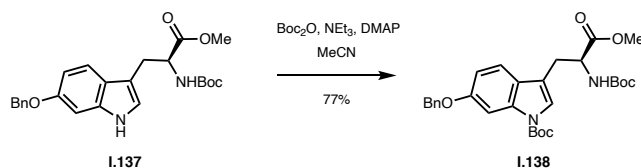
(d, $J = 7.5$ Hz, 1H), 3.61 (s, 3H), 3.23 (d, $J = 5.6$ Hz, 2H), 1.43 (s, 9H), 1.20 – 1.11 (m, 3H), 1.04 (d, $J = 7.3$ Hz, 12H).



Benzyl ether **I.137**

I.136 (0.240 g, 0.413 mmol, 1.0 equiv) was dissolved in THF (2.0 mL) and TBAF (0.496 mL of 1.0 M solution, 1.2 equiv) was added dropwise. The reaction was stirred at RT for 1 h before quenching with saturated ammonium chloride. The organic layer was diluted with ethyl acetate and the aq layer was back extracted with ethyl acetate three times. The organic layers were combined, washed with brine, and then dried over sodium sulfate. The combined organic layers were filtrated and concentrated under vacuum. The crude product was purified via flash column chromatography (20-40% EtOAc in hexane). Product fractions were cut, collected, and concentrated to furnish **I.137** (0.100 g, 0.235 mmol, 57%) as an off-white solid.

^1H NMR (500 MHz, CDCl_3) δ 7.35 (dd, $J = 8.4, 0.7$ Hz, 1H), 7.31 – 7.24 (m, 5H), 7.07 – 7.02 (m, 3H), 6.76 (s, 1H), 6.68 – 6.61 (m, 2H), 5.64 (s, 1H), 5.12 (s, 2H), 3.60 (s, 3H), 3.21 (d, $J = 5.6$ Hz, 2H), 1.42 (s, 9H).

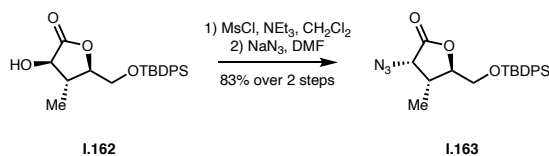


Carbamate **I.138**

I.137 (0.109 g, 0.257 mmol, 1.0 equiv) was dissolved in acetonitrile (1.5 mL). Triethylamine (0.107 mL, 0.771 mmol, 3.0 equiv) was added, followed by Boc anhydride (0.062 g, 0.283 mmol, 1.1 equiv) and DMAP

(0.003 g, 0.026 mmol, 0.1 equiv). The reaction mixture was stirred at RT for 12 h. The reaction mixture was diluted with ethyl acetate before washing twice with saturated ammonium chloride, then twice with brine. The organic layer was dried over sodium sulfate, filtered, and concentrated *in vacuo*. The crude material was purified by flash column chromatography (15-20% EtOAc in hexane). The product fractions were cut, collected, and concentrated to yield **I.138** (0.104 g, 0.198 mmol, 77%) as a white solid.

^1H NMR (600 MHz, CDCl_3) δ 7.32 – 7.26 (m, 5H), 7.10 – 7.05 (m, 3H), 6.94 (dd, $J = 8.6, 2.0$ Hz, 1H), 6.88 (s, 1H), 5.22 (s, 2H), 5.05 (d, $J = 8.3$ Hz, 1H), 4.62 (d, $J = 7.4$ Hz, 1H), 3.61 (s, 3H), 3.30 – 3.22 (m, 2H), 1.55 (s, 9H), 1.42 (s, 9H).

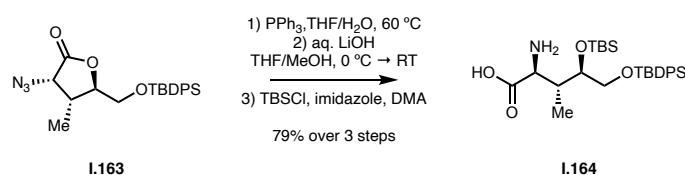


Aza-lactone **I.163**

A solution of **I.162** (1.53 g, 3.99 mmol, 1.0 equiv) and triethylamine (0.833 mL, 5.98 mmol, 1.5 equiv) in 20 mL of dichloromethane was cooled to 0 °C, followed by the dropwise addition of methanesulfonyl chloride (0.339 mL, 4.39 mmol, 1.1 equiv). The reaction mixture was allowed to warm to RT. After 1 h, the reaction mixture was quenched with saturated aq ammonium chloride, followed by extraction with three portions of ethyl acetate. The combined organic extracts were washed with aq saturated brine, dried over sodium sulfate, filtered, and concentrated. The crude residue was re-dissolved in 20 mL of anhydrous dimethylformamide and sodium azide (0.778 g, 12.0 mmol, 3.0 equiv) was added in a single portion. The resulting suspension was stirred for 12 h. The reaction mixture was diluted with water and then extracted with three portions of ethyl acetate. The combined organic extracts were washed with aq saturated brine, dried over sodium sulfate, filtered, and concentrated. The crude residue was purified by flash column chromatography (1-40% ethyl acetate/hexane) to isolate **I.163** (1.36 g, 3.32 mmol, 83%) as a white solid.

^1H NMR (500 MHz, CDCl_3) δ 7.63 (dq, $J = 8.3, 1.7$ Hz, 4H), 7.49 – 7.37 (m, 6H), 4.54 (dd, $J = 8.0, 1.5$ Hz, 1H), 4.19 – 4.14 (m, 1H), 3.91 (ddd, $J = 11.8, 2.8, 1.6$ Hz, 1H), 3.70 (ddd, $J = 11.8, 2.7, 1.5$ Hz, 1H), 2.74 (td, $J = 7.3, 4.0$ Hz, 1H), 1.25 (s, 1H), 1.09 (dd, $J = 7.2, 1.5$ Hz, 3H), 1.06 (d, $J = 1.5$ Hz, 9H).

^{13}C NMR (126 MHz, CDCl_3) δ 173.19, 135.74, 135.62, 132.69, 132.22, 130.26, 128.12, 85.40, 77.45, 77.20, 76.95, 64.04, 61.17, 35.79, 26.95, 19.34, 13.29.



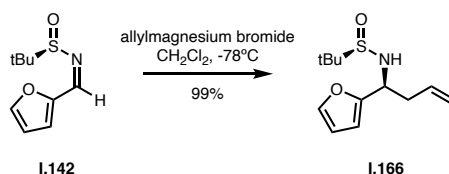
Amine **I.164**

I.163 (0.200 g, 0.488 mmol, 1.0 equiv) and triphenylphosphine (0.154 g, 0.586 mmol, 1.2 equiv) were suspended in 3.3 mL of a 5:1 tetrahydrofuran and water and heated to 60 °C. The reaction mixture was stirred at temperature for 12 h, then directly concentrated. The crude residue was re-dissolved in a mixture of tetrahydrofuran/methanol (3:1) and cooled to 0 °C before the dropwise addition of aq lithium hydroxide (0.018 g, 0.731 mmol, 1.5 equiv in 0.50 mL water). The reaction mixture was stirred for 2 h at 0 °C, followed by dropwise addition of 10% v/v hydrochloric acid solution until the mixture reached pH 8.0. The crude residue was concentrated under reduced pressure and re-dissolved in 2.4 mL of anhydrous dimethylacetamide. Imidazole (0.665 g, 9.76 mmol, 20 equiv) and *tert*-butyldimethylsilyl chloride (0.736 g, 4.88 mmol, 10 equiv) were added and the resulting suspension was stirred for 12 h. The reaction mixture was quenched with aq saturated ammonium chloride and extracted with three portions of ethyl acetate. The combined organic extracts were washed with aq saturated brine, dried over sodium sulfate, filtered, and concentrated. The crude residue was purified by flash column chromatography (1-20% methanol+ NH_4OH /dichloromethane gradient) to isolate **I.164** (0.198 g, 0.384 mmol, 79%) as a colorless oil.

Sulfinyl imine I.142

4Å molecular sieves (41.3 g) were flame dried under vacuum. 129 mL of tetrahydrofuran was added, followed by (*R*)-(+)-2-methyl-2-propanesulfonamide (5.00 g, 41.3 mmol, 1.0 equiv). Furfural (3.97 mL, 41.3 mmol, 1.0 equiv) was added, followed by pyrrolidine (0.345 mL, 4.13 mmol, 0.1 equiv). The reaction flask was fitted with a reflux condenser and heated to 66 °C for 7 h. The reaction was cooled to RT before filtering through a pad of celite, rinsing with dichloromethane. The filtrate was concentrated *in vacuo*. The crude material was purified using flash column chromatography (10-15% EtOAc in hexane) to yield **I.142** (7.56 g, 37.9 mmol, 93%) as an off white oil.

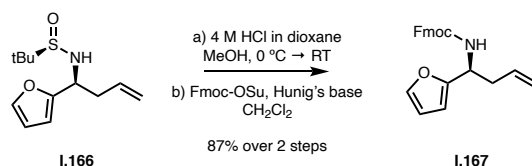
¹H NMR (500 MHz, CDCl₃) δ 8.39 (s, 1H), 7.64 (d, *J* = 1.6 Hz, 1H), 7.01 (d, *J* = 3.5 Hz, 1H), 6.57 (dq, *J* = 4.3, 1.2 Hz, 1H), 1.25 (d, *J* = 1.3 Hz, 9H).



Sulfonamide I.166

I.142 (0.500 g, 2.51 mmol, 1.0 equiv) was dissolved in 12.5 mL of dichloromethane and cooled to -78 °C. Allyl magnesium bromide (5.02 mL, 5.02 mmol, 2.0 equiv) was added dropwise and the reaction mixture was stirred at temperature for 30 min. The reaction was quenched with saturated ammonium chloride and the mixture was allowed to warm to RT before diluting the organic layer with dichloromethane. The aq layer was back extracted thrice with dichloromethane, after which the combined organic extracts were washed with brine, dried over sodium sulfate, filtered, and concentrated under vacuum. The crude material was purified by flash column chromatography (25-100% EtOAc in hexane) to yield **I.166** as an off-white oil (0.598 g, 2.48 mmol, 99%).

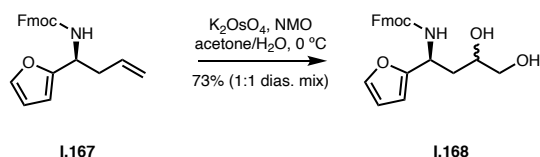
^1H NMR (500 MHz, CDCl_3) δ 7.37 (dd, $J = 1.9, 0.9$ Hz, 1H), 6.34 – 6.29 (m, 1H), 6.22 (d, $J = 2.4$ Hz, 1H), 5.71 (ddt, $J = 17.2, 10.2, 7.1$ Hz, 1H), 5.23 – 5.13 (m, 2H), 4.54 (td, $J = 6.7, 4.8$ Hz, 1H), 3.55 (d, $J = 4.8$ Hz, 1H), 2.75 – 2.61 (m, 2H), 1.19 (s, 9H).



Amine I.167

A solution of **I.166** (0.490 g, 2.03 mmol, 1.0 equiv) in 10 mL of methanol was cooled to 0 °C before the addition of 4.0 M HCl in dioxane (2.54 mL, 10.2 mmol, 5.0 equiv). The reaction was allowed to stir at RT for 30 min or until TLC indicated the disappearance of starting material. The crude reaction mixture was directly concentrated and then redissolved in 10 mL dichloromethane. DIPEA (1.06 mL, 6.09 mmol, 3.0 equiv) and Fmoc-OSu (0.788 g, 3.05 mmol, 1.5 equiv) were added to the reaction mixture and stirred for 1 h. The reaction was quenched with saturated ammonium chloride. The aq layer was back extracted thrice with dichloromethane, after which the combined organic extracts were washed with brine, dried over sodium sulfate, filtered, and concentrated under vacuum. The crude material was purified by flash column chromatography (10-20% EtOAc in hexane) to yield **I.167** (0.632 g, 1.74 mmol, 87%) as a white foam.

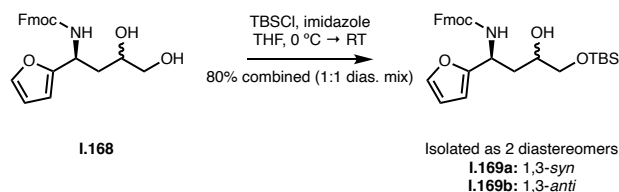
^1H NMR (500 MHz, CDCl_3) δ 7.78 (d, $J = 7.6$ Hz, 2H), 7.60 (d, $J = 7.6$ Hz, 2H), 7.42 (t, $J = 7.5$ Hz, 2H), 7.37 (d, $J = 1.8$ Hz, 1H), 7.32 (t, $J = 7.5$ Hz, 2H), 6.32 (dd, $J = 3.2, 1.9$ Hz, 1H), 6.18 (s, 1H), 5.74 (dq, $J = 16.8, 7.7$ Hz, 1H), 5.18 – 5.08 (m, 3H), 5.00 – 4.89 (m, 1H), 4.45 (dtd, $J = 17.7, 11.8, 6.1$ Hz, 2H), 4.24 (t, $J = 6.9$ Hz, 1H), 2.63 (q, $J = 6.2$ Hz, 2H).



Diol **I.168** (dias. mix)

I.167 (0.632 g, 1.76 mmol, 1.0 equiv) was dissolved in 18 mL of a 9:1 mixture of acetone and water and cooled to 0 °C. NMO (0.412 g, 3.52 mmol, 2.0 equiv) and $K_2OsO_4 \cdot 2 H_2O$ (0.032 g, 0.088 mmol, 0.05 equiv) were added and the reaction was slowly warmed to RT overnight. The reaction was quenched with sodium sulfite and stirred for 1 h before diluting with water and dichloromethane. The aq layer was back extracted with three portions of dichloromethane before drying the combined organic layers over sodium sulfate, filtering, and concentrating *in vacuo*. The crude was purified by flash column chromatography (50-100% EtOAc in hexane with 2.5% methanol) to yield **I.168** (0.508 g 1.29 mmol, 73%) as a white foam.

1H NMR (500 MHz, $CDCl_3$) δ 7.76 (dd, $J = 7.6, 3.5$ Hz, 2H), 7.61 – 7.54 (m, 2H), 7.44 – 7.27 (m, 6H), 6.31 (dt, $J = 5.6, 2.7$ Hz, 1H), 6.25 – 6.17 (m, 1H), 5.31 – 5.25 (m, 1H), 5.08 (td, $J = 9.8, 3.4$ Hz, 1H), 4.55 (dd, $J = 10.8, 6.7$ Hz, 1H), 4.45 (dd, $J = 10.8, 6.4$ Hz, 2H), 4.21 (t, $J = 6.5$ Hz, 1H), 3.86 (d, $J = 4.0$ Hz, 1H), 3.75 – 3.56 (m, 2H), 3.54 – 3.45 (m, 1H), 1.88 (ddd, $J = 14.1, 10.7, 3.5$ Hz, 1H), 1.79 (ddd, $J = 13.9, 10.7, 2.6$ Hz, 1H).



Silyl ethers **I.169a**, **169b**

A solution of **I.168** (0.508 g, 1.29 mmol, 1.0 equiv) in THF (13 mL) was cooled to 0 °C. TBSCl (0.389 g, 2.58 mmol, 2.0 equiv) and imidazole (0.176 g, 2.58 mmol, 2.0 equiv) were added and the reaction was slowly warmed to RT. After 12 h, the reaction was quenched with saturated ammonium chloride and diluted with ethyl acetate. The aq layer was back extracted with three portions of ethyl acetate and the combined organic layers were dried over sodium sulfate and concentrated under vacuum. The crude material was purified by flash column chromatography (10-25% EtOAc in hexane). Fractions pertaining to silyl ethers

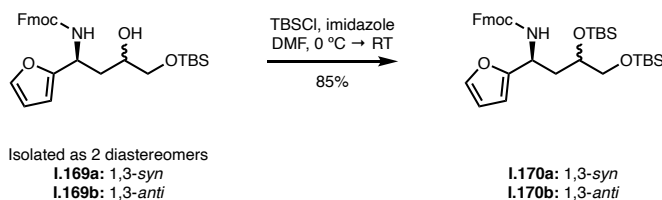
I.169a and **I.169b** were cut, collected separately, and concentrated to furnish a white foam (0.053 g, 1.04 mmol, 80% combined yield).

I.169a (1,3-*syn*)

^1H NMR (500 MHz, CDCl_3) δ 7.76 (d, $J = 7.6$ Hz, 2H), 7.58 (d, $J = 7.5$ Hz, 2H), 7.40 (t, $J = 7.5$ Hz, 2H), 7.35 (d, $J = 1.8$ Hz, 1H), 7.30 (t, $J = 7.4$ Hz, 2H), 6.32 (t, $J = 2.5$ Hz, 1H), 6.23 (s, 1H), 5.36 (s, 1H), 5.02 (d, $J = 8.4$ Hz, 1H), 4.40 (q, $J = 8.7$ Hz, 2H), 4.22 (t, $J = 7.0$ Hz, 1H), 3.60 (d, $J = 11.5$ Hz, 2H), 3.47 – 3.42 (m, 1H), 1.98 (s, 2H), 0.90 (s, 9H), 0.06 (s, 6H).

I.169b (1,3-*anti*)

^1H NMR (500 MHz, CDCl_3) δ 7.77 (d, $J = 7.6$ Hz, 2H), 7.61 (d, $J = 7.5$ Hz, 2H), 7.41 (t, $J = 7.5$ Hz, 2H), 7.37 – 7.35 (m, 1H), 7.32 (t, $J = 7.5$ Hz, 2H), 6.32 (dd, $J = 3.2, 1.8$ Hz, 1H), 6.19 (d, $J = 3.2$ Hz, 1H), 5.78 (d, $J = 8.9$ Hz, 1H), 5.14 (td, $J = 8.5, 3.9$ Hz, 1H), 4.44 (d, $J = 7.1$ Hz, 2H), 4.24 (t, $J = 7.0$ Hz, 1H), 3.71 (ddq, $J = 10.5, 7.0, 3.5$ Hz, 1H), 3.59 (dd, $J = 9.9, 4.2$ Hz, 1H), 3.51 (dd, $J = 9.9, 7.0$ Hz, 1H), 3.00 (d, $J = 3.6$ Hz, 1H), 2.00 – 1.85 (m, 2H), 0.91 (s, 10H), 0.08 (d, $J = 2.7$ Hz, 6H).



Silyl ethers I.170a, I.170b

A solution of **I.169a** or **I.169b** (0.239 g, 0.607 mmol, 1.0 equiv) in 1.2 mL dimethylformamide was cooled to 0 °C. TBSCl (0.183 g, 1.21 mmol, 2.0 equiv) and imidazole (0.083 g, 1.21 mmol, 2.0 equiv) were added and the reaction was allowed to slowly warm to RT. After 2 h, the reaction was quenched with saturated ammonium chloride and diluted with water and ethyl acetate. The aq layer was back extracted thrice with ethyl acetate and the combined organic layers were dried over sodium sulfate, filtered, and concentrated *in vacuo*. The crude was purified via flash column chromatography (10-15% EtOAc in hexane) and product

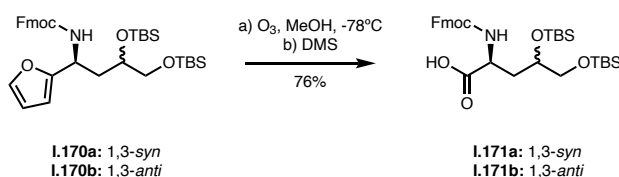
fractions were cut, collected, and concentrated to furnish **I.170a** or **I.170b** (0.261 g, 0.514 mmol, 85%) as a white foam.

I.170a (1,3-*syn*)

^1H NMR (500 MHz, CDCl_3) δ 7.77 (d, $J = 7.6$ Hz, 2H), 7.60 (d, $J = 7.5$ Hz, 2H), 7.41 (t, $J = 7.5$ Hz, 2H), 7.37 (d, $J = 1.8$ Hz, 1H), 7.32 (t, $J = 7.5$ Hz, 2H), 6.33 (dd, $J = 3.3, 1.8$ Hz, 1H), 6.23 – 6.19 (m, 1H), 5.48 (d, $J = 8.3$ Hz, 1H), 5.05 (q, $J = 7.6$ Hz, 1H), 4.43 (q, $J = 8.7$ Hz, 2H), 4.23 (t, $J = 6.9$ Hz, 1H), 3.71 – 3.58 (m, 2H), 3.44 (dd, $J = 10.0, 6.8$ Hz, 1H), 2.27 (ddd, $J = 12.8, 7.7, 4.3$ Hz, 1H), 1.97 (dt, $J = 13.7, 6.8$ Hz, 1H), 0.94 (d, $J = 7.3$ Hz, 18H), 0.13 – 0.03 (m, 12H).

I.170b (1,3-*anti*)

^1H NMR (500 MHz, CDCl_3) δ 7.78 (d, $J = 7.6$ Hz, 2H), 7.62 (t, $J = 6.8$ Hz, 2H), 7.41 (t, $J = 7.5$ Hz, 2H), 7.36 (s, 1H), 7.32 (t, $J = 7.5$ Hz, 2H), 6.32 (dd, $J = 3.3, 1.8$ Hz, 1H), 6.17 – 6.13 (m, 1H), 5.65 (d, $J = 7.9$ Hz, 1H), 5.02 (td, $J = 8.4, 4.2$ Hz, 1H), 4.51 – 4.40 (m, 2H), 4.24 (t, $J = 6.9$ Hz, 1H), 3.81 (dp, $J = 7.9, 4.0$ Hz, 1H), 3.63 (dd, $J = 10.0, 4.9$ Hz, 1H), 3.46 (dd, $J = 10.0, 7.0$ Hz, 1H), 2.25 – 2.16 (m, 1H), 2.03 – 1.94 (m, 1H), 0.96 – 0.89 (m, 18H), 0.15 – 0.07 (m, 12H).



Carboxylic acids I.171a, I.171b

A solution of **I.170a** or **I.170b** (0.041 g, 0.066 mmol, 1 equiv) in methanol (1.3 mL) was cooled to -78°C . Ozone was bubbled through the solution until the reaction mixture turned a light blue-grey. Excess ozone was removed by bubbling nitrogen through the reaction mixture at -78°C . Dimethyl sulfide (0.048 mL, 0.660 mmol, 10 equiv) was added and the reaction was allowed to stir at RT before concentrating under vacuum.

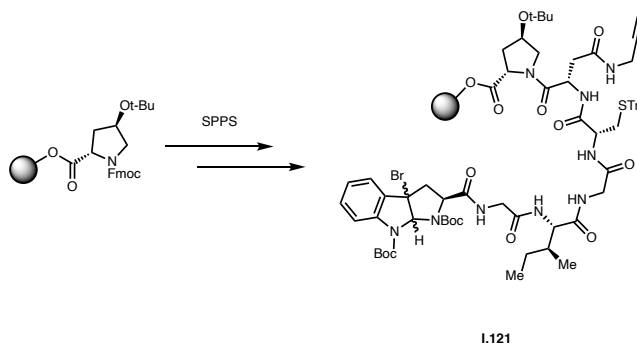
The crude material was purified by flash column chromatography (10-15% EtOAc in hexane with acetic acid) to furnish carboxylic acid **I.171a** or **I.171b** (0.030 g, 0.050 mmol, 76%) as a white foam.

I.171a (1,3-*syn*)

$^1\text{H NMR}$ (500 MHz, CDCl_3) δ 7.75 (d, $J = 7.6$ Hz, 2H), 7.59 (t, $J = 6.4$ Hz, 2H), 7.39 (t, $J = 7.5$ Hz, 2H), 7.30 (t, $J = 7.5$ Hz, 2H), 5.90 (d, $J = 6.5$ Hz, 1H), 4.48 – 4.42 (m, 2H), 4.38 (dd, $J = 10.8, 7.0$ Hz, 1H), 4.22 (t, $J = 7.0$ Hz, 1H), 3.89 (t, $J = 6.1$ Hz, 1H), 3.66 (dd, $J = 10.4, 4.6$ Hz, 1H), 3.50 (dd, $J = 10.1, 7.0$ Hz, 1H), 2.17 (dd, $J = 12.5, 6.4$ Hz, 1H), 2.01 (td, $J = 14.9, 8.0$ Hz, 1H), 0.89 (d, $J = 6.4$ Hz, 18H), 0.07 (d, $J = 2.0$ Hz, 12H).

I.171b (1,3-*anti*)

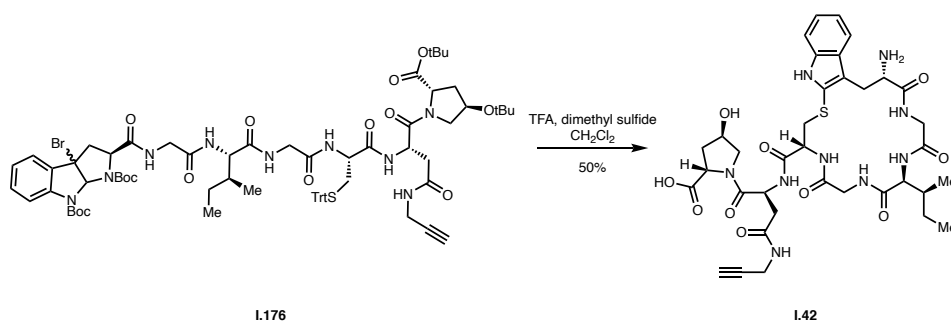
$^1\text{H NMR}$ (500 MHz, CDCl_3) δ 7.75 (d, $J = 7.6$ Hz, 2H), 7.60 (t, $J = 8.4$ Hz, 2H), 7.39 (t, $J = 7.5$ Hz, 2H), 7.33 – 7.26 (m, 2H), 5.94 (d, $J = 6.6$ Hz, 1H), 4.41 (tt, $J = 17.9, 8.8$ Hz, 3H), 4.22 (t, $J = 7.1$ Hz, 1H), 3.92 (dt, $J = 7.7, 3.7$ Hz, 1H), 3.63 (dd, $J = 10.1, 4.6$ Hz, 1H), 3.47 (dd, $J = 10.1, 7.3$ Hz, 1H), 0.90 (s, 18H), 0.11 – 0.04 (m, 12H).



Heptapeptide I.121

Fmoc-*L*-Hyp(*t*Bu)-OH was loaded on 2-chlorotrityl resin as follows: the resin (2.0 g, 2.3 mmol, 1 equiv) was suspended in 15 mL CH_2Cl_2 , followed by Fmoc-*L*-Hyp(*t*Bu)-OH (1.9 g, 4.6 mmol, 2 equiv) and DIPEA (2.0 mL, 11.5 mmol, 5 equiv). The reaction was allowed to stir at room temperature for 3 hours and then filtered and rinsed with CH_2Cl_2 . Unreacted resin sites were capped by washing thrice with a solution of

CH₂Cl₂:MeOH:DIPEA (17:2:1), followed by washing with CH₂Cl₂ x 3, DMF x 3, and CH₂Cl₂ x 3 before filtering and drying under vacuum. The peptide sequence was extended from the N-terminus using 3 equivalents of the appropriate N-Fmoc-amino acid (Propargyl-Asn(Trt), Cys(Trt), Gly, Ile, Gly, **1.123**), 3 equivalents of HATU, and 6 equivalents of DIPEA in DMF applied sequentially after Fmoc-removal of the growing sequence using 20% piperidine in DMF. A small amount of resin containing the completed heptapeptide was deprotected using 25% HFIP in CH₂Cl₂ and the product mass was confirmed using HRMS.

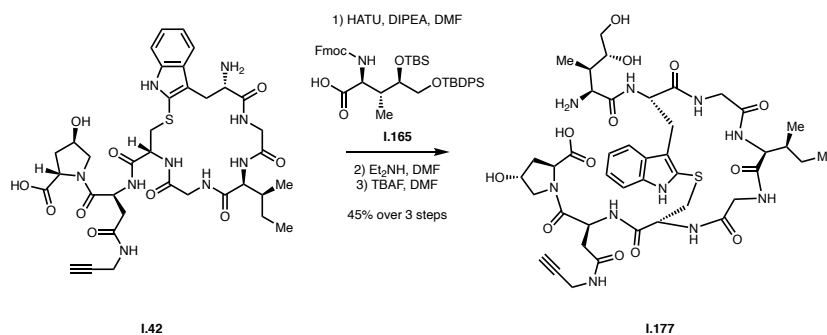


Macrocyclic heptapeptide **1.42**

A solution of TFA (7.0 mL) and dimethyl sulfide (0.512 mL, 6.98 mmol, 20 equiv) was cooled to 0 °C. Linear heptamer **1.176** (0.500 g, 3.49 mmol, 1.0 equiv) was dissolved in 1.0 mL CH₂Cl₂ and added to the reaction flask using a syringe pump over the course of 1 h. The reaction was stirred at 0 °C for 12 h and then directly concentrated under reduced pressure. The crude was redissolved in MeCN and water and passed through a 0.2 μM syringe filter before purification by reversed-phase HPLC using 0.1% TFA in water (solvent A) and 0.1% TFA in acetonitrile (solvent B). The desired product was isolated using a solvent gradient of 5-70% solvent B over 30 minutes. The product fractions were carefully cut, collected, and concentrated under vacuum to yield **1.42** (0.140 g, 1.75 mmol, 50%) as an off-white solid.

¹H NMR (500 MHz, CD₃OD) δ 7.65 (d, *J* = 8.0 Hz, 1H), 7.37 (d, *J* = 8.1 Hz, 1H), 7.23 – 7.16 (m, 1H), 7.10 (t, *J* = 7.6 Hz, 1H), 4.49 – 4.41 (m, 2H), 4.34 (dd, *J* = 8.7, 4.5 Hz, 1H), 4.28 (t, *J* = 7.3 Hz, 1H), 4.14 – 4.01 (m, 3H), 3.93 (dd, *J* = 3.7, 2.3 Hz, 2H), 3.84 – 3.74 (m, 4H), 3.66 – 3.56 (m, 2H), 3.43 (dd, *J* = 13.8, 4.3

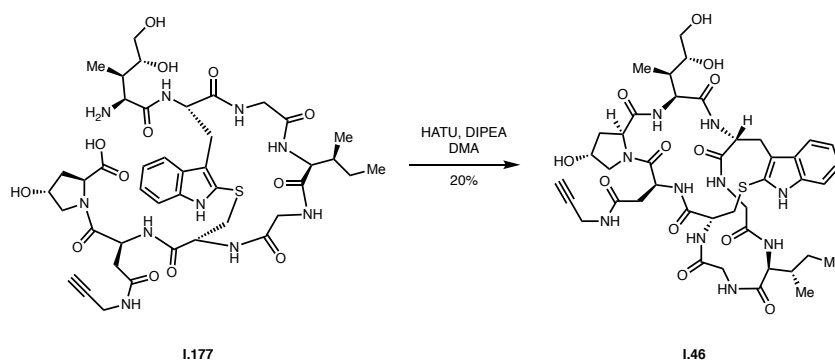
Hz, 1H), 3.28 – 3.20 (m, 1H), 3.15 (dd, $J = 13.8, 8.5$ Hz, 1H), 2.91 (dd, $J = 7.2, 1.7$ Hz, 2H), 2.67 (dd, $J = 15.3, 5.3$ Hz, 1H), 2.62 – 2.53 (m, 2H), 2.24 (ddd, $J = 12.1, 8.4, 2.8$ Hz, 1H), 2.05 (ddt, $J = 12.0, 8.3, 4.2$ Hz, 1H), 1.99 – 1.84 (m, 2H), 1.64 – 1.55 (m, 1H), 1.21 (tq, $J = 15.1, 7.4$ Hz, 1H), 0.98 – 0.89 (m, 6H).



Monocyclic octamer I.177

To a suspension of carboxylic acid **I.165** (0.051 g, 0.069 mmol, 1.1 equiv) and HATU (0.026 mg, 0.069 mmol, 1.1 equiv) in 1.3 mL DMF was added DIPEA (0.033 mL, 0.188 mmol, 3.0 equiv). The reaction mixture was allowed to stir for 30 minutes before the addition of macrocycle **I.42** (0.050 g, 0.063 mmol, 1.0 equiv). After 12 hours, diethylamine (0.065 mL, 0.627 mmol, 10 equiv) was added and the resulting mixture stirred for an additional hour before directly concentrating under reduced pressure. After drying, the crude residue was re-dissolved in 1.3 mL DMF and cooled to 0 °C before addition of 1.0 M tetrabutylammonium fluoride solution in tetrahydrofuran (0.470 mL, 0.470 mmol, 7.5 equiv). After 2 hours, the reaction mixture was brought to RT and treated with hexamethyldisiloxane (0.133 mL, 0.627 mmol, 10 equiv) to destroy any excess fluoride. The mixture was directly concentrated before re-dissolving the crude in MeCN/DMF and passing through a 0.2 μ M syringe filter. The filtered mixture was purified by reversed-phase HPLC, using 0.1% TFA in water (solvent A) and 0.1% TFA in acetonitrile (solvent B). The desired product was isolated using a solvent gradient of 5-60% solvent B over 30 minutes and product fractions were cut, collected, and concentrated under reduced pressure to furnish **I.177** (0.026 g, 0.028 mmol, 45% over 3 steps) as a pale yellow oil.

^1H NMR (500 MHz, CD_3OD) δ 7.70 – 7.55 (m, 1H), 7.30 (t, J = 7.7 Hz, 1H), 7.15 (d, J = 9.5 Hz, 1H), 7.05 (t, J = 7.7 Hz, 1H), 5.09 (s, 1H), 4.91 (s, 44H), 4.87 (s, 24H), 4.69 (s, 1H), 4.57 (s, 1H), 4.45 (dd, J = 15.1, 7.6 Hz, 2H), 4.31 – 4.01 (m, 2H), 4.00 – 3.87 (m, 4H), 3.87 – 3.78 (m, 3H), 3.74 – 3.54 (m, 3H), 3.54 – 3.40 (m, 1H), 3.35 (s, 2H), 3.31 (dq, J = 3.1, 1.6 Hz, 14H), 3.19 – 3.08 (m, 2H), 2.87 (t, J = 3.0 Hz, 1H), 2.61 – 2.55 (m, 2H), 2.24 (s, 2H), 2.08 – 1.99 (m, 3H), 2.00 – 1.83 (m, 1H), 1.60 (s, 2H), 1.29 (s, 2H), 1.06 – 0.90 (m, 9H), 0.21 (d, J = 7.1 Hz, 1H).

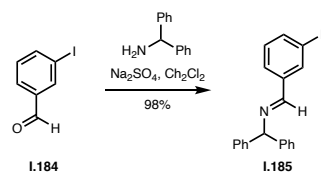


Bicyclic octamer **1.46**

To a suspension of **1.177** (26.0 mg, 0.028 mmol, 1.0 equiv) and HATU (0.094 mg, 0.248 mmol, 9.0 equiv) in 6.9 mL DMA was added DIPEA (0.046 mL, 0.262 mmol, 9.5 equiv). The resulting reaction mixture was stirred at ambient temperature for 12 h, after which the crude was directly concentrated and passed through a 0.2 μm syringe filter. The filtered mixture was purified by reversed-phase HPLC, using 0.1% TFA in water (solvent A) and 0.1% TFA in acetonitrile (solvent B). The desired product was isolated using a solvent gradient of 5-60% solvent B over 30 minutes. Product fractions were isolated and concentrated in vacuo to yield bicycle **1.46** (0.006 mg, 0.006 mmol, 20%) as a pale yellow oil.

^1H NMR (500 MHz, CD_3OD) δ 7.74 (d, J = 8.1 Hz, 1H), 7.25 (d, J = 7.8 Hz, 1H), 7.12 (t, J = 7.5 Hz, 1H), 7.04 (t, J = 7.5 Hz, 1H), 5.40 (s, 1H), 4.80 – 4.72 (m, 4H), 4.64 – 4.46 (m, 3H), 4.33 – 4.20 (m, 1H), 4.14 (dd, J = 17.3, 7.6 Hz, 2H), 4.03 (d, J = 17.8 Hz, 2H), 3.93 (d, J = 16.6 Hz, 3H), 3.75 (t, J = 11.3 Hz, 3H),

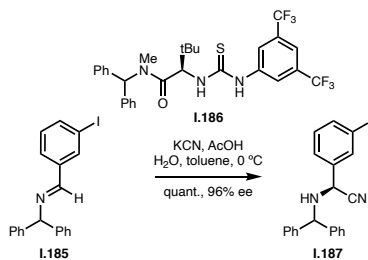
3.67 – 3.50 (m, 6H), 3.42 (d, $J = 15.0$ Hz, 2H), 3.37 – 3.27 (m, 69H), 3.27 – 3.13 (m, 4H), 3.11 – 2.93 (m, 2H), 2.92 (s, 1H), 2.64 – 2.46 (m, 2H), 2.42 (dd, $J = 13.1, 6.8$ Hz, 1H), 2.31 (d, $J = 2.3$ Hz, 2H), 2.07 (s, 2H), 1.77 – 1.55 (m, 5H), 1.29 (s, 8H), 1.21 – 1.15 (m, 2H), 1.07 (dd, $J = 7.2, 1.7$ Hz, 3H), 0.96 – 0.86 (m, 11H).



Imine I.185

Sodium sulfate (3.71 g, 26.1 mmol, 1.4 equiv) was added to a flame-dried reaction flask and suspended in 27.3 mL of CH_2Cl_2 . 3-iodobenzaldehyde (4.87 g, 21.0 mmol, 0.770 equiv) was added, followed by benzhydrylamine (5.00 g, 27.3 mmol, 1.0 equiv). The reaction flask was capped and allowed to stir at room temperature for 4 h. After completion of the reaction, the crude was filtered and directly concentrated before redissolving in CH_2Cl_2 and eluting through a silica plug using a solvent mixture of 9:1:0.1 hexane:EtOAc: NEt_3 . The eluted fractions were concentrated under reduced pressure to yield **I.185** (10.7 g, 26.8 mmol, 98%) as an off-white oil.

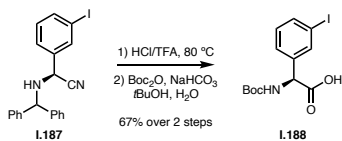
^1H NMR (500 MHz, CDCl_3) δ 8.32 (s, 1H), 8.23 (t, $J = 1.7$ Hz, 1H), 7.75 (dd, $J = 7.7, 1.8$ Hz, 2H), 7.41 – 7.36 (m, 4H), 7.36 – 7.30 (m, 4H), 7.25 – 7.21 (m, 1H), 7.15 (t, $J = 7.8$ Hz, 1H), 5.60 (s, 1H).



Aminonitrile I.187

A flask was charged with KCN (16.4 g, 25.2 mmol, 2.0 equiv) and 31.5 mL toluene and cooled to at 0 °C for 10 min under N₂. Acetic acid (0.86 mL, 15.1 mmol, 1.2 equiv) and water (0.91 mL, 50.3 mmol, 4.0 equiv) were added sequentially and the N₂ inlet was removed. The suspension was stirred at 0 °C for 20 min, after which the N₂ inlet was restored and a toluene solution of imine **I.185** (5.00 g, 12.6 mmol, 1.0 equiv) and **I.186** (0.146 g, 0.252 mmol, 0.020 equiv) was added over the course of several minutes. The flask containing the solution mixture was rinsed 3 times with additional toluene and the rinses were added to the reaction mixture. The N₂ inlet was removed and the mixture was allowed to stir at 0 °C for 24 h. The reaction was allowed to warm to room temperature and treated with () mL of a 0.2 g/mL aqueous K₂CO₃ solution. The mixture was transferred to a separatory funnel and after vigorous mixing and removal of the aqueous layer, the organic layer was washed with another portion of K₂CO₃ solution and then with brine. The organic layer was dried over sodium sulfate and concentrated under reduced pressure. The crude was purified by flash column chromatography (5-12% EtOAc in hexane). Product fractions were carefully cut, collected, and concentrated to yield **I.187** (5.34 g, 12.6 mmol, quantitative yield) as a clear oil. A sample of the product was determined to be 96% e.e. by chiral HPLC analysis (ChiralCel OD-H, 2% *i*PrOH in hexane).

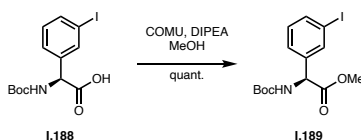
¹H NMR (500 MHz, CDCl₃) δ 7.89 (t, *J* = 1.9 Hz, 1H), 7.72 (dt, *J* = 7.9, 1.4 Hz, 1H), 7.58 – 7.49 (m, 3H), 7.44 (dt, *J* = 6.3, 1.2 Hz, 2H), 7.38 (t, *J* = 7.6 Hz, 2H), 7.35 – 7.27 (m, 3H), 7.26 – 7.21 (m, 3H), 7.15 (t, *J* = 7.8 Hz, 1H), 5.23 (s, 1H), 4.55 (d, *J* = 12.3 Hz, 1H), 2.14 (d, *J* = 12.1 Hz, 1H).



Carboxylic acid I.188

Aminonitrile **I.187** (0.200 g, 0.471 mmol, 1 equiv) was added to a reaction flask, followed by a 1:1 solution of TFA and 0.5 N HCl. The reaction flask was sealed and heated to 80 °C for 18 h. The reaction mixture was cooled to room temperature, transferred to a separatory funnel, and then washed with diethyl ether twice. The aqueous layer was then concentrated under reduced pressure, redissolved in 1.2 mL water, then basified to pH 10 using 1 N NaOH. The reaction mixture was warmed to room temperature and to the mixture was added 2.3 mL THF and Boc₂O (0.154 g, 0.704 mmol, 1.5 equiv). After consumption of starting material, the reaction mixture was cooled to 0 °C, acidified to pH 2-3, then extracted with diethyl ether. The reaction crude was purified by flash column chromatography (30% EtOAc in hexane with 1% acetic acid). Product fractions were cut, collected, and concentrated to yield **I.188** (0.124 g, 0.316 mmol, 67% over 2 steps) as an off-white foam.

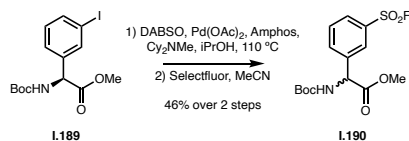
¹H NMR (500 MHz, CDCl₃) δ 11.89 (s, 1H), 7.75 (d, *J* = 17.7 Hz, 1H), 7.63 (dt, *J* = 7.9, 1.4 Hz, 1H), 7.38 (t, *J* = 9.0 Hz, 1H), 7.07 (t, *J* = 7.8 Hz, 1H), 5.04 (d, *J* = 5.2 Hz, 1H), 1.42 (s, 5H), 1.24 (d, *J* = 5.4 Hz, 5H).



Methyl ester **I.189**

To a solution of **I.188** (0.185 g, 0.490 mmol, 1.0 equiv) in 2.45 mL MeOH was added COMU (0.231 g, 0.540 mmol, 1.1 equiv), followed by DIPEA (0.094 mL, 0.540 mmol, 1.1 equiv). The reaction was allowed to stir at room temperature for 3 h and then quenched with saturated ammonium chloride. The aqueous layer was back extracted thrice with EtOAc and the combined organic layers were washed with brine and dried over sodium sulfate. The crude was concentrated under reduced pressure and then purified by flash column chromatography (15-25% EtOAc in hex) to yield **I.189** (0.192 g, 0.490 mmol, quantitative yield) as a white foam.

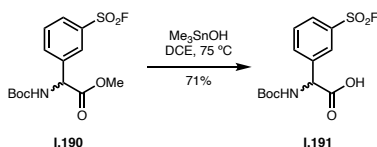
^1H NMR (500 MHz, CDCl_3) δ 7.69 (s, 1H), 7.64 (d, $J = 7.9$ Hz, 1H), 7.33 (d, $J = 7.8$ Hz, 1H), 7.07 (t, $J = 7.8$ Hz, 1H), 5.64 (d, $J = 7.4$ Hz, 1H), 5.25 (d, $J = 7.3$ Hz, 1H), 3.71 (s, 3H), 1.42 (s, 7H).



Sulfonyl fluoride **I.190**

I.189 (0.265 g, 0.677 mmol, 1.0 equiv), DABSO (0.0977 g, 0.406 mmol, 0.6 equiv), $\text{Pd}(\text{OAc})_2$ (0.0076 g, 0.0339 mmol, 0.05 equiv), AmPhos (0.018 g, 0.0677 mmol, 0.10 equiv), were all added to a pressure tube and suspended in 6.77 mL of $i\text{PrOH}$. N,N -dicyclohexylmethylamine (0.435 mL, 2.03 mmol, 3 equiv) was added and the reaction vessel was sealed and heated to 110°C . The reaction was allowed to stir at temperature for 1 h, after which the mixture was cooled and Selectfluor (0.432 g, 1.22 mmol, 1.8 equiv) and 0.153 mL of MeCN was added. The reaction was stirred at room temperature for 3 h and then filtered through a pad of celite. The flowthrough was washed with saturated aqueous sodium thiosulfate followed by brine. The organic layer was concentrated under reduced pressure and then purified via flash column chromatography (25% EtOAc in hexane) to yield **I.190** (0.110 g, 0.317 mmol, 46% over 2 steps) as an off-white solid.

^1H NMR (500 MHz, CDCl_3) δ 8.01 (t, $J = 1.9$ Hz, 1H), 7.95 (d, $J = 8.0$ Hz, 1H), 7.82 (d, $J = 7.9$ Hz, 1H), 7.63 (t, $J = 7.9$ Hz, 1H), 5.88 – 5.83 (m, 1H), 5.44 (d, $J = 6.7$ Hz, 1H), 3.75 (s, 3H), 1.42 (s, 9H).



Carboxylic acid **I.191**

I.190 (0.110 g, 0.317 mmol, 1.0 equiv) was dissolved in 3.17 mL DCE. Me_3SnOH was added and the reaction flask was sealed and heated 75 °C. The reaction mixture was stirred for 2 h after which the reaction was quenched with 1 N HCl. The organic layer was washed with water thrice followed by brine. The organic layer was concentrated under reduced pressure and then purified by flash column chromatography to furnish **I.191** (0.075 g, 0.225 mmol, 71%) as a white solid.

^1H NMR (500 MHz, CDCl_3) δ 8.17 – 8.12 (m, 1H), 8.07 (d, $J = 12.9$ Hz, 1H), 7.98 (d, $J = 7.9$ Hz, 1H), 7.87 (d, $J = 7.8$ Hz, 1H), 7.65 (t, $J = 7.9$ Hz, 1H), 5.25 (d, $J = 4.5$ Hz, 1H), 1.21 (s, 9H).

Chapter 3: An introduction to cycloheximide

3.1. Cycloheximide: overview

Cycloheximide (CHX, **2.1**, **Figure 3.1 A**), also known as naramycin A or actidione, is a reversible, small molecule inhibitor of eukaryotic ribosomes^{51,52}. CHX binds to the exit site (E-site) of actively elongating ribosomes, blocking tRNA translocation and leading to polysome stabilization^{53,54}. Originally isolated from the gram-positive bacterium *Streptomyces griseus* in 1946, CHX has gained considerable notoriety due to its wide antifungal activity and extensive use as a biochemical tool for studying protein synthesis. CHX is limited to employment in an *in vitro* setting due to its toxicity and mutagenicity; its use as an agricultural fungicide has noticeably declined as the health risks associated with the natural product have become better understood. Nevertheless, the molecule remains one of the of the most well-known glutarimide natural products.

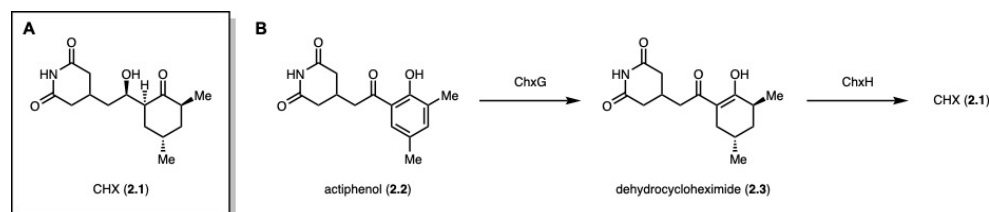


Figure 3.1. A and B) The biosynthesis of cycloheximide (CHX, **2.1**) is believed to proceed through the synthesis of actiphenol (**2.2**), another glutarimide-containing natural product that shares the same carbon framework as CHX.

The biosynthesis of CHX is governed by an acyltransferase-less (AT-less) type I polyketide synthase (PKS). Cloning, sequencing, and characterization of a gene cluster from the *Streptomyces* species YIM65141 revealed 10 genes within the *chx* cluster that encode for the following: an acyl carrier protein (ChxC), an amidotransferase for glutarimide synthesis (ChxD), an acyltransferase (ChxB), the AT-less type I PKS for polyketide backbone synthesis (ChxE), an enoylreductase (ChxG), a ketoreductase (ChxH), a cytochrome P450 oxidoreductase (ChxI), a carboxylic acid reductase (ChxJ), and two regulator proteins (ChxA and ChxF). The same machinery is also credited with the production of actiphenol, a related

compound that contains a phenol in lieu of the cyclohexanone and displays weak inhibitory activity against translation despite housing the same carbon skeleton as cycloheximide (**Figure 3.1 B**)⁵⁵. Given the co-production of the inhibitors in several *Streptomyces* species, the biosynthesis of CHX is believed to proceed through a phenol-to-cyclohexanone reduction that necessitates ChxG and ChxH. However, further details of the tailoring steps to produce CHX from actiphenol have yet to be elucidated.

3.2. Mechanism of action

Despite the historic and widespread use of CHX for protein and translational studies, the inhibitor's binding site within the ribosome was not known until relatively recently. A report from Jun Liu's lab at Johns Hopkins published in 2010 detailed a series of footprinting experiments showing that both CHX and the structurally related lactimidomycin (LTM, **2.4**) protect a single cytidine nucleotide (C3993) in the E-site of the 60S ribosomal subunit and were therefore proposed to share the same binding pocket⁵⁴.

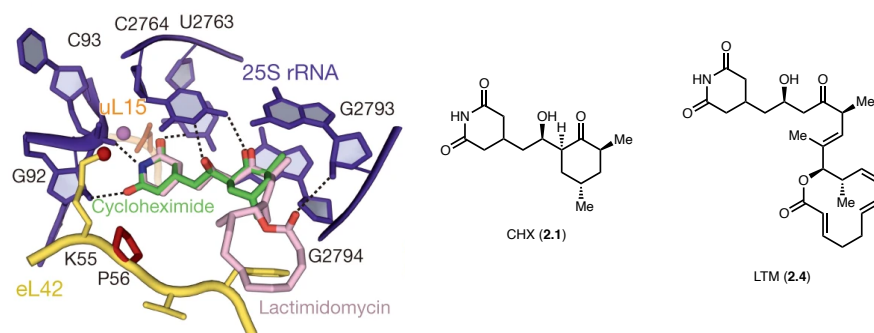


Figure 3.2. X-ray crystallography structures of CHX (green) overlaid with LTM (pink) binding within the same E-site pocket of the 80S ribosome from *S. cerevisiae*. Reproduced with permission from Schneider-Poetsch *et al*⁵⁶.

Cross resistance to yeast L28 mutants provided further corroboration to this claim. The results gleaned by Schneider-Poetsch *et al.* were a monumental step forward in determining both the probable binding site as well as proposing a mechanistic model for the action of CHX, despite the lack of structural data of inhibitor-ribosome complexes. The work published by the Liu lab was later validated by the crystal structure

determination of the *S. cerevisiae* 80S ribosome in complex with a suite of inhibitors, including CHX (**Figure 3.2**)⁵⁶.

A particular focus on eukaryote-specific inhibitors revealed that despite the chemical diversity of the compounds, all were found in close proximity to either mRNA or tRNA binding sites as opposed to the peptide exit tunnel (a more common binding site for bacterial antibiotics). CHX and LTM were found to bind in the large ribosomal subunit E-site, forming contacts with the universally conserved nucleotides of the 25S rRNA and a portion of the eukaryote-specific eL42 protein. It is noteworthy that the glutarimide and the secondary hydroxyl of both inhibitors form crucial hydrogen bond interactions within the pocket, while fewer concrete small molecule-protein contacts are explicitly detailed regarding the cyclohexanone of CHX and the macrolactone of LTM.

The E-site accommodates deacylated tRNAs after peptide bond formation, but before their release in the cytoplasm. Relative to the A- and P-site, the E-site is the most diverse across species. The presence of two rRNA residues specific to the bacterial E-site is believed to occlude the binding of LTM and possibly CHX as well, possibly explaining the selectivity of these E-site inhibitors for eukaryotic ribosomes. The impressive work of de Loubresse *et al.* included solving the structure of the yeast ribosome in complex with the tri-nucleotide CCA to recapitulate the acceptor end of the deacylated tRNA⁵⁶. Given the structure of CHX and LTM complexes, the glutarimide inhibitors were believed to compete with the binding of the tRNA CCA-end, occluding the association of the E-site's natural substrate. Kinetic experiments using a proflavin labelled tRNA support a competitive binding mode for both CHX and LTM, in which pre-incubation with either inhibitor abrogated the rate of tRNA binding. Curiously, these results were at odds with the conclusions drawn by the Liu lab regarding their own of E-site binding studies using radioactively labeled deacylated tRNAs, in which CHX is not believed to interfere with tRNA-ribosome association⁵⁴. As it stands, our current understanding of the precise binding mode of CHX remains incomplete.

3.3. Related eukaryotic translation inhibitors

In addition to CHX, there are several notable small molecule inhibitors of eukaryotic protein synthesis. Given the potential of translation inhibitors for both biochemical and therapeutic use, considerable interest in their mechanism of action and derivatization has persisted. While CHX is perhaps the most famous of the

glutarimide-containing natural products, several structurally related compounds include the aforementioned LTM, as well as migrastatin (**2.5**), isomigrastatin (**2.6**), and dorrigocin A and B (**2.10**) (**Figure 3.3**). However, only LTM and isomigrastatin are shown to actively inhibit eukaryotic protein synthesis; furthermore, only LTM shares the same E-site binding pocket as CHX^{54,56}. Other known E-site inhibitors include phyllanthoside (**2.8**) and chlorolissoclimide (**2.9**), both of which adopt a similar binding interaction to the glutarimide compounds, despite their drastically dissimilar chemical structures.

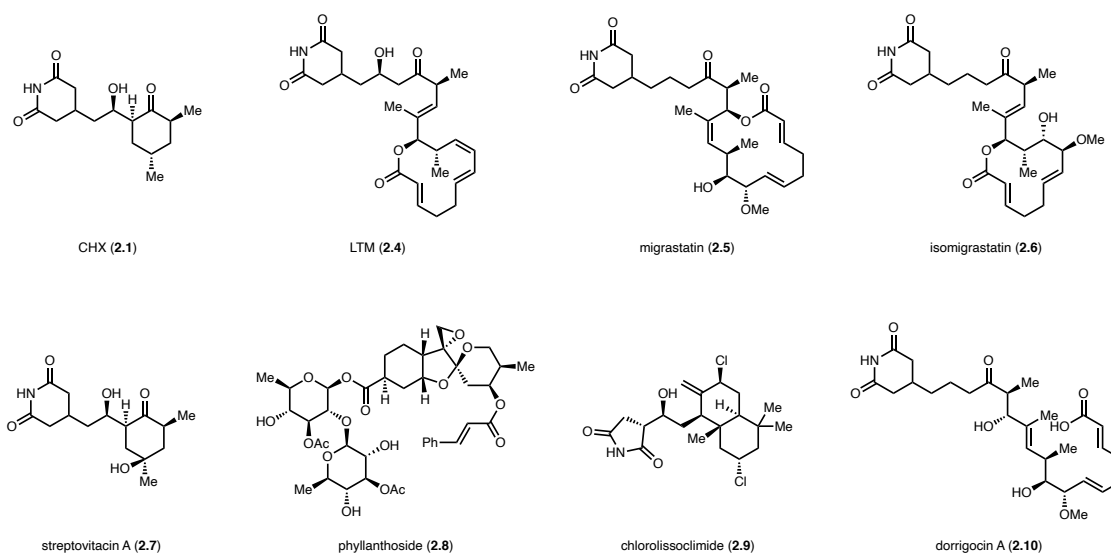


Figure 3.3. Chemical structures of several ribosome-targeting natural products.

Although CHX and LTM share the same ribosomal binding pocket, disparate polysome profiles suggest a mechanistic difference between the inhibitory action of the two compounds; while CHX is known to stabilize polysomes, LTM does not. In line with this assumption, toeprinting assays revealed that CHX allows a single translocation process before freezing ribosomal elongation, whereas LTM halts ribosomal translation at the start codon without completing a full round of elongation. However, much like CHX, there are several aspects of LTM's mechanism of action that remain a mystery. Of particular note (due to our own vested interest in the binding mode of CHX) is the lack of knowledge regarding the exact structural features that cause such a marked disparity in the inhibition of CHX vs. LTM, despite residing in the same ribosomal binding pocket with similar conformational profiles.

Like CHX, LTM inhibits eEF2-mediated translocation, though is at least tenfold more potent. Unsurprisingly, the difference in activity is mostly attributed to the sterically demanding 12-membered macrocycle housed within LTM's structure, which plausibly forms a larger network of interactions within the binding pocket due to the expanded carbon frame. The macrocycle is believed to occlude tRNA access to the E-site in a manner that is not possible by CHX; conversely, the inability of LTM to freeze actively elongating ribosomes is most likely due to its inability to access the E-site in the presence of a deacylated tRNA, leading to a depletion of polysomes.

In addition to LTM, we were also intrigued at the activity of streptovitacin A, another known natural product glutarimide (**2.7**). Identical to CHX apart from an additional hydroxyl group at carbon 13, streptovitacin A is also known to freeze polysomes upon inhibiting translation. As of the writing of this current work, there is no published structure of streptovitacin A in complex with the eukaryotic ribosome; however, it is reasonable to believe that the small molecule occupies the same binding pocket as CHX given their near identical chemical structures.

3.4. Biochemical applications of CHX

Translation inhibitors have long been employed as biochemical tools to study protein synthesis, and CHX in particular has been utilized as one of the *de facto* compounds used for measuring protein half-lives. To this day, performing a cycloheximide chase is one of the most common methods of determining protein stability in eukaryotic cells⁵⁷. More recently, the utility of CHX as a translational inhibitor has been underscored even further by its use in ribosome profiling^{58,59}.

There are several well-established methods that can be used to probe ribosome-mediated translation. The most direct method involves looking at the translation output itself, such as fluorescent tagging of newly synthesized polypeptides or proteomic mass spectrometry-based analysis. However, the advent of mRNA profiling and deep sequencing has led to the development of techniques that allow us to study the process of translation from the perspective of the mRNA template, as opposed to the protein product. Ribosome profiling, a deep-sequencing method that provides a snapshot of global translation *in vivo*, has served as an invaluable tool for studying one of the fundamental processes of molecular biology. First reported in 2009, ribosome profiling relies on the use of a small molecule inhibitor to freeze actively

elongating ribosomes (**Figure 3.4**). After isolating the ~30 nucleotide ribosome-protected fragments and converting the mRNA into a DNA library, global density maps of where the ribosome was translating as a single moment in time can be generated with subcodon resolution.

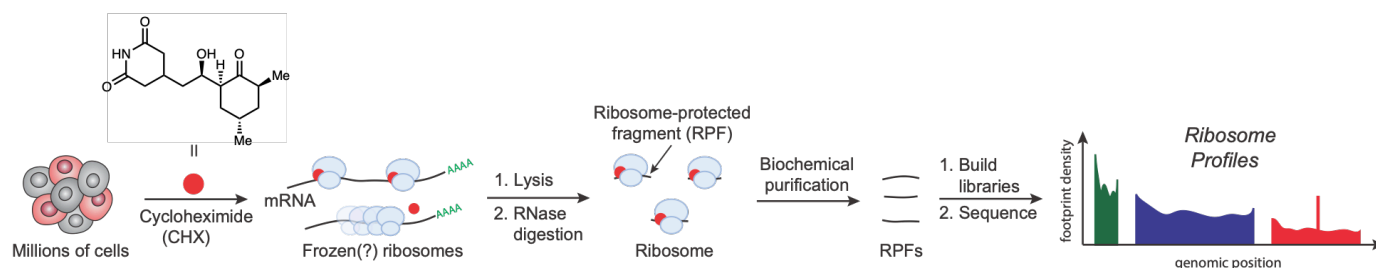


Figure 3.4. Simplified workflow of ribosome profiling. This deep-sequencing technique is reliant on the use of a small molecule inhibitor of translating ribosomes to produce a snapshot of translation.

Quantifying genome-wide rates of protein synthesis via ribosome profiling requires a suitable translation inhibitor. CHX is often employed due to its ability to stabilize the polysomes residing on the mRNA template (in contrast to an inhibitor such as LTM, which cannot freeze actively elongating ribosomes and therefore allows the protein to run off the RNA strand). There are some precautions to be noted upon the use of CHX for ribosome profiling; CHX-induced ribosomal inhibition is reversible, and therefore the drug must be included in all buffers to ensure translation does not restart before isolation of the mRNA footprints. However, even high concentrations of drug are not enough to completely stall elongation over the course of the experiment, which ultimately results in dose- and time-dependent biases^{60,61}. Regardless of the drug used, codon-level ribosome profiles are susceptible to distortion due to an accumulation of ribosomes at transcript positions that are more sensitive to the small molecule⁵⁹.

3.5. Previous total syntheses of CHX

At the time of this project's inception, there had been only one prior publication regarding the synthesis of CHX, reported in 1966 by Johnson and coworkers⁶². While the authors also boast a route to the optically active *l*-cycloheximide, the starting material is derived from the natural product itself. Previous attempts to

access CHX were unfruitful, mainly due to lack of knowledge regarding the absolute stereochemistry of the natural product. However, CHX presents a synthetically difficult target even with full knowledge of its structure; these difficulties are addressed by Johnson *et al.* as follows: first, the sensitivity of the molecule to both acidic and basic conditions (mostly attributed to the glutarimide moiety); second, the stereoselective installation of the C8 hydroxyl; and third, the installation of the axial methyl group at C13.

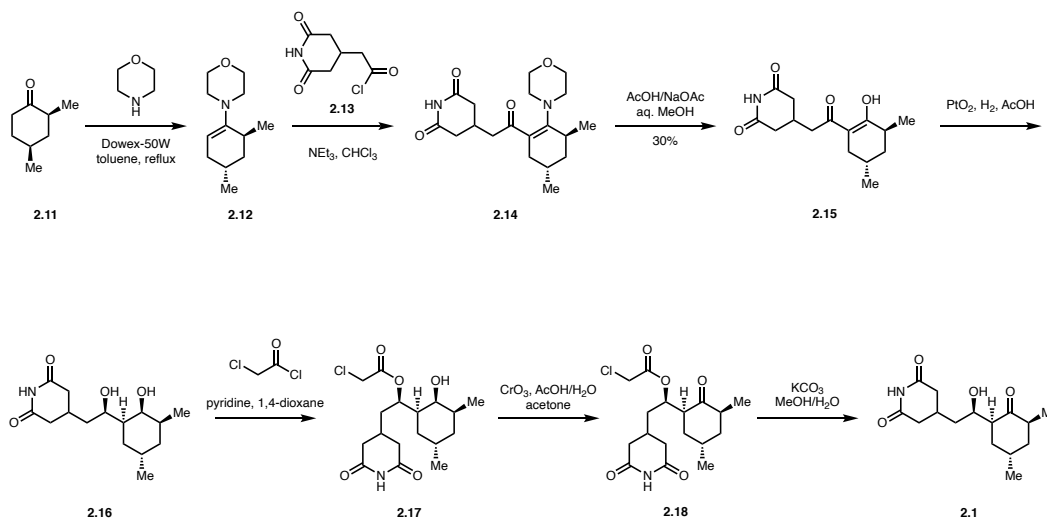


Figure 3.5. The first reported total synthesis of CHX, credited to Johnson and coworkers⁶².

With these points in mind, the total synthesis of CHX commenced with the reduction of 2,4-dimethylphenol to *cis*-2,4-dimethylcyclohexanone. Treatment with morpholine and Dowex-50W resin in refluxing toluene afforded enamine **2.12**; critically, epimerization at the C2 position allowed access to the *trans* isomer. Acylation using 3-glutarimidylacetyl chloride was performed in chloroform and triethylamine, which was directly hydrolyzed to yield intermediate **2.15**. Reduction to dihydrocycloheximide was performed in anticipation of capping the secondary hydroxyl. Acylation of the secondary hydroxyl was carried out with chloroacetyl chloride; Johnson and coworkers noted that hydrolysis of the ester resulting from protection with the simpler acetyl chloride was not possible without destroying the rest of the molecule. Following acylation, oxidation of the secondary alcohol with chromium trioxide and finally hydrolysis of the chloroacetyl

ester furnished racemic cycloheximide. The same route was used to generate the enantiopure isomer as well upon commencing the synthesis with optically pure *cis*-2,4,-dimethylcyclohexanone (**Figure 3.5**).

We found replication of the above synthesis to be difficult, and more importantly, not greatly amenable to late-stage derivatization at C11 and C13. Previously published work from our lab successfully devised a more versatile route to CHX and related analogues, laying the foundation for further mechanistic explorations of the natural product⁶³.

3.6. CHX: our goals and interests

By the time I had joined this project, the total synthesis of CHX and analogues had already been developed by Park and coworkers. The SAR uncovered by the Liao lab's previous paper revealed several CHX analogues with increased potency due to derivatization at the C13 position and we took particular interest in uncovering the specific interactions that mediate this elevated binding affinity to the ribosome. Additionally, we were intrigued at expanding the current repertoire of elongation inhibitors suitable for ribosome profiling; furthermore, we surmised that development of an effectively irreversible inhibitor would circumvent some of the drawbacks that accompany the use of CHX for this powerful biochemical assay.

The following chapters will aim to summarize the work performed by Park and coworkers as a foundation for the mechanistic exploration of the C13 CHX analogues. We will then segue into the structural and sequencing-based experiments that were performed in an effort to elucidate the binding mode of these potent elongation inhibitors. Finally, we will end with possible future inquiries relating to both CHX as well as other intriguing natural product translation inhibitors.

3.7. Laying the groundwork: the total synthesis of cycloheximide and analogues

The Liao lab's 2019 publication on the synthetic route to CHX and analogues accomplished several key goals that led to the project in its current form, the most prominent being the successful formulation of a robust total synthesis that allowed access to CHX and derivatives (and a marked improvement over the previous report by Johnson and coworkers)^{62,63}. Moreover, the versatility of the devised route allowed generation of analogues modified at the C11 and C13 centers. A noticeable dearth of knowledge regarding

the impact of the cyclohexanone methyl groups spurred us to devise a route that allowed late-stage stereodivergent installation of C11 and C13 for our own SAR interrogation.

Of course, our interest in CHX was not born purely from a desire to fill the gaps of currently available SAR and structural data. We took interest in exploring the functional group flexibility of the CHX cyclohexanone with an eye towards further functionalizing the molecule to enhance its utility for techniques such as ribosome profiling. The following chapter will summarize the work performed by Park *et al.* and elaborate how our findings set the foundation for further structural inquiry regarding CHX and related derivatives.

3.8. The synthetic route to CHX

Unsurprisingly, the quest to develop a synthetic route to CHX was fraught with numerous difficulties. Despite its deceptively innocuous appearance, CHX contains four stereocenters in tight proximity as well as a sensitive glutarimide moiety that is quick to decompose in response to strong acid or base. Our route was devised with several points in mind: first, that the glutarimide and C8 hydroxyl group would remain untouched due to their established importance for inhibitory activity; and second, that assembly of the cyclohexanone and its substituents should occur relatively late stage for ease of derivatization.

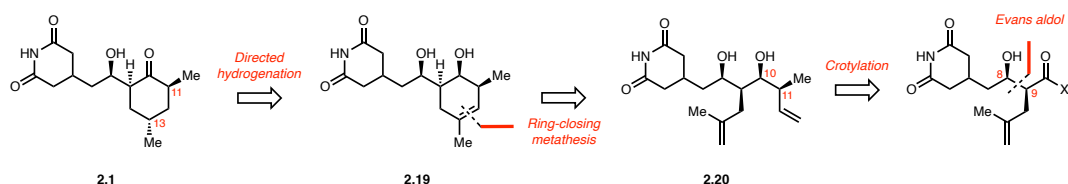


Figure 3.6. Retrosynthetic analysis for CHX and analogues. Figure reproduced from Park *et al.*

The final retrosynthetic scheme of the molecule is as follows is shown in **Figure 3.6**, which pinpoints cyclohexene **2.19** as a key intermediate; directed hydrogenation allows access to the natural product upon establishing the stereochemistry of the C13 methyl. However, one can imagine that the alkene can be leveraged for the installation of other functionalities. We envisioned that the cyclohexene could be obtained via ring closing metathesis of **2.20** following a diastereoselective crotylation. Finally, the C8 and C9 centers

were to be installed via an Evans *syn* aldol, which additionally secures the early incorporation of the glutarimide moiety.

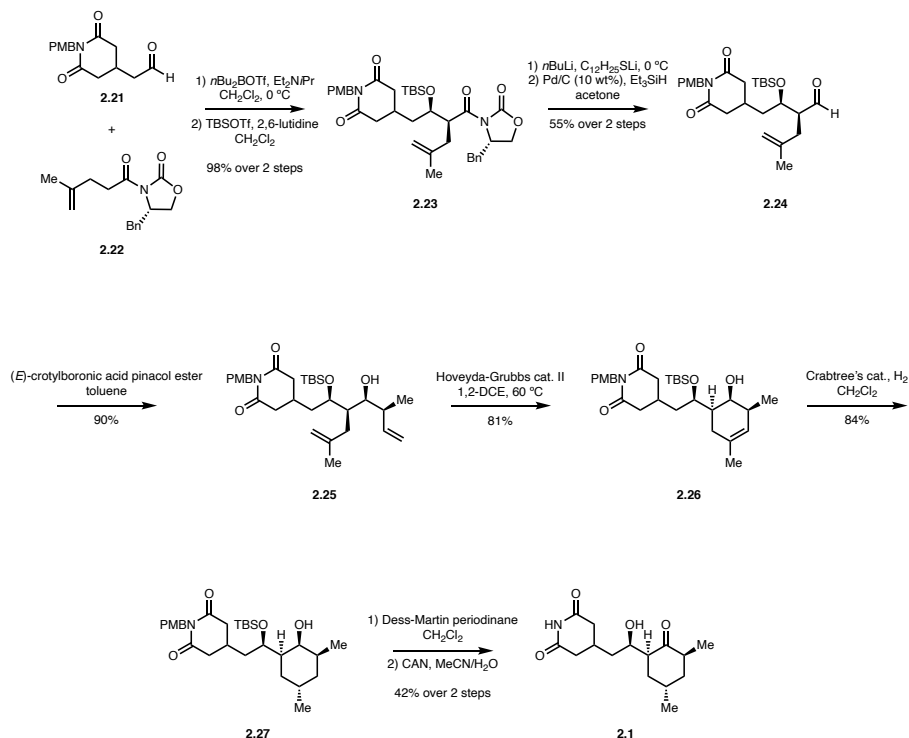


Figure 3.7. The total synthesis of CHX reported by Park and ⁶⁷coworkers. Figure reproduced from Park *et al.*

In the forward direction, the synthesis commenced with the synthesis of *N*-acetyl oxazolidinone **2.21** and *N*-PMB imide **2.22** in anticipation of the Evans aldol reaction, each obtained in a 3-step sequence from commercially available starting materials (**Figure 3.7**). The resulting aldol product was swiftly protected as the TBS ether. Conversion to the thioester using a lithium thiolate followed by Fukuyama reduction smoothly furnished aldehyde **2.24** in anticipation of diastereoselective crotylation employing *trans*-crotylboronic acid pinacol ester to establish the C10 and C11 centers of homoallylic alcohol **2.25**. RCM was performed to obtain cyclohexene **2.26**. Directed hydrogenation using Crabtree's catalyst set successfully installed the C13 methyl group in the desired configuration. Dess-Martin oxidation of the C10 alcohol followed by global

deprotection using ceric ammonium nitrate (CAN) completed the synthesis of CHX in 10% yield and 12 steps from commercially available 2-(2,6-dioxopiperidine-4-yl)acetic acid.

3.9. Analogue generation and assessment

The established route was easily amenable to accessing analogues with altered C11 and C13 substituents (**Figure 3.8**). Modification of the diastereoselective addition to aldehyde **2.24** allowed access to several C11-modified derivatives, including the C11 epimer (**2.28**) and desmethyl compounds (**2.30**). Similarly facile was obtaining the C13 epimer **2.31** by use of palladium on carbon in place Crabtree's catalyst for the directed hydrogenation of cyclohexene **2.26**.

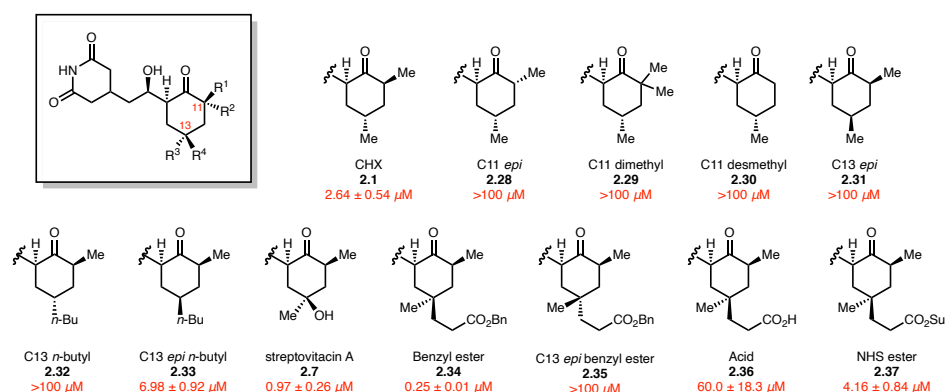


Figure 3.8. CHX analogues synthesized by Park *et al.* IC₅₀ values are shown in red. Figure reproduced from Park *et al.*⁶⁶

Compound assessment was performed using a cell-based translation assay, wherein incorporation (or lack thereof) of *O*-propargyl puromycin was used to measure inhibitory activity. To our surprise, we found the majority of compounds to be inactive. Inversion or ablation of the C11 methyl group abolished translation inhibition, as did the addition of a second methyl group; inversion at the C13 center produced a similarly inactive analogue. Replacement of the C13 methyl group with an *n*-butyl (**2.32**) was also debilitating to compound activity. Curiously, we found that inhibitory activity was recovered upon positioning

the *n*-butyl group pseudoequatorially (**2.33**), producing one of the only analogues that retained the translation inhibition of the parent compound in the initial SAR effort.

We reasoned that the unexpected results of our analogue assessment may result from an incomplete picture regarding the interactions of CHX with the ribosome binding pocket. While the crystal structure produced by de Loubresse *et al.* indicate a relatively open area surrounding the cyclohexanone (and thus fueled our initial belief that modification at C11 and C13 should be possible with little impact on binding affinity), the intolerance of the ring substituents to derivatization made us reexamine the interactions driving CHX-mediated inhibition. We surmised that the C11 and C13 methyl groups of CHX may be recapitulating binding pocket contacts that are shared among other known E-site inhibitors. LTM contains two methyl groups that mirror those of CHX; likewise, the C2 chloride of chlorolissoclimide and the C11 methyl of phyllanthoside are oriented in a similar manner to that of the C11 methyl of CHX. A more detailed inspection of the ribosome E-site led us to believe that contact with G4370, G4371, and RPL36a Phe56 within the E-site may be a requisite for retaining the inhibitory activity of CHX.

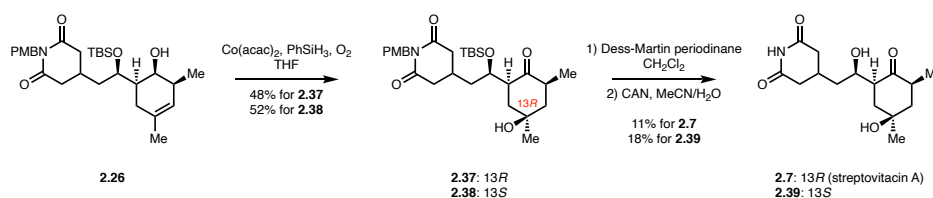


Figure 3.9. The synthesis of streptovitamin A (**2.7**) from intermediate **2.26**. Figure reproduced from Park *et al.*

Our cursory examination of other E-site inhibitors also brought another natural product to our attention. The elongation inhibitor streptovitamin A is identical to CHX in all respects except for the additional hydroxyl appended to the C13 position. Noteworthy is the observation that the C13 methyl group of streptovitamin A retains the same configuration as that found in CHX. Given the wealth of inactive CHX analogues we had thus far produced, we concluded that incorporation of an additional substituent at C13 of CHX – leaving the pseudoaxial methyl group untouched – was the most viable strategy for accessing active CHX analogues. Towards this goal, we commenced with our own synthesis of streptovitamin A and

C13-*epi*-streptovitamin A using the previously described route (**Figure 3.9**), wherein Mukaiyama hydration of cyclohexene **2.26** afforded tertiary alcohols **2.37** and **2.38** as a 1:1 diastereomeric mixture. Oxidation to the cyclohexanone followed by global deprotection were performed as previously described. As expected, streptovitamin A showed inhibitory activity against translation, boasting a calculated IC₅₀ of 0.97 ± 0.26 μM.

Drawing inspiration from streptovitamin A, we moved forward with producing synthetic derivatives with additional functional groups appended to the C13 center. We were delighted to find that cyclohexene **2.26** could be further exploited as a useful synthetic intermediate upon installation of a quaternary center through a radical-mediated cross coupling reaction (**Figure 3.10**).

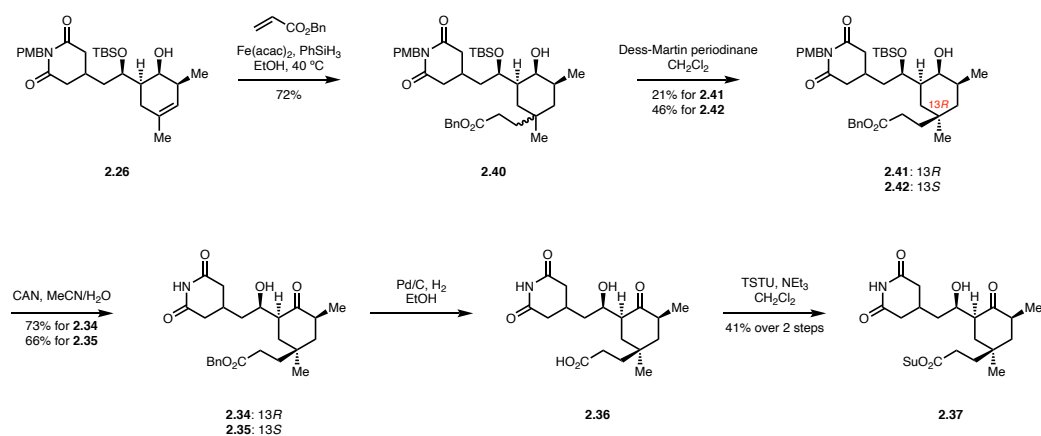


Figure 3.10. Synthesis of benzyl esters **2.34** and **2.35** and NHS ester **2.37**. Figure reproduced from Park *et al.*

Hydrogen atom transfer to cyclohexene **2.26** followed by the addition of benzyl acrylate resulted in a 2:1 diastereomeric mixture of quaternary functionalized intermediate **2.40**. Oxidation to the cyclohexanone allowed for separation of the diastereomeric mixture, which were then separately subjected to global deprotection to furnish benzyl esters **2.34** and **2.35**. Upon evaluation of the C13 functionalized benzyl esters, we found **2.34** to be approximately an order of magnitude more potent than CHX itself; in line with our expectations, diastereomer **2.35** was not active against translation. The increased potency demonstrated by the active diastereomer further bolstered our supposition that CHX derivatives elaborated at the C13 position may be driven by stabilizing interactions that mirror those of the macrolactone of LTM

within the ribosome E-site. Intrigued at this possibility, we converted active benzyl ester **2.34** to the NHS ester **2.37** over a two-step sequence, furnishing a CHX derivative functionalized with a covalent handle and with comparable inhibitory activity to the parent compound. With this, we obtained a potentially irreversible inhibitor of protein synthesis that could furthermore be leveraged as a probe to identify specific interactions within the binding pocket of the E-site with the C13-derivatized CHX analogues that may account for the increased potency demonstrated by benzyl ester **2.34**.

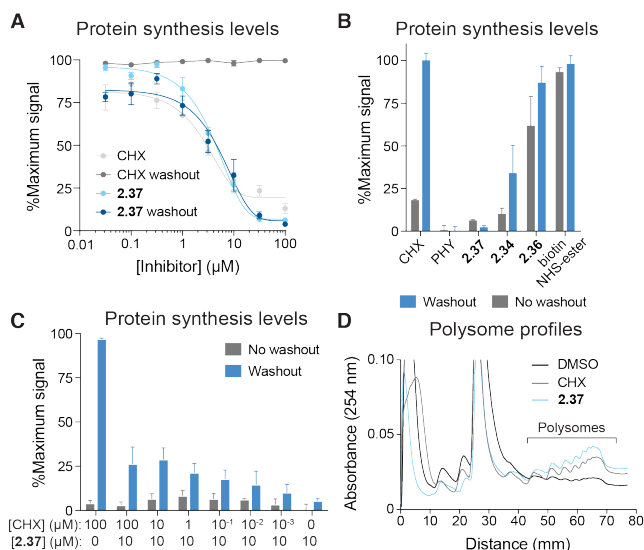


Figure 3.11. A) Dose-response curves of relative protein synthesis levels for CHX and **2.37** after being retained or washed out from cell media. **B)** Relative protein synthesis levels after compound treatments (100 μM) are retained or washed out. **C)** Relative protein synthesis levels after co-treatment with CHX and **2.37** at various doses. Cells were preincubated with CHX for 5 min before addition of **2.37**. **D)** Polysome profiles obtained from 293T cells treated with vehicle (0.1% DMSO), CHX (100 μM), or **2.37** (100 μM) for 90 min. Figure reproduced from Park *et al.*

Performing OPP-translation assays after inhibitor washout allowed us to determine whether NHS ester **2.37** irreversibly inhibited protein synthesis. We found that inhibitory activity was maintained when treating cells with **2.37**, in contrast to the recovery of protein synthesis levels in CHX-treated cells that is observed upon washout (**Figure 3.11 A and C**). Furthermore, these effects could not be attributed to either

hydrolysis of **2.37** or nonspecific effects of an NHS ester (**Figure 3.11 B**). Polysome profiles of drug-treated cells indicated that **2.37**-mediated translation maintains the integrity of the polysome unlike that of LTM and phyllanthoside (**Figure 3.11 D**). From this data, we concluded that NHS ester **2.37** mediates ribosomal inhibition in a similar manner to CHX in all respects aside from the effectively irreversible nature of the synthetic derivative. While further exploration of the activity of analogue **2.37** was conducted via IP-MS experiments, the only identified adducts formed with RPL36a were located outside the CHX binding pocket. Acylation of Lys22 by **2.37** was observed but was suspected to not hold mechanistic significance with regards actual binding mode of the analogue.

3.10. Curious behavior at carbon 13

While the effective irreversibility of NHS ester analogue **2.37** was expected given the analogue's covalent functionality, performing the same washout assay with benzyl ester **2.34** produced results that presented a point of peculiarity. We noted that inhibitor washout of cells treated with the benzyl ester compound did not fully restore protein synthesis levels. We attributed most of this activity to the increased potency relative to CHX, but our curiosity was piqued at the possibility of a more beguiling reason underlying the reluctance of the benzyl ester analogue to exit the E-site binding pocket. With the total synthesis of CHX and analogues now completed, we turned our attention to generating a more varied compound library. The SAR uncovered by Park and coworkers gave us a clear direction with regards to the modifications that were tolerated by the parent compound. Therefore, the next leg in this journey focused solely on producing and characterizing analogues derivatized at C13.

Chapter 4: Semi-synthetic route to CHX C13-amido analogues

4.1. Introduction: how to access C13-functionalized CHX analogues

While we were pleased with the goals accomplished with the 2019 publication of Park *et al.*, there were unsurprisingly several questions that remained in the wake of our lab's initial publication on the total synthesis of CHX and analogues. Our SAR of CHX revealed that the cyclohexanone was unexpectedly inflexible to modification, especially with regards to the C11 methyl group. However, we did find that installation of a quaternary center at the C13 center did allow resulting analogues to retain the inhibitory action of the parent compound, provided that the configuration of the methyl group remained pseudoaxial. Intriguingly, we found that in some cases, these C13-derivatized analogues had both increased potency as well as a reluctance to exit their respective binding site (putatively the ribosome E-site pocket). And while these effects may simply be explained through a general increase in lipophilicity, our interest was roused. The natural course of action to address our curiosities was a more thorough exploration of the C13-functionalized CHX analogues.

Of course, the issue of how to execute the library generation of such analogues was our primary concern. It was not outside the realm of feasibility to utilize the route developed by Park and coworkers; however, the synthetic route was developed with versatility in mind. Furthermore, completing the synthesis is not a trivial task – generation of NHS analogue **2.37** is a linear 12 step sequence with an overall 2.5% yield. Given the results of our initial SAR wherein we no longer saw derivatization at C11 as a viable option, we wondered if the versatility of the route could be abandoned in favor of step economy. We thus set out on devising a streamlined route towards C13-functionalized CHX analogues that would allow for rapid library generation. The following chapter encompasses text and figures from a pending publication⁶⁴ that is reproduced with consent from the co-authors.

4.2. A semi-synthesis of C13-amido CHX derivatives

Our desires for a streamlined route came to fruition in the form of a du Bois amination. A 2013 publication by Roizen and coworkers report the rhodium-mediated amination of tertiary C-H bonds, and furthermore included cycloheximide as part of their substrate scope⁶⁵. We delightedly exploited the stereospecific amination, finding it to be both extremely scalable in addition to its brevity. Starting from the natural product,

the C8 hydroxyl group of CHX was capped as a TMS ether before being subjected to intermolecular C-H amination. As reported by Roizen *et al.*, we found that the aryl sulfamate was indeed installed at the C13 of CHX to afford a single diastereomer, attributing the steric congestion surrounding the other tertiary C-H bonds to the selectivity of the insertion. Global deprotection of the aryl sulfamate furnished amine **2.45** in anticipation of further functionalization via amide bond formation (**Figure 4.1**).

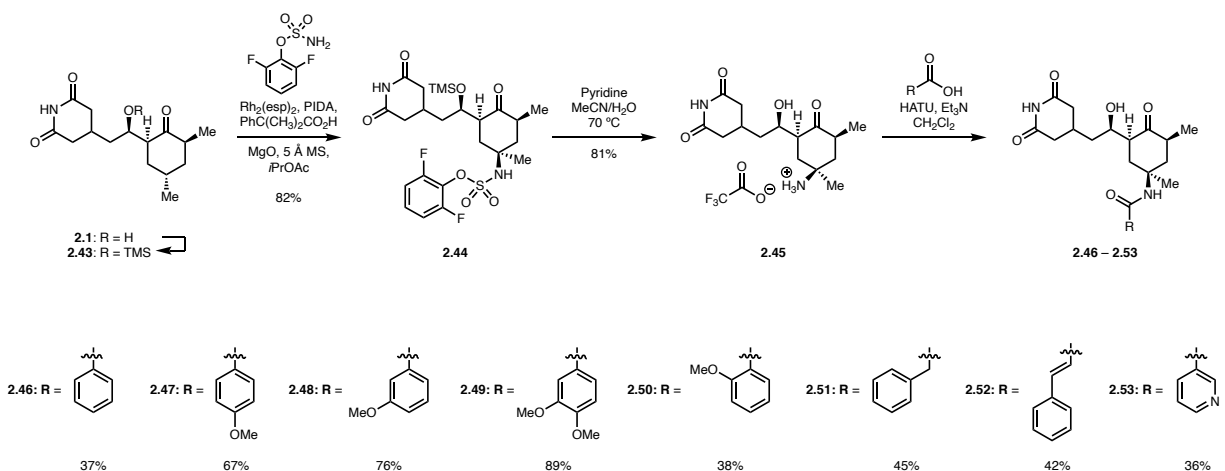


Figure 4.1. A semisynthetic route to CHX derivatives that employs a stereoselective C-H amination.

Leveraging this stereoselective C-H amination followed by *N*-acylation of the resulting CHX amine, we were able to generate a library of C13-amido CHX analogues in a rapid and facile manner. *In vivo* assessment showed that many of these amide derivatives were active against translation (**Figure 4.2**). Of note was the extremely potent CHX benzamide compound **2.46**, which boasts a calculated IC₅₀ of 63 nM, which is approximately 40 times more active than CHX in halting protein synthesis. Furthermore, our in-cell translation assays indicated that like benzyl ester and NHS ester analogues **2.34** and **2.37**, the effects of **2.46**-induced translation inhibition are not completely reversed upon inhibitor washout. This was corroborated by the results of polysome profiling cells after treatment with benzamide **2.46**, which appears to stabilize polysomes to a similar manner as the parent compound. However, it is noteworthy that the integrity of the polysome could be achieved with a single dose of **2.46** in comparison to the high concentrations of CHX needed in all buffers post cell lysis due to its rapidly reversible inhibition.

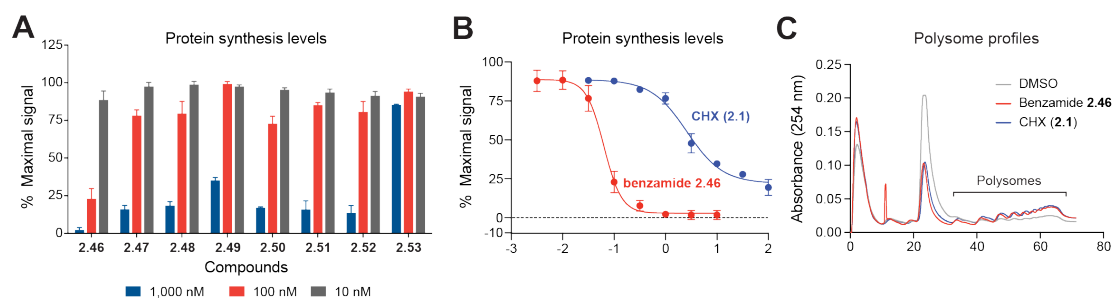


Figure 4.2. **A)** Relative protein synthesis levels after treatment with C13-modified CHX derivatives at various doses. Error bars represent SE for $n=3$. **B)** Dose-response curves show relative protein synthesis levels (% maximum signal, y axis) after treatment with CHX or **2.46** versus vehicle (0.1 % DMSO v/v). Error bars represent SE for $n=3$. **C)** Polysome profiles obtained from 293T cells treated with vehicle (0.1 % DMSO v/v), CHX (100 μ M), or **2.46** (100 μ M) for 30 min.

4.3. DMS-MaPSeq of CHX and 2.46

While producing a CHX analogue with such potent translation inhibition was exciting, we had yet to address the molecular basis of translation inhibition by benzamide **2.46**. To investigate these questions, I conducted dimethyl sulfate (DMS) mutational profiling with sequencing (DMS-MaPseq) with CHX and benzamide **2.46** to determine accessibility of rRNA nucleotides in the presence or absence of compounds^{66,67}. DMS footprinting is a widely utilized technique for structural analysis of RNAs and RNA-protein complexes that exploits the selective DMS-induced methylation of unpaired adenines and cytosines at their Watson-Crick base-pairing positions. The position of these chemical lesions can then be detected upon reverse transcriptase (RT) enzyme cDNA synthesis. While many methods are truncation-based due to the RT enzyme termination transcription upon reaching a modified nucleotide, more recently developed methods utilize thermostable RT enzymes that instead encode DMS modifications as mismatches. These mutational profiling techniques have been successfully used to characterize the differences in the accessibility of rRNA nucleotides and by proxy differences in ribosomal conformation in response to treatment with different protein synthesis inhibitors⁶⁷.

I therefore pre-treated 293T cells with 350 μ M of CHX or 350 μ M benzamide **2.46** for 10 min at 37 $^{\circ}$ C before adding DMS to each plate. RNA was isolated from each condition and subjected to library

preparation as previously described⁶⁸. I found that 293T cells pretreated with CHX or **2.46** revealed strong protection of C4341 relative to the DMSO control (**Figure 4.3**). C4341 is a key residue in the 28S rRNA that hydrogen bonds CHX and its observed protection upon compound treatment corroborates that **2.46** occupies the canonical CHX binding pocket.

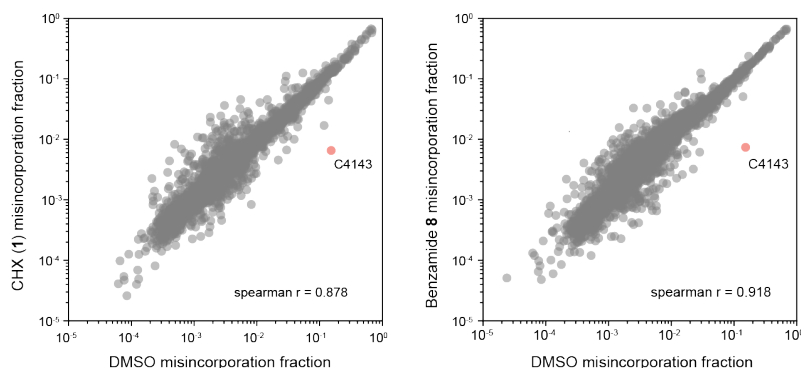


Figure 4.3. Scatterplots showing mutation rates of 28S and 18 rRNA due to DMS modification comparing *in vivo* pretreatment with CHX (left) or **2.46** (right) relative to DMSO pretreatment.

4.4. Abandoned efforts towards photo-labeling the ribosome

In addition to the structural analysis of **2.46**-bound ribosomes, we were interested in leveraging a photoaffinity-based approach to identify the drug-protein and drug-RNA interactions that are formed by the C13-amido CHX compounds. This endeavor was unfortunately abandoned for several reasons and led us to pursue DMS-MaPSeq studies of CHX and **2.46** instead (*vide supra*).

Our foray into a photo-crosslinking strategy was inspired by work published by the Myers' group in 2018 describing a technique for in-cell click selective crosslinking with RNA sequencing profiling (icCL-seq)⁶⁹. Mortison and coworkers successfully mapped tetracycline binding sites on the human ribosome using a combination of proteomics and RNA-sequencing via a dual-functionalized tetracycline probe. The small molecule was appended with a tag containing both a photoreactive diazirine for crosslinking and a terminal azide for click-mediated enrichment. Cells treated with the functionalized tetracycline were crosslinked, followed by protein and RNA isolation. RNA interaction sites were identified by converting RNA fragments to DNA by ligation of an adapter sequence before reverse transcription. RNA fragments

containing a crosslinked adduct result in truncated DNA products, which were then mapped back to the ribosomal RNA within the tetracycline binding pocket to identify the interaction sites at nucleotide resolution.

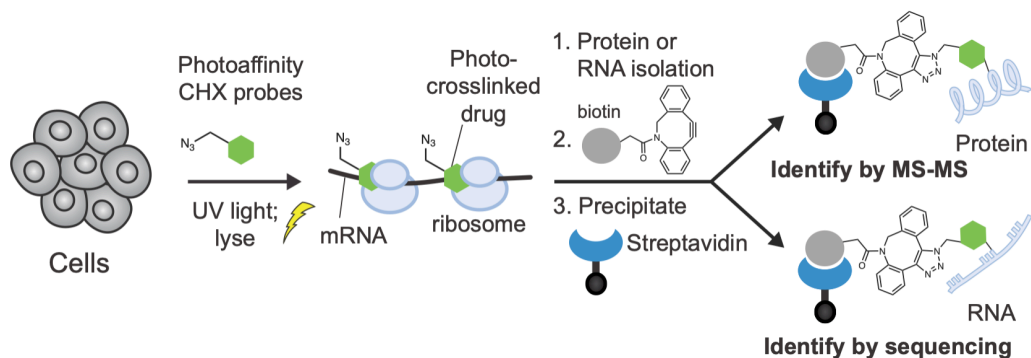


Figure 4.6. Simplified workflow of icCL-seq to identify small molecule interaction sites with protein and RNA.

We believed that a similar strategy would allow us to identify both the ribosomal protein residues and RNA structures that interact with the C13-amido CHX compounds (**Figure 4.6**). We were especially intrigued at the possibility of enriching tRNAs through this protocol, which would suggest that a non-competitive binding mode to the ribosome E-site, in contrast to the proposed competitive mechanism of CHX inhibition. Adapting the route reported by Mortison and coworkers for a minimal diazirine-azide tag, I synthesized three CHX analogues that contain a photo-labile diazirine as well as a click-compatible pull-down handle, two of which exploit the benzamide scaffold of derivative **2.46**. Satisfyingly, I found that all three compounds inhibited protein synthesis and washout was not sufficient to fully reverse the inhibitory effects of these derivatives (**Figure 4.6**).

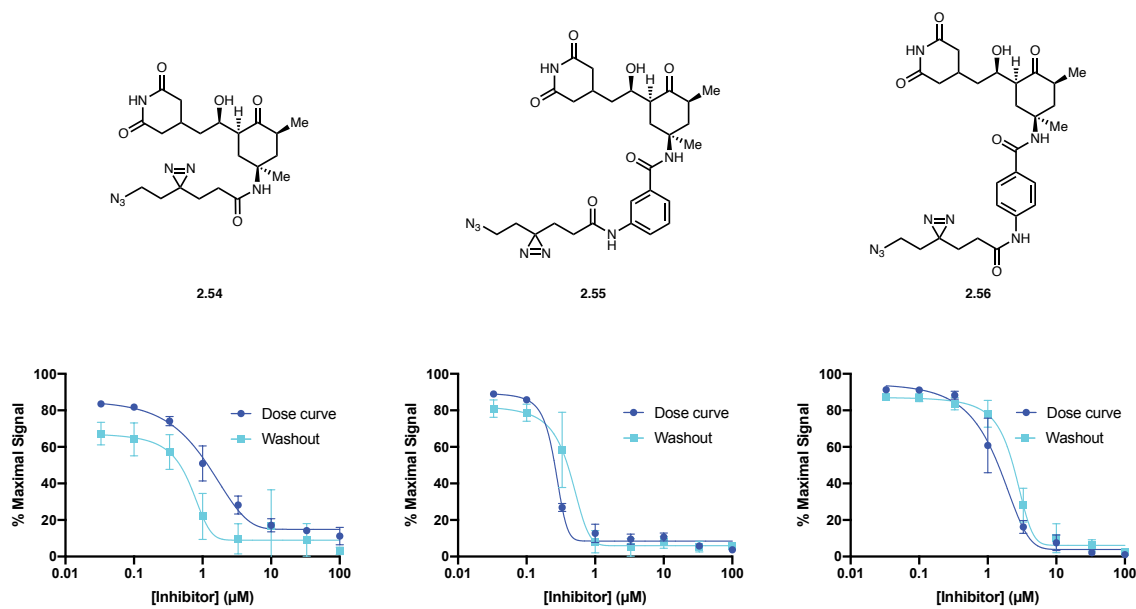


Figure 4.7. Dose response curves show relative protein synthesis levels for cells treated with **2.54** (left), **2.55** (center), and **2.56** (right) with and without compound washout.

With this in hand, I decided to perform the icCL-seq protocol with meta-substituted benzamide **2.55**, which was the most potent of the three photo-CHX molecules we synthesized. Though the entire pipeline was followed through to completion, there were issues with the adapter sequences reported in the original paper. We found that the primer design was not compatible with MiSeq sequencing technology used, resulting in an inability to demultiplex the reads generated from library synthesis. Although there were initially aspirations to repeat the protocol after reworking the adapter design of the entire workflow, these desires were abandoned. We also floated the idea of performing a simpler mass spectrometry-based analysis on the photo-CHX probes without RNA-based sequencing, but instead decided to go forward with DMS-MaPSeq in lieu of any utilization of the photo-crosslinking-probes for the publication of the 2021 CHX manuscript.

4.5. Summary and conclusion

The culmination of this project resulted in the discovery C13-functionalized CHX derivatives with significantly enhanced potencies. Characterization of benzamide **2.46** using structural and sequencing-

based analyses revealed that **2.46** stabilizes polysomes in a sustained manner has potential as an improved probe for studying protein synthesis. These derivatives can be accessed in a rapid and facile manner via semi-synthesis starting from commercially available CHX. We were successful in ascertaining that **2.46** shares the same binding pocket as CHX using DMS-MaPSeq; these results have been further corroborated by to-be-published cryo-EM structures⁶⁴. Ribosome profiling studies comparing the footprint sizes produced from **2.46**- vs CHX-treated cells also support our observations of sustained inhibition as demonstrated by in-cell translation assays. Of course, one of the lingering questions that plagued us was the reason behind the sustained inhibition exhibited by **2.46** and several other of the C13-amido CHX analogues. We also quite enamored with the idea that of **2.46** may be forming an interaction network similar to that of LTM, wherein the aminobenzoyl of **2.46** is positioned similarly to the macrolactone of LTM, i.e. towards the solvent exposed space that the E-site tRNA would normally occupy. However, given the reversible nature of LTM-induced inhibition, this still doesn't provide a full mechanistic explanation for the sustained inhibition of **2.46** and related derivatives. Unveiling the full mechanistic mystery of these derivatives will most likely require further work.

4.6. Experimental section

Materials and Methods

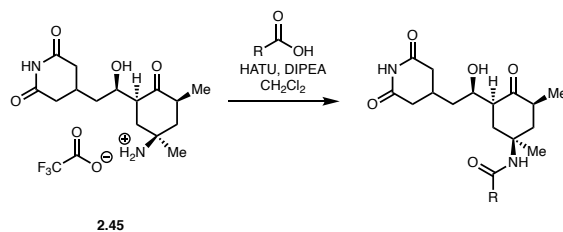
Organic Chemistry. All reactions were performed in oven-dried or flame-dried glassware under a positive pressure of nitrogen unless otherwise noted. Column chromatography was performed with a Biotage Isolera system employing silica gel 60 (230-400 mesh, Silicycle). Celite filtration was performed using Celite® 545 (EMD Millipore). Analytical thin-layer chromatography (TLC) was performed using 0.25 mm silica gel 60 F254 (EMD Millipore). TLC plates were visualized by fluorescence quenching under ultraviolet light (UV) and exposure to a solution of ceric ammonium molybdate, *p*-anisaldehyde, or potassium permanganate stain followed by heating on a hot plate. Reversed-phase chromatography was performed on an Agilent 1200 series HPLC using water and acetonitrile as a mobile phase and Agilent Pursuit C18 as a stationary phase.

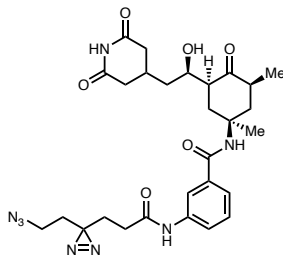
Commercial reagents and solvents were used as received with the following exceptions: tetrahydrofuran (THF), diethyl ether (Et₂O), dichloromethane (CH₂Cl₂), toluene (PhMe), acetonitrile (MeCN), and *N,N*-dimethylformamide (DMF) were degassed with argon and passed through a solvent purification system (designed by Pure Process Technology) utilizing alumina columns.

NMR spectra were recorded with a Varian INOVA-500 spectrometer, are reported in parts per million (δ), and are calibrated using residual undeuterated solvent as an internal reference (CDCl₃: δ 7.26 for ¹H NMR and δ 77.00 for ¹³C NMR; CD₃CN: δ 1.94 for ¹H NMR and δ 118.26; CD₃OD: δ 3.31 for ¹H NMR and δ 49.00 for ¹³C NMR). Data for ¹H NMR spectra are reported as follows: chemical shift (δ ppm) (multiplicity, coupling constant (Hz), integration). Multiplicities are reported as follows: s = singlet, d = doublet, t = triplet, q = quartet, m = multiplet, br = broad, or combinations thereof. High-resolution mass spectra (HRMS) were recorded using electrospray ionization (ESI) mass spectroscopy experiments on an Agilent 6210 TOF LC/MS.

Cell Culture. For cell culture, all media were supplemented with 100 U mL⁻¹ penicillin and 100 μ g mL⁻¹ streptomycin (Life Technologies) and fetal bovine serum (FBS, Peak Serum). K562 cells were maintained in RPMI-1640 (Life Technologies), 10% FBS. 293T cells were maintained in Dulbecco's Modified Eagle Medium (DMEM, Life Technologies) supplemented with 10% FBS. All cell lines were authenticated by STR profiling and routinely tested for mycoplasma (Sigma-Aldrich).

Representative reaction for amide bond formation





2.55

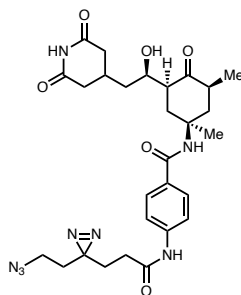
Amide 2.55

Following the representative procedure above, amide 2.54 was obtained as a colorless oil (6.5 mg, 0.011 mmol, 34%).

¹H NMR (500 MHz, CD₃OD) δ 7.90 (s, 1H), 7.62 (d, *J* = 8.8 Hz, 1H), 7.44 (dt, *J* = 7.8, 1.5 Hz, 1H), 7.38 (td, *J* = 7.9, 1.8 Hz, 1H), 4.18 (m, 1H), 3.35 (s, 1H), 3.22 (td, *J* = 6.7, 1.7 Hz, 2H), 2.83–2.55 (m, 5H), 2.46 (dd, *J* = 13.1, 5.8 Hz, 1H), 2.38 (d, *J* = 11 Hz, 3H), 2.24 (td, *J* = 7.6, 1.7 Hz, 2H), 2.13–2.05 (m, 1H), 2.01 (t, *J* = 13 Hz, 1H), 1.86 (td, *J* = 7.5, 1.7 Hz, 2H), 1.83 (s, 3H), 1.69 (td, *J* = 6.7, 1.8 Hz, 2H), 1.58–1.41 (m, 2H), 1.01 (d, *J* = 6.5 Hz, 3H)

¹³C NMR (126 MHz, CD₃OD) δ 212.80, 174.22, 174.10, 171.38, 168.83, 138.47, 128.59, 125.91, 122.55, 118.72, 65.53, 53.25, 50.74, 45.70, 44.88, 40.40, 39.59, 37.95, 37.63, 36.54, 32.00, 30.25, 28.07, 27.59, 26.37, 21.80, 13.45.

HRMS (ESI) (*m/z*) calc'd for C₂₈H₃₆N₈O₆Na [M+Na]⁺: 603.2656, found 603.2637.



2.56

Amide 2.56

Following the representative procedure above, amide **2.56** was obtained as a colorless oil (7.0 mg, 0.012 mmol, 36%).

^1H NMR (500 MHz, CD_3OD) δ 7.71 (d, J = 8.3 Hz, 2H), 7.63 (d, J = 8.8 Hz, 2H), 4.18–4.13 (m, 1H), 3.21 (t, J = 6.6 Hz, 2H), 2.80–2.58 (m, 5H), 2.49–2.42 (m, 1H), 2.40–2.34 (m, 3H), 2.23 (t, J = 7.6 Hz, 2H), 2.08 (t, J = 11.7 Hz, 1H), 1.99 (t, J = 13 Hz, 2H), 1.85 (t, J = 7.6 Hz, 2H), 1.80 (s, 3H), 1.68 (t, J = 6.7 Hz, 2H), 1.57–1.44 (m, 2H), 1.01 (d, J = 6.4 Hz, 3H)

^{13}C NMR (126 MHz, CD_3OD) δ 214.21, 175.63, 175.52, 172.75, 169.73, 142.82, 132.08, 129.19, 127.33, 120.24, 67.03, 54.62, 52.18, 47.09, 46.46, 41.88, 41.00, 39.36, 39.13, 37.96, 33.41, 31.76, 29.44, 28.99, 27.75, 23.19, 14.81.

HRMS (ESI) (m/z) calc'd for $\text{C}_{28}\text{H}_{36}\text{N}_8\text{O}_6\text{Na}$ $[\text{M}+\text{Na}]^+$: 603.2656, found 603.2637.

O-Propargyl Puromycin (OPP) Flow Cytometry Translation Inhibition Assays⁷⁰

Representative procedure:

K562 cells were plated into 96-well plates (10^5 cells in 100 μL media per well) in R10 media (RPMI with glutamine, 10% FBS and 1% penicillin-streptomycin) in triplicate per condition. Stock solutions of inhibitors CHX and benzamide **2.46** were prepared in DMSO (100 mM). Stock solutions of O-propargyl puromycin (OPP, 120 mM) were prepared in DMSO.

Well #	1	2	3	4	5	6	7	8	9	10
CHX (μM)	0	0	100	32	10	3.2	1	0.32	0.1	0.032
OPP (μM)	0	20	20	20	20	20	20	20	20	20
DMSO (%)	0.12	0.12	0.12	0.12	0.12	0.12	0.12	0.12	0.12	0.12

Table S=4.1. Concentrations of each reagent for dose-curve analysis.

Inhibitor (100 μ M to 31.6 nM final concentration in R10) or DMSO (0.1% final concentration in R10) was added to cells in triplicate, and the cells were incubated at 37 °C for 30 minutes (**Table 4.1**). The cells were then treated with *O*-propargyl puromycin (20 μ M final concentration in R10) or DMSO (0.12% final concentration in R10), and the cells were incubated at 37 °C for 60 minutes. The media was removed, and the cells were washed with PBS twice. The cells were then fixed in 1% formaldehyde in PBS at 0 °C for 15 min. The formaldehyde solution was removed, and the cells were washed with PBS once. The cells were permeabilized by re-suspension in 20 μ L of PBS containing 0.1% saponin and 2% BSA at room temperature. After 10 minutes, the Click-iT Cell Reaction Kit (Life Technologies) was used to tag the alkyne-labeled peptides with MB 488 picolyl azide (Click Chemistry Tools, 10 μ M final concentration). After 30 minutes at room temperature, the reaction solution was removed, and the cells were washed twice in PBS containing 0.1% saponin and 2% BSA, resuspended in the same buffer, and analyzed by flow cytometry ($>10^4$ events/well).

Gating was performed as previously described⁷¹. Briefly, a polygon gate was drawn to exclude dead cells using forward and side scatter. Then, a bi-range gate was set up to exclude approximately 99% of DMSO-treated cells to define a FITC-positive population. A maximum signal was obtained when cells were only treated with OPP, and a minimum signal was obtained when cells were only treated with DMSO. % Maximal signal was defined as $(\text{FITC}_{\text{drug,OPP}} - \text{FITC}_{\text{DMSO,DMSO}}) / (\text{FITC}_{\text{DMSO,OPP}} - \text{FITC}_{\text{DMSO,DMSO}})$. From these values, a dose-response curve was generated using GraphPad Prism.

Compound Washout Experiments

K562 cells were plated into 96-well plates (10^5 cells in 100 μ L media per well) in R10 media in triplicate per condition. After being treated with drugs (see above for details) or DMSO (0.1% v/v) in R10, the cells were incubated at 37 °C for 30 min and were then washed twice with R10 and resuspended in 0.1% DMSO in R10. The washes were not performed for non-washout samples. The cells were treated with *O*-propargyl puromycin (20 μ M final concentration in R10) or DMSO (0.11% v/v) at 37 °C for 60 min. Fixation, permeabilization, cycloaddition, and flow cytometry analysis were performed as described above.

DMS-MaPSeq and data processing

Whole cell DMS-MaPSeq was carried out with CHX and benzamide **2.46** as previously described⁶⁸. 293T cells were grown in 15 cm² tissue culture plates to roughly 80% confluency. Cells were treated with 350 μ M of CHX, 350 μ M benzamide **2.46**, or vehicle for 10 min at 37 °C before adding 600 μ L of dimethylsulfate (DMS) to each plate, gently swirling to mix. DMS-treated cells and no DMS-treated cells were included as additional controls. The DMS modification was quenched by the addition of 10 mL of a solution of 30% v/v 2-mercaptoethanol in PBS to each plate. Cells were transferred to a conical tube, pelleted, washed with PBS, and then resuspended in 1 mL TRIzol, after which RNA isolation was performed according to manufacturer protocol. RNA samples were resuspended in 50 μ L of RNase-free water and quantified by NanoDrop.

10 μ g of RNA was used for library preparation as outlined in McClary *et al.* RNA was fragmented with 10 mM ZnCl₂ and incubated for 5 minutes at 95 °C before quenching with 20 mM EDTA on ice. Samples were ethanol precipitated and size selected using a 10% TBE-Urea PAGE gel, staining with SYBR Gold in TBE, and cutting out a slice between 60 and 70 bp. Size-selected fragments were gel extracted and purified before performing 3' end healing with T4 polynucleotide kinase (NEB) followed by linker ligation to AppCACTCGGGCACCAAGGA/3ddC/ using T4 RNA ligase 2 truncated K227Q (NEB). Residual linker was degraded by the addition of yeast 5'-deadenylase and RecJ exonuclease. 10 μ M L reverse transcription reactions were carried out using half of the ligated RNA and adding 1X first strand buffer, 0.5 mM dNTPs, 0.5 μ L SUPERase-In, 100 nM of RT primer (5Phos/AGATCGGAAGAGCGTCGTGTAGGGAAAGAGTGTAGATCTCGGTGGTCCG/iSP18/CACTCA/iSP18/TTCAGACGTGTGCTCTTCCGATCTGTCCTTGGTGCCCGAGT), 5 mM dithiothreitol, and 0.5 μ M TGIRTIII (InGex) for 1 hour at 60 °C. Full-length RT products were purified using a 10% TBE-Urea PAGE gel, followed by gel extraction and purification. cDNA was circularized using CircLigase II (EpiCentre) and prepared for Illumina sequencing using forward primer AATGATACGGCGACCACCGAGATCTACAC and barcoded reverse primer CAAGCAGAAGACGGCATACGAGATNNNNNNNNGTGGAGTTCAGACGTGTGCTCTTCC. 15 cycles of PCR were performed using Phusion High-Fidelity DNA polymerase (NEB). Full-length libraries were gel purified from a 10% TBE-PAGE gel, quantified by bioanalyzer, pooled, and sequenced. The

libraries were sequenced for 150 cycles, single end on an Illumina NextSeq with roughly 20 million reads allocated per condition.

Raw sequencing reads were trimmed and aligned to rRNA reference indices using DMS-MaPseq data analysis software provided at https://github.com/borisz264/mod_seq/. Briefly, the 3' linker sequence was trimmed from all reads and the 5'-most 3 nucleotides were removed. Pre-processed reads were fed into ShapeMapper 2.0 to count mismatches relative to human ribosomal 28S and 18S sequences (NCBI accession NR_003287.2 for 28S, and X03205.1 for 18S).

icCL-seq protocol

icCL-Seq was performed following the protocol as previously described by Mortison and coworkers⁶⁹. A375 cells were grown to 80% confluency in 15 cm plates and treated with either 20 μ M photo-CHX **2.55** or DMSO (final concentration 1% v/v). Duplicate plates were treated to be used as non-crosslinked controls. Cells were incubated at 37 °C for 3 hours, after which the media was fully aspirated and cells were washed with 2 x 10 mL of cold Hank's Balanced Salt Solution (HBSS). The HBSS was removed and plates were crosslinked for 20 minutes on ice at 365 nm using a Stratalinker 1800 at 5 cm from the UV source. Non-crosslinked controls were kept on ice under ambient light for 20 min. Following crosslinking, cells were directly lysed with 5 mL TRIzol. RNA isolation was performed using the Direct-zol RNA Miniprep Kit (Zymo Research).

RNAs were quantified and conjugated to DBCO-PEG4-Desthiobiotin using copper-free click chemistry. RNA was added to an aq mixture of 40 U SUPERaseIN and 1 mM DBCO-PEG4-Desthiobiotin (40 μ g RNA per 100 μ L reaction mixture, 1% v/v DMSO) and incubated in an Eppendorf Thermomixer at 37 °C, 800 rpm, for 4 h. The RNAs were then purified using the RNA Clean & Concentrator-25 Kit (Zymo Research). RNA samples were dried and resuspended in 18 μ L of RNase-free water, then denatured at 95 °C for 60 s before addition of 2 μ L RNA Fragmentation Reagent (Ambion) and heating at 95 °C for 90 s. 2 μ L of Fragmentation Stop Solution were added and samples were immediately purified using the RNA Clean & Concentrator-25 Kit.

10 μ g of RNA per sample was dried and subjected to end repair by resuspending in 1 μ L 10X PNK buffer, 1 μ L SUPERaseIN, 1 μ L FastAP alkaline phosphatase (Thermo), 2 μ L T4 PNK, and 5 μ L RNase-

free water. Reactions were incubated at 37 °C for 1 h, and directly subjected to adapter ligation by addition of 1 µL of 50 µM adenylated adapter (5rApp/AGATCGGAAGAGCGGTTCAG/3ddC/ for drug-treated samples or /5rApp/AGATCGGAAGAGCGGTTCAG/3TEGDesthioBiotin/ for DMSO-treated samples), 1 µL T4 RNA Ligase Buffer, 1 µL T4 RNA Ligase 1, High Concentration (NEB), 1 µL of 100 mM DRR, and 6 µL of 50% PEG8000. Adapter ligation was carried out for 3 h at 25 °C. Following incubation, samples were diluted with 10 µL of RNase-free water and purified using the RNA Clean & Concentrator-25 Kit. Unligated adapter was digested by the addition of 1 µL RNA 5' pyrophosphohydrolase (RPPH), 1 µL RecJ_r, 2 µL NEB Buffer 2, and 6 µL RNase-free water. Samples were incubated at 37 °C for 1 h, followed by dilution with 40 µL RNase-free water and purification using the RNA Clean & Concentrator-5 Kit (Zymo Research). Following ligation, RNA samples were annealed to the RT primer by addition of 2 µL of 2 µM RT primer (5phos/DDDNNAACNNNNAGTCGGAAGAGCGTCGTGAT/iSp18/GGATCC/iSp18/TACTGAACCGC), 1 µL RNasin Plus (Promega), 2 µL of 10 mM dNTPs, and 12 µL RNase-free water. Samples were heated at 65 °C for 5 min, then cooled to 25 °C for 1 min. 2 µL of 100 mM DTT, 8 µL of SSIV, and 2 µL of SuperScript IV (Thermo) were added to each reaction, and extension was performed at 25 °C for 3 min, 42 °C for 5 min, and 52 °C for 30 min, after which the samples were cooled to 4 °C.

Sample enrichment was performed via streptavidin capture: Dynabeads MyOne Streptavidin C1 were washed and resuspended in bead binding buffer (100 mM Tris, pH 7.0, 1 M NaCl, 10 mM EDTA, 0.2% Tween20) and 20 µL was added to each sample along with 5 U RNase I_r. Samples were rotated at room temperature for 1 h. The beads were placed on a magnet and the supernatant was removed. Beads were washed with 5 x 0.5 mL of wash buffer (100 mM Tris, pH 7.0, 4 M NaCl, 10 mM EDTA, 0.2 Tween20) and 2 x 0.5 mL of 1X PBS. Enriched samples were eluted using 50 µL 5 mM D-biotin in 1X PBS, incubating in an Eppendorf Thermomixer at 37 C for 30 min at 1500 rpm. Following incubation, samples were placed on a magnet and the supernatant was collected. The elution was repeated using an additional 50 µL elution buffer. The eluted cDNAs were purified using the DNA Clean and Concentrator-5 kit (Zymo research), following the protocol for purifying ssDNA.

Circularization was performed by adding 2 µL of 10X CirLigase II Buffer, 1 µL of 50 mM MnCl₂, and 1 µL CirLigase II. Samples were incubated at 60 °C for 2 h, followed by purification with the DNA Clean and

Concentrator-5 kit, using the protocol for isolating ssDNA. PCR amplification was carried out adding 10 μ L of 5X Q5 Reaction Buffer, 1 μ L of 10 mM dNTPs, 1 μ L of 10 μ M P3 primer (CTGAACCGCTCTTCCGATCT), 1 μ L of 10 μ M P5 primer (ACACGACGCTCTTCCGATCT), 16.5 μ L nuclease-free water, and 0.5 μ L of Hot Start High-Fidelity DNA Polymerase. Reactions were amplified for a single cycle with the following program:

98 °C for 60 s,

98 °C for 15 s,

62 °C for 30 s,

72 °C for 45 s,

Reactions were then purified using the DNA Clean and Concentrator-5 kit.

Library amplification and barcoding was performed using the Universal Illumina Forward Primer (5'-AATGATACGGCGACCACCGAGATCTACACTCTTTCC CTACACGACGCTCTTCCGATC*T-3') and barcoded reverse primers (5'-CAAGCAGAAGACGGCATAACGAGATNNNNNNNNGTGACT GGAGTTCACTGAACCGCTCTTC CGATCT -3') on a qPCR thermal cycler. Amplification was carried out with the following program:

98 °C for 60 s,

1 cycle of

98 °C for 60 s,

62 °C for 20 s,

72 °C for 60 s,

Followed by N cycles with

98 °C for 15 s,

70 °C for 20 s,

72 °C for 60 s,

Amplifications were monitored using 20X Evagreen. Library samples were purified using Omega Mag-Bind TotalPure NGS and analyzed using an Agilent Bioanalyzer 2100. The purified libraries were pooled and sequenced on an Illumina MiSeq genome analyzer.

References

- (1) Block, S. S.; Stephens, R. L.; Barreto, A.; Murrill, W. A. Chemical Identification of the Amanita Toxin in Mushrooms. *Science* **1955**, *121* (3145), 505–506. <https://doi.org/10.1126/science.121.3145.505>.
- (2) Wieland, T.; Faulstich, H. Fifty Years of Amanitin. *Experientia* **1991**, *47* (11–12), 1186–1193. <https://doi.org/10.1007/bf01918382>.
- (3) Garcia, J.; Costa, V. M.; Carvalho, A.; Baptista, P.; Pinho, P. G. de; Bastos, M. de L.; Carvalho, F. Amanita Phalloides Poisoning: Mechanisms of Toxicity and Treatment. *Food Chem Toxicol* **2015**, *86*, 41–55. <https://doi.org/10.1016/j.fct.2015.09.008>.
- (4) Wieland, T. Peptides of Poisonous Amanita Mushrooms. *Springer Ser Mol Biology* **1986**. <https://doi.org/10.1007/978-3-642-71295-1>.
- (5) Walton, J. D.; Hallen-Adams, H. E.; Luo, H. Ribosomal Biosynthesis of the Cyclic Peptide Toxins of Amanita Mushrooms. *Peptide Sci* **2010**, *94* (5), 659–664. <https://doi.org/10.1002/bip.21416>.
- (6) Luo, H.; Hallen-Adams, H. E.; Scott-Craig, J. S.; Walton, J. D. Ribosomal Biosynthesis of α -Amanitin in *Galerina Marginata*. *Fungal Genet Biol* **2012**, *49* (2), 123–129. <https://doi.org/10.1016/j.fgb.2011.12.005>.
- (7) Luo, H.; Hong, S.-Y.; Sgambelluri, R. M.; Angelos, E.; Li, X.; Walton, J. D. Peptide Macrocyclization Catalyzed by a Prolyl Oligopeptidase Involved in α -Amanitin Biosynthesis. *Chem Biol* **2014**, *21* (12), 1610–1617. <https://doi.org/10.1016/j.chembiol.2014.10.015>.
- (8) Bushnell, D.; the ..., C.-P. of. Structural Basis of Transcription: α -Amanitin–RNA Polymerase II Cocystal at 2.8 Å Resolution. **2002**. <https://doi.org/10.1073/pnas.251664698>.
- (9) Klug, A. STRUCTURAL BIOLOGY: A Marvellous Machine for Making Messages. *Science* **2001**, *292* (5523), 1844–1846. <https://doi.org/10.1126/science.1062384>.
- (10) Liu, X.; Farnung, L.; Wigge, C.; Cramer, P. Cryo-EM Structure of a Mammalian RNA Polymerase II Elongation Complex Inhibited by α -Amanitin. *J Biol Chem* **2018**, *293* (19), 7189–7194. <https://doi.org/10.1074/jbc.ra118.002545>.
- (11) Pahl, A.; Lutz, C.; Hechler, T. Amanitins and Their Development as a Payload for Antibody-Drug Conjugates. *Drug Discov Today Technologies* **2018**, *30*, 85–89. <https://doi.org/10.1016/j.ddtec.2018.08.005>.
- (12) Davis, M.; Preston, J. A Conjugate of Alpha-Amanitin and Monoclonal Immunoglobulin G to Thy 1.2 Antigen Is Selectively Toxic to T Lymphoma Cells. *Science* **1981**, *213* (4514), 1385–1388. <https://doi.org/10.1126/science.6115471>.
- (13) Figueroa-Vazquez, V.; Ko, J.; Breunig, C.; Baumann, A.; Giesen, N.; Pálfi, A.; Müller, C.; Lutz, C.; Hechler, T.; Kulke, M.; Müller-Tidow, C.; Krämer, A.; Goldschmidt, H.; Pahl, A.; Raab, M. S. HDP-101, an Anti-BCMA Antibody–Drug Conjugate, Safely Delivers Amanitin to Induce Cell Death in Proliferating and Resting Multiple Myeloma Cells. *Mol Cancer Ther* **2021**, *20* (2), 367–378. <https://doi.org/10.1158/1535-7163.mct-20-0287>.
- (14) Moldenhauer, G.; Salnikov, A. V.; Lüttgau, S.; Herr, I.; Anderl, J.; Faulstich, H. Therapeutic Potential of Amanitin-Conjugated Anti-Epithelial Cell Adhesion Molecule Monoclonal Antibody Against Pancreatic Carcinoma. *Jnci J National Cancer Inst* **2012**, *104* (8), 622–634. <https://doi.org/10.1093/jnci/djs140>.

- (15) Jonkers, I.; Lis, J. T. Getting up to Speed with Transcription Elongation by RNA Polymerase II. *Nature Reviews Molecular Cell Biology* **2015**, *16* (3), 167–177. <https://doi.org/10.1038/nrm3953>.
- (16) Core, L. J.; Waterfall, J. J.; Lis, J. T. Nascent RNA Sequencing Reveals Widespread Pausing and Divergent Initiation at Human Promoters. *Science (New York, N.Y.)* **2008**, *322* (5909), 1845. <https://doi.org/10.1126/science.1162228>.
- (17) Nojima, T.; Gomes, T.; Grosso, A.; Kimura, H.; Dye, M. J.; Dhir, S.; Carmo-Fonseca, M.; Proudfoot, N. J. Mammalian NET-Seq Reveals Genome-Wide Nascent Transcription Coupled to RNA Processing. *Cell* **2015**, *161* (3), 526–540. <https://doi.org/10.1016/j.cell.2015.03.027>.
- (18) Mayer, A.; di Iulio, J.; Maleri, S.; Eser, U.; Vierstra, J.; Reynolds, A.; Sandstrom, R.; Stamatoyannopoulos, J. A.; Churchman, S. L. Native Elongating Transcript Sequencing Reveals Human Transcriptional Activity at Nucleotide Resolution. *Cell* **2015**, *161* (3), 541–554. <https://doi.org/10.1016/j.cell.2015.03.010>.
- (19) Wieland, T.; Gótzendórfer, * Christa; Dabrowski, J.; Lipscomb, W. N.; Shoham, and G. Unexpected Similarity of the Structures of the Weakly Toxic Amanitin (S)-Sulfoxide and the Highly Toxic (-R)-Sulfoxide and Sulfone As Revealed by Proton Nuclear Magnetic Resonance and X-Ray Analysis¹. *Biochemistry* **1983**, *22*, 1264–1271.
- (20) Faulstich, H.; Trischmann, H.; Wieland, T.; Wulf, E. Ether Derivatives of Alpha-Amanitin. Introduction of Spacer Moieties, Lipophilic Residues, and Radioactive Labels. *Biochemistry-us* **1981**, *20* (22), 6498–6504. <https://doi.org/10.1021/bi00525a031>.
- (21) MORRIS, P. W.; VENTON, D. L. Regiospecific Arylazo Substitution into A-amanitin with Retention of Inhibitory Properties against Eukaryotic Class II RNA Polymerase. *Int J Pept Prot Res* **1983**, *21* (4), 419–430. <https://doi.org/10.1111/j.1399-3011.1983.tb03123.x>.
- (22) Matinkhoo, K.; Pryma, A.; Todorovic, M.; Patrick, B. O.; Perrin, D. M. Synthesis of the Death-Cap Mushroom Toxin α -Amanitin. *J Am Chem Soc* **2018**, *140* (21), 6513–6517. <https://doi.org/10.1021/jacs.7b12698>.
- (23) ZANOTTI, G.; BIRR, C.; WIELAND, T. ANALOGS OF AMANIN. *Int J Pept Prot Res* **1981**, *18* (2), 162–168. <https://doi.org/10.1111/j.1399-3011.1981.tb02054.x>.
- (24) May, J. P.; Perrin, D. M. Tryptathionine Bridges in Peptide Synthesis. *Peptide Science* **2007**, *88* (5), 714–724. <https://doi.org/10.1002/bip.20807>.
- (25) Horton, D. A.; Bourne, G. T.; Smythe, M. L. Exploring Privileged Structures: The Combinatorial Synthesis of Cyclic Peptides. *J Comput Aid Mol Des* **2002**, *16* (5–6), 415–431. <https://doi.org/10.1023/a:1020863921840>.
- (26) Zorzi, A.; Deyle, K.; Heinis, C. Cyclic Peptide Therapeutics: Past, Present and Future. *Curr Opin Chem Biol* **2017**, *38*, 24–29. <https://doi.org/10.1016/j.cbpa.2017.02.006>.
- (27) Wieland, T.; Jochum, C.; Faulstich, H. Optimierung Der Synthese von Indolyl-(2)-thioäthern Aus Derivaten Des Tryptophans Und Des Cysteins. *Liebigs Ann Chem* **1969**, *727* (1), 138–142. <https://doi.org/10.1002/jlac.19697270117>.
- (28) Anderson, M. O.; Shelat, A. A.; Guy, R. K. A Solid-Phase Approach to the Phallotoxins: Total Synthesis of [Ala 7]-Phalloidin. *J Org Chem* **2005**, *70* (12), 4578–4584. <https://doi.org/10.1021/jo0503153>.

- (29) May, J. P.; Perrin, D. M. Intraannular Savige–Fontana Reaction: One-Step Conversion of One Class of Monocyclic Peptides into Another Class of Bicyclic Peptides. *Chemistry - A European Journal* **2008**, *14* (11), 3404–3409. <https://doi.org/10.1002/chem.200701088>.
- (30) Savige, W.; Fontana, A. New Method of Linking Tryptophan to Cysteine Sulphydryl Groups in Peptides and Proteins. *Journal of the Chemical Society, Chemical Communications* **1976**, *0* (15), 600–601. <https://doi.org/10.1039/c39760000600>.
- (31) Wieland, T.; Birr, C.; Zanotti, G. L,L-3,6-[Methanothio(2,3-indolo)Methano]Piperazine-2,5-dione, the Smallest Phallotoxin Model. *Angewandte Chemie Int Ed Engl* **1978**, *17* (1), 54–55. <https://doi.org/10.1002/anie.197800541>.
- (32) ZANOTTI, G.; MÖHRINGER, C.; WIELAND, T. Synthesis of Analogues of Amaninamide, an Amatoxin from the White Amanita Virosamushroom. *Int J Pept Prot Res* **1987**, *30* (4), 450–459. <https://doi.org/10.1111/j.1399-3011.1987.tb03353.x>.
- (33) ZANOTTI, G.; D'AURIA, G.; PAOLILLO, L.; TRIVELLONE, E. Synthetic Amatoxin Analogues. *Int J Pept Prot Res* **1988**, *32* (1), 9–20. <https://doi.org/10.1111/j.1399-3011.1988.tb00920.x>.
- (34) Wieland, T.; Georgi, V. Über Die Inhaltsstoffe Des Grünen Knollenblätterpilzes, XXVIII. Synthesen von B-Methyl- γ -hydroxy-leucin Und B-Methyl- γ . Δ -dihydroxy-leucin, Zwei Vermuteten Amanitin-Bausteinen. *Liebigs Ann Chem* **1967**, *700* (1), 133–148. <https://doi.org/10.1002/jlac.19667000117>.
- (35) Bartlett, P. A.; Tanzella, D. J.; Barstow, J. F. Stereoselective Synthesis of the Dihydroxyisoleucine Constituent of the Amanita Mushroom Toxins. *Tetrahedron Letters* **1982**, *23* (6), 619–622. [https://doi.org/10.1016/s0040-4039\(00\)86905-1](https://doi.org/10.1016/s0040-4039(00)86905-1).
- (36) Zhao, L.; May, J. P.; Blanc, A.; Dietrich, D. J.; Loonchanta, A.; Matinkhoo, K.; Pryyma, A.; Perrin, D. M. Synthesis of a Cytotoxic Amanitin for Biorthogonal Conjugation. *ChemBioChem* **2015**, *16* (10), 1420–1425. <https://doi.org/10.1002/cbic.201500226>.
- (37) Lutz, C.; Simon, W.; Werner-Simon, S.; Pahl, A.; Müller, C. Total Synthesis of A- and B-Amanitin. *Angewandte Chemie Int Ed* **2020**, *59* (28), 11390–11393. <https://doi.org/10.1002/anie.201914935>.
- (38) Siegert, M. J.; Knittel, C. H.; Süßmuth, R. D. A Convergent Total Synthesis of the Death Cap Toxin A-Amanitin. *Angewandte Chemie Int Ed* **2020**, *59* (14), 5500–5504. <https://doi.org/10.1002/anie.201914620>.
- (39) May, J. P.; Fournier, P.; Pellicelli, J.; Patrick, B. O.; Perrin, D. M. High Yielding Synthesis of 3 α -Hydroxypyrrolo[2,3-b]Indoline Dipeptide Methyl Esters: Synthons for Expedient Introduction of the Hydroxypyrroloindoline Moiety into Larger Peptide-Based Natural Products and for the Creation of Tryptathionine Bridges. *The Journal of organic chemistry* **2005**, *70* (21), 8424–8430. <https://doi.org/10.1021/jo051105t>.
- (40) Posadaz, A.; Biasutti, A.; Casale, C.; Sanz, J.; Amat-Guerri, F.; Garcia, N. A. Rose Bengal-Sensitized Photooxidation of the Dipeptides Trp-Phe, Trp-Tyr and Trp-Trp. Kinetics, Mechanism and Photoproducts. *Photochem Photobiol* **2004**. <https://doi.org/10.1562/2004-03-03-ra-097>.
- (41) Ley, S. V.; Cleator, E.; Hewitt, P. R. A Rapid Stereocontrolled Synthesis of the 3 α -Hydroxy-Pyrrolo[2,3- b]Indole Skeleton, a Building Block for 10 b -Hydroxy-Pyrazino[1',2':1,5]Pyrrolo[2,3- b]Indole-1,4-Diones. *Org Biomol Chem* **2003**, *1* (20), 3492–3494. <https://doi.org/10.1039/b308288a>.

- (42) Kamenecka, T. M.; Danishefsky, S. J. Discovery through Total Synthesis: A Retrospective on the Himastatin Problem. *Chem - European J* **2001**, *7* (1), 41–63. [https://doi.org/10.1002/1521-3765\(20010105\)7:1<41::aid-chem41>3.0.co;2-d](https://doi.org/10.1002/1521-3765(20010105)7:1<41::aid-chem41>3.0.co;2-d).
- (43) Ruiz-Sanchis, P.; Savina, S. A.; Acosta, G. A.; Albericio, F.; Álvarez, M. Orthogonal Protecting Groups in the Synthesis of Tryptophanyl-Hexahydropyrroloindoles. *Eur J Org Chem* **2012**, *2012* (1), 67–73. <https://doi.org/10.1002/ejoc.201101057>.
- (44) Feng, Y.; Holte, D.; Zoller, J.; Umemiya, S.; Simke, L. R.; Baran, P. S. Total Synthesis of Verruculogen and Fumitremorgin A Enabled by Ligand-Controlled C–H Borylation. *J Am Chem Soc* **2015**, *137* (32), 10160–10163. <https://doi.org/10.1021/jacs.5b07154>.
- (45) Liu, G.; Cogan, D. A.; Ellman, J. A. Catalytic Asymmetric Synthesis of Tert-Butanesulfinamide. Application to the Asymmetric Synthesis of Amines. *J Am Chem Soc* **1997**, *119* (41), 9913–9914. <https://doi.org/10.1021/ja972012z>.
- (46) Barros, O. S. do R.; Sirvent, J. A.; Foubelo, F.; Yus, M. Diastereoselective Allylation and Crotylation of N-Tert -Butanesulfinyl Imines with Allylic Alcohols. *Chem Commun* **2014**, *50* (52), 6898–6901. <https://doi.org/10.1039/c4cc02317j>.
- (47) Chandrasekhar, S.; Rambabu, Ch.; Prakash, S. J. Total Synthesis of 6-Epiprelactone-V via a Syn-Selective Oxygen Tethered Intramolecular Michael Reaction. *Tetrahedron Lett* **2006**, *47* (7), 1213–1215. <https://doi.org/10.1016/j.tetlet.2005.12.012>.
- (48) Hanessian*, S.; Sumi, K. On the Stereochemical Divergence in the Conjugate Addition of Lithium Dimethylcuprate/Trimethylsilyl Chloride to α -Alkoxy and α -Ureido α,β -Unsaturated Esters. *Synthesis* **1991**, *1991* (12), 1083–1089. <https://doi.org/10.1055/s-1991-28396>.
- (49) Hanessian, S.; Wang, W.; Gai, Y.; Olivier, E. A General and Stereocontrolled Strategy for the Iterative Assembly of Enantiopure Polypropionate Subunits: Synthesis of the C19–C28 Segment of Rifamycin S from a Single Chiron. *J Am Chem Soc* **1997**, *119* (42), 10034–10041. <https://doi.org/10.1021/ja970251g>.
- (50) Vila-Perelló, M.; Pratt, M. R.; Tulin, F.; Muir, T. W. Covalent Capture of Phospho-Dependent Protein Oligomerization by Site-Specific Incorporation of a Diazirine Photo-Cross-Linker. *Journal of the American Chemical Society* **2007**, *129* (26), 8068–8069. <https://doi.org/10.1021/ja072013j>.
- (51) Ennis, H. L.; Lubin, M. Cycloheximide: Aspects of Inhibition of Protein Synthesis in Mammalian Cells. *Science* **1964**, *146* (3650), 1474–1476. <https://doi.org/10.1126/science.146.3650.1474>.
- (52) Baliga, B. S.; Pronczuk, A. W.; Munro, H. N. Mechanism of Cycloheximide Inhibition of Protein Synthesis in a Cell-Free System Prepared from Rat Liver. *J Biol Chem* **1969**, *244* (16), 4480–4489. [https://doi.org/10.1016/s0021-9258\(18\)94343-7](https://doi.org/10.1016/s0021-9258(18)94343-7).
- (53) Obrig, T.; Culp, W.; McKeehan, W.; Hardesty, B. The Mechanism by Which Cycloheximide and Related Glutarimide Antibiotics Inhibit Peptide Synthesis on Reticulocyte Ribosomes. *J Biological Chem* **1971**, *246* (1), 174–181.
- (54) Schneider-Poetsch, T.; Ju, J.; Eyler, D. E.; Dang, Y.; Bhat, S.; Merrick, W. C.; Green, R.; Shen, B.; Liu, J. O. Inhibition of Eukaryotic Translation Elongation by Cycloheximide and Lactimidomycin. *Nat Chem Biol* **2010**, *6* (3), nchembio.304. <https://doi.org/10.1038/nchembio.304>.

- (55) Yin, M.; Yan, Y.; Lohman, J. R.; Huang, S.-X.; Ma, M.; Zhao, G.-R.; Xu, L.-H.; Xiang, W.; Shen, B. Cycloheximide and Actiphenol Production in *Streptomyces* Sp. YIM56141 Governed by Single Biosynthetic Machinery Featuring an Acyltransferase-Less Type I Polyketide Synthase. *Org Lett* **2014**, *16* (11), 3072–3075. <https://doi.org/10.1021/ol501179w>.
- (56) Loubresse, N. de; Prokhorova, I.; Holtkamp, W.; Rodnina, M. V.; Yusupova, G.; Yusupov, M. Structural Basis for the Inhibition of the Eukaryotic Ribosome. *Nature* **2014**, *513* (7519), nature13737. <https://doi.org/10.1038/nature13737>.
- (57) Kao, S.-H.; Wang, W.-L.; Chen, C.-Y.; Chang, Y.-L.; Wu, Y.-Y.; Wang, Y.-T.; Wang, S.-P.; Nesvizhskii, A.; Chen, Y.-J.; Hong, T.-M.; Yang, P.-C. Analysis of Protein Stability by the Cycloheximide Chase Assay. *Bio-protocol* **2015**, *5* (1). <https://doi.org/10.21769/bioprotoc.1374>.
- (58) Ingolia, N. T.; Ghaemmighami, S.; Newman, J. R.; Weissman, J. S. Genome-Wide Analysis in Vivo of Translation with Nucleotide Resolution Using Ribosome Profiling. *Science* **2009**, *324* (5924), 218–223. <https://doi.org/10.1126/science.1168978>.
- (59) Ingolia, N. T. Ribosome Footprint Profiling of Translation throughout the Genome. *Cell* **2016**, *165* (1), 22–33. <https://doi.org/10.1016/j.cell.2016.02.066>.
- (60) Gerashchenko, M. V.; Gladyshev, V. N. Translation Inhibitors Cause Abnormalities in Ribosome Profiling Experiments. *Nucleic Acids Res* **2014**, *42* (17), e134–e134. <https://doi.org/10.1093/nar/gku671>.
- (61) Husmann, J. A.; Patchett, S.; Johnson, A.; Sawyer, S.; Press, W. H. Understanding Biases in Ribosome Profiling Experiments Reveals Signatures of Translation Dynamics in Yeast. *Plos Genet* **2015**, *11* (12), e1005732. <https://doi.org/10.1371/journal.pgen.1005732>.
- (62) Johnson, F.; Starkovsky, N. A.; Paton, A. C.; Carlson, A. A. The Total Synthesis of Cycloheximide. *J Am Chem Soc* **1966**, *88* (1), 149–159.
- (63) Park, Y.; Koga, Y.; Su, C.; Waterbury, A. L.; Johnny, C. L.; Liao, B. B. Versatile Synthetic Route to Cycloheximide and Analogues That Potently Inhibit Translation Elongation. *Angew Chem-ger Edit* **2019**, *131* (16), 5441–5445. <https://doi.org/10.1002/ange.201901386>.
- (64) Koga, Y.; Hoang, E. M.; Park, Y.; Keszei, A. F. A.; Murray, J.; Shao, S.; Liao, B. B. Synthesis and Structural Basis of C13- Aminobenzoyl Cycloheximide Derivatives That Potently Inhibit Translation Elongation. **2021**.
- (65) Roizen, J. L.; Zalatan, D. N.; Du Bois, J. Selective Intermolecular Amination of C-H Bonds at Tertiary Carbon Centers. *Angewandte Chemie Int Ed* **2013**, *52* (43), 11343–11346. <https://doi.org/10.1002/anie.201304238>.
- (66) Zubradt, M.; Gupta, P.; Persad, S.; Lambowitz, A. M.; Weissman, J. S.; Rouskin, S. DMS-MaPseq for Genome-Wide or Targeted RNA Structure Probing in Vivo. *Nat Methods* **2017**, *14* (1), 75–82. <https://doi.org/10.1038/nmeth.4057>.
- (67) Wu, C. C.-C.; Zinshteyn, B.; Wehner, K. A.; Green, R. High-Resolution Ribosome Profiling Defines Discrete Ribosome Elongation States and Translational Regulation during Cellular Stress. *Mol Cell* **2019**, *73* (5), 959-970.e5. <https://doi.org/10.1016/j.molcel.2018.12.009>.
- (68) McClary, B.; Zinshteyn, B.; Meyer, M.; Jouanneau, M.; Pellegrino, S.; Yusupova, G.; Schuller, A.; Reyes, J. C. P.; Lu, J.; Guo, Z.; Ayinde, S.; Luo, C.; Dang, Y.; Romo, D.; Yusupov, M.; Green, R.; Liu, J.

O. Inhibition of Eukaryotic Translation by the Antitumor Natural Product Agelastatin A. *Cell Chem Biology* **2017**, *24* (5), 605-613.e5. <https://doi.org/10.1016/j.chembiol.2017.04.006>.

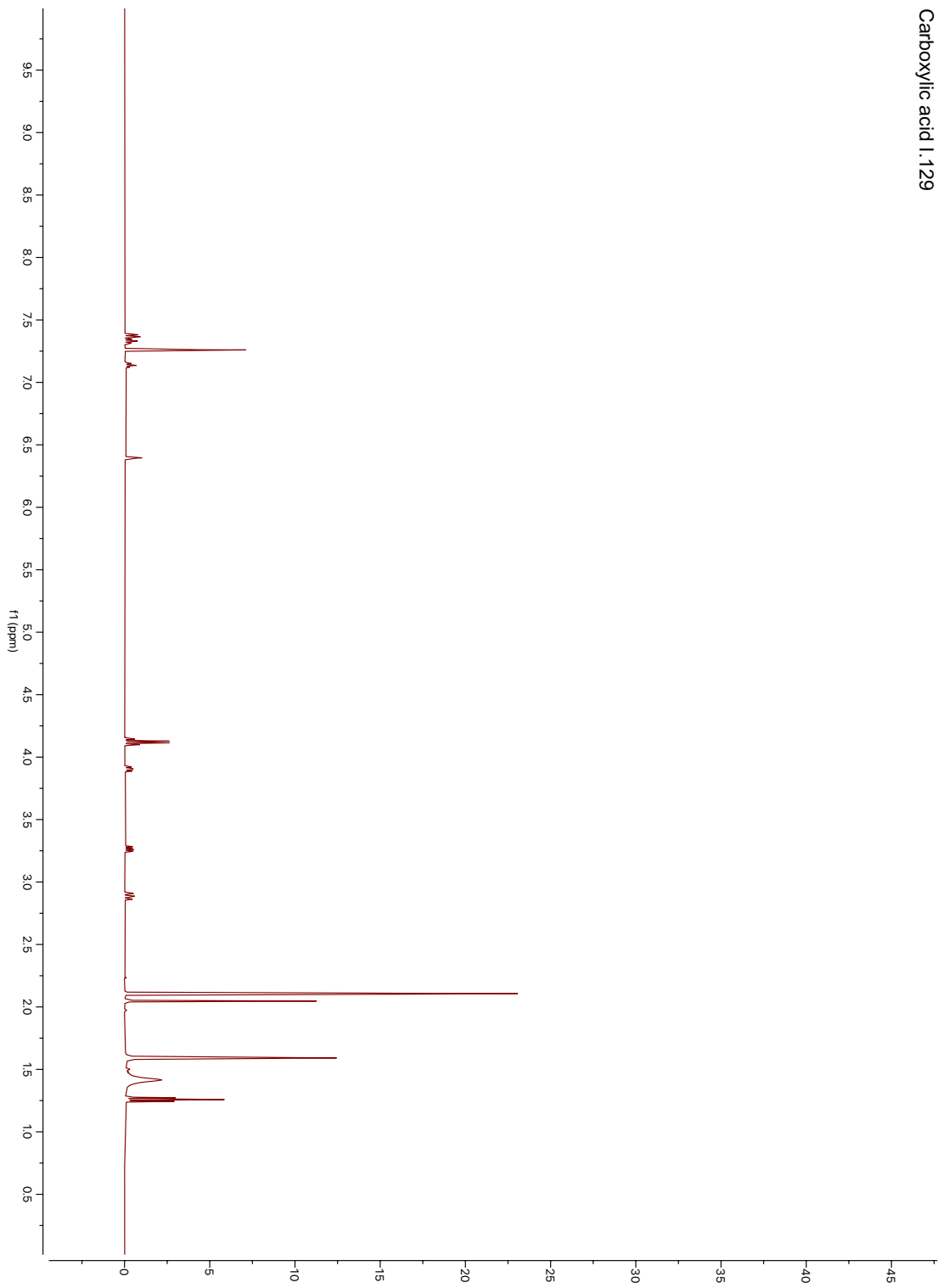
(69) Mortison, J. D.; Schenone, M.; Myers, J. A.; Zhang, Z.; Chen, L.; Ciarlo, C.; Comer, E.; Natchiar, K. S.; Carr, S. A.; Klaholz, B. P.; Myers, A. G. Tetracyclines Modify Translation By Targeting Key Human RRNA Substructures. *Biorxiv* **2018**, 256230. <https://doi.org/10.1101/256230>.

(70) Liu, J.; Xu, Y.; Stoleru, D.; Salic, A. Imaging Protein Synthesis in Cells and Tissues with an Alkyne Analog of Puromycin. *Proc National Acad Sci* **2012**, *109* (2), 413–418. <https://doi.org/10.1073/pnas.1111561108>.

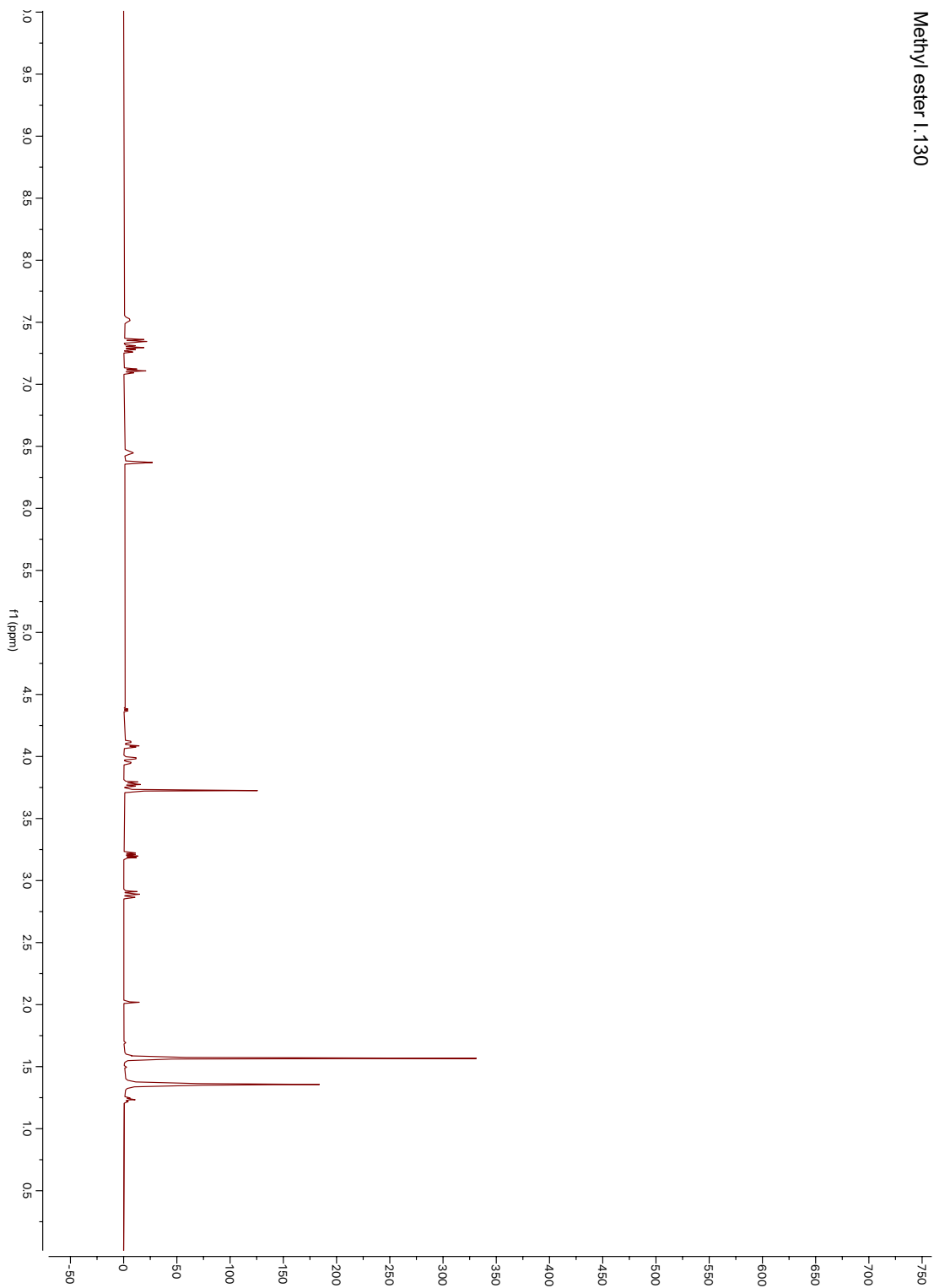
(71) Park, Y.; Koga, Y.; Su, C.; Waterbury, A. L.; Johnny, C. L.; Liao, B. B. Versatile Synthetic Route to Cycloheximide and Analogues That Potently Inhibit Translation Elongation. *Angewandte Chemie Int Ed* **2019**, *58* (16), 5387–5391. <https://doi.org/10.1002/anie.201901386>.

Appendix A: Catalog of Spectra

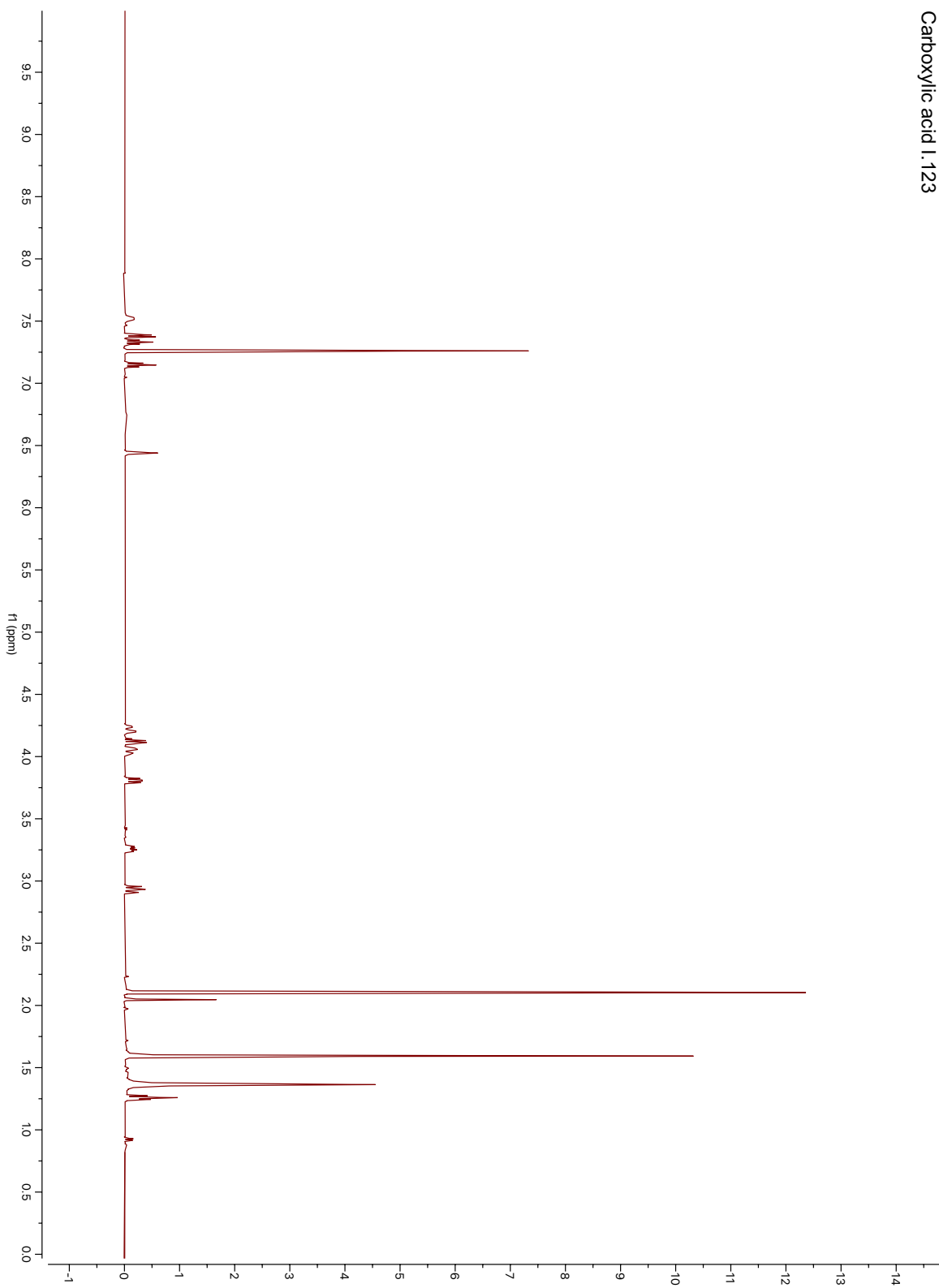
Carboxylic acid 1:129



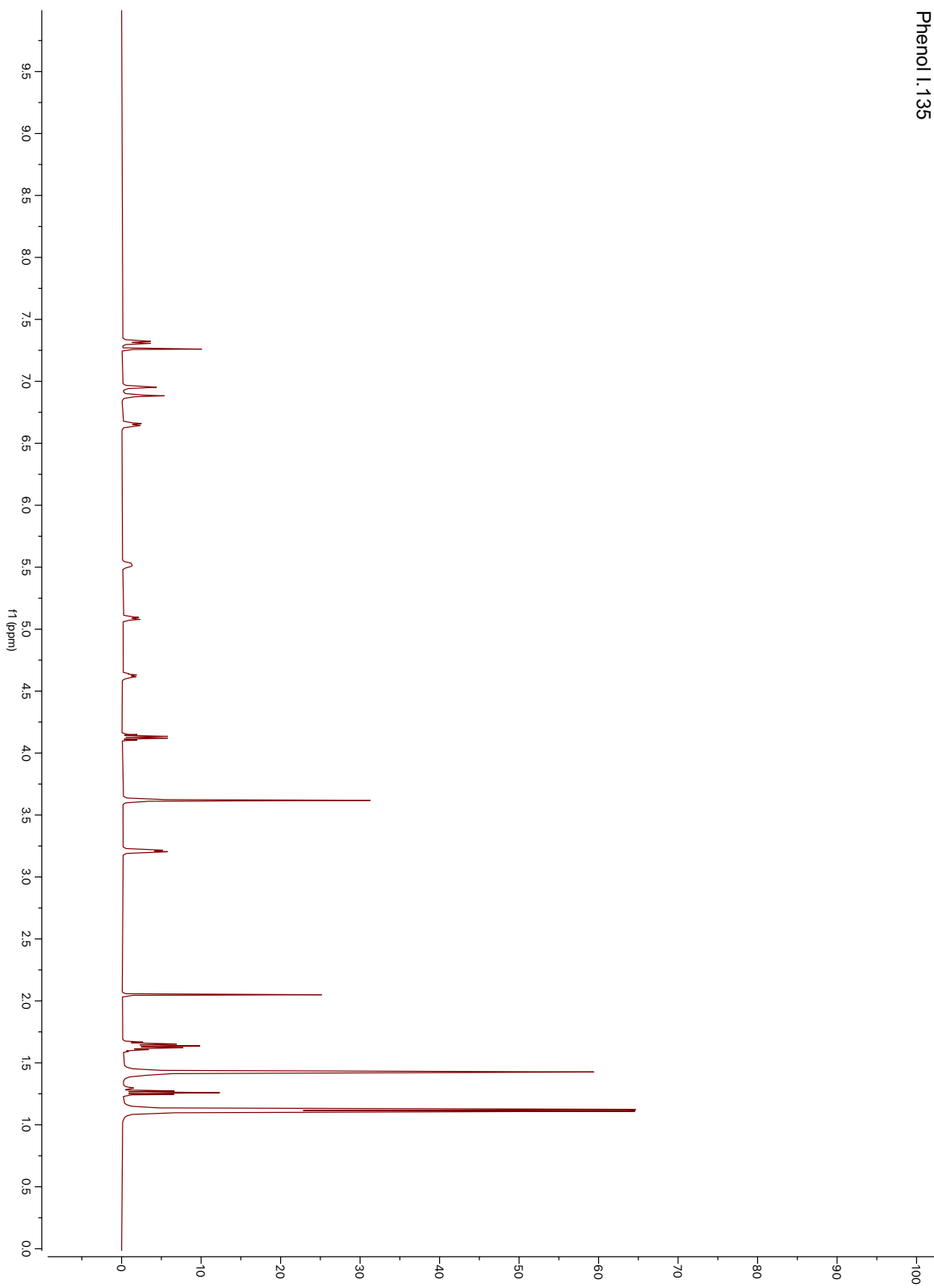
Methyl ester 1.130



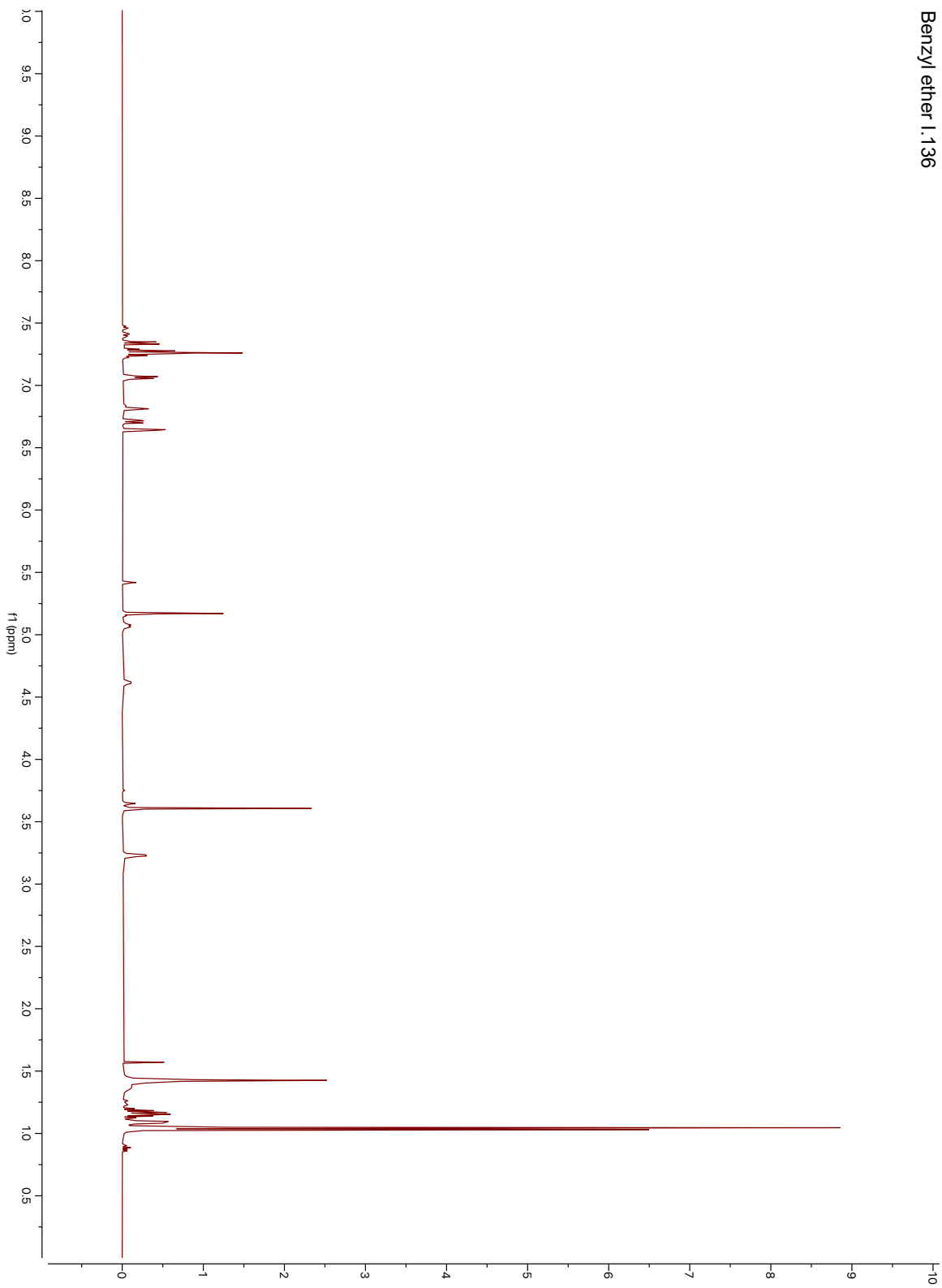
Carboxylic acid I. 123



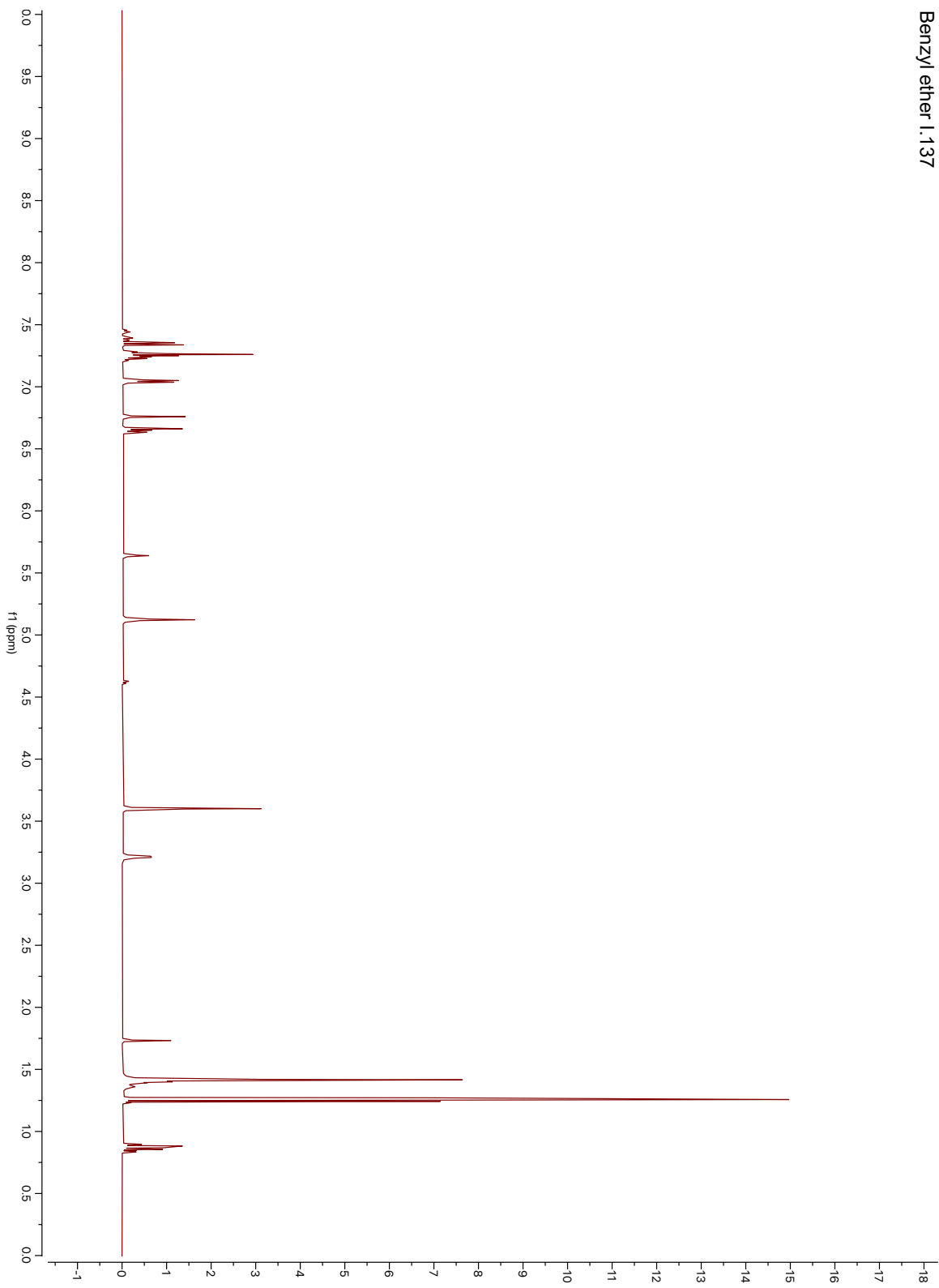
Phenol I.135



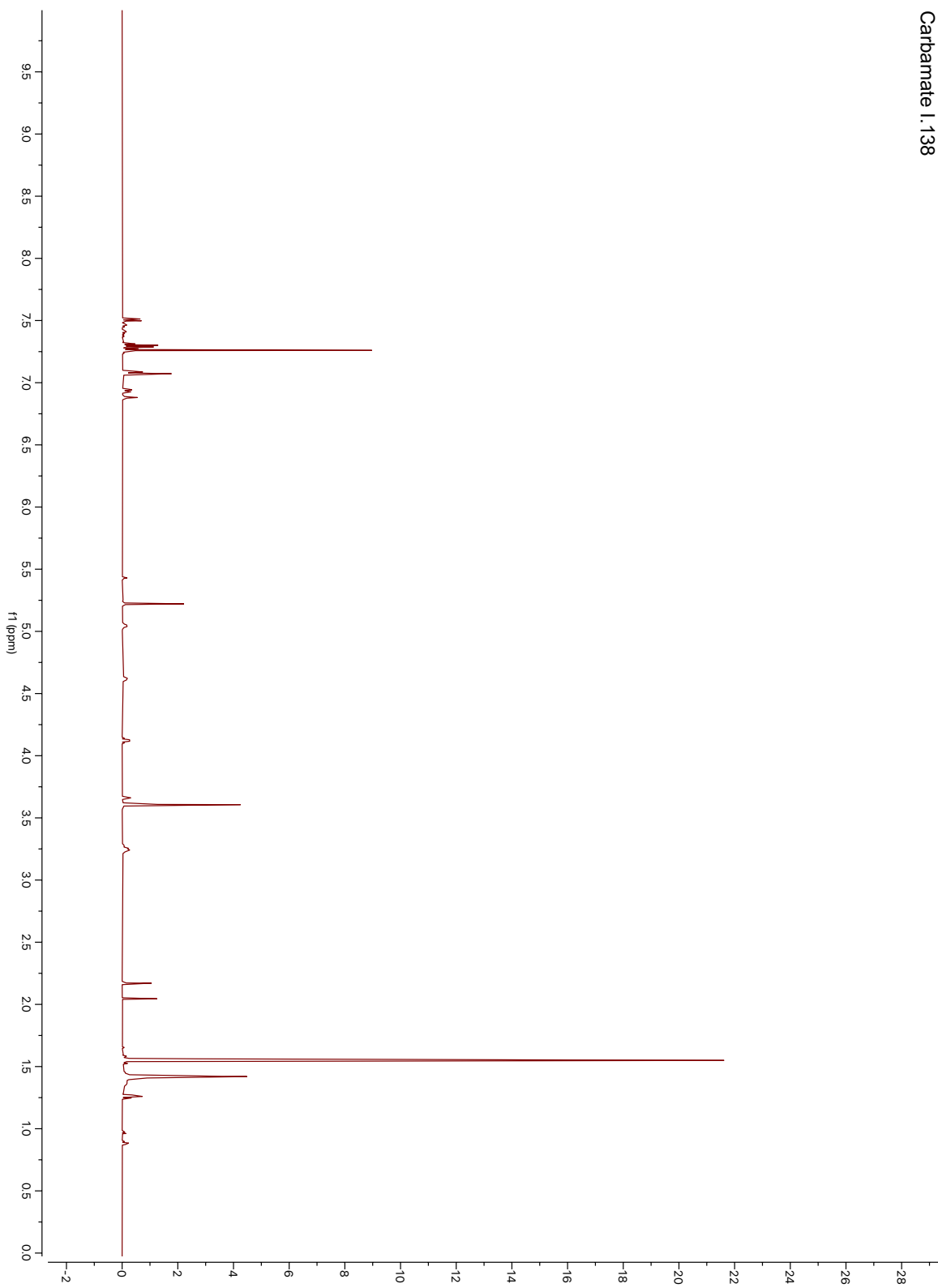
Benzyl ether 1.136



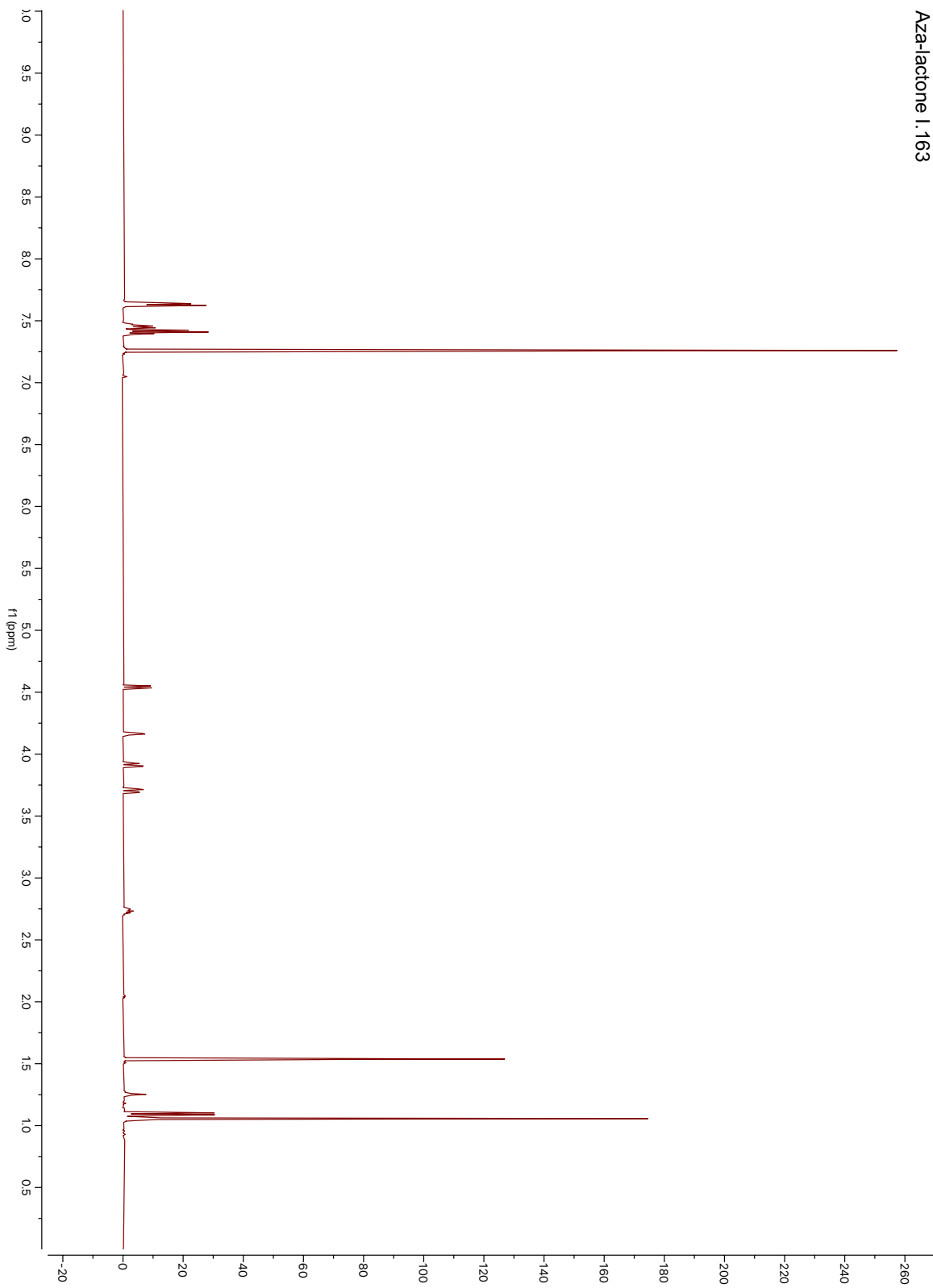
Benzyl ether 1.137



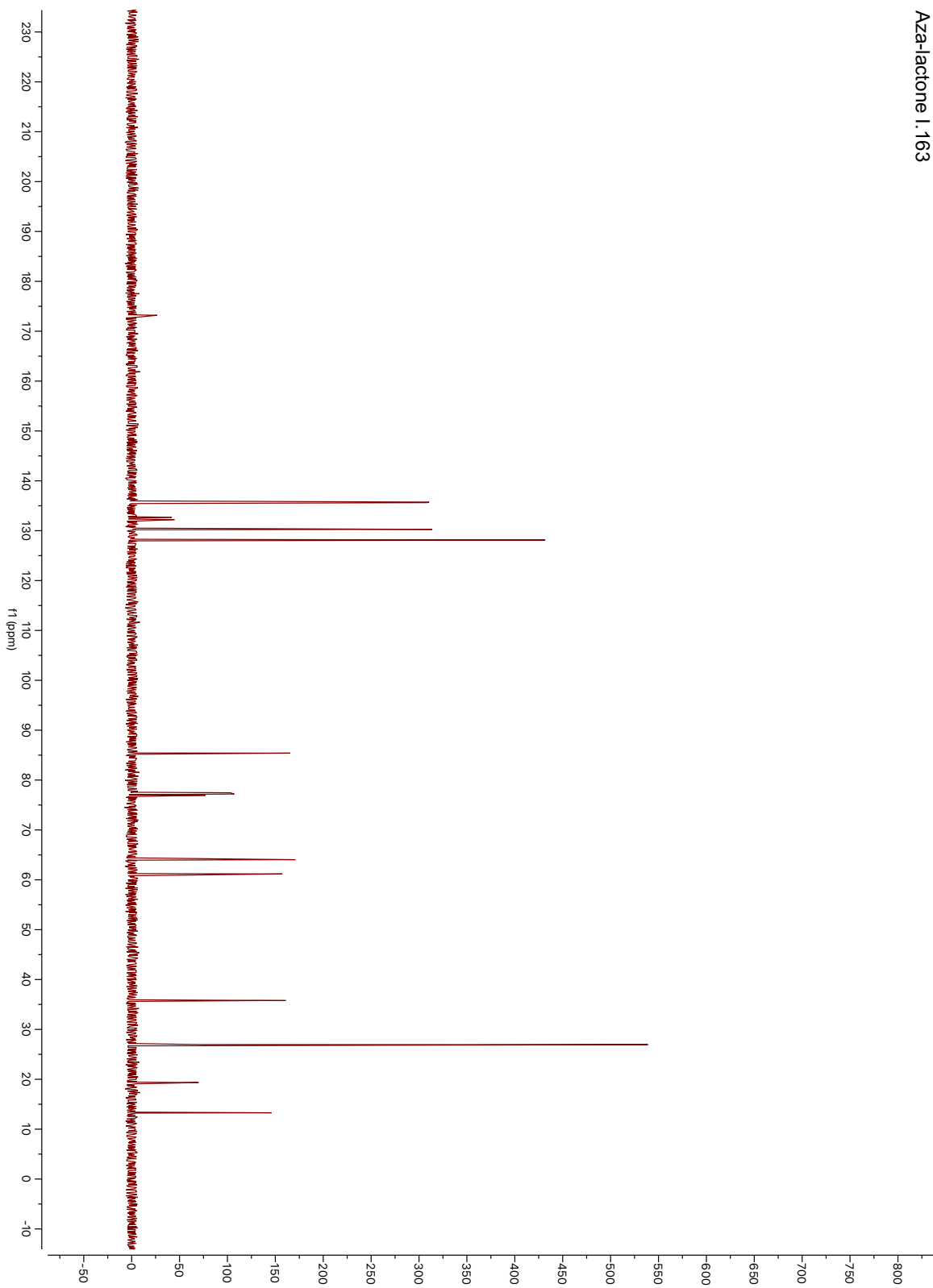
Carbamate 1.138



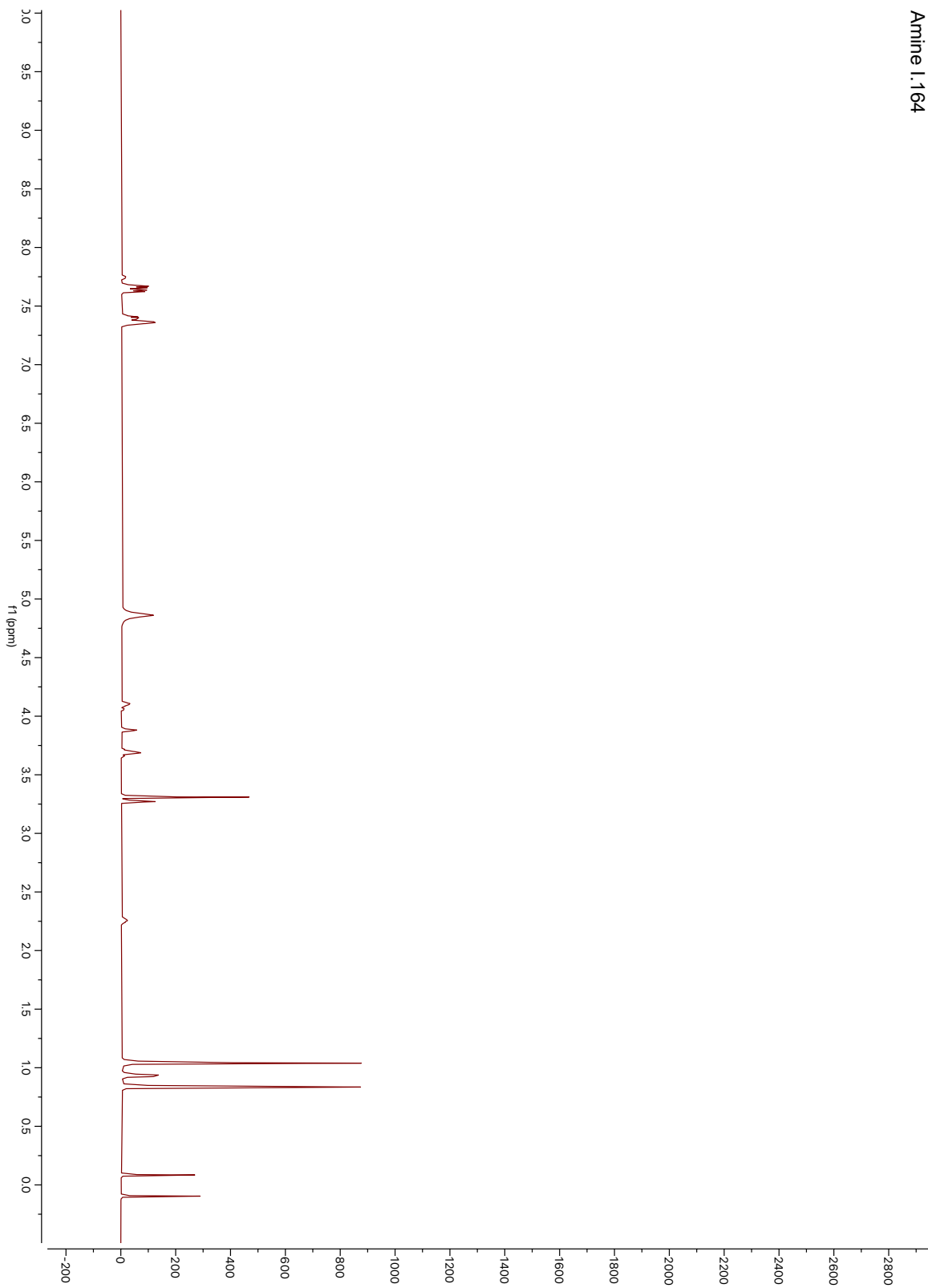
Aza-lactone I. 163



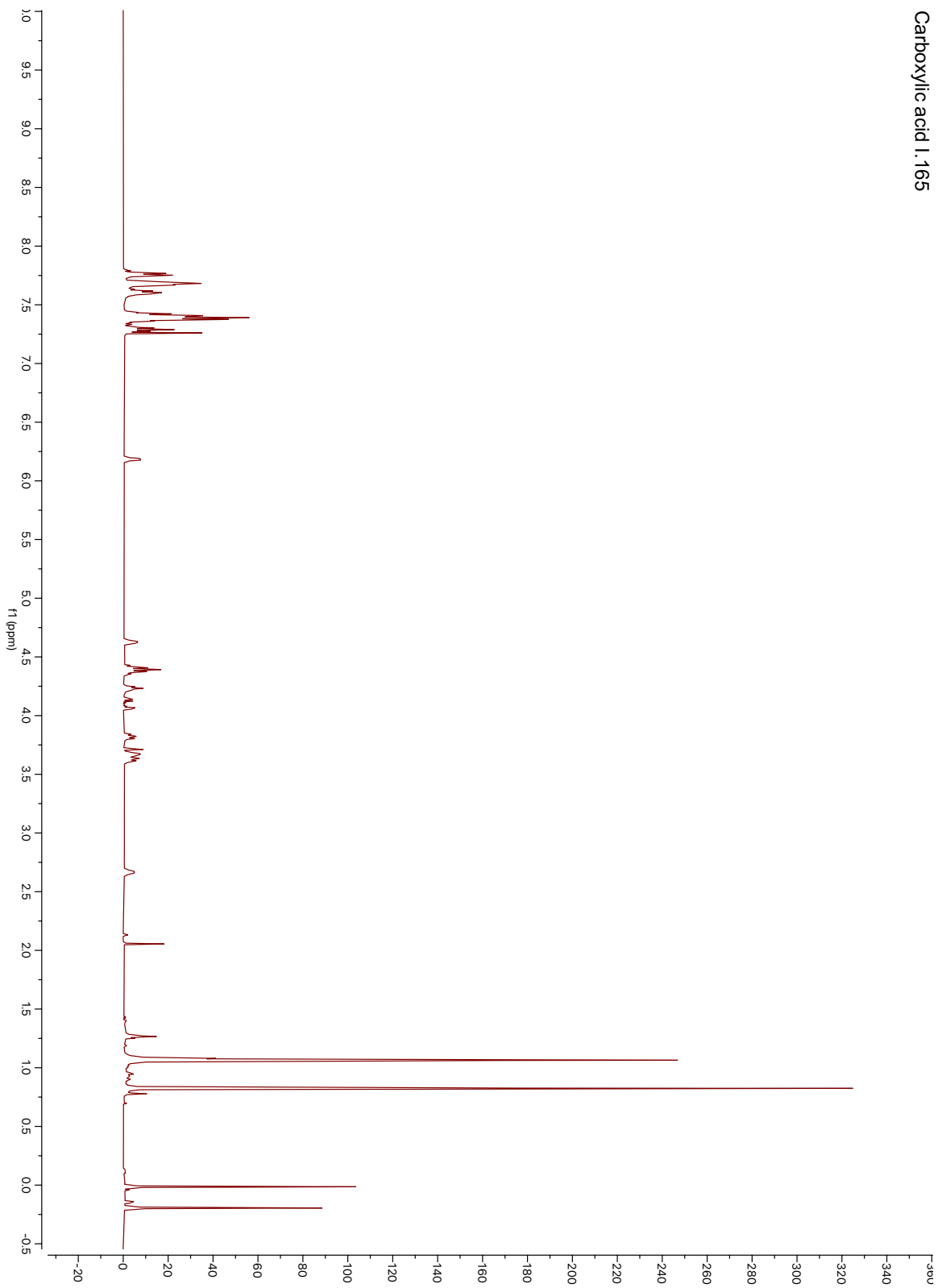
Aza-lactone I. 163



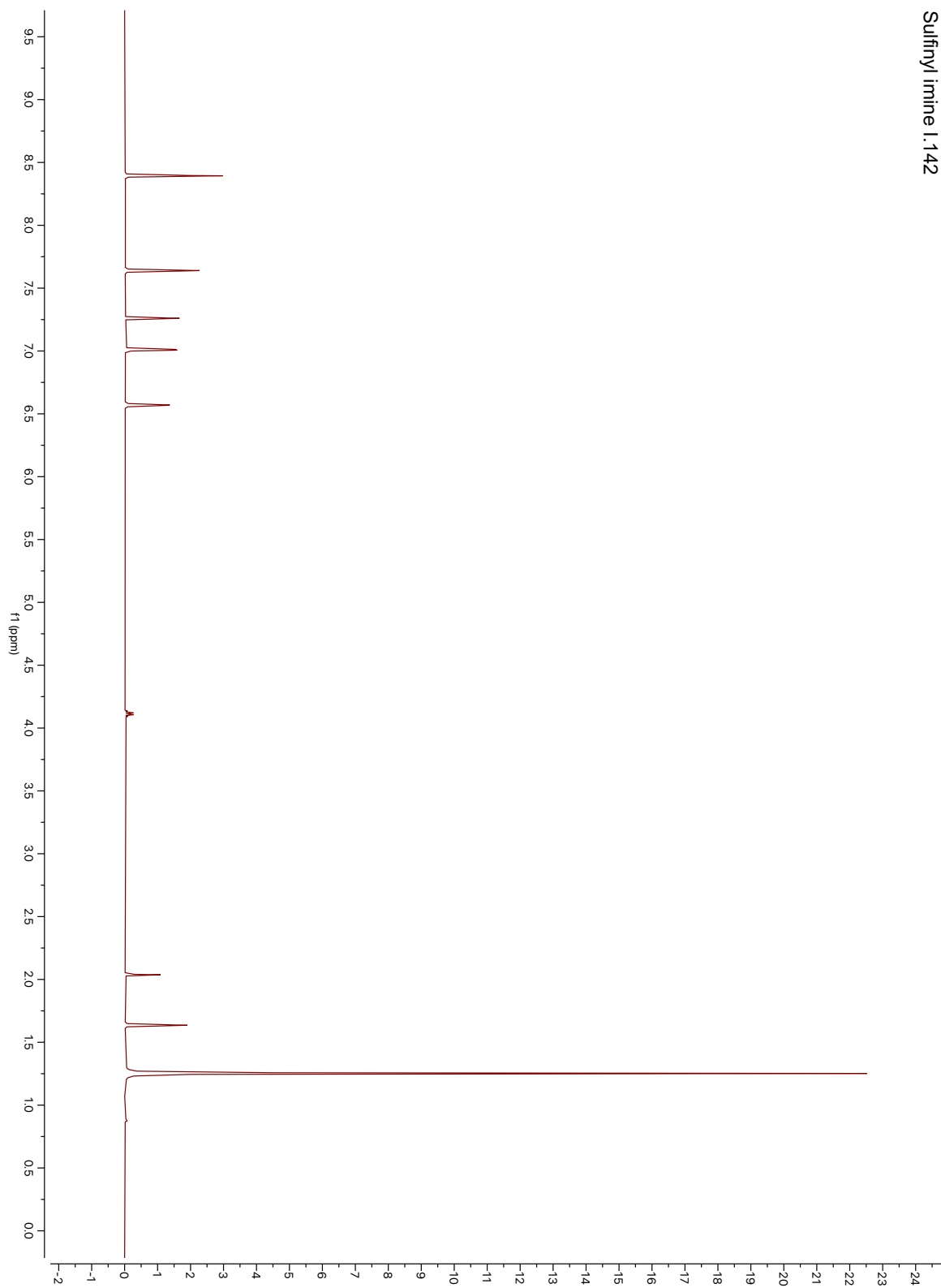
Amine I.164



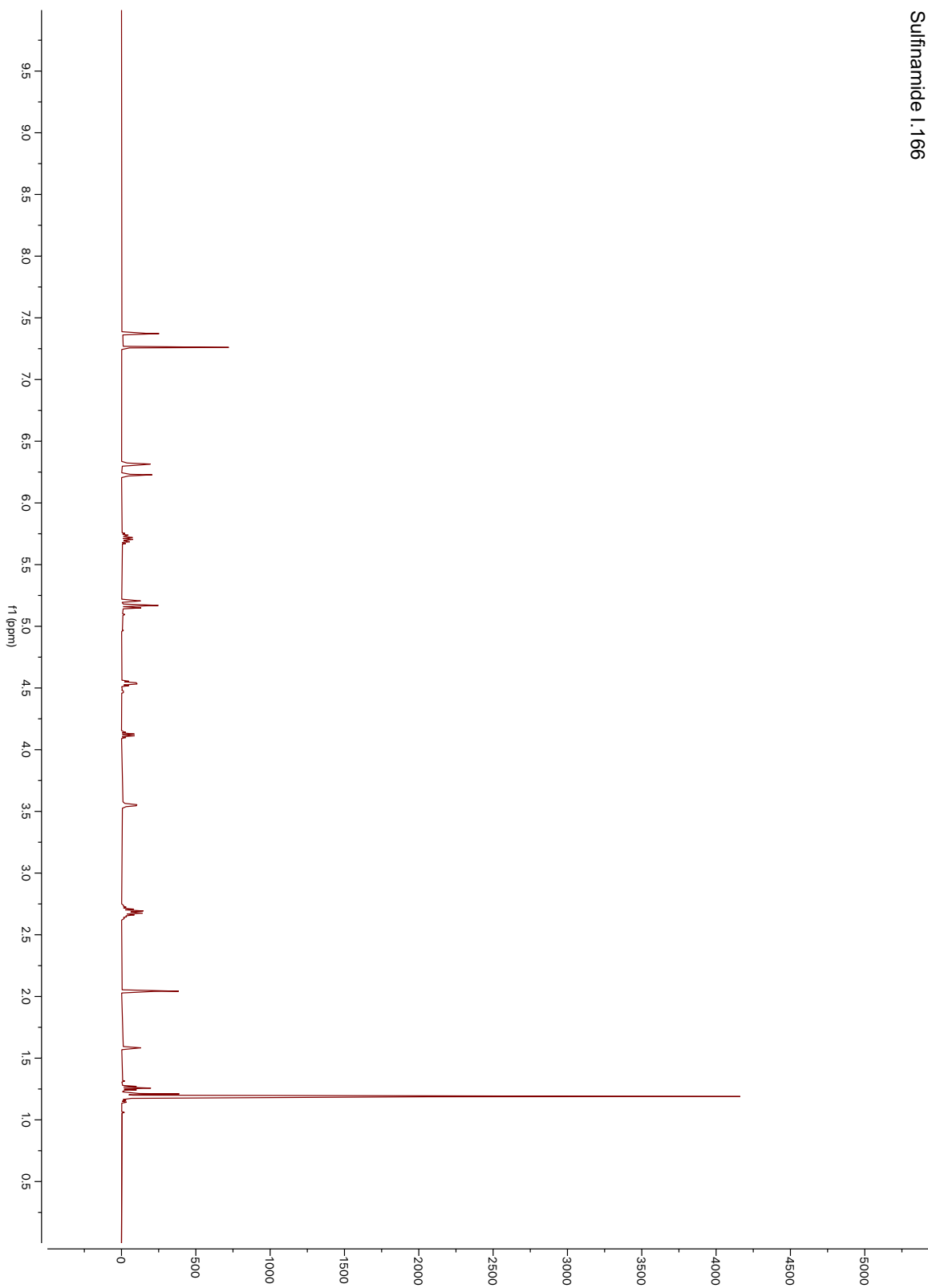
Carboxylic acid 1.165



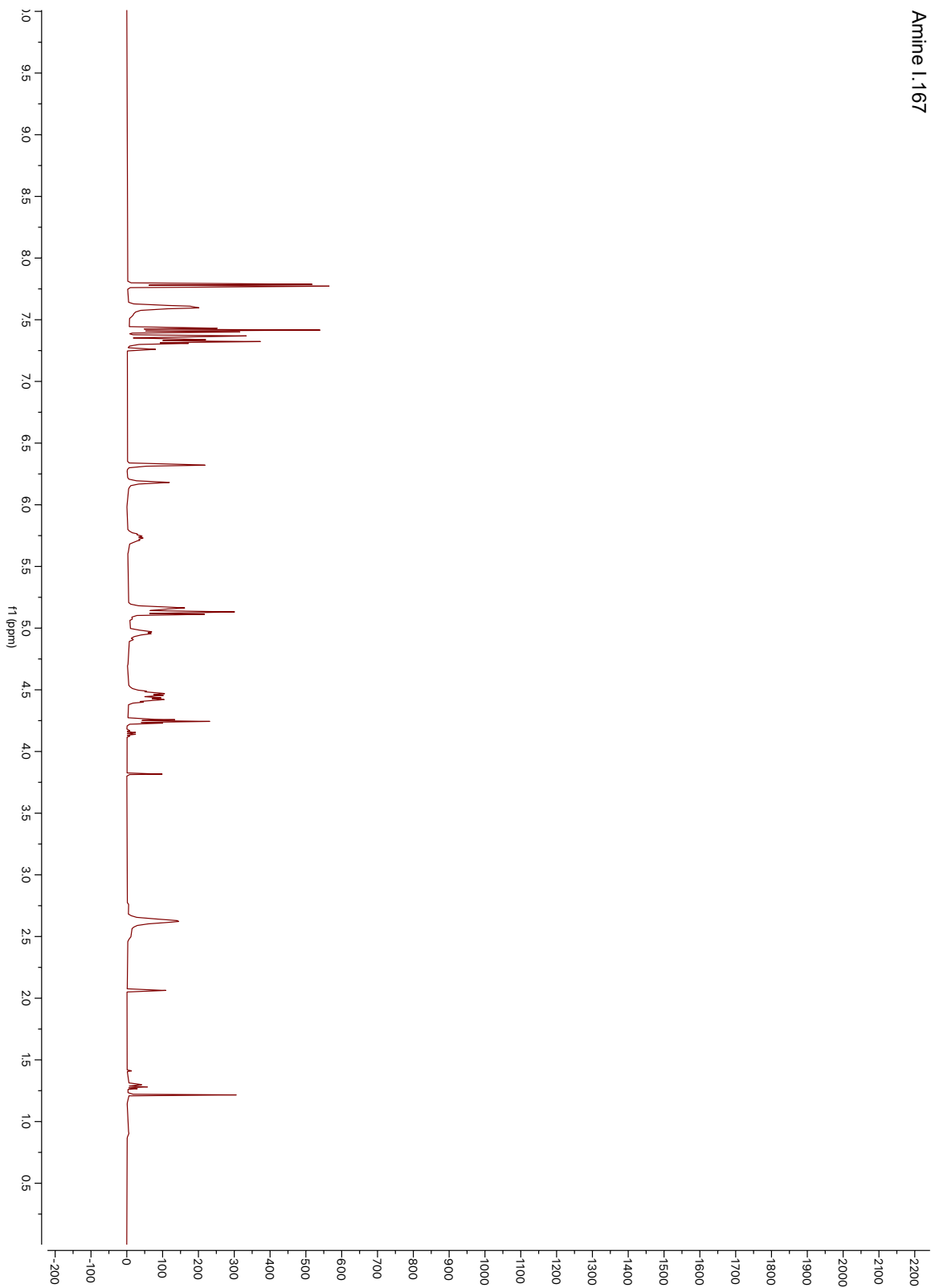
Sulfanyl imine I.142



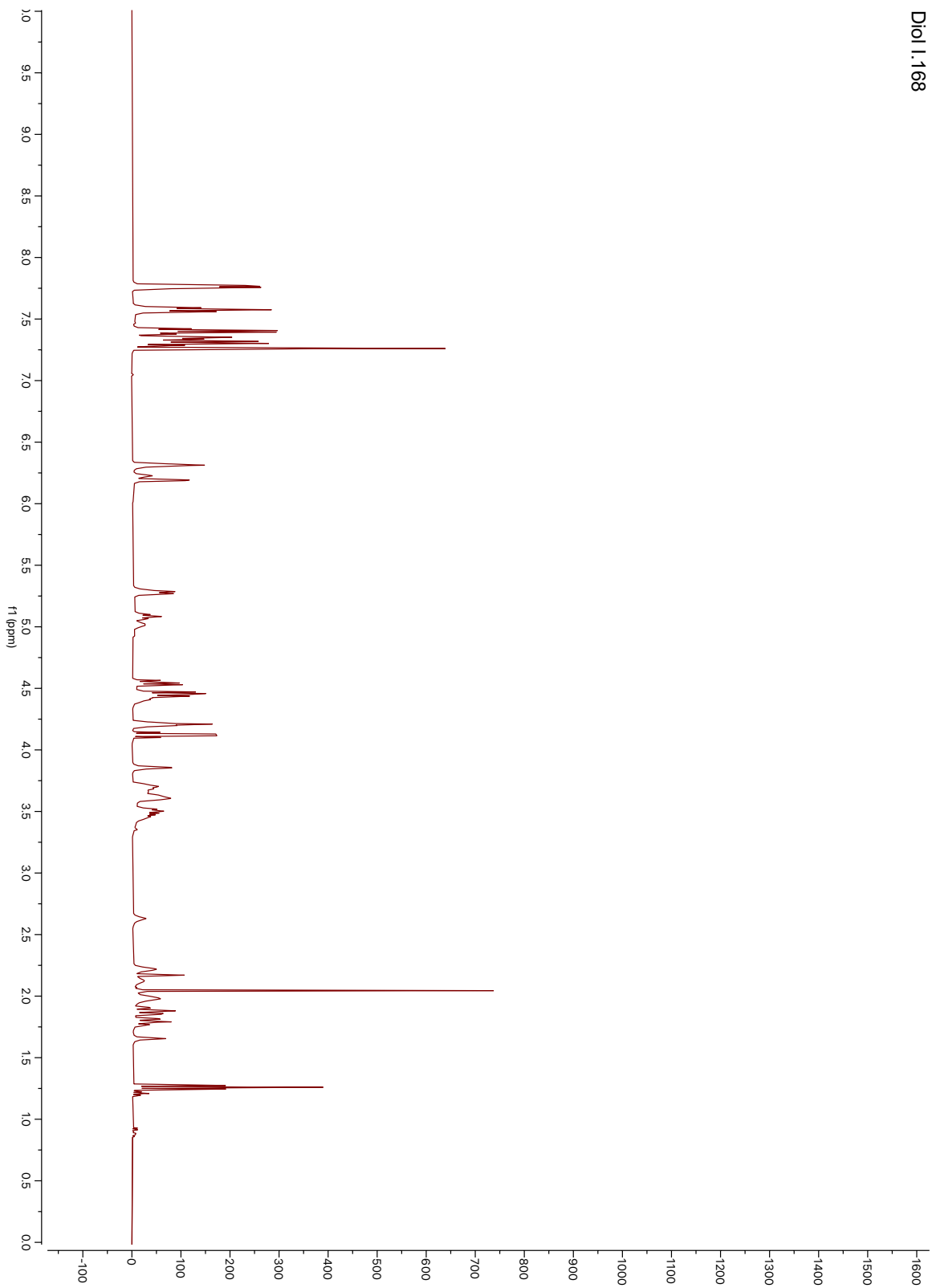
Sulfonamide I.166



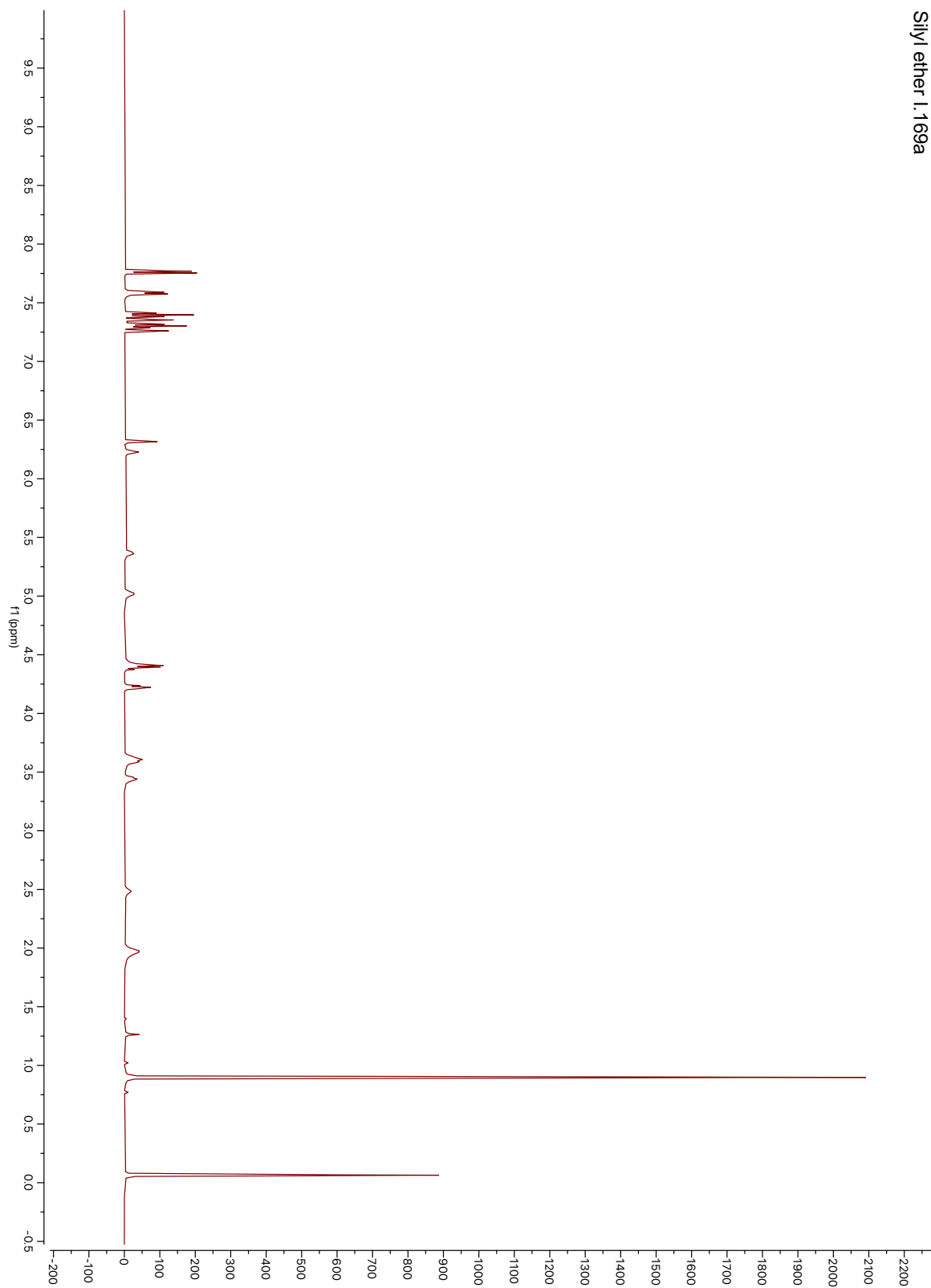
Amine I.167



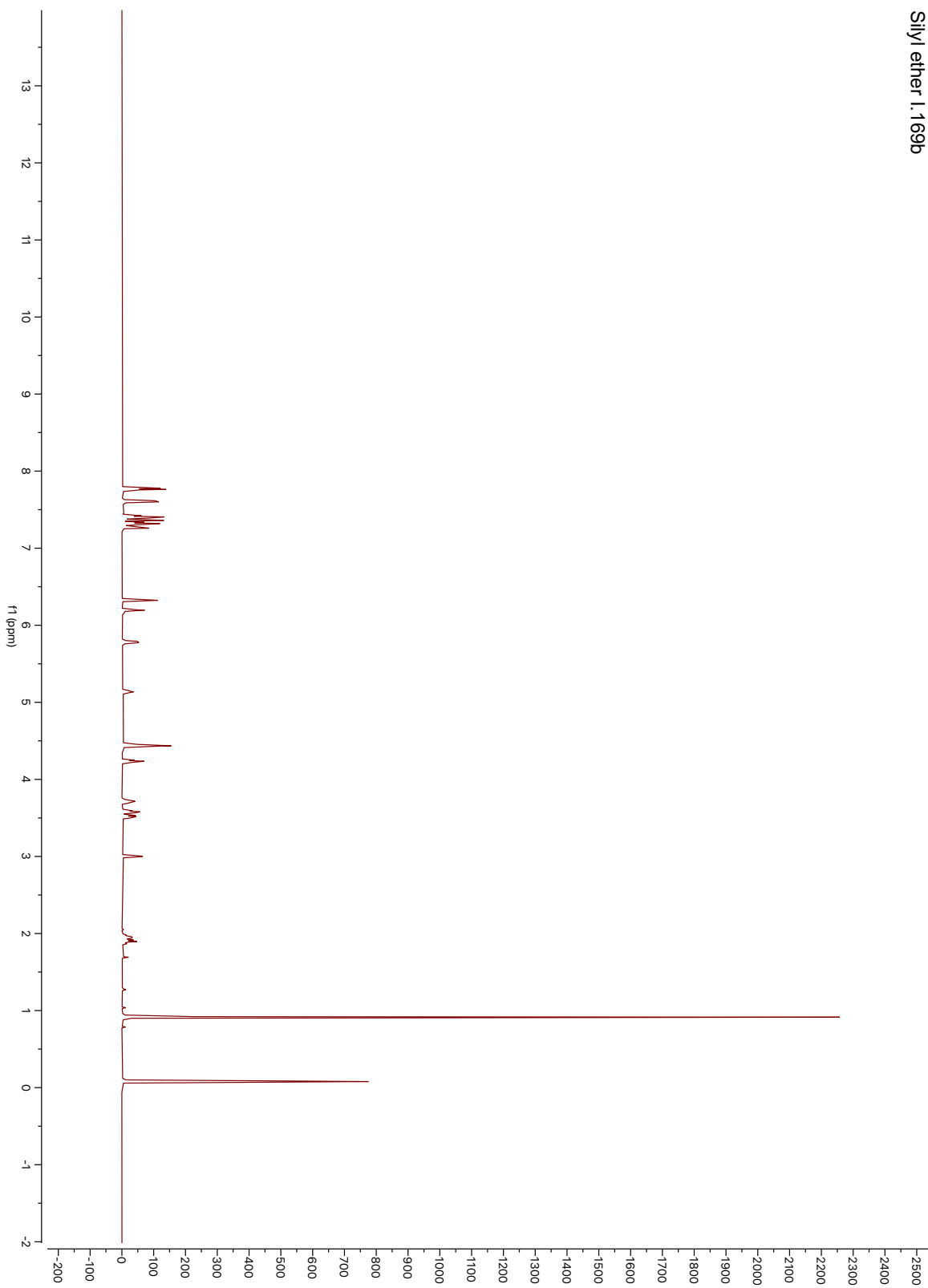
Diol I.168



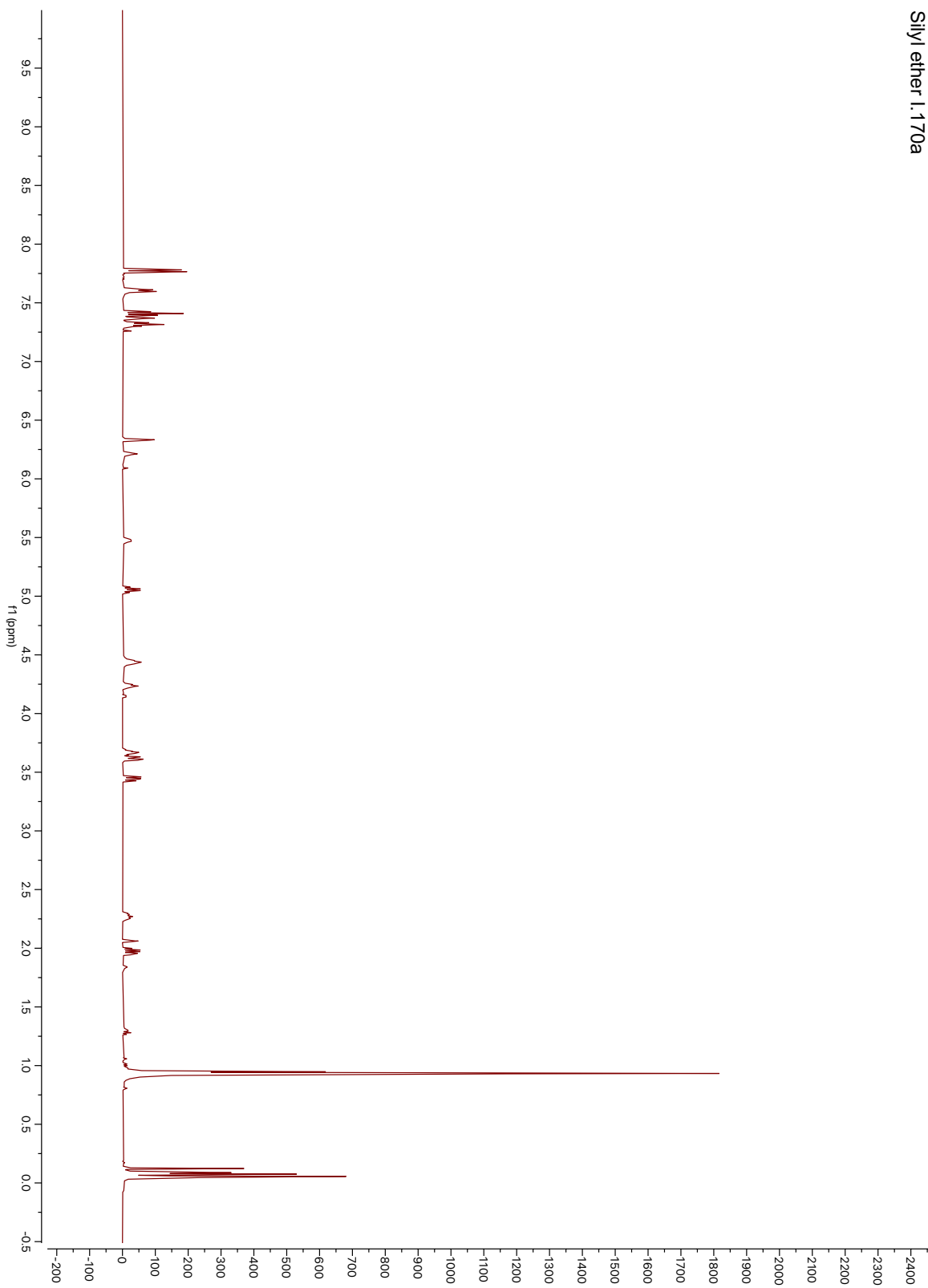
Silyl ether 1.169a



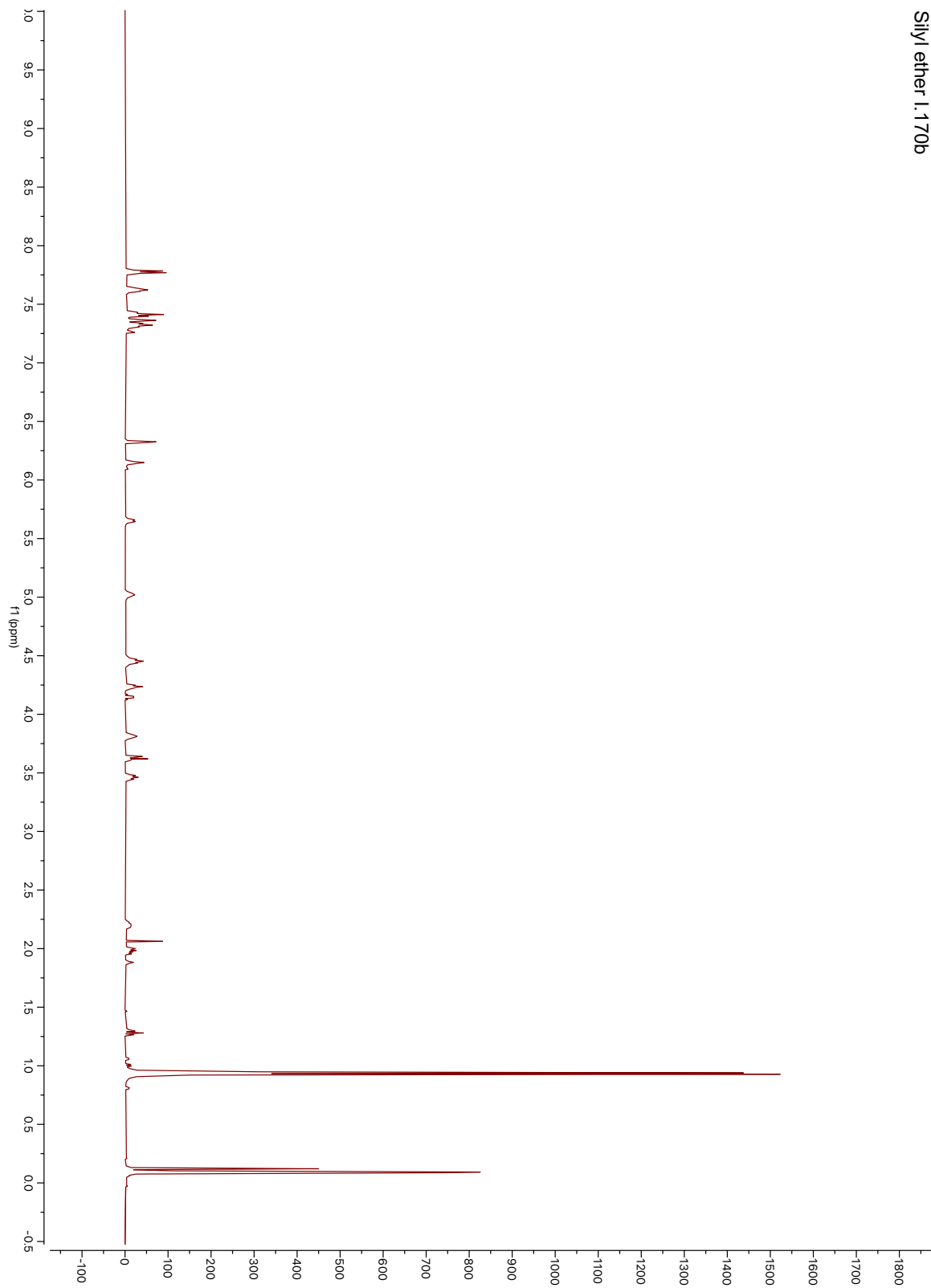
Silyl ether 1.169b



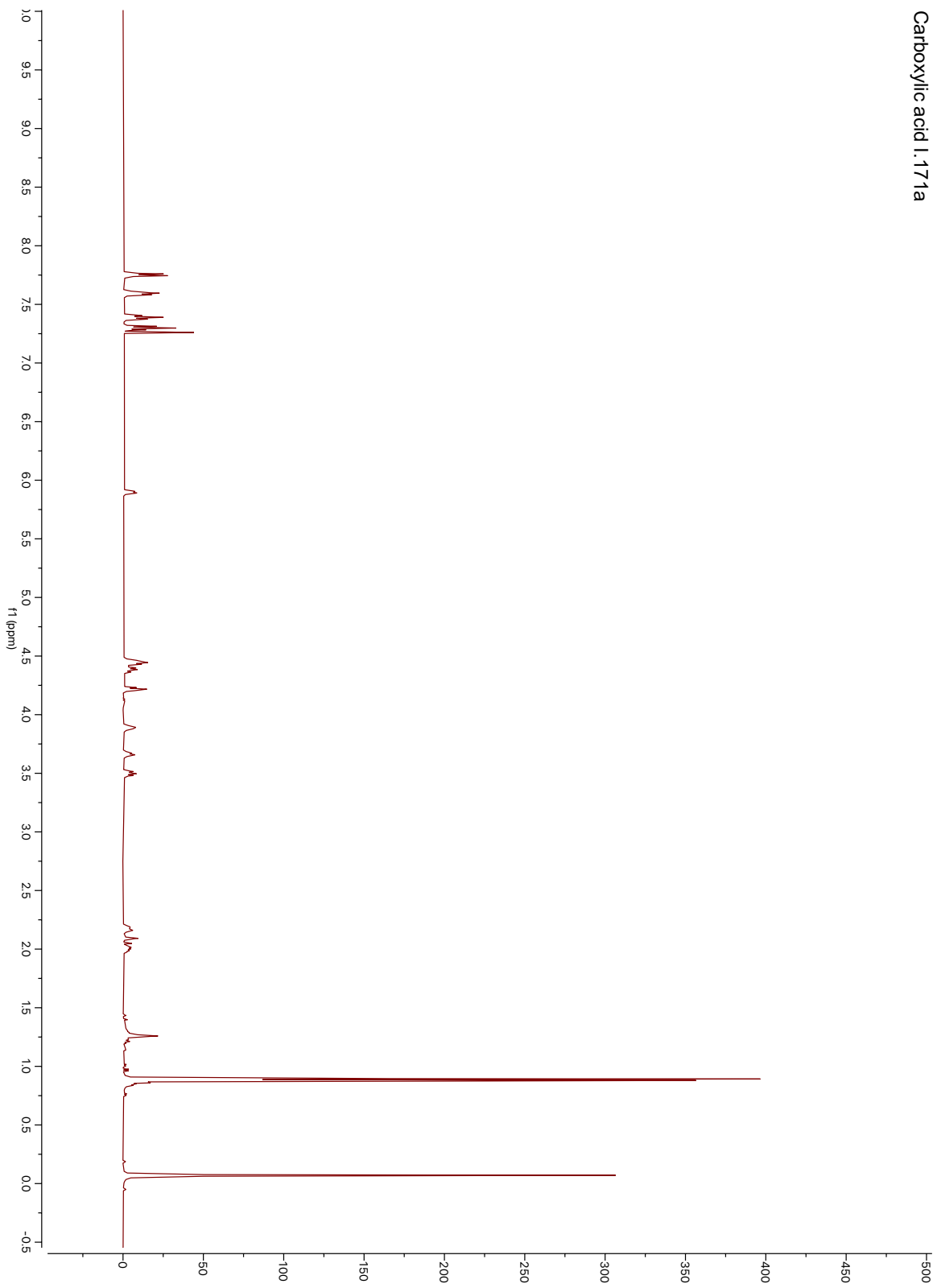
Silyl ether 1.170a



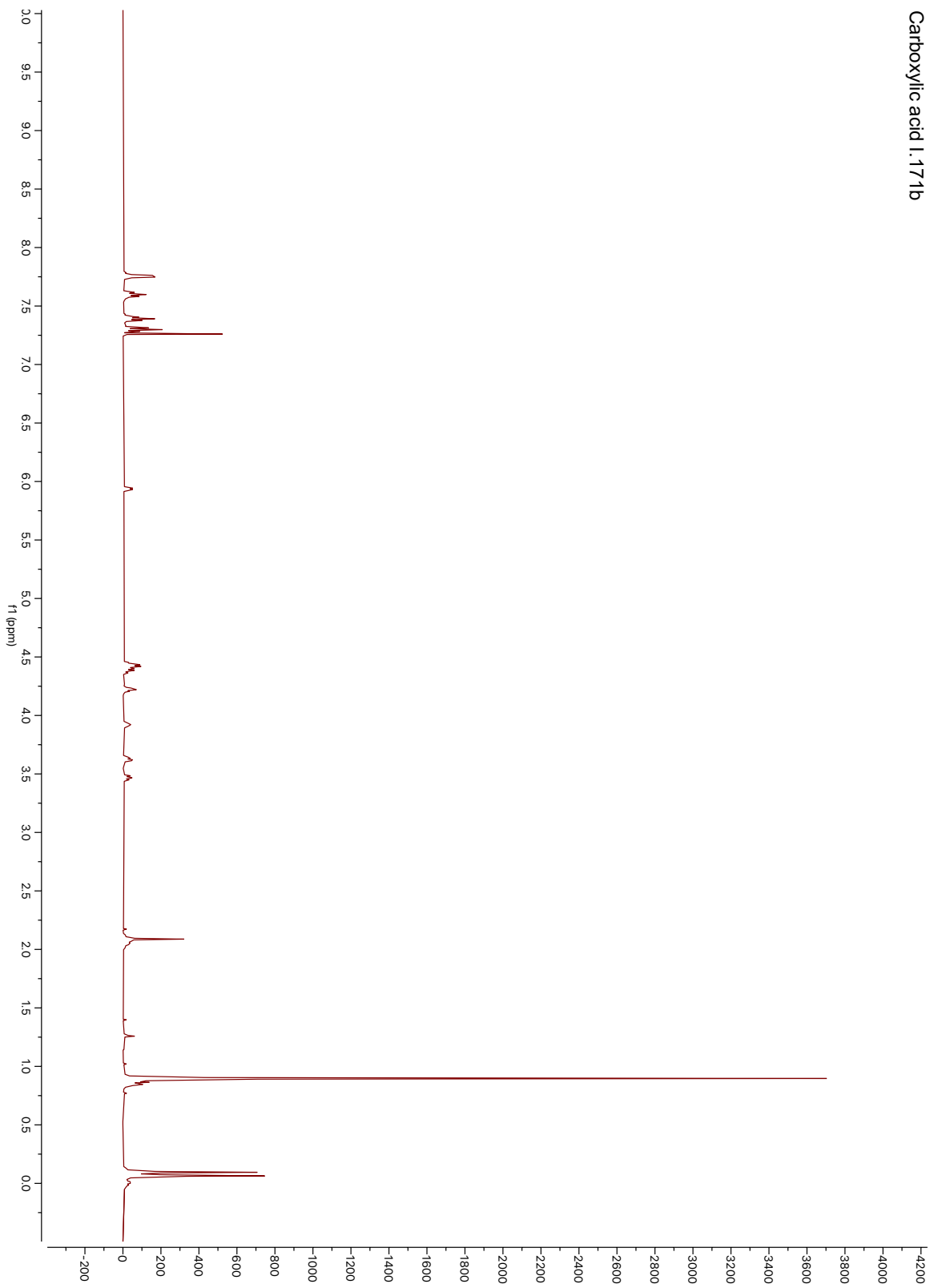
Silyl ether 1.170b



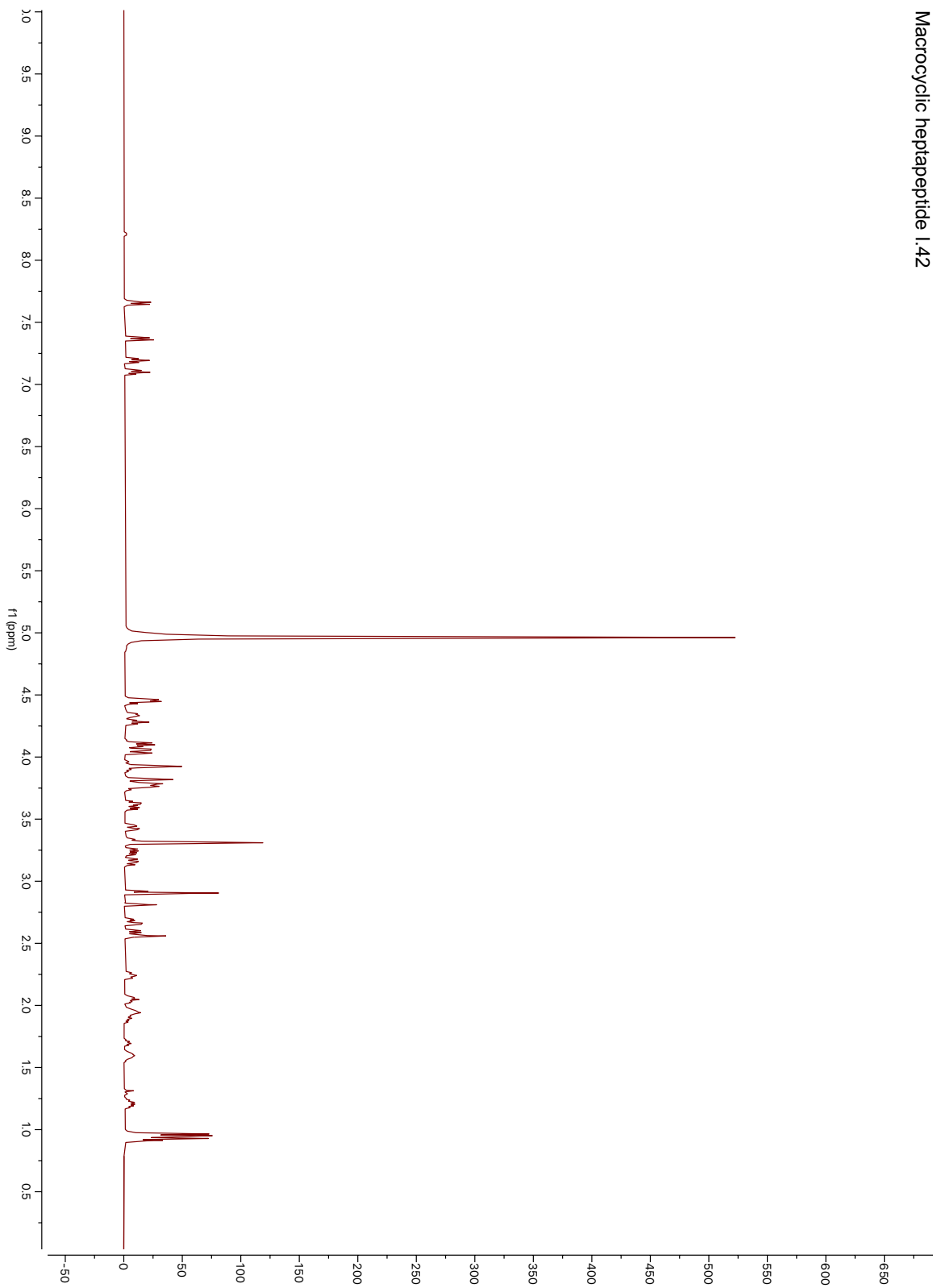
Carboxylic acid 1.171a



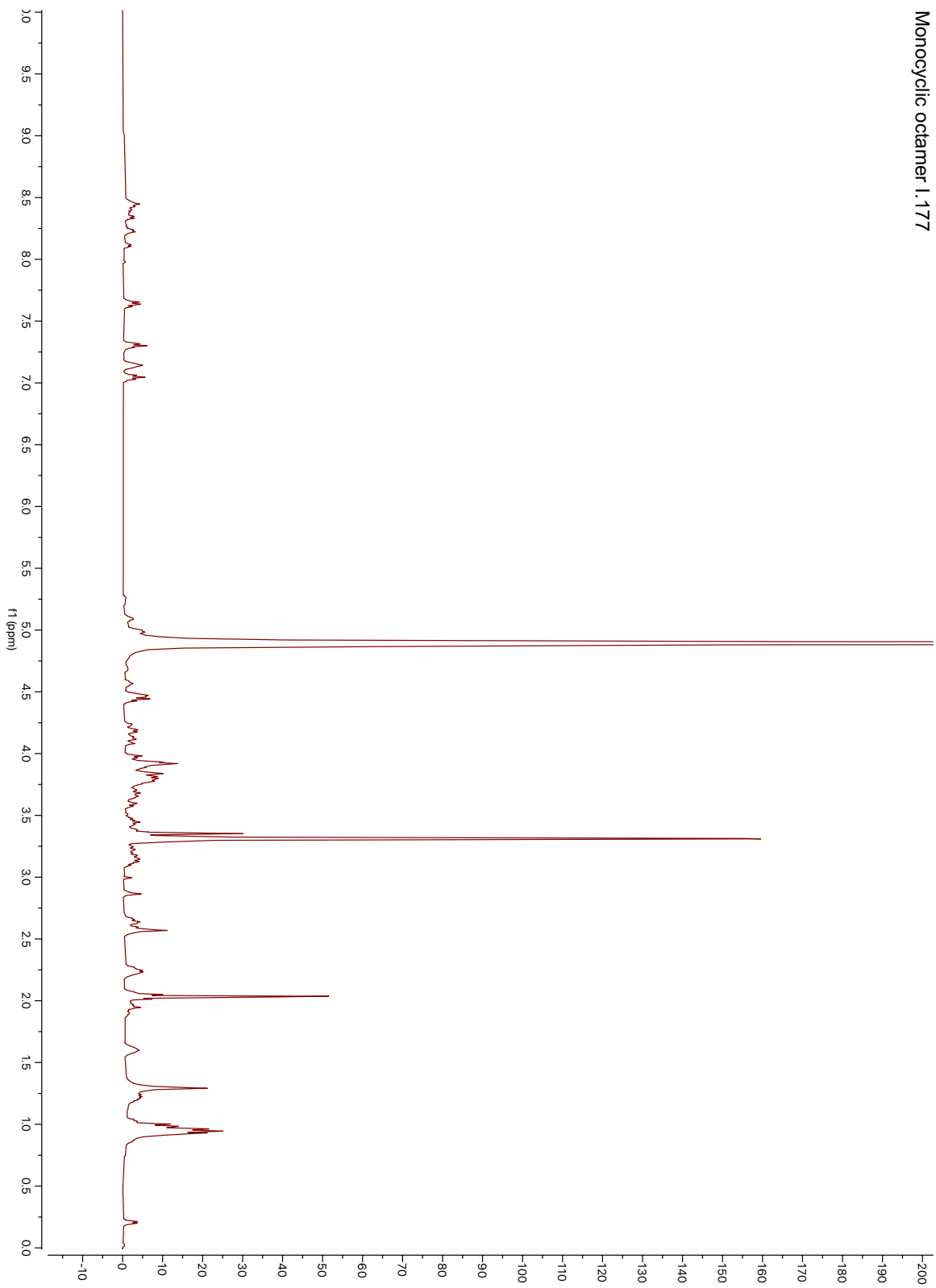
Carboxylic acid 1.171b



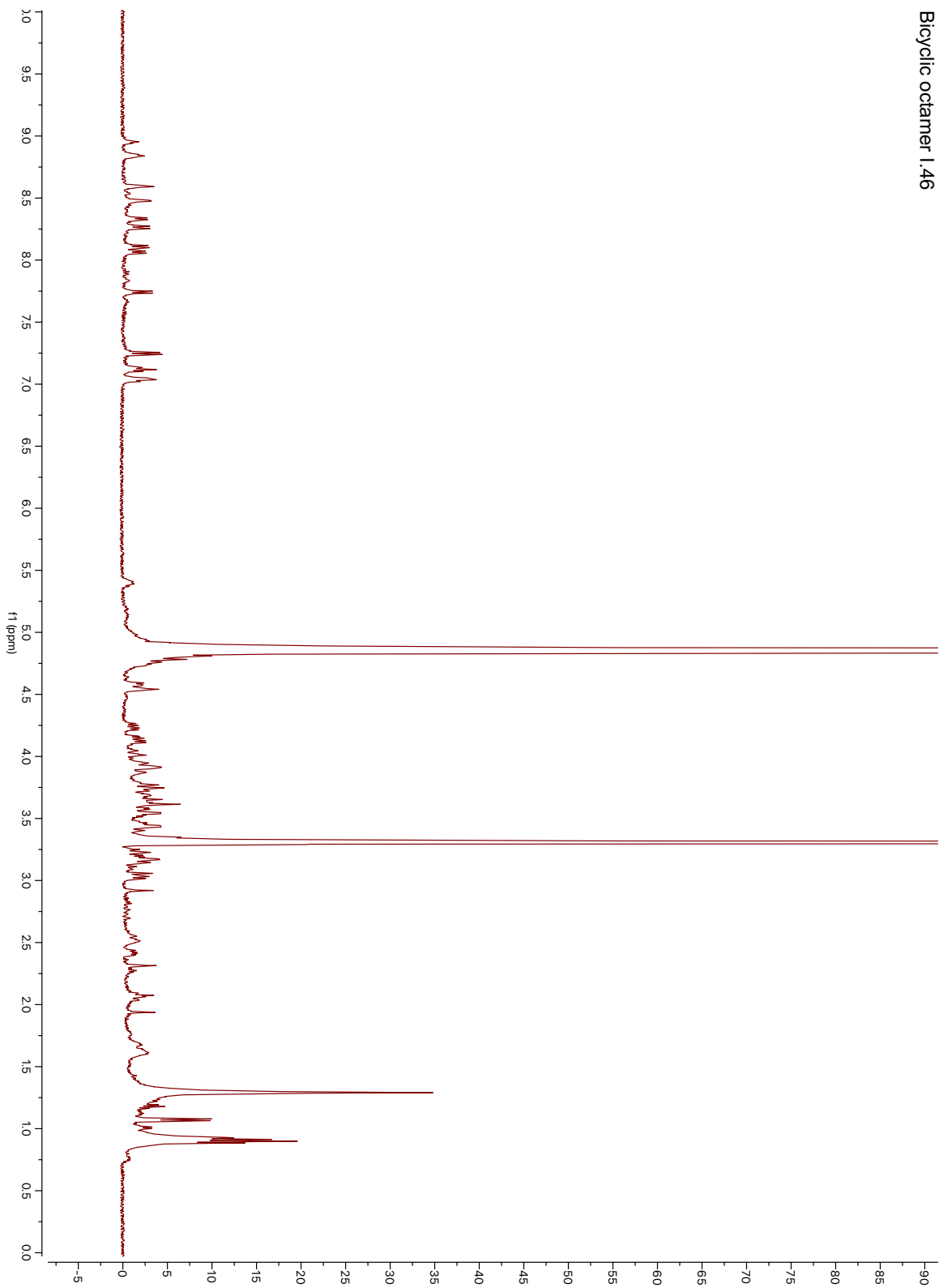
Macrocyclic heptapeptide 1.42



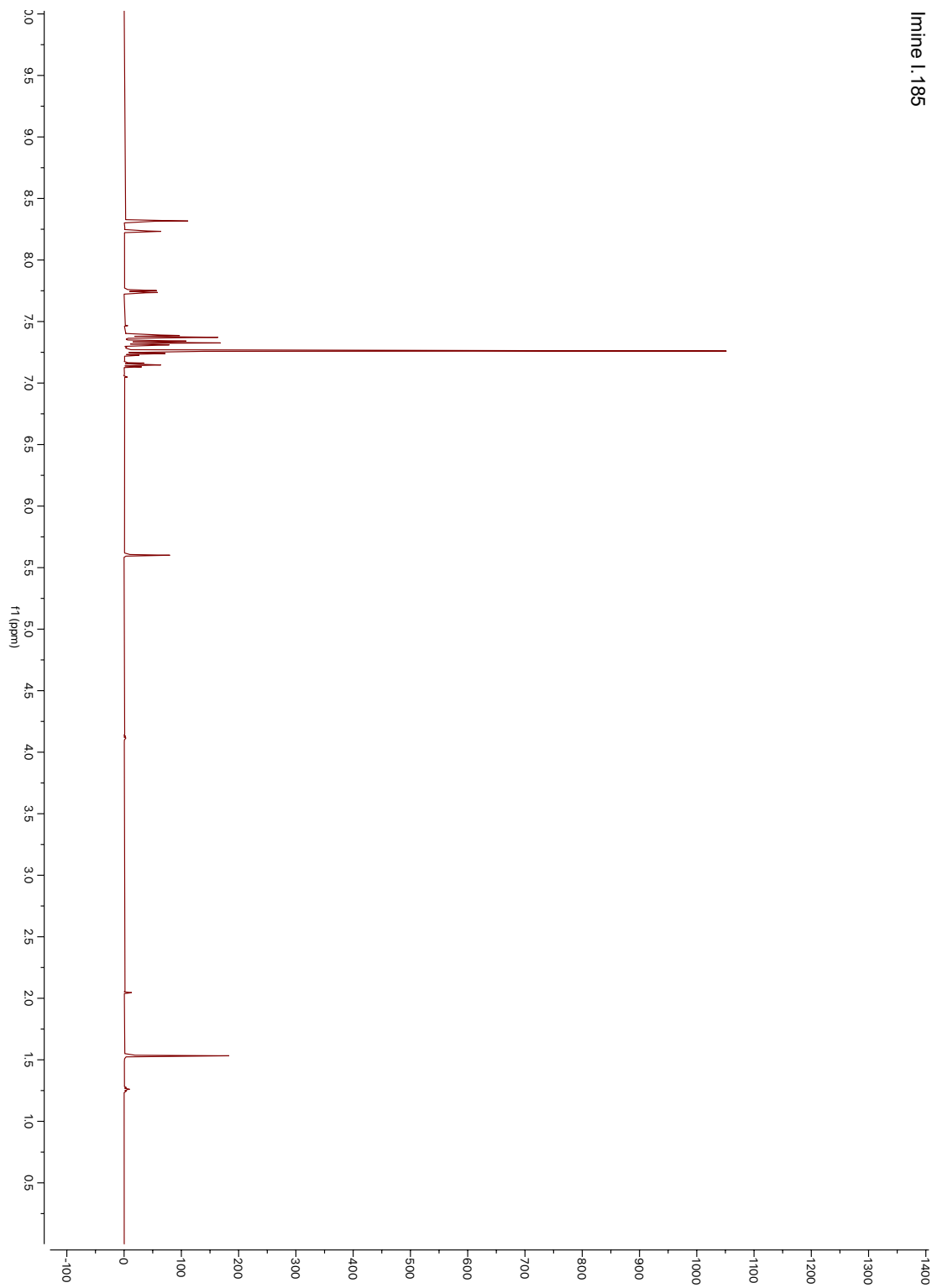
Monocyclic octamer 1.177



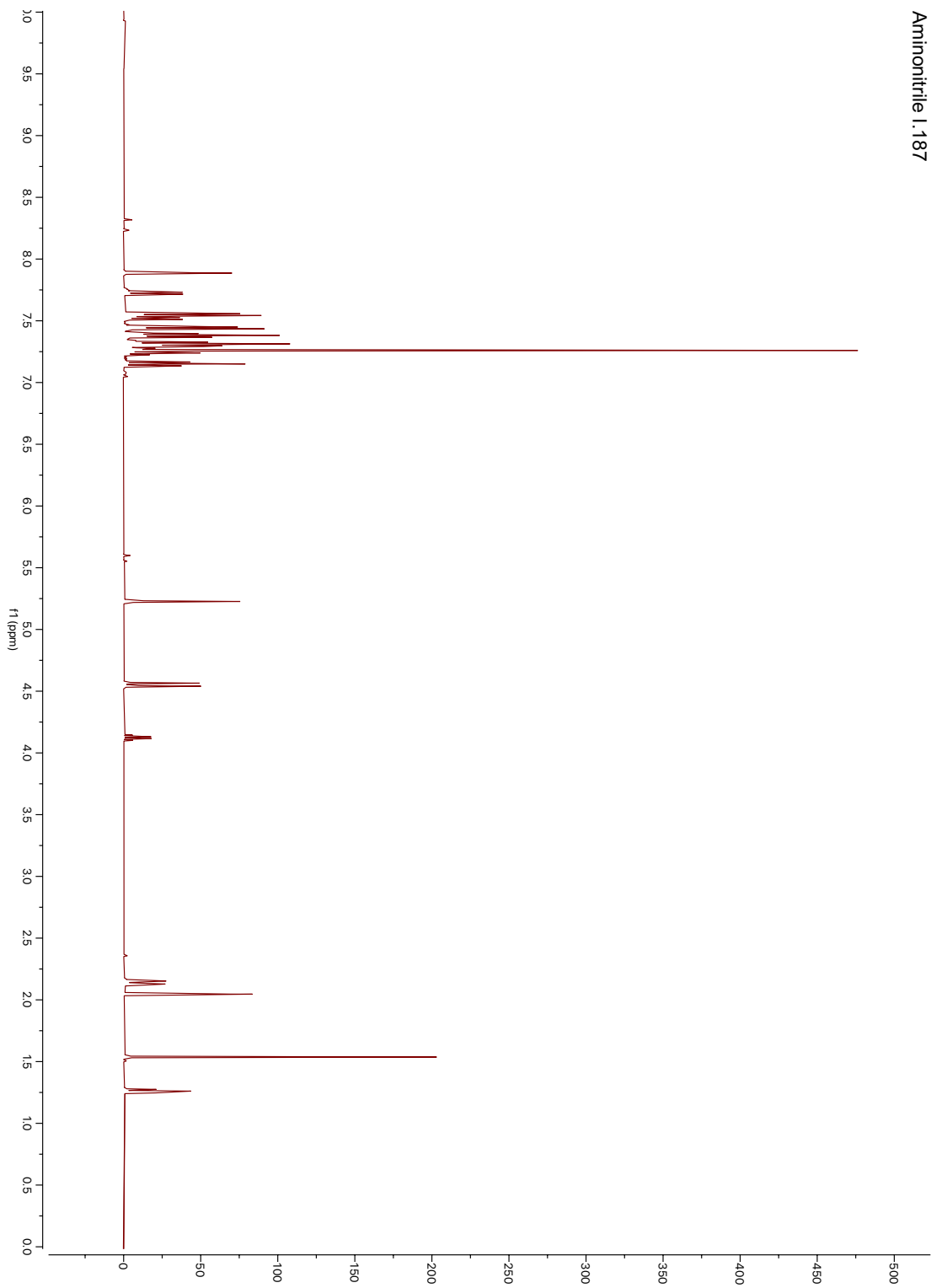
Bicyclic octamer 1.46



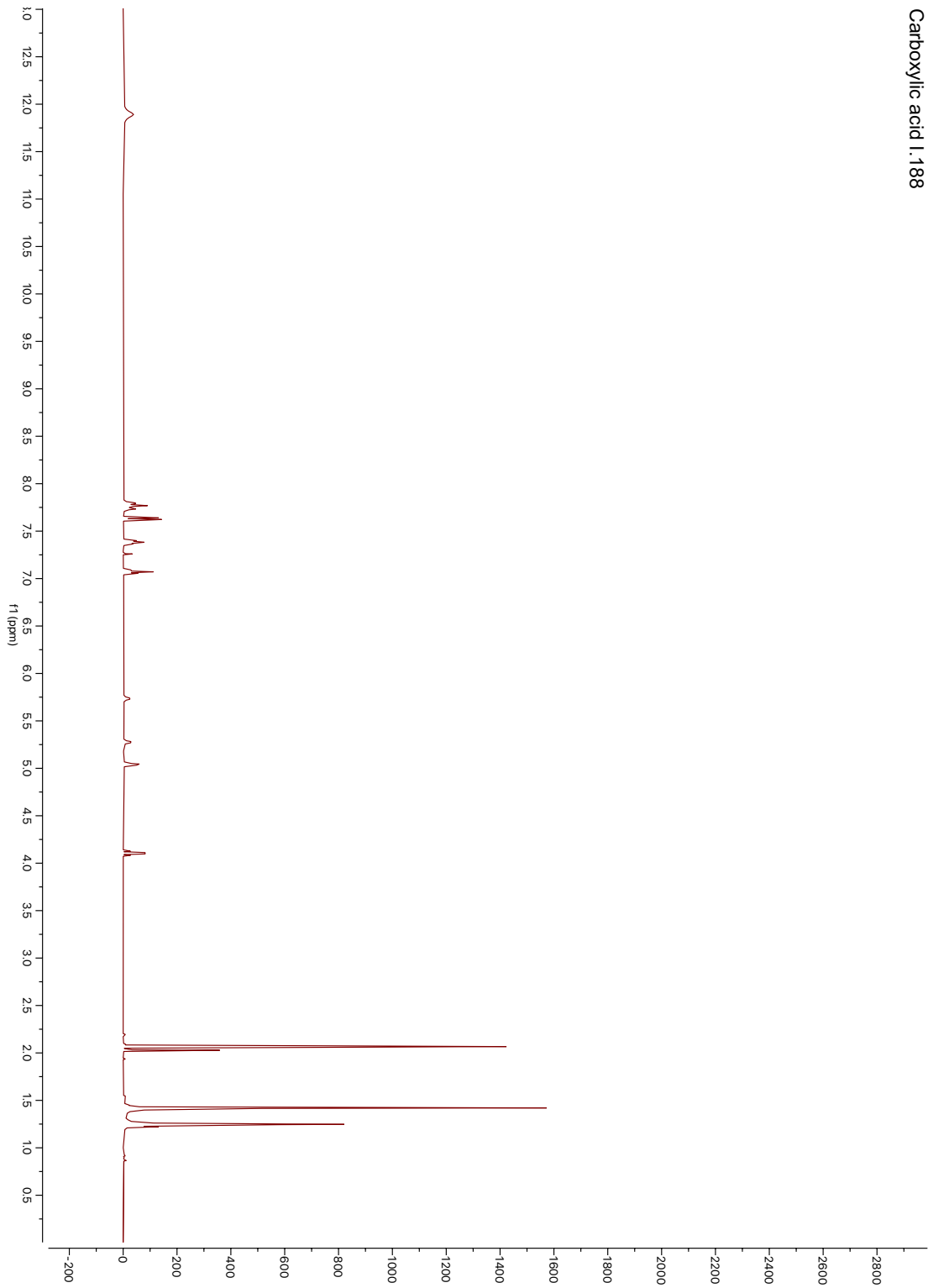
Imine 1.185



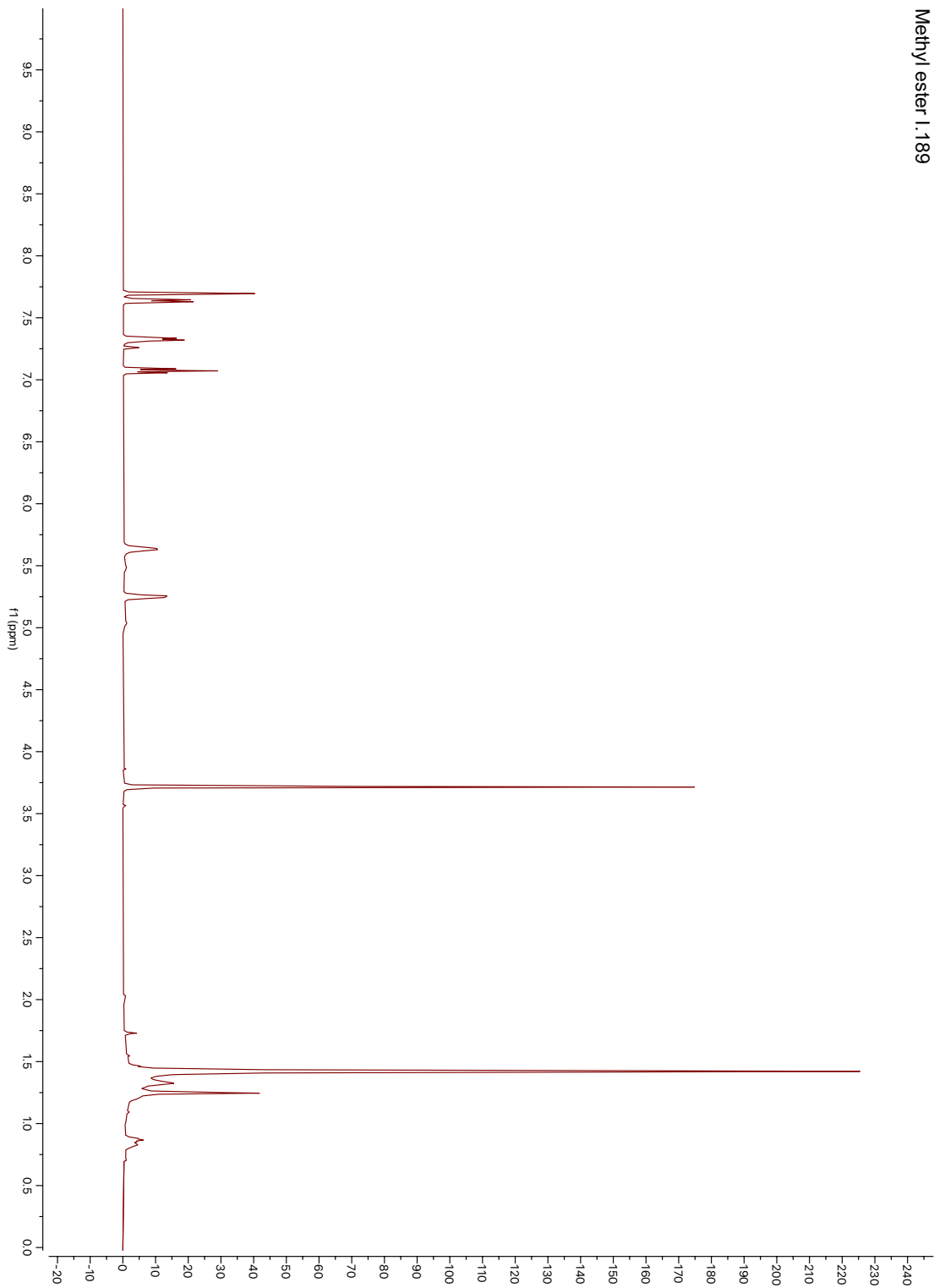
Aminonitrile 1.187



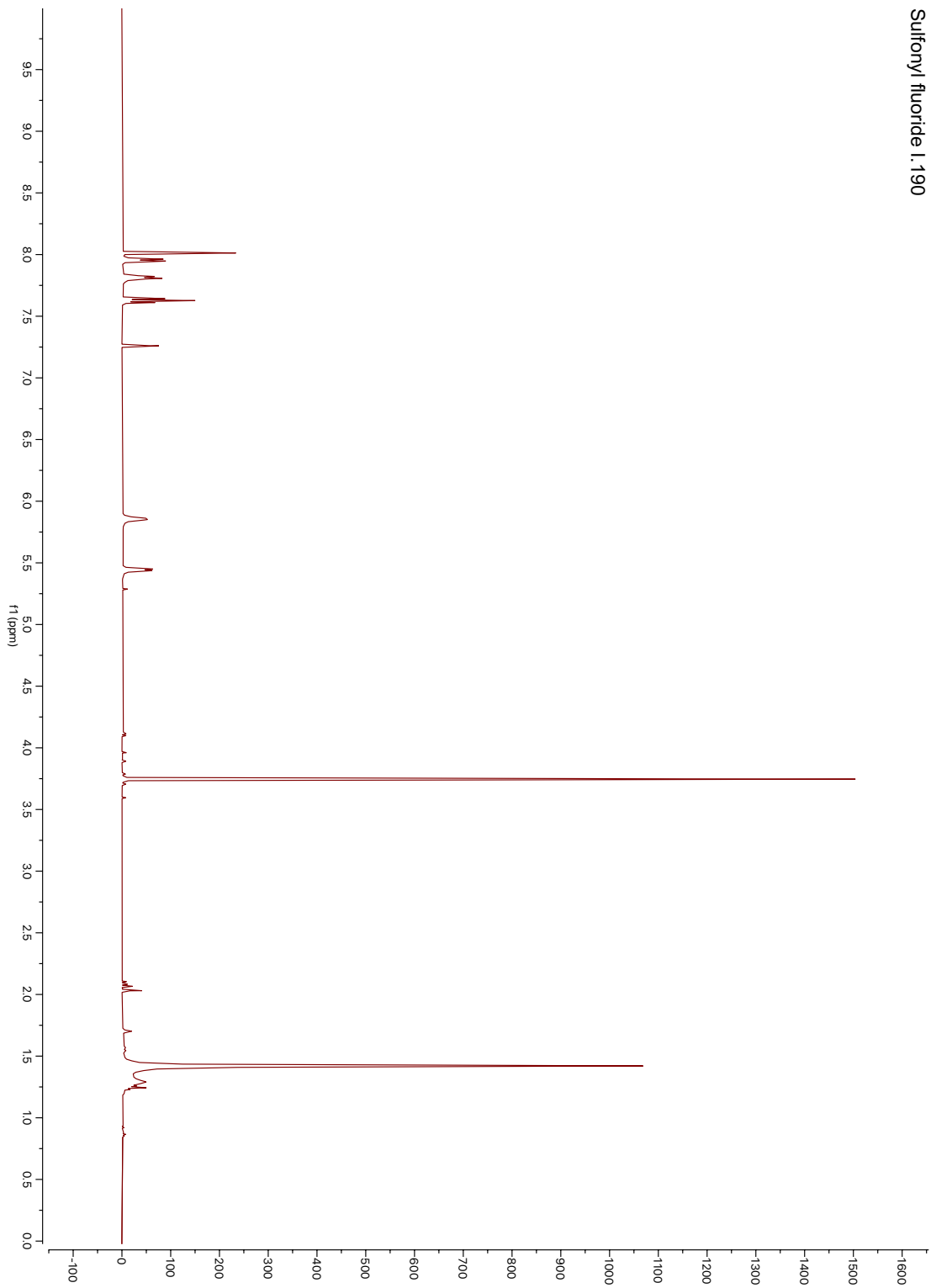
Carboxylic acid 1.188



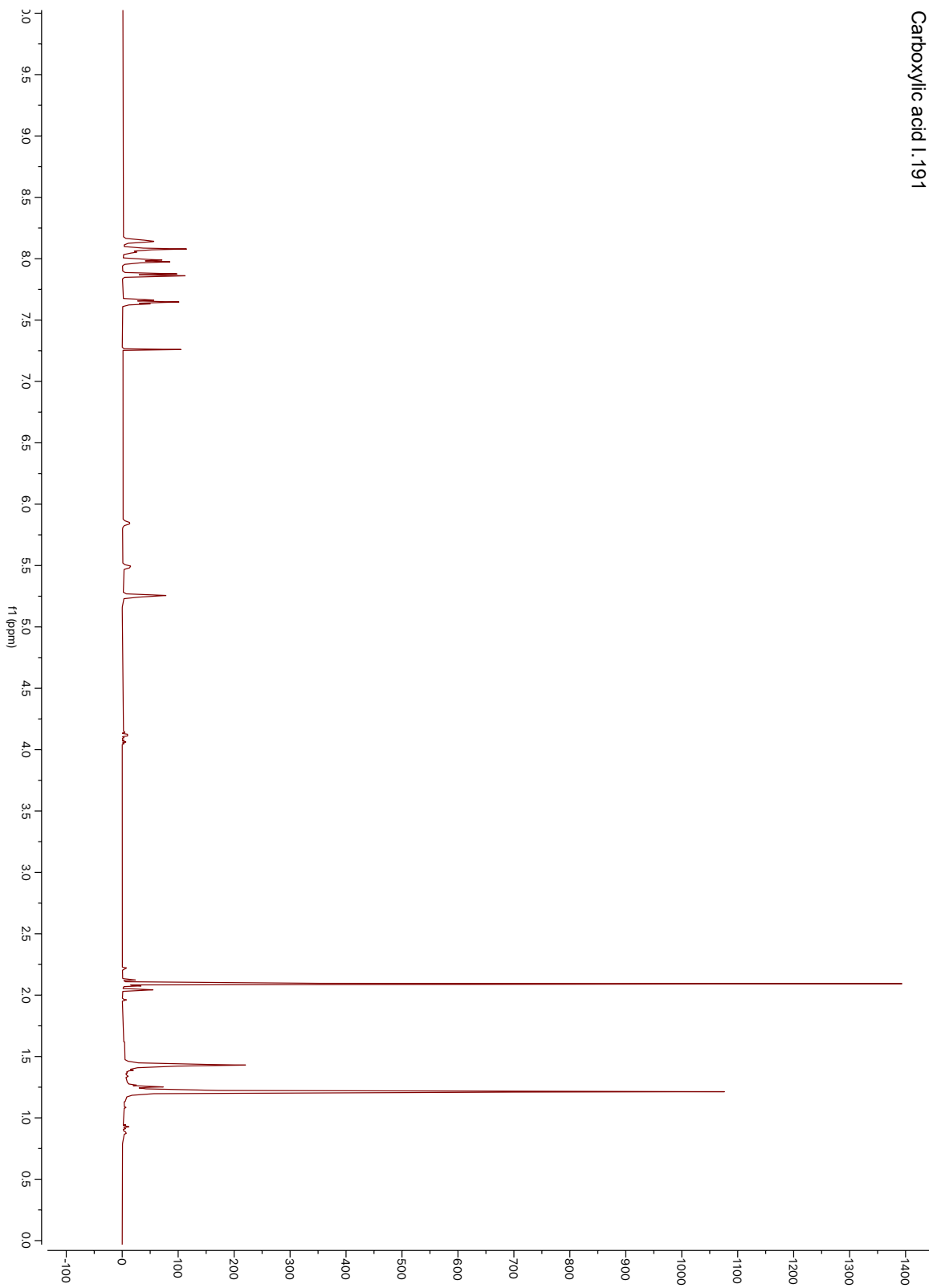
Methyl ester 1.189



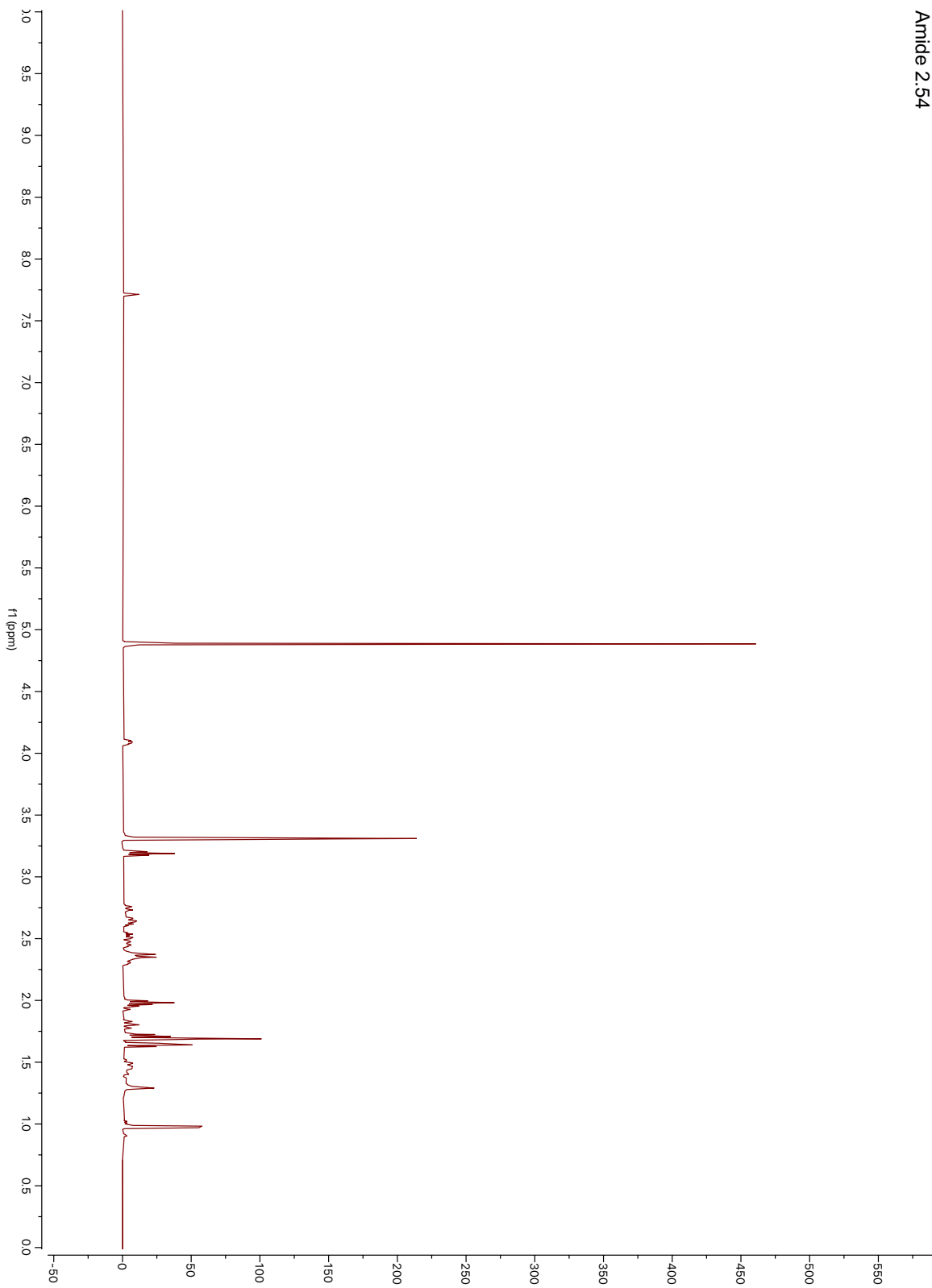
Sulfonyl fluoride 1.190



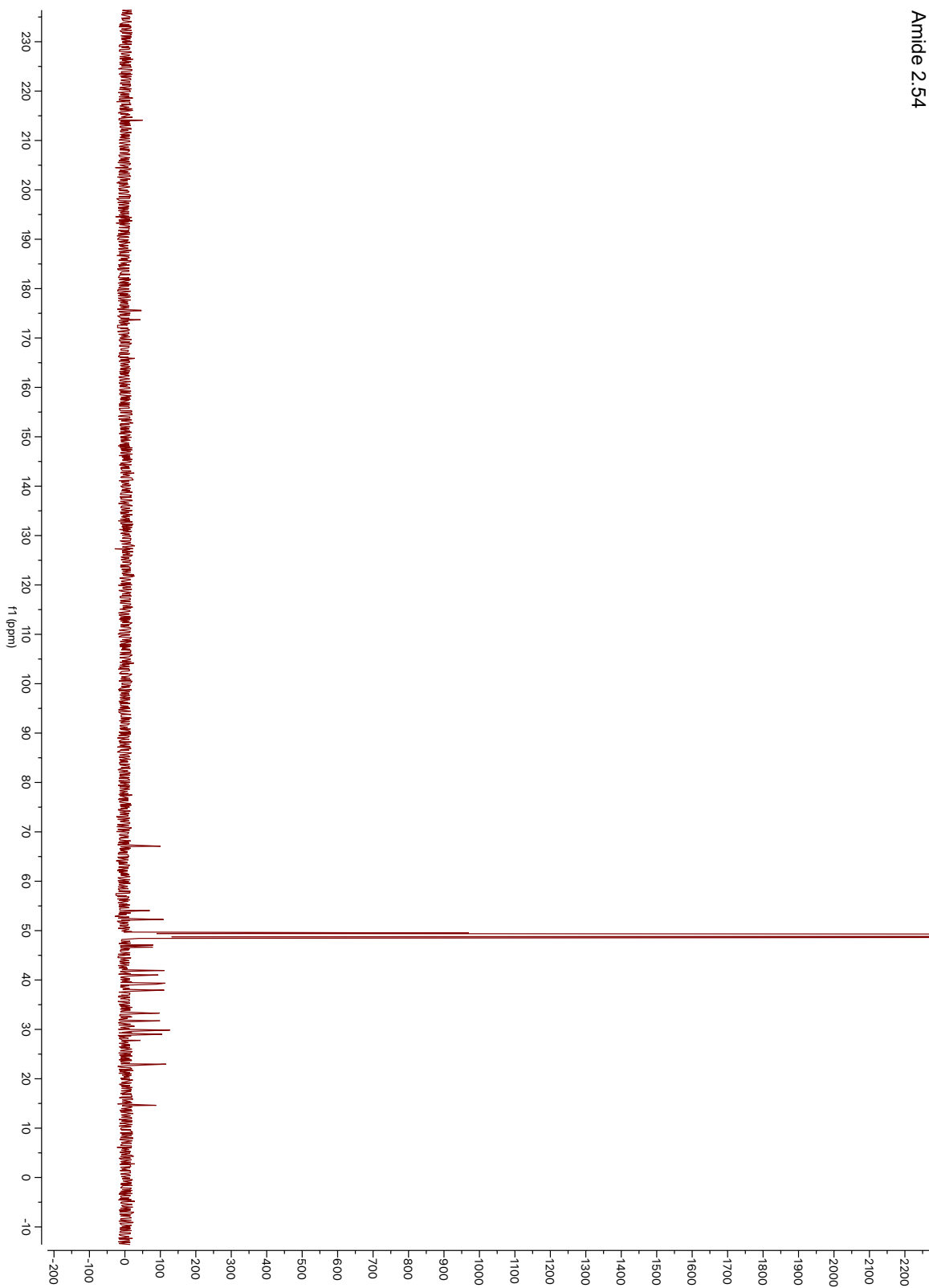
Carboxylic acid 1.191



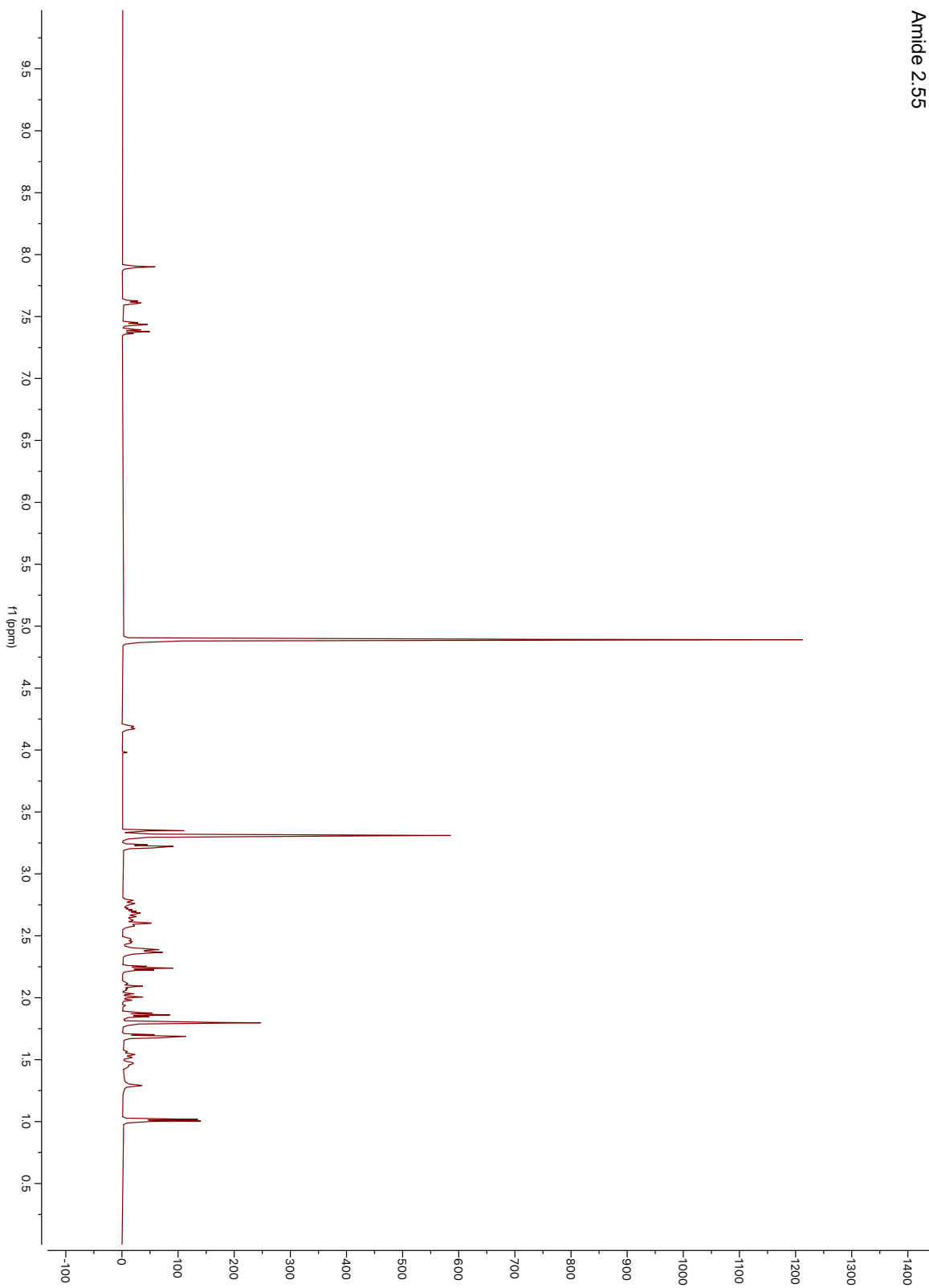
Amide 2.54



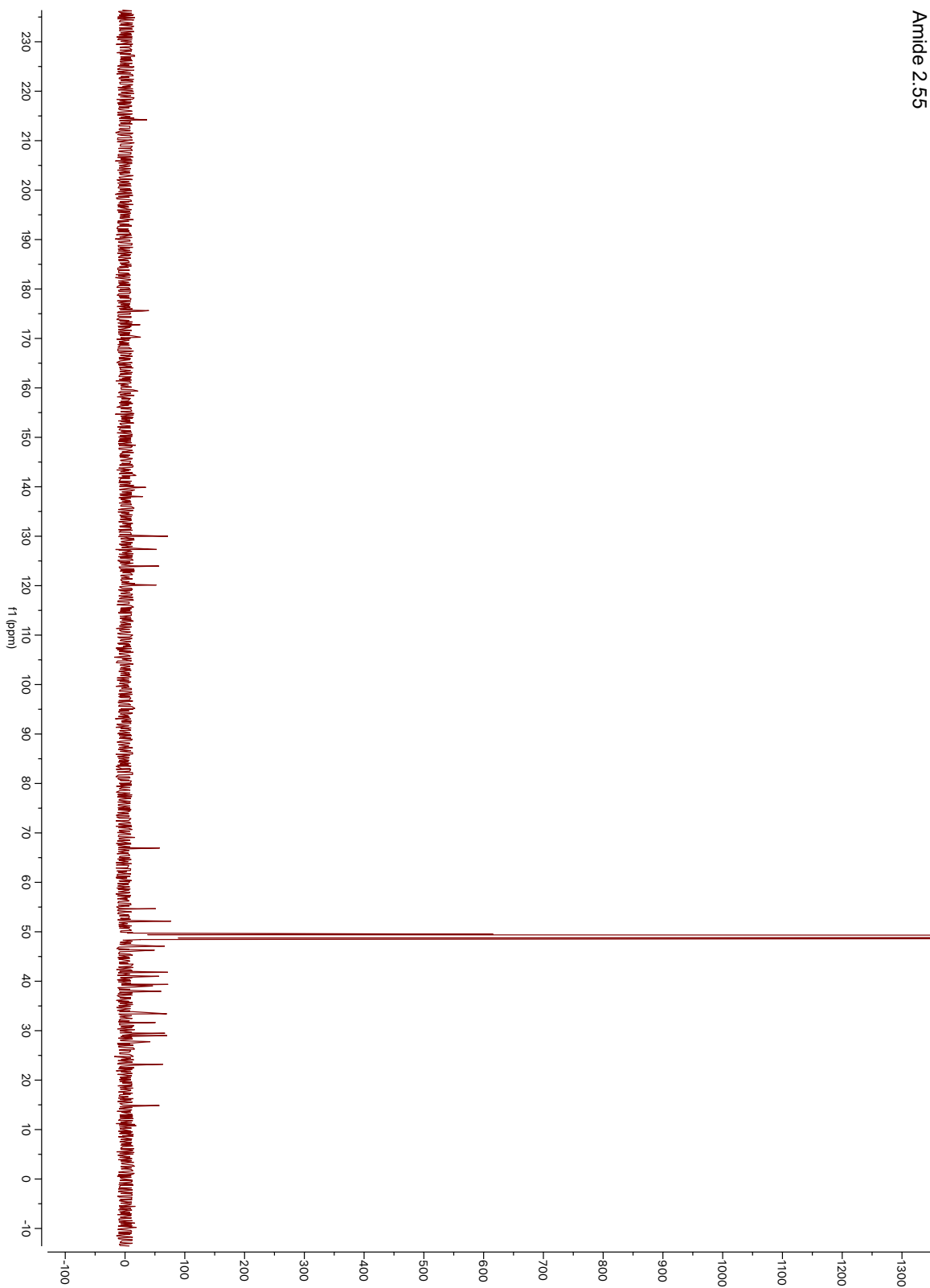
Amide 2.54



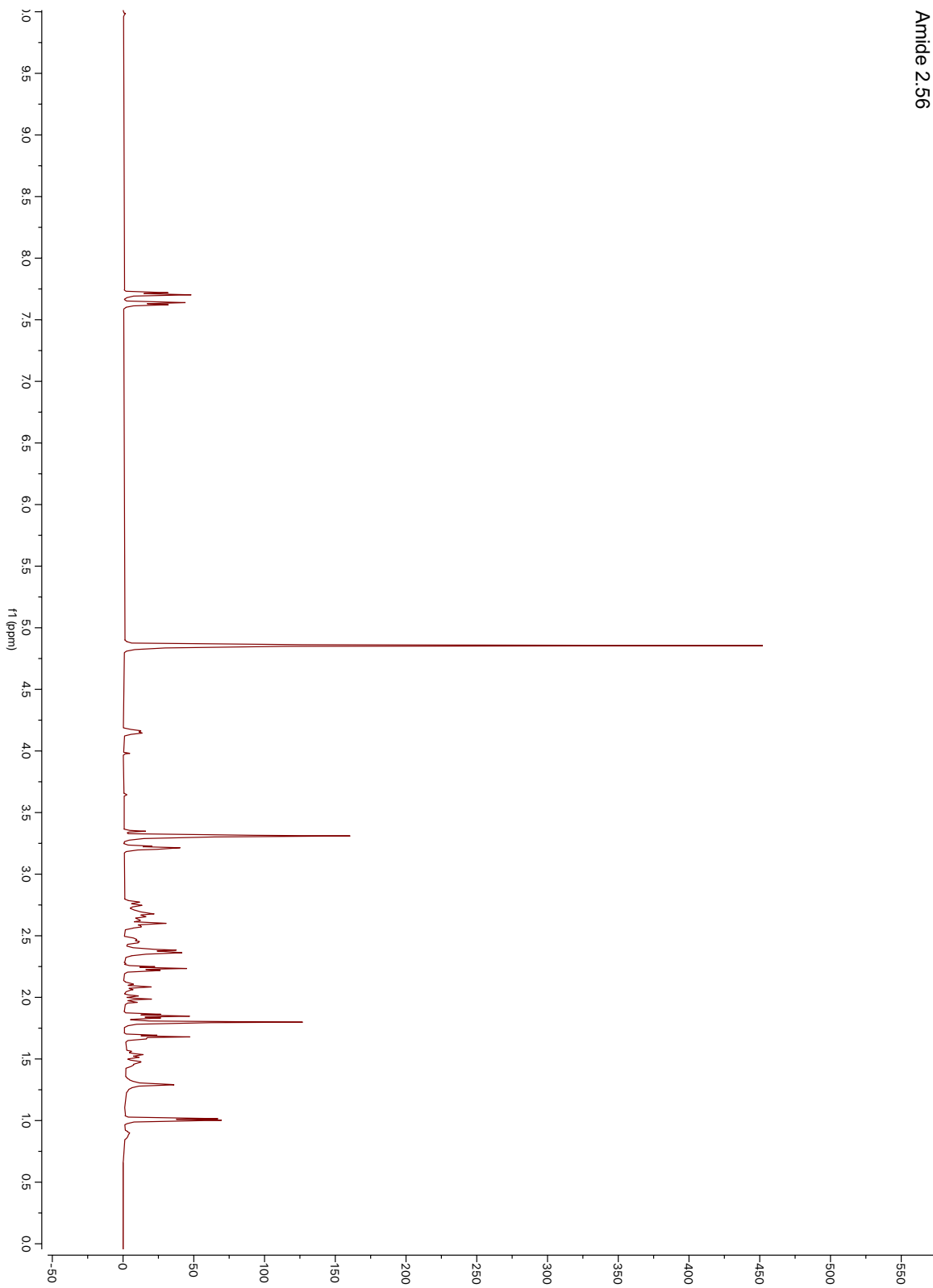
Amide 2.55



Amide 2.55



Amide 2.56



Amide 2.56

